Zeitschrift: IABSE reports of the working commissions = Rapports des commissions de travail AIPC = IVBH Berichte der Arbeitskommissionen

Band: 34 (1981)

Rubrik: Session 2: Structural modelling for numerical analysis

SESSION 2

June 3 rd, 1981

Structural Modelling for Numerical Analysis

Modélisation structurelle pour l'analyse numérique

Modellierung von Konstruktionen für die numerische Analyse

Part 1
Morning Session

Chairman: **Prof. P.G. Bergan, Norway**

Introductory Reporter: **Prof. Dr. Ch. Meyer, USA**
Dynamic Finite Element Analysis of Reinforced Concrete Structures[1])

Part 2
Afternoon Session

Chairman: **Prof. W.C. Schnobrich, USA**

Introductory Reporter: **Prof. Dr. J.H. Argyris**
G. Faust, K.J. Willam, F.R.G.[2])
Finite Element Modelling of Reinforced Concrete Structures[1])

[1]) Published in Introductory Report IABSE Colloquium, Delft 1981, Volume - Band 33.

[2]) The Introductory Report was delivered by Willam.

Leere Seite
Blank page
Page vide

Nonlinear Analysis of Concrete Structures by the Imposed Deformations Method. Comparison with experimental results.

Analyse non-linéaire de structures en béton par la méthode des déformations imposées. Comparaison avec des résultats expérimentaux.

Nichlineare Berechnung von Betonkonstruktionen mit der Methode aufgezwungener Verformungen.

ANTONIO AGUADO
Associate Professor

JUAN MURCIA
Professor

ANTONIO MARÍ
Assistant Professor

Polytechnic University of Barcelona
Barcelona, Spain

SUMMARY

This paper presents a method to analyse structures with nonlinear materials, using the superposition of linear problems in which the actions can be of any kind: imposed deformations, loads, displacements. In the same way, the characteristics of the numerical resolution process are exposed and finally an application example is presented in which the results obtained by other analytical methods are compared with the ones obtained experimentally.

RÉSUMÉ

Dans cet exposé on présente une méthode d'analyse de structures avec des matériaux non-linéaires en utilisant la superposition de problèmes linéaires dans lesquels les actions peuvent être de n'importe quel type: déformations imposées, charges, déplacements. Cette méthode peut s'utiliser manuellement ou avec un computer, si bien ici on utilise l'ordinateur. En dernier lieu, on présente un exemple d'application avec lequel on compare les résultats obtenus par d'autres méthodes et avec des résultats expérimentaux.

ZUSAMMENFASSUNG

In diesem Berich wird eine Methode für die Berechnung von Konstruktionen mit nichtlinearen Materialien gegeben. Wir benutzen die Überlagerung von aufgezwungenen Verformungen, Lasten, Verschiebungen. Wir beschreiben auch die Merkmale der numerischen Lösungsmethode und geben ein Anwendungsbeispiel, in dem wir die erzielten Ergebnisse mit denen anderer analytischer Methoden und mit Experimenten vergleichen.

1. INTRODUCTION

The concrete nonlinear behaviour and its influence in hyperstatic structures made out of prismatic pieces is known since the beginning of this century, although its adoption by the different national normatives was made later. The research on this subject can be made by any of the existing methods which go from the so called "exact methods" until the "approximated methods". Those in the first group demand the simultaneous fulfilment of the different conditions which form the structural analysis such as: equilibrium, compatibility and material conditions. Those included in the second group normally imply the partial fulfillment of the previous conditions, but they have the advantage of giving, in general, simple solutions more or less precise regarding the exact solution.

The nonlinear analysis (by the material) of structures can be made, from our point of view, according to compact analysis or to separative analysis:

1.- In the compact analysis, the material nonlinear characteristics are introduced in each section, changing its mechanical properties (i.e. area, inertia, modulus of elasticity, etc...) This fact sticks out the mechanical treatment of the structure with an equilibrium preponderance.

2.- In the separative analysis, the nonlinear traits of the material are introduced in each section (or zone) as a virtual action of geometrical kind (strain or imposed rotation) (1). This fact means a geometrical treatment of the structure with compatibility preponderance.

In each of these two ways of analysis, there are methods of direct resolution or through iterations. This case implies generally the utilization of computers, hypothesis of great precision, etc...

Inside the general framework of nonlinear methods of analysis, which we have just established, the method set out below fits into the exact methods treating the problem by a separative analysis in which we can work with linear problems superposing them, and obtaining the right solution by iterations.

2. PROPOSED ANALYSIS METHOD

2.1 Calculation Bases

The material behaviour is presented on a section level by a nonlinear diagram Moment-curvature (M-C) which means a section by section treatment and therefore, we do not work with concentrate rotations in plastic hinges . (Diagram M-θ) (1), (2).

The diagram shape M-C is not intrinsic to the method of analysis, and we can use any of the diagrams adopted by the different authors (G. MACCHI (1), A.L. BAKER (2)), as: curve, bilinear, trilinear, etc... Fig. 1. In case of using multilinear

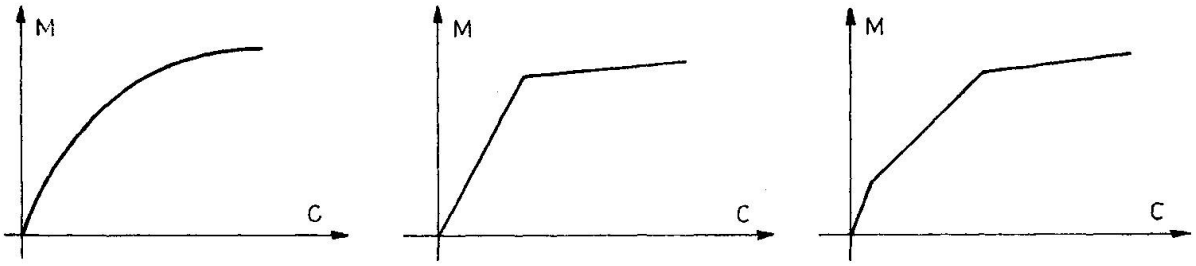

Fig. 1 Moment-Curvature diagrams.

diagrams the slope of any of the straight lines must not be null, because we will have problems in the numerical resolution.

The M-C diagrams have been obtained numerically according to G. MACCHI and E. SIVIERO (3) where the tension stiffening is considered as a mean to achieve a greater precision when we analyse the structure in service situation.

The method allows to analyze the structure behaviour in front of any action: loads, strains (increases and gradients of temperature, shrinkage, creep, etc...) and displacements (bearing settlements, etc...).

As data issue for the calculation steps in which the method is detached, we have: the actions working in the structure (they can be any of those mentioned before) and the Moment-curvature diagrams of each section Fig. 2.b.

In this case we have not considered the strains caused by shear or axial forces although the proposed method can consider these strains as another virtual action.

2.2 Calculation steps

In the first step, we take the actions working in the structure and we make a linear calculation of it, taking the stiffness to bending $K_o = EI$ (Fig. 2.a). This way we obtain the effects (moment, shear, axial force, etc...) to which each section is submitted.

With the structure linear calculation in this step, we have got a balanced and compatible solution, but it does not fulfill with the real characteristics of the material. In a generical section, the solution obtained by the calculation is represented by the point A (Fig. 2.a) while the fulfillment of the material conditions would require to be in the point B (Fig. 2.b).

In the second step the curvature increases (ΔC_1), of each section between the real curvature and the one obtained in the calculation of the first step (C_A), are not generally compatible. If the structure is isostatic, these strains mean an increase of strain, but no forces are shown; however in a hyperstatic structure besides the strains increase some hyperstatic effects are shown.

The calculation in this second step is made by a linear calculation with the initial traits of the structure (bending stiffness Ko) taking imposed deformations

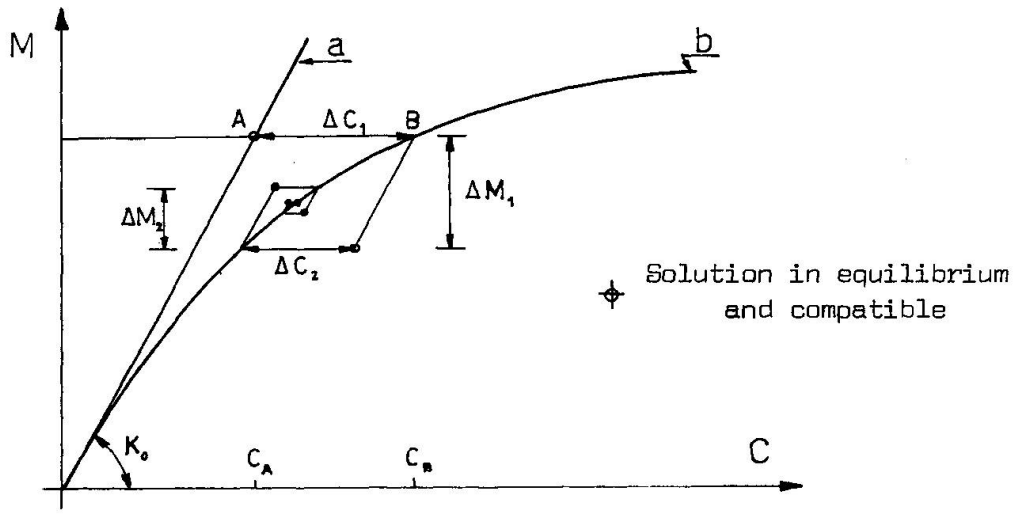

Fig. 2 Sectional study of the proposed analysis method.

(Curvature increases ΔC_1) as virtual actions in each section. With these calculations we get the hyperstatic load effects which make compatible the curvature system; in a section this hyperstatic moment is given by ΔM_1. Fig. 2. Structural analysis procedure taking imposed deformations (curvatures system) as actions can be seen in ref. (4).

Since we work below the dominion of small strains in each of these two calculation steps, either the superposition of the deflection system (y) or the superposition of the curvature system ($c \simeq y''$) are valid, and so the superposition principle can be applied in the analysis in first order. Consequently we superpose to the forces obtained in the first step those deduced in the second one, getting in a section the point 1. This point is on a parallel to the initial stiffness K_0 since we work with this stiffness in the two linear problems.

The point 1 represents a balanced and compatible solution to the problem, although it does not fulfill the real characteristics of the material. This is why it would be necessary to introduce, as action, the strain system given by the different curvatures increases ΔC_2 of each section.

The determination of the hyperstatic forces system (ΔM_2) caused by this curvature system (ΔC_2) is made in the same way to the one mentioned previously. Thus, this procedure implies an iterating process in which we pivot over the material real conditions for each iteration. We get the final solution when the forces system (ΔM_i) vanishes. In this moment (point S) we have a balanced and compatible solution which fulfills the material traits.

As we have seen this process does not impose any conditions about which must be the situation the structure is found. This is why is valid either for service situations or for situations next to failure. In the same way this process is valid in front of any kind of action (strain, loads, movements) working in the structure which is considered in the first calculation step, while in the second step we take the curvature increases ΔC as another (virtual) action.

2.3 Numerical resolution

In order to reflect the material nonlinear behaviour through the diagram M-C in each section, an accurate definition is needed for all the sections of the different elements. In the numerical resolution each element is divided in n parts being determined in every of them a diagram M-C representing all the sections of it. The number of parts n depends on the kind of structural elements (constant or veriable inertia, reinforcement distribution) and it often changes between 1 and 5, being in the practice the most common n=3.

Every one of the linear problems representing both calculation steps can be approached either by compatibility or equilibrium and its resolution can be achieved by any of the existing calculation methods, which means that the process of the nonlinear analysis exposed here by, has a great flexibility according to the resolution system.

Since the initial characteristics (stiffness or flexibility matrix) of the structure are kept, in order to simplify the calculations, it is interesting to systematize them. We have to use, for that, the same method in the two steps and this calculation, in its turn, must systematize at the maximum the operations to be done.

To obtain the numerical solution a convergence criterion defining the end of the iterations must be fixed. Its number depends on different factors: precision defining the final solution, solution being the issue for the analysis (first step) numerical process used, etc.

As follows we study the incidence of every one.

a.- The precisions is influenced in one hand by the adopted convergence criterion. In this case it is established according to a certain percentatge of the initial effects in some definite sections e.g.:

$$\Delta M_i \leq \alpha \cdot M_o$$

where

ΔM_i = Increase of moments in the fixed sections for two consecutives iterations.
α = Fixed percentatge according to the criterion (values below 5%)
M_o = Bending moment in the fixed sections obtained in the first step, and the other hand, the number of sections in which the mentioned criterion is verified, in this case, we have taken the sections at the edge of each bar.

b.- In a hyperstatic structure the moment law deduced from the first calculation step depends on the stiffness K_o adopted. Thus, if this stiffness is near the ultimate value, the number of iterations is going to be small, in the opposite case this number will increase.

c.- The numerical process can follow the described theorical process which graph is made in Fig. 2, or can reckon among the results obtained in the first calcula

tion step and those of the previous iteration to the one being reckoned. With this procedure the convergence proves to be faster.

In the examples presented in (4), (5), considering between 2% and 4%, and establishing the convergence criterion in both edge sections of every bar, the number of iterations needed to reach the numerical solution, were 2 or 3 for service situations and something higher (5 or 6) for situations near failure.

Finally the method of analysis said above, can be applied manually (for small grade of hyperstaticity structures, e.g. a bridge) or by computer (in high grade of hyperstaticity structures e.g., frames).

3. EXAMPLE : COMPARISON WITH EXPERIMENTAL RESULTS.

We have shown until this point the validity of this method from a theoretical point of view. An enlargement of the subject as well as its comparison with analytical methods can be seen in the ref. (4). To conclude we are going to show its practical validity by the comparison with experimental results.

As experimental test we will take one of the test sequences made by A. MATTOCK (6) on a continuous beam of two spans (Fig. 3) with a concentrated load at the middle of one of them. The choice of this test brings us an additional advantage since it allows us to compare at the same time the results with those achieved by other analytical methods, which have been explained by A. GRELAT (7) and A. APARICIO (8).

The Moment-curvature diagrams (M-C) of the sections were obtained numerically by computer and then an adjustement of trilinear diagrams to them was made. Nevertheless and as we have said, the kind of diagram M-C is not intrinsic to the proposed method. The use of multilinear diagrams (trilinear in this case) has the advantage on one hand of getting and accurate adjustement regarding the one got numerically, and on the other hand it allows to obtain a simple expression of the curvature increases (ΔC) taken as virtual actions in the second calculation step. This fact is to the advantage of calculations systematization mentioned previously.

To obtain the diagram MC concrete contribution between cracks (tension stiffening) has been considered. This way we obtain a better precision in the structure behaviour in front of service load, which according to A. GRELAT can be evaluated in this case up to 20%. (7)

The results obtained by the different methods are presented in Fig. 4 by a Moment-load diagram corresponding to the sections where the load is applied (section B) and the support one (section C).

In the proposed analysis method the value to a load $P_u = 70{,}4$ KN has been considered as ultimate moment since the result obtained experimentally $P_u = 74{,}2$ KN. Fig. 4 can be due to a hardening of the steel stress-strain diagram after the

yielding point.

The results exposed in the mentioned diagram state the accurate precision of the proposed method, as well as the other analytical methods regarding the experimental results either in failure situations or in service situations (in the last the consideration of the tension-stiffening has an special influence).

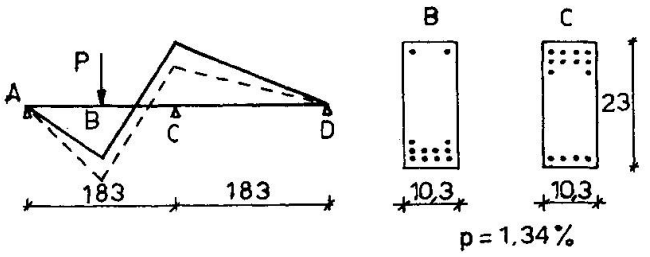

Fig. 3 Analysed structure.

Thus, if we accept the accurate precision of the analytic methods the argument will be centred in the advantages and disadvantages of each one. We would like to review those advantages and disadvantages as a way of concluding, regarding the method we are proposing.

4. CONCLUSIONS

In the field of linear structures this method allows to work with any kind of action (load, strain, movements) and specially with imposed deformations due to increases and gradients of temperature (5), shrinkage, creep, etc...

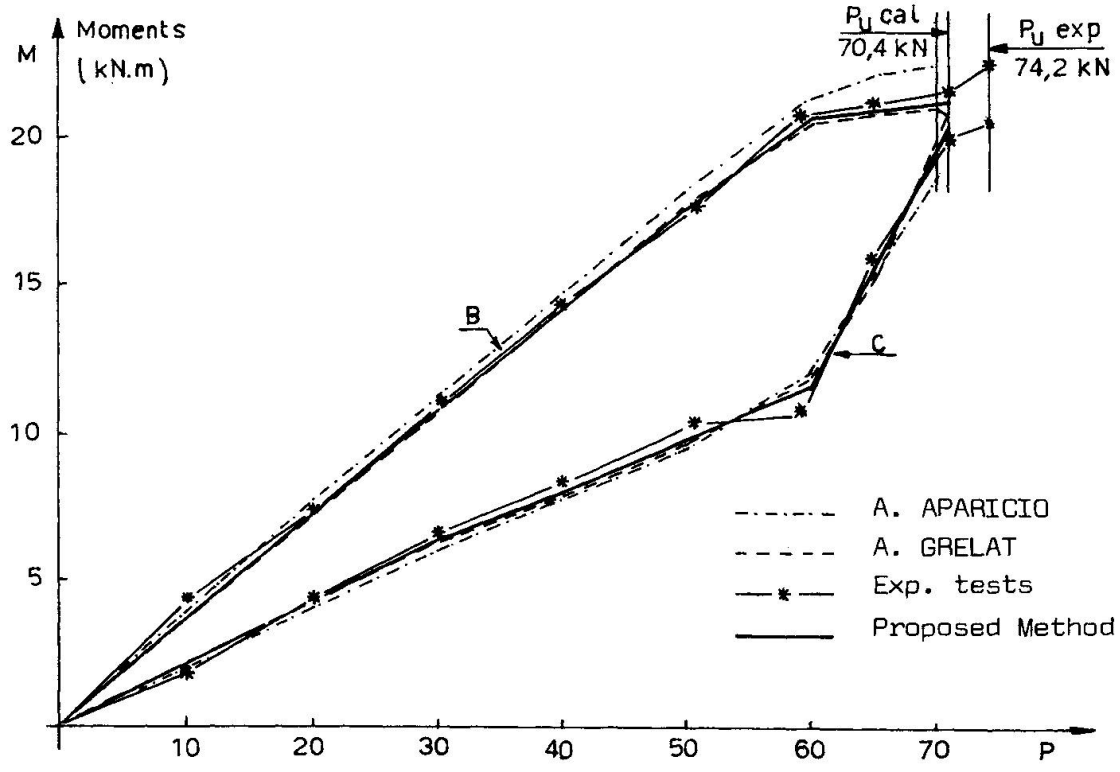

Fig. 4 Bending Moment evolution in a continuous beam under increasing load.

The method belongs to the group of "exact methods" since the conditions of equilibrium, compatibility and material constitutives are fulfilled. The comparison with experimental results confirms the accuracy with a great precision of the numerical solution.

The practical application of the method has a great independence regarding the concrete procedure of resolution of both steps, since it can be approached by compatibility methods and by equilibrium methods.

We always work with linear problems with only one stiffness or flexibility matrix. This is the reason why they can be superposed validly. In the method resolution by computer this trait allows to take advantage of common blocks, decreasing the execution time and the capacity of memory needed.

Finally, this method has a great field of application since it allows to analyze any kind of linear structure: Bridges (5), continuous beams, multistory frames (4), etc.

REFERENCES

1. MACCHI, G., "Méthode des rotations imposées, Exposé de la méthode et exemple de calcul," C 10-2, C.E.B., International Course on Structural Concrete, L. N.E.C., Lisbon, 1973.
2. BAKER, A.L.L., "The ultimate-load theory applied to the design of reinforced and prestessed concrete frames," Concrete Publications, Ltd. London, 1956, pp. 91.
3. MACCHI, G. and SIVIERO, E., "Deformability of prismatic reinforced concrete members with rectangular cross-section under combined bending and axial load," Bulletin d'information nº 101, "Structures hiperstatiques," Juillet 1974.
4. AGUADO, A., "Estudio del análisis no lineal de estructuras de hormigón mediante superposición de problemas lineales en deformaciones", Universidad Politécnica de Barcelona, Tesis doctoral, Barcelona, Febrero 1980.
5. AGUADO, A. and MURCIA, J., "Nonlinear analysis of concrete structures by imposed deformation method. Application to the study of load and temperature effects," C.E.B., Comission 2, "Structural Analysis," Meeting at Venice, October 1980.
6. MATTOCK, A., "Redistribution of design bending moments in reinforced concrete continuous beams," The Institution of Civil Engineers, Vol. 13, (Session 1958.59).
7. GRELAT, A., "Comportement non linéaire et stabilité des ossatures en béton armé," Annales de l'Institut Technique du Bâtiment et des Travaux Publics, nº 366, Novembre 1978.
8. APARICIO, A., "Estudio de la evolución hasta la rotura por solicitaciones normales de tableros contínuos de puentes de hormigón armado o pretensado," Universidad de Santander, Tesis doctoral, Santander, Abril 1980.

Essentials for discrete crack analysis

L'essentiel en ce qui concerne le calcul des fissures distinctes

Das Wichtigste über die Berechnung mit diskreten Rissen

JOHAN BLAAUWENDRAAD
Professor of Civil Engineering
Delft University of Technology,
Rijkswaterstaat, Bouwresearch,
Utrecht, The Netherlands

HENK J. GROOTENBOER
Dr. Ir., Research Member
Twente University of Technology,
Department of Mechanical Engineering,
Enschede, The Netherlands

SUMMARY

Reinforced concrete structures sometimes display a failure behaviour which is dominated by one or a few discrete sharp cracks. An analysis can only predict such failure types if discrete cracks are allowed to develop in any direction, and to cross any element. It is argued that equilibrium models in the finite element method meet the requirements for an accurate simulation of this cracking problem.

RÉSUMÉ

Le comportement à la rupture de constructions en béton armé est souvent déterminé par quelques fissures distinctes. Seul une analyse permettant le développement de fissures dans toute direction, à travers tout élément, est capable de prévoir une telle rupture. Il est démontré que la méthode des éléments finis à condition d'équilibre, correspond aux exigences d'une simulation précise de la fissuration.

ZUSAMMENFASSUNG

Das Verhalten von Stahlbetonkonstruktionen wird manchmal von einem oder mehreren diskreten Rissen bestimmt. Um dieses Verhalten gut vorhersagen zu können, verwendet man am besten finite Elemente, die in verschiedenen Richtungen reissen können. Es wird gesagt, dass Gleichgewichtsmodelle die Anforderungen an die genaue Risssimulation erfüllen können.

1. SCOPE

Structural analysis of reinforced concrete is done, roughly speaking, in two distinct ways. One uses either an approach in which cracks are smeared out, or one uses single sharp interelement cracks. The first approach, using an average stiffness of cracked elements, seems to apply well in all cases where one can observe cracks in concrete which tend to be diffuse and spread over a large zone. The latter approach, handling interelement sharp cracks, is promising for the analysis of structures in which one or a few discrete cracks dominate the behaviour. Both approaches have their advantages and draw-backs.
The smeared out approach can give widely different results for crack propagation depending on the choice of the finite element mesh, and is, therefore, unobjective. Bažant [*1*] has proposed a propagation criterion to overcome this serious problem. Using the same concept as in fracture mechanics of sharp cracks and accounting for the effect of bond-slip across the crack, he refines the modelling in terms of element-wide blunt smeared crack band.
The paper presented here enters into the subject of an analysis with discrete cracks and aims for an enhancement of the single sharp interelement crack approach. Untill now, one splits each node in two when the crack advances, requiring node renumbering and changes in topological connectivity of the mesh with the necessary recalculations of the structural stiffness matrix. Moreover it can be necessary to vary the direction of the interface between two finite elements and move the location of the mode into which the crack is about to advance. The big advantage of this approach above the smeared out concept is the fact that actual crack spacings and widths can be predicted. The present method maintains these advantages and avoids the forementioned difficulties. The element mesh needs not be changed any more and single cracks are allowed to propagate in each possible direction regardless the chosen mesh. In this way the approach becomes suitable for the analysis of complete concrete structures. We will discuss the requirements to meet this goal.

2. PHENOMENA TO BE MODELLED

An adequate model to analyze a reinforced structure accounting for single cracks at arbitrary spacings, which is capable to predict correct crack widths and crack spacings, must meet the following requirements:

a. Constitutive laws for plain concrete must be available, including a crushing criterion and a cracking criterion. A similar requirement holds for the reinforcement bar.
b. A proper model has to be chosen for the description of the force transfer in a crack. This model must allow for shear stresses and normal stresses in the crack layer due to aggregate interlock. A relation between these stresses and the corresponding relative displacements of the crack faces (shift and dilatancy) must be available.
c. A suitable model has to be chosen for the bond-slip zone in between the reinforcement bar and the surrounding concrete. This model must provide a relation between the shear stress and normal (radial) stress on the one hand and the corresponding displacement components (parallel and radial) on the other hand.
d. The complex local state of stress at an intersection of a crack and a reinforcement bar, with typical high gradients for stresses, must be approached as close as possible. The reinforcement bar acts as a flexible connection between the two crack faces.

In order to make good predictions of the crack widths, the real bond spring behaviour near the crack must be modelled.
So the abrupt change of sign of bond shear stresses at the crack must be accounted for in this respect. A similar want applies for the dowel action of the reinforcement bar due to a parallel shift of the crack faces relative to each other. However this feature seams to be of much less influence on the behaviour of the structure than the bond-slip phenomenon. Dowel action will develop only noticeably after the structure has already started to fail.

e. The correct failure mechanism must be predicted. From experimental evidence, for instance [2], we know that the ultimate load capacity of a structure strongly depends on the crack pattern. This applies especially for failure modes due to combinations of bending moment and shear force. Failure is induced then by one or a few dominating cracks and displays a brittle character. An inaccurate destination of the crack position may influence the ultimate load seriously. The analysis model must also apply, of course, for ductile models of failure, as is the case in pure bending for low percentages of main reinforcement.

3. FINITE ELEMENT REALIZATION

The authors feel that the requirements listed in section 2 are best met if two decisions are made concurrently:

a. The finite element formulation must allow for single cracks at discrete arbitrary spacings. The specifications of the program must be so conceived, that no crack direction is enforced by the element mesh or by the way the program was written. A crack can come into being at any position in the mesh and can from there propagate in any direction through any element.

b. A proper description of the stress state is of much importance. Therefore, out of all known finite element formulations, an equilibrium model, which starts from assumed stress fields, is the most promising one [3]. The authors particularly prefer a modified version of the hybrid model [4] using (what has been called) *natural boundary displacements* [5]. This finite element model is used in combination with the *initial strain* concept to process nonlinear effects.

We will discuss these two decisions in more detail. The explanation will be restricted to states of plane stress.

3.1. Equilibrium model for the uncracked state

Let us start with the uncracked state of reinforced concrete. We basically adopt an approach of apart two-dimensional elements of plain concrete and apart one-dimensional elements of reinforcement. Therefore, concrete elements never contain reinforcement steel. The rebar elements run in between concrete elements. The rebar element is attached to the concrete element with the aid of a bond linkage element as described in section 2c. In physical reality full interelement equilibrium of surface tractions exists. It also holds that the integral of bond stresses along a rebar element yields the stress resultants in the cross-section of a rebar element. To model this properly, one needs a finite element formulation which basically is an equilibrium model. The wide-spread stiffness models concentrate on compatibility rather than on equilibrium, and are therefore less suited with regard to our requirements. The equilibrium model, used by the authors, has been derived from the hybrid model proposed by Pian [4].

This model starts from the following assumptions:
- stresses σ_{ij} are in equilibrium with the given load q_i all over the volume V_e of an element.
- it is not enforced a priori that the strains ε_{ij} are compatible with the displacement field u_i over the volume V_e of an element.
- on the interelement boundaries A_e nor continuity of tractions ($\bar{p}_i = \overset{+}{p}_i$) is enforced a priori, nor compatibility of displacements ($\bar{u}_i = \overset{+}{u}_i$).
- on the external boundary it is adopted that displacements u_i take the prescribed value u_i° at the part A_u of the boundary. However, it is not enforced that the element tractions p_i equalize the given load p_i° at the part A_p of the boundary.

All these appointments result in one variational condition to be fulfilled for all M elements:

$$\sum_{e=1}^{M} \left[\iiint_{V_e} \left\{ \varepsilon_{ij} - \frac{1}{2}\left(u_{i,j} + u_{j,i}\right) \right\} \delta\sigma_{ij} \, dV + \right.$$

$$\left. + \iint_{A_e} \left(\bar{u}_i - \overset{+}{u}_i\right) \delta p_i \, dA - \iint_{A_e} \left(\bar{p}_i + \overset{+}{p}_i\right) \delta u_i \, dA \right] +$$

$$+ \iint_{A_p} \left(-p_i + p_i^\circ\right) \delta u_i = 0 \qquad (1)$$

Application of the divergence theorem and re-ordering of terms yields

$$\sum_{e=1}^{M} \left\{ \iiint_{V_e} \varepsilon_{ij} \, \delta\sigma_{ij} \, dV - \oiint_{A_e} p_i \, \delta u_i \, dA \right\} + \iint_{A_p} p_i^\circ \, \delta u_i \, dA = 0 \qquad (2)$$

In this expression the surface integral must be taken over the full boundary A_e of each element, also for the elements which join the external boundary A_p. We now introduce the constitutive law, using the flexibility relation for strains and stresses:

$$\varepsilon_{ij} = F_{ijkl} \, \sigma_{ij} \qquad (3)$$

This enables us to make the following interpretation of the variational condition (2). When introducing the functional F:

$$F = \sum_{e=1}^{M} \left\{ - \iiint_{V_e} \frac{1}{2} F_{ijkl} \, \sigma_{ij} \sigma_{kl} \, dV + \oiint_{A_e} p_i \, u_i \, dA \right\} - \iint_{A_p} p_i^\circ \, u_i \, dA \qquad (4)$$

the condition can be restated:

$$\delta F(\sigma_{ij}, u_i) = 0 \qquad (5)$$

The functional F must be stationary in respect of variations of the element stresses σ_{ij} and the element boundary displacements u_i. This facilitates to choose a stress distribution over the whole element volume and to restrict ourselves to a distribution for the displacements which is defined along the element edges only.

Normally, this variational principle is used as follows. One choses nodes at the element corners and these nodes are common for all elements which join together at that position. In case of plane stress, one defines two degrees of freedoms for the displacements in each node and has to interpolate the displacements along the element boundaries. This means that the displacement fields for the several elements are interconnected. On the contrary, stress interpolations are full indepently chosen within each element. Execution of the variational process yields a set of equations similar to the standard stiffness method. This type of finite element method, referred to as *hybrid* method, appears to the user as a displacement method type of analysis. Fig. 1 shows the degrees of freedom in such an analysis (left part of figure).

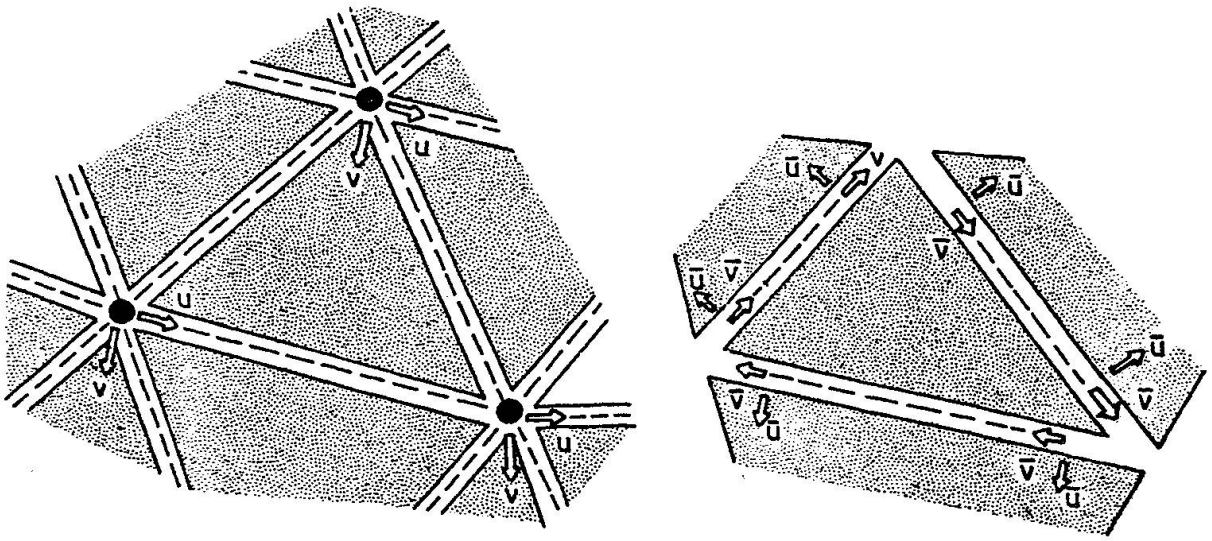

Fig. 1 Standard type of hybrid elements (left) and modified model with natural boundary displacements (right).

It will be clear that the hybrid method does not fully meet the requirements for a good crack analysis, stated in section 2. We still lack the wanted interelement stress continuity. The stress parameters can be eliminated per element without any assurance that stresses (tractions) will take the same values $\bar{\sigma}_{ij}$ and σ^{+}_{ij} at different sides of the interelement boundary.

This assurance does be got, if one so modifies the hybrid method, that degrees of freedom are not common to alle elements joining at a corner, but only common for two elements which share one single straight edge.
If one, additionally, uses the same distribution for the tractions (stresses) in both elements and above that also for the displacements along this edge, interelement stress continuity will be achieved automatically. Said in another way, one then gets a more natural stress transfer across element boundaries, and for that reason the name *natural boundary displacements* was introduced [5].Mathematically, the natural degrees of freedom are Lagrangian multipliers in a variational scheme. The method has been applied for the discrete crack analysis, reported in [6] and [7]. In this analysis a triangle is chosen and linear stress interpolations are applied, in connection with linearly varying natural boundary displacements. Fig. 1 shows in the right hand part a picture of the degrees of freedom which are needed in that case. It will be clear that special care must be taken for the programming of such a type of analysis, but using a frontal solution scheme, one will not have too big problems. The rebar element to be used in this method is of the special type shown in Fig. 2. The interaction between concrete elements, and rebar elements is performed by natural boundary displacements, and the force transfer from one rebar element to another rebar element by standard degrees of freedom.

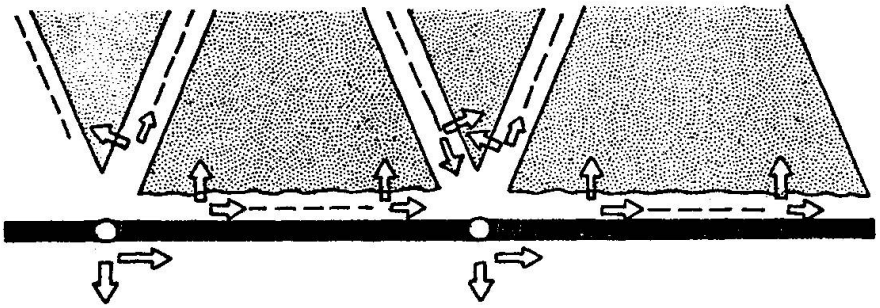

Fig. 2 Special type of reinforcement bar element in the equilibrium model with natural boundary displacements

3.2. Equilibrium model in the cracked state

We now consider the cracked state of a reinforced concrete structure. For the purpose of this paper we assume that just one crack occurs per element, but in general more cracks may cross an element.
Let us first observe a cracked concrete element that is not linked to a rebar element. Everyting is available in the formulation for elements with natural boundary displacements to handle this crack. A shear stress and normal stress in the crack can develop and full continuity of these stresses has been preserved between the faces of the two element parts after cracking.

Fig. 3 shows crack displacements u_i, u_j and v which have been chosen in [6]. These quantities, defining the crack opening and the crack shift, are processed as initial strains, as is done for all other nonlinear effects.
It is highly questionable if this approach would be possible in the standard stiffness method based on an assumption for the displacement field. Quite surely one needs additional degrees of freedom in that case.

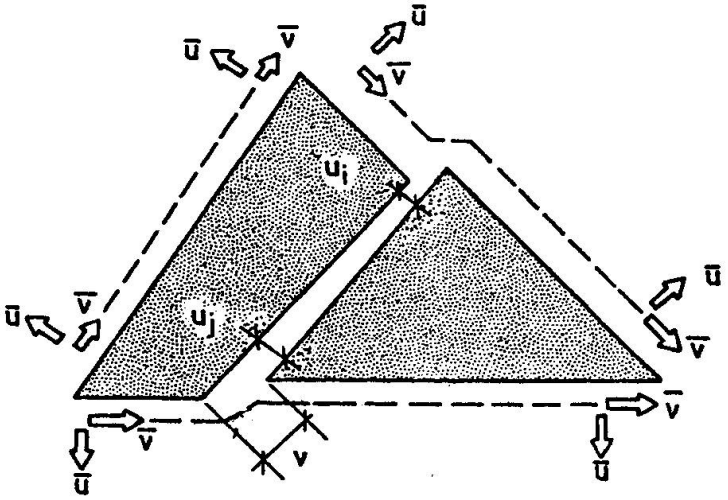

Fig. 3 *Crack displacements u_i, u_j and v are handled as initial strains. No additional degrees of freedom are needed.*

Now we move to observe a cracked concrete element that has been linked to a rebar element. In this case an intersection of the crack and the rebar element can occur, and abrupt gradients for the bond stresses and dowel stresses will come into being. Especially the dowel action of the reinforcement bar asks for additional features in the model. This is achieved by assuming an additional stress field in the cracked concrete element. This extra field must fullfil the continuity of stresses in the crack, but must additionally allow for the rapidly changing distribution of tractions between the element edge and the rebar. It has been shown in [6] that this can be achieved with the triangular elements for concrete described above. Now extra degrees of freedom are needed in the natural boundary displacements. The displacements discontinuities Δu° and Δv° in the natural displacements on the boundary have been introduced for this purpose, see Fig. 4.

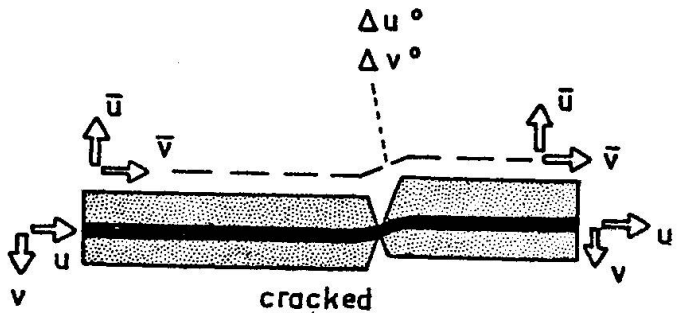

Fig. 4 *To account for dowel action, one needs additional degrees of freedom Δu° and Δv° and extra discontinuous stress fields*

The crack displacements u_i, u_j and v are treated as initial strains in the analysis and the discontinuities Δu^o and Δv^o in the natural boundary displacements determine an additional set of equations which has to be solved simultaneously with the global set of degrees of freedom which already exists in the uncracked state. This global set remains unchanged, no re-analysis of the stiffness matrix being needed. If dowel action is disregarded, the extra set of equations will not be needed.

We see that it is easy to handle internal element displacement discontinities. Obviously it is far more easy than in a formulation based on a displacement field interpolation over the whole element volume.

4. EVALUATION

In this final section some reflections of more comtemplative nature are presented. One may ask after the convergence of the process and put the question if the algorithm does yield correct internal crack displacements and the correct failure mechanism.

4.1. The advantage of an equilibrium model

To judge the chance for a correct crack displacement prediction, we may use an energy examination. When a crack crosses a structure, the two separated parts may move relative to each other. A displacement mechanism may occur in which the parts displace in a rigid body mode. Then, the energy dissipation in the crack, must be equal to the work performed by the external loading. Only when the stresses in the crack are in equilibrium with the external loading, we do get from this equality the correct internal crack displacement associated with a rigid body mode displacement of the structural parts. In the hybrid element formulation the stresses over an arbritrary line are in general not in equilibrium with the external loading, so we may not expect to get the correct internal crack displacements. And even when, after cracking, a rigid body mode is possible, we are not sure to find this mode in our calculation. In the element formulation with natural boundary displacements the stresses on the element boundaries are in equilibrium with the external loading. This applies however also for the stresses along any arbitrary line. So with this model we can expect to find the right crack displacement. And, what is even more important, we can expect to find the right failure mechanism.
Calculations performed with the MICRO-model have shown that with this model the different kinds of failure as bending failure, shear failure or combinations of these two can be analysed with great accuracy. This applies for ductile behaviour as well as brittle behaviour.
Fig. 5 shows a typical result for a brittle failure in shear.

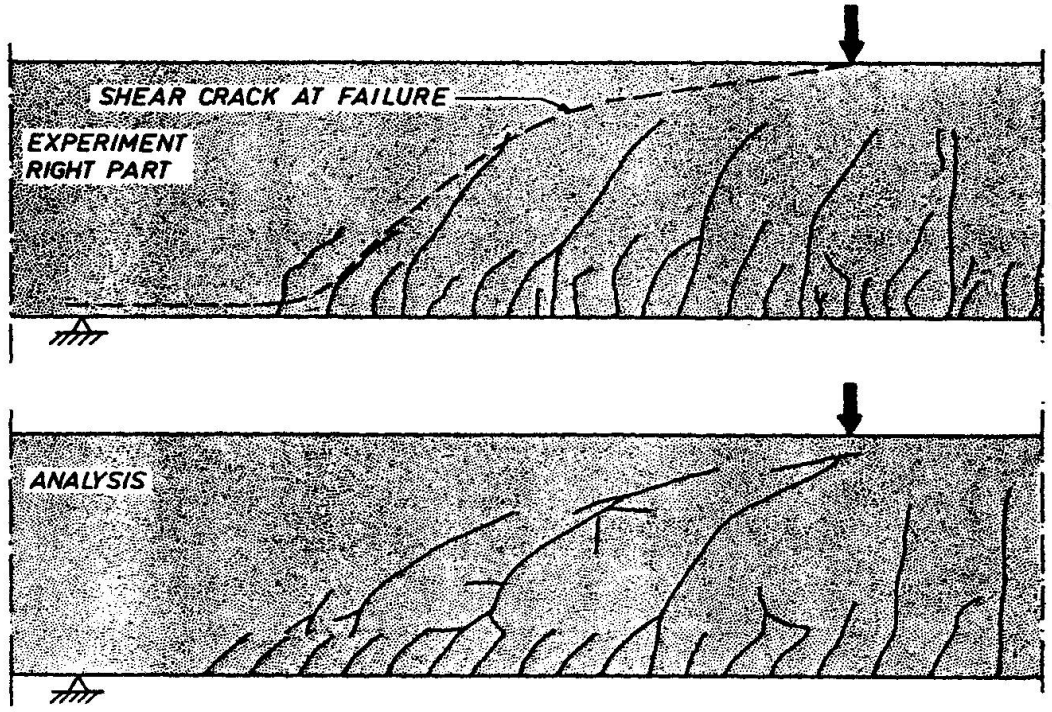

Fig. 5. A typical result for an analysis in which a few single sharp cracks dominate the brittle shear failure

4.2. Parellel stiffness versus serial stiffness

We want to make another comment on the use of an equilibrium model on the basis of an assumed stress field. Most research-workers apply the stiffness method on the basis of an assumed field of displacements and use the concept of smeared-out cracks with a scheme for numerical integration. This means, mostly, that they can make use of standard finite element programs for the analysis of cracked reinforced structures. It proves that such models are well suited for the prediction of ductile bending failure, but they yield bad predictions for brittle shear failure. The authors feel that this is due to the limited possibilities of the smeared-out concept with numerical integration to model a failure mechanism in which only a few cracks will be formed. Because of the assumed displacement field, and therefore an assumed strain field of limited freedom, the effect of the individual Gaussian points in one element is of a parallel nature and is not serial. Only an element, in which all integration points have been cracked, has the possibility of stressless deformation, but even when all integration points of the element are cracked, while the crack direction is not exactly the same in these points, the element has still a residual stiffness. This results in an over-estimation of the failure load and a much larger crack zone at failure than in reality. In a model with an assumed stress field such problems do not arise. The strain field is now free to develop and even can reach an infinite value at a crack. Because of the use of the constitutive law in a flexibility form, the stiffnesses are chained serially.

Then it is possible to develop a single sharp crack and a more correct failure mechanism is awaited for.

4.3. Convergence and crack propagation

Cracks tend to come in being abruptly, but in the MICRO/1 program crack displacements only can grow gradually. This has been reached by introducing a fictitious visco-plastic model for the behaviour of the crack layer. The convergence of this model does not only depend on the fictitious time integration procedure but also on the validity of the assumption that the unbalanced stresses in the crack will decline when the crack displacements are altered. From a physical point of view this seems obvious, but this will certainly not be the case for all finite element models. The best guarantee to get convergence is an accurate description of the internal crack displacements, as is the case in the MICRO/1 program.

When increasing the load on the structure, cracks may whether or not propagate. In fact one needs a proper criterion to decide on this matter. In each loading step one must correctly predict whether a new crack will come into being, or an existing crack will propagate, or maybe both at the same time. No doubt the real stress state around a crack tip shows a singularity with high stress peaks. One can choose for a suited energy criterion as is done for crack propagation in metals. Bažant has proposed such an approach in the framework of smeared out cracks. Until now the authors used a much simpler criterion. The stress field at the tip of a crack is not adapted. Instead, to account for the stress singularity, the allowable tensile stress is lowered down 20 percent in uncracked elements which are positioned at a crack tip. It has been found in this way that a good balance exists between the propagation of existing cracks and the origin of new ones.

REFERENCES

1. BAŽANT, Z.D.: Advances in Deformation and Failure Models for Concrete. Introductory Report IABSE Colloquium on Advanced Mechanics of Reinforced Concrete, Delft 1981.

2. GIJSBERS, F.B.J.: Experimental Investigation with regard to shear capacity of reinforced concrete beams with a rectangular cross-section. Report TNO-IBBC: BI-77-17/04.1.01252, Rijswijk (Z.H.), 1977 (in Dutch).

3. FRAEIJS DE VEUBEKE, B.: Displacement and Equilibrium Models in the Finite Element Method. Stress Analysis, John Wiley, London 1965.

4. PIAN, T.H.H.: Derivation of element stiffness matrices by assumed stress distributions. AIAA Journal, Vol. 2, pp. 1333-1336, 1964.

5. BLAAUWENDRAAD, J.: Formalism and Insight in Mechanics Models. Doctoral Thesis, Delft 1973 (in Dutch).

6. GROOTENBOER, H.J.: Finite element analysis of two-dimensional reinforced concrete structures, taking account of nonlinear physical behaviour and the development of discrete cracks. Doctoral Thesis, Delft University Press, 1979.

7. GROOTENBOER, H.J.; LEIJTEN, S.F.C.H.; BLAAUWENDRAAD, J.: Concrete Mechanics, Numerical models for reinforced concrete structures in plane stress. Heron, no. 1c, 1981.

Non-Linear Finite Element Strategies for Bridge Slabs

Stratégies pour l'analyse non-linéaire des dalles de pont à l'aide d'éléments finis

Nichtlineare Finite-Elemente-Strategien für Brückenplatten

R. J. COPE
Senior Lecturer

P. V. RAO
Research Fellow

Department of Civil Engineering, Liverpool University,
Liverpool, England.

SUMMARY
Bridge slabs have to carry repeated applications of heavy concentrated loading. Simple modelling strategies for realistic post-cracking analysis are presented with results from two element formulations. Acceleration techniques and criteria for establishing convergence are discussed.

RÉSUMÉ
Les dalles de pont doivent subir des applications réitérées de charges lourdes et concentrées. Ce rapport présente des stratégies simples qui mettent en modèle avec réalisme le comportement après fissuration et donne des résultats de deux configurations d'éléments. On discute les techniques d'accélération et les critères pour établir la convergence.

ZUSAMMENFASSUNG
Brückenplatten müssen wiederholte schwere und konzentrierte Lasten tragen. Über einfache Strategien, die das Verhalten im gerissenen Zustand realistisch modellieren, wird, zusammen mit Ergebnissen von zwei Elementenformulierungen, berichtet. Beschleunigungsmethoden und Konvergenzkriterien werden besprochen.

1. INTRODUCTION

The recent introduction of a limit state based design code in the U.K. [1] gives bridge engineers a choice in selection of analytical procedures. Use of non-linear methods would allow advantage to be taken of moment redistribution and 'membrane' action, but for such methods to become acceptable, they would have to be reliable and efficient. Non-linear finite element procedures show promise for a wide range of complex structural forms, not only as a primary analytical tool, but also for arriving at empirical design formulae.

High computing costs, specialised and sometimes subjective analytical techniques, at present associated with some finite element methods, are not appealing features. The expense of computing can be, to some extent, eased by selection of simple material models. However, modelling of the composite material has not advanced sufficiently for general section/element level force-displacement characteristics to be specified. The behaviour of the composite has to be built up from those of its constituents.

Non-linear analysis is performed by incremental, iterative procedures. By using acceleration schemes to expedite convergence, considerable savings can be made in computing costs. However, for objectivity of analysis, well behaved formulations have to be used and indices established to monitor convergence and degradation of stiffnesses. It is essential that analytical response is not distorted by the numerical procedure employed.

In this paper, finite element methods for bridge slab design are considered. Material models are described for predicting detailed load history and for use in design. Suitable indices for monitoring behaviour are established and a study of the BFGS acceleration procedure to reduce the number of iterations is reported. Unless stated otherwise, the analytical results presented were obtained using the Irons-Razzaque [2] general quadrilateral element. This is a non-conforming displacement model using numerical integration at 4 Gauss stations in plan and 5 integration stations through the depth [3]. Transverse shear strains are set to zero at the Gauss stations.

2. MATERIAL BEHAVIOUR MODELLING

Perfect bond is assumed between concrete and steel so a continuous strain field results over each element. Individual cracks are not represented, but 'smeared' over an area governed by the finite element mesh size. Flexural and in-plane stiffness components are obtained by superimposing concrete and steel effects. Concrete moduli are determined at the three-dimensional grid of integration stations. Steel reinforcement is represented by its axial stiffness in the correct direction and at the correct depth at the nearest Gauss station.

2.1 Concrete

Unstressed concrete is assumed to be isotropic. Although several multi-axial stress-strain relationships have been proposed for plain concrete, uniaxial values have been used. This is primarily because variations induced by fabrication and the limited accuracy of testing procedures, especially when prototype structures are concerned, make it difficult to justify a higher level of sophistication. A wide range of studies of slabs has shown that behaviour is relatively insensitive to the compressive stress-strain relationship used.

In the authors' approach, effective direct strains in the current principal strain directions are determined from:

$$\varepsilon_1^* = \frac{1}{1 - \upsilon^2} (\varepsilon_1 + \upsilon \varepsilon_2) \quad \text{and} \quad \varepsilon_2^* = \frac{1}{1 - \upsilon^2} (\upsilon \varepsilon_2 + \varepsilon_1) \qquad (1)$$

where $\varepsilon_{1,2}$ are the current principal strains and υ is Poisson's Ratio, which is assumed constant until cracking or crushing occurs, when it is set to zero. Compressive stresses are determined using a relationship proposed by Popovics, together with a plateau of constant strain between peak stress and a strain of 0.0035 [4]. Beyond that strain level, the stress drops to zero.

2.2 Composite Action

Most of the difficulties in simulating slab behaviour stem from the way reinforced concrete loses its tensile strength after cracking. In tension, a linear stress-strain relationship with a descending branch to simulate tension stiffening has been used with some success [4]. Much of the data on tension stiffening is based on studies of one-way bending, and the authors' tensile 'stress'-strain curve was designed to give good predictions of behaviour for a range of steel percentages [3]. The effectiveness of the model with cracks inclined to reinforcement cannot be gauged with confidence, because of the limited amount of experimental data available. Gilbert and Warner [5] have developed a tension stiffening model based on modifications to the stiffness of reinforcement. At the present time, there is a lack of generality in this approach and more work needs to be done to provide a basis for selection.

To follow repeated load application, an unloading curve parallel to the initial tangent has been found to give reasonable results [6]. However, for slabs that have been subjected to an unknown load history prior to analysis, best results are given when tension stiffening is ignored [6].

Two types of material model have been used. In the first, effective strains are determined in the current principal strain directions as described above. The effective stresses in these directions are obtained from the uniaxial relationship [4], and then resolved into Cartesian components for evaluation of mobilised internal resisting forces. With this approach, shear stress-strain is not modelled explicitly. Crack directions are only notional and they 'swing' in step with the current strain field.

In the second approach, material property axes are fixed in the prevailing principal strain directions at the end of iterations for the load increment in which cracking first occurs. The above uniaxial relationships are used in these directions, together with a constant in-plane shear modulus. Under subsequent loading, the principal strain directions can be significantly different to the directions of the material property axes. As a result, use of stress determination in fixed material property directions can result in poor predictions of behaviour, and the authors have used a strategy to rotate material property axes when intersecting crack patterns are present [4].

The changes in direction of principal values can be caused by a different load arrangement or can be due to internal redistribution of resisting forces. An indication of the magnitudes of swing in principal directions for a model skew slab bridge subjected to highway type loading can be seen in Table 1. Details of experimental and analytical studies of the slab, which was numbered 1A, are given in [6, 8]. The slab had a realistic steel arrangement with bars placed parallel and normal to the simply supported edges. The results presented are for a uniformly distributed loading equivalent to 1.2 times the self weight, and for monotonically increasing increments of 20kN. applied to a bogie of the design vehicle positioned as indicated in Fig. 1.

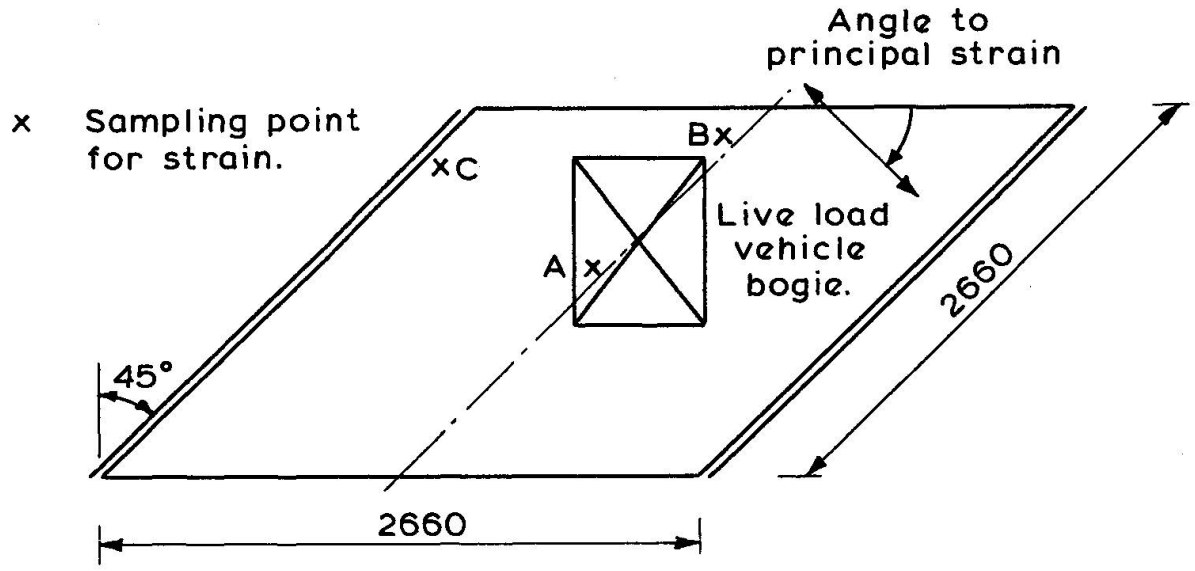

Fig. 1 Model Skew Slab

It can be seen that the principal strains are predicted to rotate considerably by the varying 'crack' direction method, whereas fixing the material property axes limits the rotation. The principal moments were obtained by integrating stresses through the depth at the Gauss stations and linearly interpolating to nodal points. Rotations of principal moments are less than those for strains, due to the influence of the reinforcement, and prior to yielding of steel there is a greater degree of agreement in their prediction. The large differences in principal angles for moments at C' and strains at C is due to the rapidly varying strain field in the obtuse corner.

Load	Linear Strain			Varying Crack Direction						Fixed Crack Direction					
				Strain			Moment			Strain			Moment		
	A	B	C	A	B	C	A'	B'	C'	A	B	C	A'	B'	C'
1.2xSelf Weight	38	20	72	37	19	73	40	27	112	37	19	73	40	27	112
+ 20kN.	35	15	79	33	11	88	44	36	115	34	16	89	44	32	111
+ 40kN.	34	13	81	29	7	89	46	34	114	34	15	90	46	28	109
+ 60kN.	33	12	82	28	2	90	44	33	107	34	14	90	42	24	104
+ 80kN.	32	12	82	28	1	92	44	32	112	33	14	91	42	20	107
+ 100kN.	32	11	83	22	- 1	93	43	29	108	32	14	91	39	20	109
+ 120kN.	31	11	83	21	- 4	94	43	28	108	32	14	91	39	19	103
+ 140kN	31	11	83	20	- 5	96	43	25	101	32	15	91	37	19	103
+ 150kN.	31	11	83	22	- 9	96	42	30	103	32	15	91	36	17	100
+ 160kN.	31	11	83	16	- 9	95	42	35	103	32	15	91	35	16	97
+ 170kN.	31	11	83	17	- 7	95	41	33	112	33	15	91	34	14	100

Table 1 Inclination of Principal Strain and Moment

Bazant [7] has commented on the inadmissibility of using orthotropic models because of their lack of directional invariance. He suggests that such models are reasonable when principal stresses do not rotate. The authors have found

that the 'varying crack direction' model gives the better overall comparison with experimental results [6, 8], and is satisfactory for design or assessment purposes.

3. MONITORING INDICES

Ideally, measurements of both equilibrium and displacement convergence are needed to terminate the iterative procedure at a given level of loading. Measures in common use depend on the differences between applied and mobilised resisting forces and iterative displacement vectors. Some of the norms presented in recent literature [3, 9, 10, 11] are examined to assess their suitability for use in analyses of concrete slabs.

For illustration, results from analyses of a reinforced concrete skewed slab (slab 2B of [6]) are discussed. The slab used is a one-fifth scale model and contains a realistic distribution of reinforcement. It is the most flexible of the slabs studied and thus presents the severest test for non-linear procedures. The analyses were performed using a 6x6 mesh [6], with a constant stiffness matrix, and no tension stiffening allowance for the concrete. Response values at four load levels with the design vehicle positioned as shown in Fig. 1, are presented for discussion. These cover response of the slab prior to yielding of the reinforcement.

3.1 Force and Displacement Norms

The authors have used two norms with consistent results [3]. A norm of out-of-balance loads in any direction (j) as defined by:

$$R_j = \frac{100 \times \sqrt{\Sigma (P_i - F_i)^2}}{\sqrt{\Sigma P_i^2}} \qquad (2)$$

where P_i is an applied nodal load, F_i is the corresponding internally mobilised force and the summations are taken over the global degrees of freedom in direction j. When there is no applied loading in a particular direction the denominator in (2) is set arbitrarily to 100, thus reducing R_j to a Euclidean norm. In this case it is not used to automatically control the number of iterations.

A norm of iterative displacements is defined as:

$$D_j = 100 \frac{(d_{j,max} - d_j)}{(d_{j,max})} \qquad (3)$$

where d_j is the Euclidean norm of the total displacement in direction j in the current iteration, and $d_{j,max}$ is the maximum d_j from previous iterations at the current load level. Experience has shown that satisfactory results are obtained when both norms are small in the transverse direction, but after yielding of reinforcement the number of iterations has to be limited when one of them is small.

Values of maximum displacement are compared in Fig. 2. The iterations at each load level were stopped when equilibrium and displacement norms of $R_3 = 2\%$ and $D_3 = 0.02\%$ were satisfied. There was some cracking on application of self weight, and although there was relatively little change in displacement, 31 iterations were needed to satisfy the equilibrium norm. This was due partly to

the unsymmetrical distribution of reinforcement about the slab's median plane. The addition of 20kN, via the idealised design vehicle, caused considerable cracking of concrete as evidenced by the big rise in deflection. 109 iterations were needed to satisfy the equilibrium norm. 72 iterations were needed for the next load increment of 20kN. With 60kN applied to the vehicle, a few bars behaved non-linearly and a maximum of 500 iterations were performed. At this stage, there was a 10% out-of-balance of equilibrium as measured by the norm R_3 and some of the implications of this are discussed below.

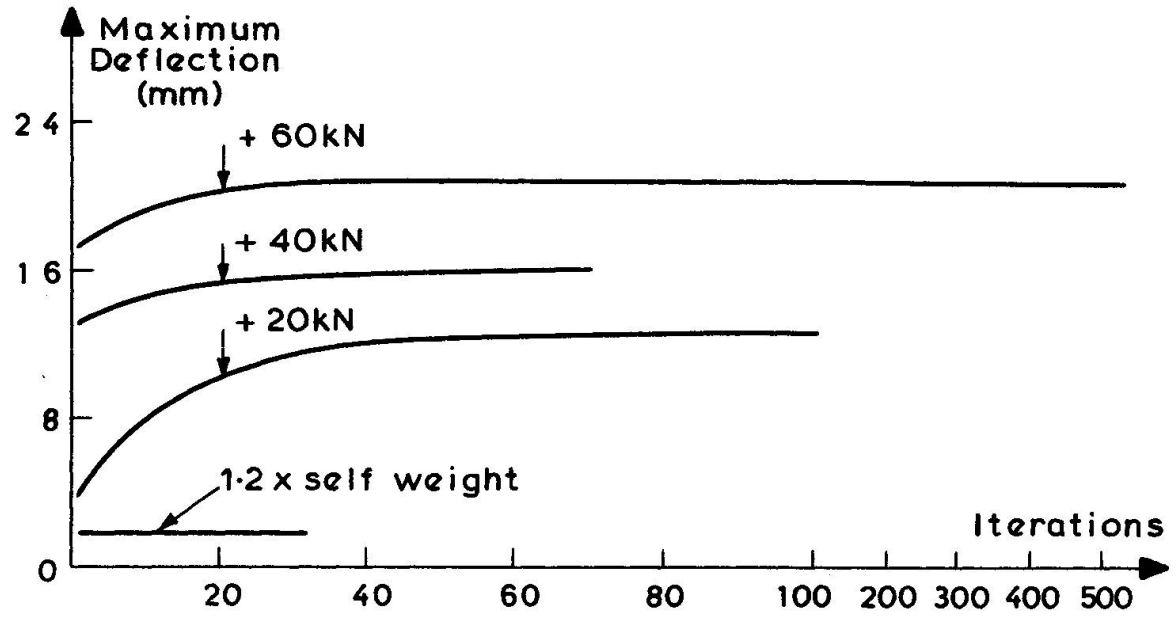

Fig. 2 Variation of Maximum Deflection

These results are typical for skew slabs, although the most flexible of the steel arrangements studied was selected to give the severest test of the procedure. At these load intensities, the biggest release of energy is in the first iteration. The rate of displacement convergence is very small after about 30 iterations and slabs reach an approximately steady state without equilibrium norms being satisfied.

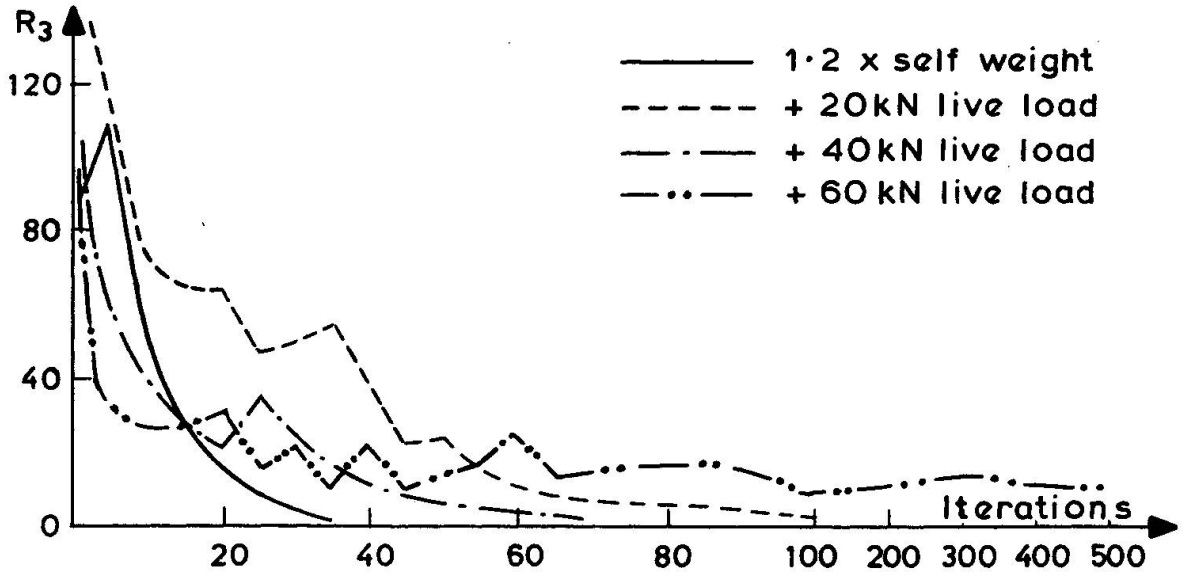

Fig. 3 Variation of R_3

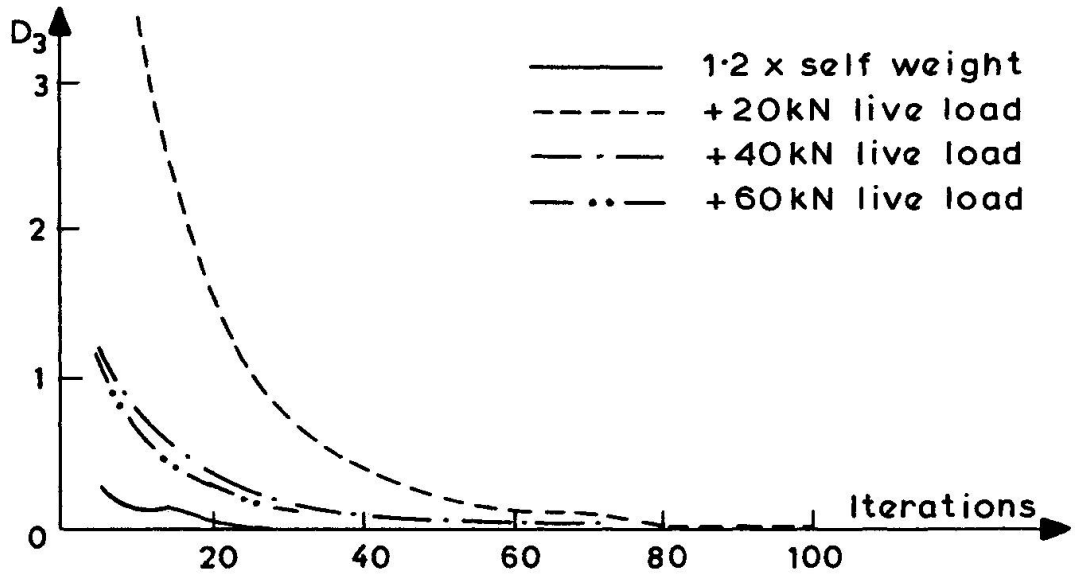

Fig. 4 Variation of D_3

The variations of the norms in the transverse direction (j = 3) are shown in Figs. 3 and 4. The high levels of R_3, at the start of iterations, indicates that most of the 'cracking' occurs on load application with substantial release of energy. At vehicle loads of 20kN and 40kN, although R_3 fluctuates, it ultimately reaches a small value. However, at 60kN, and for higher load increments, the norm R_3 tends to stabilise at a certain level, about 10% in this instance.

Examination of the force norms in other directions shows that they are still large, even when the transverse force norm R_3 has become small. Bergan and Holland [12] have noted that unbalanced loads can form self-equilibrating groups, with little influence on overall response, and a study of beams [8] has shown that the relative magnitudes of axial and couple norms are governed by the chosen shape functions. It thus seems unlikely that force norms will always converge to zero, even when a large number of iterations are performed. Bathe and Cimento [10] have observed that the modified Newton-Raphson procedure can diverge when out-of-balance forces increase during iterations.

As engineers are accustomed to relying on equilibrium checks, non-convergence of R_3 to zero is disquieting. However, engineers use linear harmonic analysis with confidence, and when a finite number of harmonics are used, there are sets of spurious self-equilibrating forces present and non-satisfaction of equilibrium norms. The analogy is a loose one, but as analytical results give satisfactory agreement with experimental values [6, 8] there is perhaps no cause for undue concern. Analyses of a wide range of slabs, in which out-of-balance forces fluctuated, gave acceptable results, and to the authors' knowledge, no divergent solution has been reported in the literature.

The transverse displacement norm D_3, which measures the rate of convergence, rather than absolute convergence, is shown in Fig. 4. Behaviour is less fluctuating with values approaching zero asymptotically.

3.2 Scaled Force and Displacement Norms

Chrisfield has recommended use of scaled norms [9] for terminating iterations. His norms are:

$$\bar{R}_j = \frac{\sqrt{\Sigma\ (\bar{P}_i - \bar{F}_i)^2}}{\text{Max}\left(\sqrt{\Sigma\ \bar{P}_i^{\,2}}, \sqrt{\Sigma\ \bar{r}_i^{\,2}}\right)} \tag{4}$$

and

$$\bar{D}_j = \frac{\sqrt{\Sigma\ \bar{\delta}_i^{\,2}}}{\sqrt{\Sigma\ \bar{U}_i^{\,2}}} \tag{5}$$

where $\bar{P}_i = P_i/\sqrt{K_{ii}}$ is the component of the nodal load in the j-direction, scaled by the reciprocal of the square root of the corresponding diagonal tangential stiffness coefficient at the beginning of the increment. The corresponding internally mobilised force F_i is scaled to give $\bar{F}_i$, and the $\bar{r}_i$ are similarly scaled reaction components at supported nodes. The displacement norm is obtained from $\bar{U}_i = \sqrt{K_{ii}}.U_i$ and $\bar{\delta}_i = \sqrt{K_{ii}}.\delta_i$, where U_i is the total accumulated displacement and δ_i is the displacement component obtained from the iteration. Analyses using limits of 10^{-4} on $\bar{R}_j$ and $\bar{D}_j$ to terminate iterations are referenced in [9].

Values of $\bar{R}_j$ and $\bar{D}_j$ for the analyses described in 3.1 are shown in Figs. 5, 6. On the whole, their behaviour is similar to that of the norms proposed by the authors. Similar fluctuations exist and there seems to be no advantage to compensate for the additional computing costs necessary to determine these norms. It should be stated that the tangential stiffness coefficients were determined using an arbitrary, small, positive value for concrete modulus at cracked integration stations. For the comparisons shown, a value of 0.05 times the uncracked concrete modulus was used.

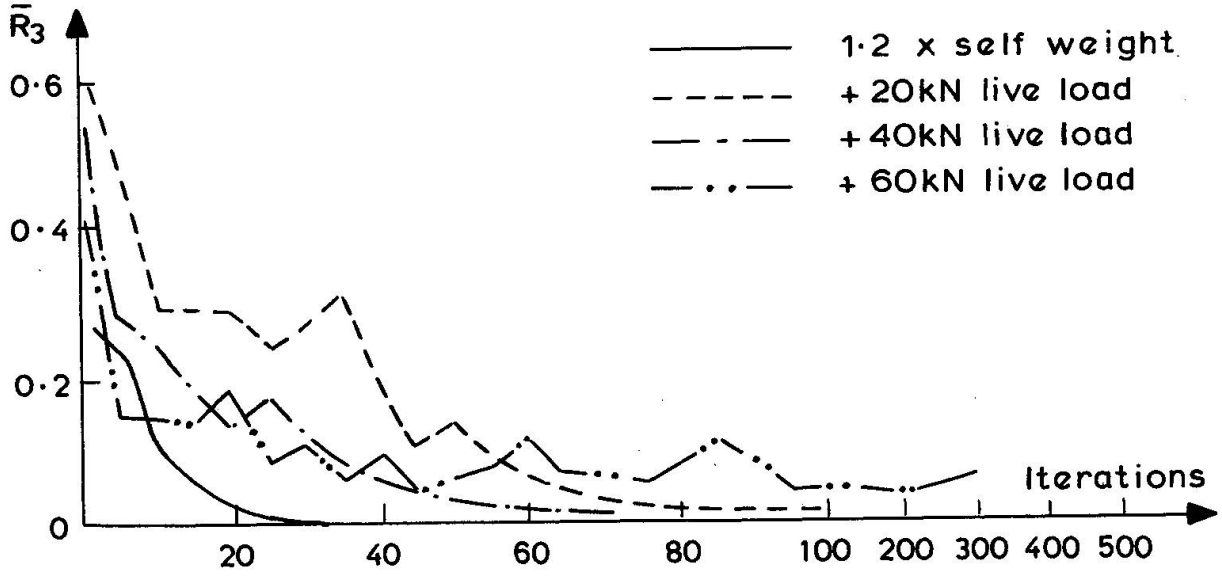

Fig. 5 Variation of $\bar{R}_3$

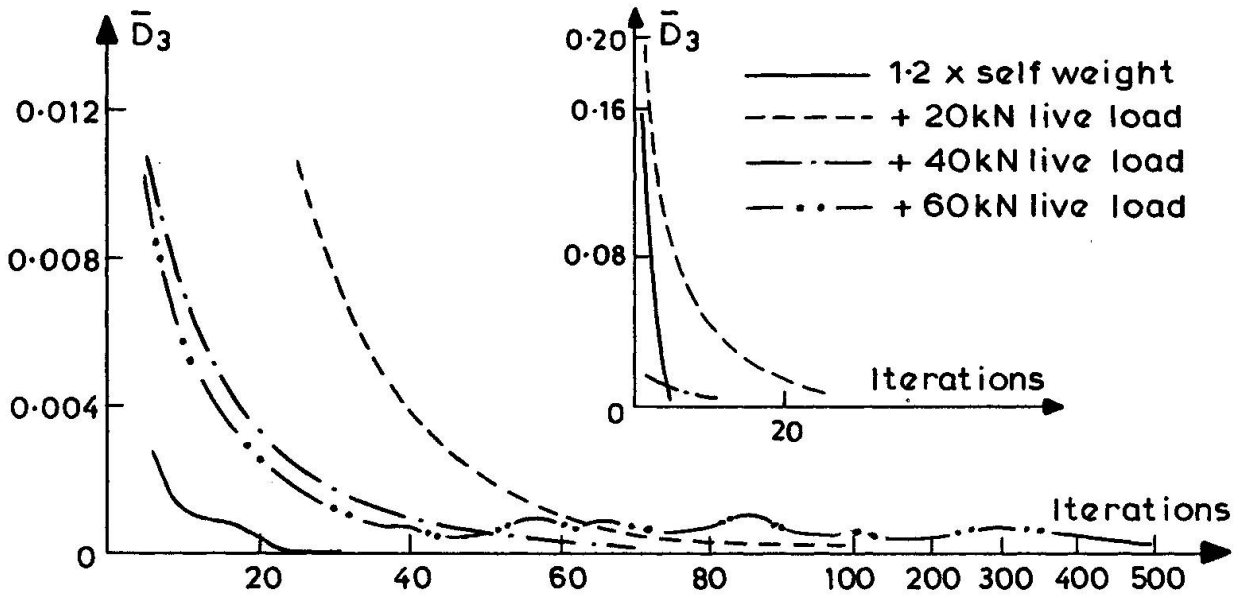

Fig. 6 Variation of $\bar{D}_3$

3.3 Energy Norms

Since both force and displacement monitoring is important, Bathe and Cimento [10] have recommended use of energy norms. The energy released during an iteration equals the work done, W, by the out-of-balance loads moving through the corresponding iterative displacements, thus:

$$W = \sum_j \sum_i (P_i - F_i).\delta_i \qquad (6)$$

Values of W with iterations, for the analyses described in 3.1, are given in Table 2. It is clear from these results that most of the energy release, prior to yielding of reinforcement, occurs during the first few iterations. This is consistent with other reported observations [3, 13].

Iteration	1	5	10	20	30	40	50	70	100	500
1.2 x Self Weight	2250	60	20	1	-	-	-	-	-	-
+ 20kN.	24000	15000	7500	2050	730	310	125	15	2	-
+ 40kN.	107000	2250	1200	300	210	60	20	2	-	-
+ 60kN.	8250	2250	1100	660	400	170	225	140	120	125

Table 2 Values of W with Iterations

The feasibility of using the ratio of energy released during an iteration to the maximum energy released in a previous iteration of that particular load increment has been studied [8]. A value varying between 0.01 and 0.025 gives acceptable results for the mesh size examined. The smaller value is used for the initial stages of intense cracking. Using such a norm results in solutions similar to those obtained using a limit of about 30 iterations, which is consistent with the results of 3.1.

3.4 Structural Integrity

To check structural integrity, strains can be monitored to assess crack widths, possible loss of ductility and extent of yielding. By studying the material damage predictions for a particular class of structure, experience can be gained and used as guides for designers. Since a numerical technique is being employed for analysis, a numerical measure is needed for any automated decision making.

Bergan [14] has advocated use of a current stiffness parameter, which attempts to express the stiffness at the current load level in terms of the initial linear stiffness. This parameter depends on the incremental load and displacement values. For the slab analysed above, it has the values 0.72, 0.09, 0.25 and 0.21 at 1.2 x self weight, and with live loads of 20kN, 40kN and 60kN, respectively, and the value 0.01 close to failure. Because the rate of stiffness degradation in concrete slabs is not uniform and decreases after first cracking, the parameter does not decrease monotonically. Also, before a single parameter could be used with confidence, experience is needed to see how it is affected by local as opposed to global failure.

An alternative indicator that could be used is the amount of energy being released due to structural damage, W. If the work done by the out-of-balance forces due to iterative displacements does not diminish or grows, there is a clear indication that the structure, or part of it, cannot sustain the applied loading.

4. ACCELERATION OF CONVERGENCE

From a study of numerical acceleration schemes [3,8], the recently implemented BFGS procedure [15] has been selected as the most efficient one available. Bathe and Cimento [10] have published results from studies of reinforced concrete beam behaviour and here, some of the effects of using the procedure to analyse slabs are presented. All of the numerical work reported was performed on a CDC 7600 computer using a constant stiffness matrix based on unstressed material properties.

4.1 Parameters STOL and CONDMAX

The two parameters of prime concern to users of the BFGS procedure are STOL and CONDMAX. STOL governs the number of line searches and iterations, and is set to a value between 0 and 1. It has been reported that as the value increases towards unity, although the number of line searches decreases, the number of iterations needed increases [15]. Analyses using STOL = 0.1 and 0.5 are presented. The decision to select a new search direction is taken by comparing the quadratic form of the stiffness matrix, with respect to the iterative displacement vector, with its previous value. This number is estimated and compared with the value of CONDMAX. It has been recommended that CONDMAX = 10^5, [15], leads to stable solutions. Here, results are presented for CONDMAX equal to 10^5 and 10^{10}.

4.2 Comparison of Solutions

Analysis of skew slab 2B of [8], with no tension stiffening, should provide a severe test of the method as it is the most flexible of the designs studied. Table 3 shows values of central deflection predicted and the numbers of iterations necessary to satisfy the prescribed norms. These were R_3 = 2% and D_3 = 0.02% for all analyses, with a maximum of 80 iterations performed in a load increment for an accelerated solution and 300 iterations for the solution without

acceleration. It can be seen that the use of the BFGS acceleration scheme reduced the number of iterations necessary to reach an equilibrium state, but for the two cases marked with an asterisk the procedure has converged to the wrong position. However, even in these two instances of unacceptable predictions, the procedure 'corrects' itself at higher load levels. This desirable feature occurs because internal forces are equilibrated to the total applied load.

Load	Without Acceleration	STOL = 0.1		STOL = 0.5	
		CONDMAX=10^5	CONDMAX=10^{10}	CONDMAX=10^5	CONDMAX=10^{10}
1.2xSelf Wt	1.3/ 31	1.3/13	6.3*/36	5.3*/34	1.3/ 9
+ 20kN	8.8/109	9.0/51	8.7 /29	8.5 /32	9.0/29
+40kN	11.4/ 72	11.5/27	11.5 /20	11.5 /30	11.5/25
+60kN	14.1/300	13.8/80	14.0 /80	13.9 /80	13.9/80

Table 3 Central Deflection/Number of Iterations

Further analyses to examine predicted response up to 20kN of live load are given in Table 4. In the analysis with no acceleration, the maximum energy release occurred during the sixth iteration of the 5kN load increment. From these results it is clear that considerable cracking occurs almost immediately and that the state of the slab at 1.2 times self weight is almost unstable. These results show that caution should be used if prediction of response during the initial phase of extensive cracking is required, but for most purposes there does not appear to be a serious problem.

Load	Without Acceleration	CONDMAX = 10^{10}	
		STOL = 0.5	STOL = 0.1
1.2 x Self Weight	1.33/ 31	1.31/ 9	6.26/36
+ 5kN	6.66/129	6.87/57	6.64/23
+ 10kN	7.14/ 53	7.30/19	7.30/16
+ 15kN	7.98/118	8.03/30	7.96/14
+ 20kN	8.70/ 64	8.68/14	8.69/20

Table 4 Central Deflection/Number of Iterations

A more detailed comparison of the predictions is given by examining the principal strains at the Gauss stations closest to the centre line. These are given in Table 5. In addition to the strains at 5kN increments values are presented for a single increment of 20kN. It can be seen that the results are in line with those for displacements. All of the predictions for the live load of 20kN lie within the accuracy that can be obtained from experiment [6] and there is no evidence to support preference for any particular set of values.

For further assessment of the overall influence of solutions following different load paths, the reactions under 1.2 times the self weight, plus a live load of 60kN, are given in Table 6.

It is clear from these results that convergence is not to a unique solution, but that there is an acceptable degree of agreement for design purposes. To examine the effects of limiting the number of iterations and of changing the size of the load increment to reduce costs of computation, further analyses were performed.

Load	Without Acceleration					
1.2 x Self Weight	173	181	186	184	167	154
+ 5kN	1315	1340	1387	1344	1291	1272
+ 10kN	1333	1409	1438	1397	1303	1308
+ 15kN	1498	1579	1568	1502	1383	1352
+ 20kN	1646	1736	1703	1615	1446	1427
+ 20kN direct	1798	1807	1756	1680	1560	1511
Load	STOL = 0.5 CONDMAX = 10^{10}					
1.2 x Self Weight	173	180	186	183	167	154
+ 5kN	1305	1351	1381	1349	1296	1285
+ 10kN	1328	1412	1454	1406	1292	1278
+ 15kN	1496	1566	1583	1509	1365	1335
+ 20kN	1617	1712	1719	1620	1460	1430
+ 20kN direct	1800	1789	1825	1650	1568	1521
Load	STOL = 0.1 CONDMAX = 10^{10}					
1.2 x Self Weight	1247	1227	1246	1248	1212	1159
+ 5kN	1201	1269	1318	1301	1203	1199
+ 10kN	1337	1415	1450	1409	1287	1284
+ 15kN	1478	1561	1592	1509	1372	1367
+ 20kN	1628	1717	1715	1623	1442	1426
+ 20kN direct	1626	1721	1711	1621	1435	1414

Table 5 Midspan Principal Strains

Without Acceleration	STOL = 0.1		STOL = 0.5	
	CONDMAX=10^5	CONDMAX=10^{10}	CONDMAX=10^5	CONDMAX=10^{10}
38.0	39.5	40.5	39.2	39.8
7.1	4.2	3.5	6.5	5.1
7.6	9.1	8.3	8.0	7.9
4.9	4.5	5.7	4.3	4.7
7.1	7.3	6.1	7.4	7.5
-0.2	-0.2	0.5	-0.4	-0.2

Table 6 Reactions at 1.2 x Self Weight + 60kN

In Table 7, values of central deflection are compared for 20kN load increments. The analysis using constant stiffness was conducted with norms of R_3 = 2% and D_3 = 0.05%, but with a limit of 300 iterations in any load increment. This latter criterion governed for the 60kN and subsequent increments. The accelerated analyses used STOL = 0.5 and CONDMAX = 10^{10}. Norms of R_3 = 2% and D_3 = 0.05% were set for these analyses, but with the maximum number of iterations in an increment as specified in the Table. Two further analyses were performed without acceleration and these were controlled by the energy norm. Iterations were stopped when the ratio of the energy norms W, (see Eqn. 6) reach 0.01 and 0.02, respectively.

Load	Without Acceleration	BFGS with Maximum Iterations			Without Acceleration Energy Control	
		10	40	150	0.02	0.01
1.2 x Self Wt	1.3	1.3	1.3	1.3	1.3	1.3
+ 20kN	8.8	8.8	9.0	9.0	8.2	8.5
+ 40kN	11.4	11.5	11.5	11.5	10.1	10.6
+ 60kN	14.1	13.9	13.9	13.9	13.7	13.9
+ 80kN	17.2	16.8	17.1	17.1	16.5	17.0
+ 100kN	21.4	21.3	21.5	21.5	20.9	21.0
+ 120kN	30.9	30.6	31.0	31.1	26.6	28.7
+ 140kN	48.2	45.9	49.3	49.2	45.0	47.0
+ 150kN	59.4		60.3	60.4		
+ 160kN	82.4		71.4			

Table 7 Central Displacement

Prior to extensive yielding of reinforcement, the BFGS solution using only 10 iterations per increment is acceptable. Results obtained using 40 and 150 iterations are virtually identical. After about 30 iterations the scaling factors from the line search procedure become very small and it appears that for most problems, with a constant stiffness approach, a maximum of 10 to 15 iterations per load increment should be adequate. No value is given for the BFGS solution with 150 iteration control at 160kN, as the allowable computer time had expired. At the stages of initial cracking, the analysis using the smaller energy ratio to control iterations is acceptable, and for high load levels both analyses gave similar results.

4.3 Cost of Solutions

Costs of solutions are compared in Table 8. The values given are based on computer mill time used. At 40kN, which corresponds approximately with the serviceability load level, the BFGS solution, with a limit of 10 iterations, costs only a quarter of the effort necessary for an analysis without acceleration. However, neither it, nor the solution using the energy norm, satisfied the limits set on the force and displacement norms. From the results given in Table 3, it can be seen that the BFGS solution, with a limit of 40 iterations, satisfied those norms, and that analysis halved the time of solution.

Load	Without Acceleration	BFGS Max Iterations		Without Acceleration
		10	40	0.01
1.2 x Self Weight	11.7	5.4	5.4	3.7
+ 20kN	53.8	12.4	24.0	21.5
+ 40kN	81.9	18.8	39.7	28.2
+ 60kN	196.9	25.1	74.9	53.4
+ 80kN	311.8	31.6	104.0	82.0
+ 100kN	426.7	37.9	135.8	115.6
+ 120kN	541.9	45.0	164.0	191.7
+ 140kN	657.1	51.3	189.6	268.0

Table 8 Cost Comparison

At higher load levels, none of the solutions satisfied the limits set on the norms, but the results from the analysis without acceleration and the solution using acceleration with the 40 iteration limit are similar. When the live load is at 80kN the cost of the accelerated solution is a third of that for the analysis without acceleration. This factor reduces slowly with increasing load level to approximately 0.3 at 140kN. But as even these analyses are expensive and results obtained with 10-15 iterations are reasonable those limits can be used for most purposes.

4.4 Size of Load Increment

A further way of reducing the costs of computation is to reduce the number of intermediate load increments. From the results given in Tables 4 and 5, it appears that deflections and strains in concrete slabs are relatively insensitive to the size of load increment. To assess the effect of load increment size, results of a number of analyses are compared in Table 9.

Load	Without Acceleration		BFGS	BFGS	BFGS
	(20kN)	(40kN)	(5kN)	(20kN)	(40kN)
1.2 x Self Wt	1.3	1.3	1.3	1.3	1.3
+ 20kN	8.8	-	8.7	8.8	-
+ 40kN	11.4	11.7	11.4	11.5	11.9
+ 60kN	14.1	-	13.9	13.9	-
+ 80kN	17.2	17.3	17.0	16.8	17.1
+ 100kN	21.4	-	21.5	21.3	-
+ 120kN	30.9	29.2	30.9	30.6	29.9
+ 140kN	48.2	47.5		46.0	46.5

Table 9 Central Displacement with Load Increment

To form a basis for comparison, the central displacements predicted by the analysis without acceleration, and with up to 300 iterations, are recorded. Results of three analyses from the BFGS solution with STOL = 0.5, CONDMAX = 10^{10}, and with a limit of 10 iterations per increment are presented. It can be seen that very similar predictions are obtained from all of the analyses. A comparison of strains and principal directions at mid-span has been made [8] which confirms that use of large load steps does not distort the response. This suggests that an engineer interested in effects at a particular load level could obtain those results with quite coarse load increments.

5. SHEAR

All of the skew slabs tested in an accompanying programme of experimental tests [6,8] showed severe inclined cracking in the obtuse corner region at high load levels. The plate element formulations used for the analyses reported above sets transverse shear strain to zero and hence cannot model this behaviour.

5.1 Heterosis Formulation

A study has been initiated to investigate the use of the Mindlin plate bending theory which accounts for shear strains. The 'heterosis' element [16] appears to be the best formulation and it has been implemented in its hierarchical form. 3x3 Gauss integration in plan has been used for both flexure and in-plane

effects. Material moduli are thus set on a 3x3x5 grid of sampling stations, in contrast to the more economical 2x2x5 grid used for the previous solutions. 2x2 integration stations are used for transverse shear, but for the preliminary results presented here, the rigidity modulus of concrete has been kept constant.

Analysis	Load							
	1.2xSelf Wt	+20kN	+40kN	+60kN	+80kN	+100kN	+120kN	+140kN
Previous	1.9	12.7	16.2	21.1	28.6	40.0	62.7	96.6
Heterosis	7.9	11.6	16.8	21.6	29.3	39.9	59.3	99.1
ER = 0.01	7.6/51	10.0/11	16.4/36	21.3/41	28.8/51	38.5/51	57.4/131	98.8/241
ER = 0.02	7.5/46	9.5/ 6	16.2/26	21.2/36	28.6/46	37.6/36	54.8/76	97.4/211

Table 10 Maximum Displacement Comparison

In Table 10 values of maximum displacement for skew slab 2B are compared with results from the previous analysis. Because of the sensitivity of this particular slab to perturbations under self weight, the change in shape functions has triggered off additional cracking. However, at later load levels, the response is similar to that obtained from the previous analysis.

The work done by the out-of-balance loads is computed using only in-plane and rotational displacements, since with a constant shear modulus this formulation does not produce any transverse out-of-balance forces. The norm R_3 cannot, therefore, be used to monitor convergence. To assess the possibility of using the energy norm W to control the number of iterations, values are also presented for energy ratios, ER, of 0.01 and 0.02 (ER = energy released in current iteration divided by maximum released energy in an iteration of the load increment). The number of iterations is also presented as a guide to the relative costs of these analyses.

6. CONCLUSIONS

Application of non-linear numerical techniques to concrete structures is complicated by the lack of uniformity in stiffness degradation and by the different load-unload paths. These features make it particularly difficult to specify norms to automatically control the number of iterations to be performed. It is clear from the results of this study that no single, unambiguous and precise measure exists, and that judgement is needed to assess the results of non-linear analyses of concrete slabs.

For design of slabs, a uniaxial stress-strain relationship can be used for concrete and tension stiffening effects need not be simulated. Analyses in which orthotropic material property axes are not fixed in directions dictated by initial cracking give better comparisons with experimental results than those in which 'crack' directions are fixed. Acceptable results can be obtained using the BFGS acceleration procedure and relatively coarse load increments to reduce the cost of analysis.

In skew slabs there is a need to implement formulations which do not employ Kirchhoff's restraints. The heterosis finite element formulation of the Mindlin plate theory promises to be a suitable approach and further studies are being undertaken to examine the possibility of incorporating the effects of inclined cracking.

REFERENCES

1. BS5400 for the Design of Steel, Concrete and Composite Bridges, London, 1978.

2. Baldwin, J. T., Razzaque, A., Irons, B. M. 'Shape Function Routine for an Isoparametric Thin Plate Element', Int. Jnl. for Num. Meth. in Eng'g, V7, 1973.

3. Cope, R. J., Rao, P. V., Clark, L. A. 'Nonlinear Design of Concrete Bridge Slabs using Finite Element Procedures', Nonlinear Design of Concrete Structures, Univ. of Waterloo, 1980.

4. Cope, R. J., Rao, P. V., Clark, L. A., Norris, P. 'Modelling of Reinforced Concrete Behaviour for Finite Element Analysis of Bridge Slabs', Numerical Methods for Nonlinear Problems, V1, Pineridge Press, 1980.

5. Gilbert, R. I., Warner, R. F. 'Tension Stiffening in Reinforced Concrete Slabs', Proc. ASCE, V104, ST12, 1978.

6. Cope, R. J., Rao, P. V. 'Reinforced Concrete Skewed Bridge Slabs', Advanced Mechanics of Reinforced Concrete, IABSE Colloquium, Delft, 1981.

7. Bažant, Z. P. 'Advances in Deformation and Failure Models for Concrete', IABSE Colloquium, Delft, 1981.

8. Cope, R. J., Rao, P. V. 'Behaviour of Reinforced Concrete Bridge Slabs', Technical Report, Dept. Civil Eng'g, Univ. of Liverpool, 1981.

9. Chrisfield, M. A. 'A Faster Modified Newton-Raphson Iteration', Computer Methods in App. Mechs. and Eng'g, 20, 1979.

10. Bathe, K. J. and Cimento, A. P. 'Some Practical Procedures for the Solution of Nonlinear Finite Element Equations', Computer Methods in App. Mechs. and Eng'g, 22, 1980.

11. Cope, R. J., Rao, P. V., Edwards, K. 'Nonlinear Finite Element Analysis Techniques for Concrete Slabs', Numerical Methods for Nonlinear Problems, V1, Pineridge Press, 1980.

12. Bergan, P. G., Holland, I. 'Nonlinear Finite Element Analysis of Concrete Structures', Computer Methods in App. Mechs. and Eng'g, V17/18, 1979.

13. Cedolin, L., Nilson, A. H. 'A Convergence Study of Iterative Methods applied to Finite Element Analysis of Reinforced Concrete', Int. Jnl. for Num. Methods in Eng'g, V12, 1978.

14. Bergan, P. G., Holland, I., Söreide, T. H. 'Use of Current Stiffness Parameter in Solution of Nonlinear Problems', Energy Methods in Finite Element Analysis, J. Wiley & Sons, 1979.

15. Matthies, H., Strang, G. 'The Solution of Nonlinear Finite Element Equations', Int. Jnl. for Num. Methods in Eng'g, V14, 1979.

16. Hughes, T. J. R., Cohen, M. 'The "Heterosis" Finite Element for Plate Bending', Computers and Structures, V9, 1978.

Advanced Mechanics of Reinforced Concrete in Structural Fire Analysis

Méthodes nouvelles de la mécanique du béton armé pour l'analyse des structures soumises au feu

Neue Verfahren im Stahlbeton für die Berechnung von Tragwerken im Brandfall

JEAN-CLAUDE DOTREPPE
Research Associate F.N.R.S.
Department of Civil Engineering, University of Liège
Liège, Belgium

SUMMARY
A numerical model for the analysis of concrete structures in a fire environment is presented. This model is based on the finite element method with subdivision of the cross section in a rectangular mesh. A particular formulation is used for the evaluation of thermal effects in a discretized structure and for the step-by-step analysis of a structure submitted to increasing temperatures. A comparison between theoretical and experimental results is made for a continuous T beam loaded and heated unsymmetrically.

RÉSUMÉ
On présente un modèle numérique pour l'étude du comportement au feu des structures en béton. Ce modèle est basé sur la méthode des éléments finis avec subdivision de la section droite en mailles rectangulaires. On propose une formulation particulière pour l'étude des effets thermiques dans une structure discrétisée et pour l'analyse incrémentielle d'une structure soumise à température croissante. On effectue une comparaison entre résultats théoriques et expérimentaux pour une poutre en T continue chargée et chauffée de manière non symétrique.

ZUSAMMENFASSUNG
Ein numerisches Modell für die Untersuchung des Brandverhaltens von Betontragwerken wird vorgelegt. Dieses Modell beruht auf der finiten Elemente Methode mit Diskretisierung des Querschnittes in rechteckige Maschen. Eine besondere Formulierung für die Untersuchung der thermischen Effekte in einem diskretisierten Tragwerk und für die inkrementelle strukturelle Analyse unter zunehmender Temperatur wird vorgeschlagen.
Ein Vergleich zwischen theoretischen und experimentellen Ergebnissen für einen durchlaufenden, unsymmetrisch erwärmten und belasteten T-Träger wird durchgeführt.

1. INTRODUCTION

The thermomechanical behaviour of reinforced concrete structures in a fire environment is a very complicated problem. The best way to verify this statement is to attend a fire test. The phenomena observed during the experiment show that an analytical treatment of this problem is rather involved.

The usual way of determining the fire resistance of structural elements is to perform fire tests. Nevertheless the information needed for a rational design for fire safety cannot be provided only by results from standard tests. As testing facilities are rather limited such tests are not sufficient to represent the behaviour of all structural elements under fire conditions, since the evaluation of structural response should also account for different conditions of restraint due to the building system. Furthemore fire tests are rather expensive.

The need for analytical predictions of thermal and structural responses has grown more and more intensively. Though much progress has been made in the field of mechanics of reinforced concrete [2], very few research has up to now been devoted to fire problems due to the lack of knowledge of the material properties at elevated temperatures and the difficulty of modeling the structural behaviour. Significant advances have recently been made in the works of Anderberg [1], Bresler [3], Kordina and Klingsch [8].

In this paper a numerical model for the evaluation of the fire resistance of reinforced concrete structures is presented. A comparison between calculated and experimental results shows the efficiency of the model.

2. MATERIAL PROPERTIES AT ELEVATED TEMPERATURES

A structural fire resistance problem may be subdivided in two distinct parts :

1. a thermal problem i.e. evaluation of the temperature distribution in the element during the development of fire ;

2. a mechanical problem, i.e. study of the mechanical behaviour of the element due to the temperature increase calculated at point 1 and evaluation of the fire endurance of the element.

To solve these problems analytically, it is necessary to collect data on thermophysical (point 1) and mechanical (point 2) properties of the materials used, i.e. steel and concrete. Furthemore, due to the high temperatures reached, the variations of temperature affect significantly the properties of these materials, and this must be taken into account in the numerical model.

Experimental research has been made in various laboratories [1] [3] [8], and also in Belgium [5], but the experimental results display appreciable differences mainly in the case of concrete. Simplified methods for the evaluation of the fire endurance only require the determination of classical mechanical properties, i.e. ultimate strength in tension and compression, yielding stress and modulus of elasticity. In a step-by-step numerical analysis, these characteristics are not sufficient, and information concerning the instantaneous stress-strain relation is necessary.

Experimental investigations (cf [5]) show that the stress-strain diagram depends not only on the temperature reached, but also on preloading. This factor has clearly a favourable influence on the strength of concrete at elevated temperatures.

Thermal creep of concrete and steel has also a non negligible influence. Creep models have been proposed for both materials, but they appear quite involved. Furthermore research people do not still agree on the form of the creep laws and on the importance of the phenomenon. Thus this question remains open.

As temperature and stress vary from one point to another, a rigorous analysis of the problem should be based on a stress (σ) versus strain (ε) relation of the following type :

$$f(\sigma, \tilde{\sigma}, \varepsilon, \theta, t) = 0 \qquad (1)$$

where $\tilde{\sigma}$: stress history
θ : temperature
t : time

Such a relation characterizing the material behaviour under varying loading and temperature conditions has not yet been determined.

The analytical models used in this study are described in reference [5].

3. TEMPERATURE DISTRIBUTION IN THE ELEMENTS

The first problem to be solved is the modeling of the environment created by a fire. Several factors influence the severity and duration of a fire, but it is not reasonable to take them into account in performing fire tests. In order to simplify comparisons between fire test results from different laboratories, it has been decided to refer to the same thermal program. This is known as the standard ISO curve adopted in the ISO 834 Recommendations [7] and defined by the following temperature versus time relation :

$$\theta - \theta_o = 345 \log_{10} (8\,t + 1) \qquad (2)$$

t = time in minutes
θ_o = initial temperature

The distribution of temperature in the elements is governed by the following non linear partial differential equation :

$$\frac{\partial}{\partial x}\left(\lambda_x \frac{\partial \Theta}{\partial x}\right) + \frac{\partial}{\partial y}\left(\lambda_y \frac{\partial \Theta}{\partial y}\right) + \frac{\partial}{\partial z}\left(\lambda_z \frac{\partial \Theta}{\partial z}\right) + Q = c\,p\,\frac{\partial \Theta}{\partial t} \qquad (3)$$

with various boundary conditions

$\lambda_x, \lambda_y, \lambda_z$ (x, y, z, θ) : coefficients of thermal conductivity
c (x, y, z, θ) : specific heat
ρ (x, y, z, θ) : density
Q(x, y, z, θ) : distribution of internal sources

The most difficult problem is the determination of the density of heat flow Φ transmitted to the element.This can be written as follows :

$$\Phi = h(\theta_e - \theta) + \sigma_o\, \varepsilon_{es}\, (T_e^4 - T^4) \qquad (4)$$

θ_e, T_e : temperature and absolute temperature of the environment
h : coefficient of convection

σ_o : Stefan-Boltzman constant

ε_{es} : resultant emissivity factor between the environment and the surface of the element

Due to the high temperatures reached, the radiation term becomes rapidly preponderant. The preceding parameters cannot be determined analytically, but the following values have been adopted on the basis of numerical tests :

$$h = 25 \text{ W/m}^2\text{. K} \qquad \varepsilon_{es} \simeq 0,5 \tag{5}$$

The temperature distribution has to be obtained by numerical methods. The finite element and finite difference methods have been used in this study [5]. In both cases, reasonable agreement has been found between theoretical and experimental results.

4. NUMERICAL PROCEDURE FOR THE THERMOMECHANICAL ANALYSIS OF REINFORCED CONCRETE STRUCTURES IN A FIRE ENVIRONMENT

4.1. General structure of the computer program

The general structure of the computer program is given in figure 1. It can be derived from the analysis of a structural element submitted to fire. Before fire external loads are applied on the element. After starting of fire the increase of temperature induces several thermal effects and a reduction of the bearing capacity. The numerical procedure must be able to analyse these phenomena and to predict failure corresponding to the fire endurance of the element.

The 1st part of the computer program is devoted to the evaluation of the structural behaviour of the beam at ambient temperature under static loads. This is an extension to beams of the method developed previously for slabs [4]. Preference has been given to the formulation proposed in a parallel study by Hand et al. [6].

The 2nd and 3rd parts correspond to the thermomechanical response of the structural element during the development of fire. This analysis is made step-by-step. For the thermal analysis a finite difference program has been incorporated in the general program.

The increase of temperature leads to mechanical transformations analysed in part 3. The variation of displacements, strains, thermal stresses is calculated. An iterative procedure appears which will be described in § 4.3. If the element does not collapse, a new increment of time is applied, corresponding to an increase of the environmental temperature and the procedure is repeated.

Failure is detected by applying the classical Ryan and Robertson criterion on the rate of displacement

$$\frac{\Delta f}{\Delta t} \leq \frac{\ell^2}{9000\ h} \tag{6}$$

ℓ = length of the span
h = effective height

4.2. Evaluation of thermal effects in a discretized structure

The procedure used for the evaluation of thermal effects in a discretized structure is based on the classical assumption that plane sections remain plane. The

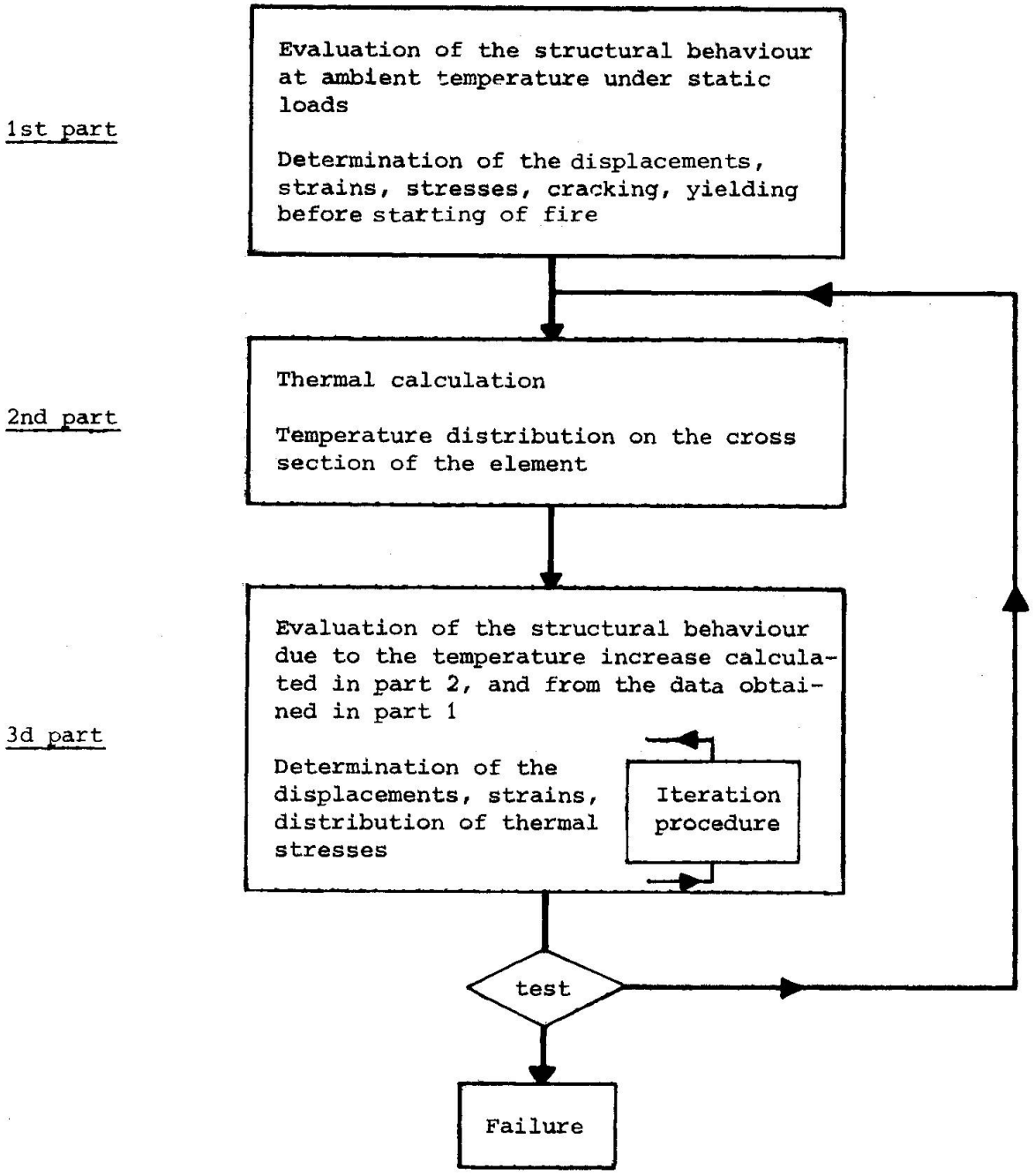

Figure 1 : General structure of the computer program

increase of displacement during a time step is given by :

$$\Delta u = \Delta u_o - z \frac{d\Delta w}{dx} \tag{7}$$

The "effective" strains, i.e. strains related stresses can be obtained by adding to the strains associated with the preceding displacement field, those corresponding to full restraint of the element :

$$\Delta\varepsilon = - \alpha \Delta\theta + \frac{d\Delta u}{dx} = - \alpha \Delta\theta + \Delta\varepsilon_o + z \Delta\chi \tag{8}$$

α : coefficient of thermal expansion
χ : curvature

The additional thermal stresses can be derived from the preceding equation :

$$\Delta\sigma = E \Delta\varepsilon = E(- \alpha \Delta\theta + \Delta\varepsilon_o + z \Delta\chi) \tag{9}$$

The quantities $\Delta\varepsilon_o$ and $\Delta\chi$ must be determined so as to satisfy equilibrium equations. In a statically determinate beam these conditions reduce to :

$$\int_\Omega \Delta\sigma \, d\Omega = 0 \qquad \int_\Omega \Delta\sigma \, z \, d\Omega = 0 \tag{10}$$

By substituting (9) in (10), one gets :

$$\begin{aligned} \Delta\varepsilon_o \int_\Omega E \, d\Omega + \Delta\chi \int_\Omega E \, z \, d\Omega &= \int_\Omega E \, \alpha \, \Delta\theta \, d\Omega \\ \Delta\varepsilon_o \int_\Omega E \, z \, d\Omega + \Delta\chi \int_\Omega E \, z^2 \, d\Omega &= \int_\Omega E \, \alpha \, \Delta\theta \, z \, d\Omega \end{aligned} \tag{11}$$

The discretization can be introduced here. The beam is divided in finite elements and the cross section is divided in subslices forming a rectangular mesh (figure 2). Let nc be the number of horizontal layers and nt the number of vertical layers. The discretization in a rectangular mesh corresponds to evaluating in a discretized way the integrals of equation (11), which leads to :

$$\begin{aligned} \int_\Omega E \, d\Omega &= \sum_{i=1}^{nc} \sum_{j=1}^{nt} E_{ij} \, \Omega_{ij} = E\Omega^* \\ \int_\Omega E \, z \, d\Omega &= \sum_{i=1}^{nc} \sum_{j=1}^{nt} E_{ij} \, S_{ij} = ES^* \\ \int_\Omega E \, z^2 \, d\Omega &= \sum_{i=1}^{nc} \sum_{j=1}^{nt} E_{ij} \, I_{ij} = EI^* \\ \int_\Omega E \, \alpha \, \Delta\theta \, d\Omega &= \sum_{i=1}^{nc} \sum_{j=1}^{nt} E_{ij} \, \alpha_{ij} \, \Delta\theta_{ij} \, \Omega_{ij} = \Delta N_\theta \\ \int_\Omega E \, \alpha \, \Delta\theta \, z \, d\Omega &= \sum_{i=1}^{nc} \sum_{j=1}^{nt} E_{ij} \, \alpha_{ij} \, \Delta\theta_{ij} \, S_{ij} = \Delta M_\theta \end{aligned} \tag{12}$$

By using the preceding notations, equations (11) may be written as follows :

$$\begin{Bmatrix} \Delta N_\theta \\ \Delta M_\theta \end{Bmatrix} = \begin{bmatrix} E\Omega^* & ES^* \\ ES^* & EI^* \end{bmatrix} \begin{Bmatrix} \Delta\varepsilon_o \\ \Delta\chi \end{Bmatrix} \tag{13}$$

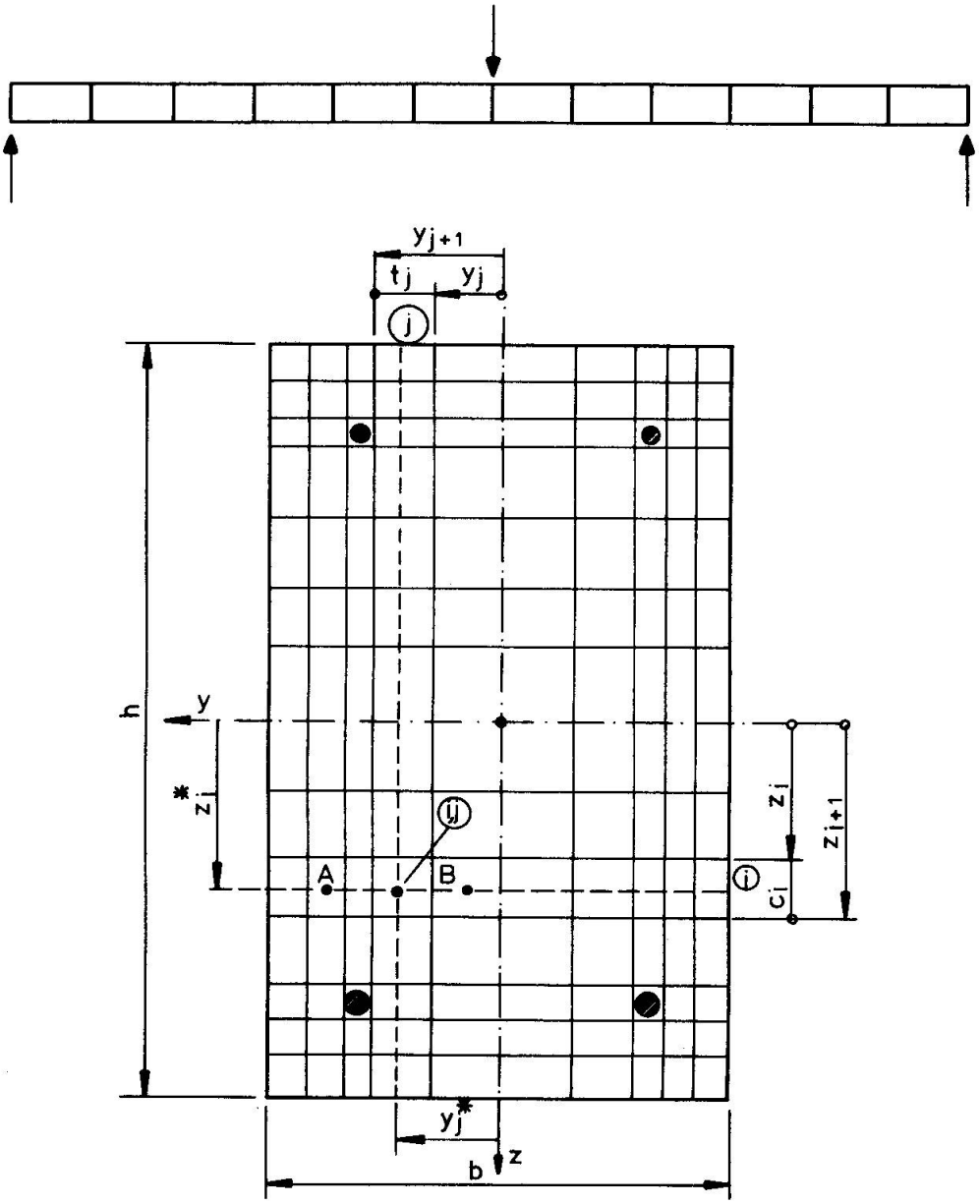

Figure 2 : Discretization of the beam and of the cross section

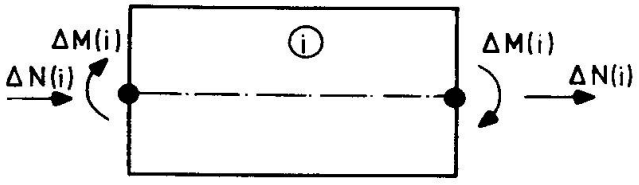

Figure 3 : Thermal equivalent nodal forces

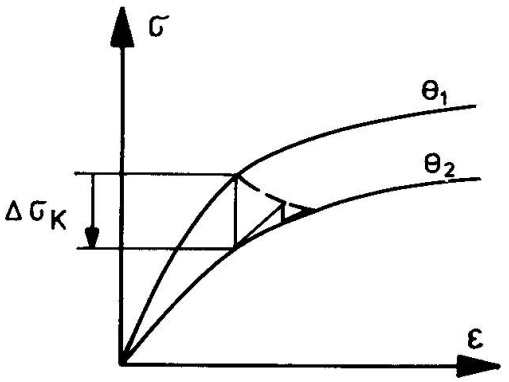

Figure 4 : Iterative procedure

which gives the thermal equivalent forces in a discretized element (figure 3). For the whole structure these forces must be combined between adjacent elements. As can be seen a coupling between membrane and flexural effects appears similar to the one described in [4] and [6].

4.3. Numerical iterative prodedure

In a classical thermoelastic problem thermal effects are calculated by applying the well-known Duhamel's principle. The structure is first restrained against any displacement ; equivalent restraint forces are computed and next applied to the element.

The problem is more involved in this case for several reasons :

- The restraint forces must be evaluated for a discretized structure as indicated in the preceding paragraph ;
- The structure is analysed step-by-step. This means that Duhamel's principle must be applied at each time or temperature increment ;
- Due to several nonlinearities (stress-strain diagram, cracking, crushing), an iterative procedure occurs leading to progressive structural modifications during each increment.

At the beginning of each time or temperature increment, the structure tangent stiffness matrix is updated to reflect any changes in material properties which have taken place. Inelastic effects within the increment are taken into account by the initial stress method, in which pseudo-loads are iteratively redistributed through the structure using the tangent stiffness computed at the beginning of each increment and modified during the iterative procedure.

At the beginning of the time or temperature increment the correction forces consist in thermal equivalent forces $\{\Delta F_\Theta\}$ that can be obtained from equation (13). The temperature variations during a time step cause a subsequent change in the stress-strain law (figure 4). This temperature dependent shift gives rise to another set of correction forces.

The associated correction stress is the difference $\Delta\sigma_K$ between two stress-strain laws for the same strain and different temperatures (see figure 4). This stress difference is transformed into equivalent forces by the usual following procedure :

$$\Delta N_K = \sum_{i=1}^{nc} \sum_{j=1}^{nt} (\Delta\sigma_K)_{ij}\, \Omega_{ij} \qquad (14)$$

$$\Delta M_K = \sum_{i=1}^{nc} \sum_{j=1}^{nt} (\Delta\sigma_K)_{ij}\, S_{ij}$$

and for the equivalent nodal forces

$$\{\Delta F_K\} = \int_\Omega [B]^T \begin{Bmatrix} \Delta N_K \\ \Delta M_K \end{Bmatrix} d\Omega \qquad (15)$$

For the i^{th} time increment, the first approximation to the incremental displacements is calculated from

$$[K]_i^{(o)}\ \{\Delta u\}_i^{(o)} = \{\Delta F\}_i^{(o)} \qquad (16)$$

where $[K]_i^{(o)}$ is the tangent stiffness matrix at the beginning of the i^{th} increment.

$$\{\Delta F\}_i^{(o)} = \{\Delta F_\Theta\}_i + \{\Delta F_K\}_i \qquad (17)$$

These nodal forces are redistributed through the structure. But inelastic actions occur due to the nonlinearity of stress-strain diagrams, cracking and crushing of concrete, which leads to an iterative procedure. Numerical tests show that the iterations are mainly due to the formation of new cracks. The stress released in a crack is temperature dependent and is given by

$$\{\Delta\sigma\}_{cr} = R_b(\theta) \tag{18}$$

Successive iterations take the form

$$[K]_i^{(r)} \{\Delta u\}_i^{(r)} = \{\Delta F\}_i^{(r)} \tag{19}$$

where $[K]_i^{(r)}$ is the stiffness matrix updated at the beginning of the r^{th} iteration in the i^{th} increment

$\{\Delta F\}_i$ is mainly due to the formation of new cracks in the preceding iteration.

The total incremental displacements for the i^{th} time increment (after N iterations) is then given by :

$$\{\Delta u\}_i = \sum_{r=o}^{N} \{\Delta u\}_i^{(r)} \tag{20}$$

The incremental stresses are obtained by adding those corresponding to the preceding incremental displacements to the restraint stresses - $E\,\alpha\,\Delta\theta$.

5. EXAMPLE : T BEAM ON 3 SUPPORTS

To demonstrate the accuracy of the numerical results which can be obtained from the described procedure a continous T beam on 3 supports has been analysed and the theoretical results compared with test results obtained at the Technical University of Braunschweig [9].

The loading and heating system is presented in figure 5. The beam is loaded and heated unsymmetrically. The thermal program is applied according to the ISO 834 Recommendations [7]. The dimensions of the cross section and reinforcement arrangement are indicated on figure 6. The beam is subdivided in 20 finite elements. The whole beam has to be considered due to the lack of symmetry, but only one half of the cross section for the division in subslices.

Figure 7 shows the temperature increase in the tension steel near the corners. There is a good agreement between theoretical and experimental results. As can be seen the temperature increases rapidly at these points : $\sim$ 600°C after 1 hour and more than 800°C after 2 hours.

The structural behaviour of a continuous beam or a beam with fixed ends is completely different from that of a simply supported beam. In the latter case, large deflections occur due to the steep thermal gradient on the cross section. In a hyperstatic beam, the same thermal gradient produces an increase of the bending moment on the supports, while the deflections remain rather small.

The variation of the bending moment on the central support of the T beam analysed here is indicated on figure 8. After $\sim$ 1 hour, the bending moment tends to become constant. This corresponds to the formation of a plastic hinge on the central support. Again there is a good agreement between theoretical and experimental results.

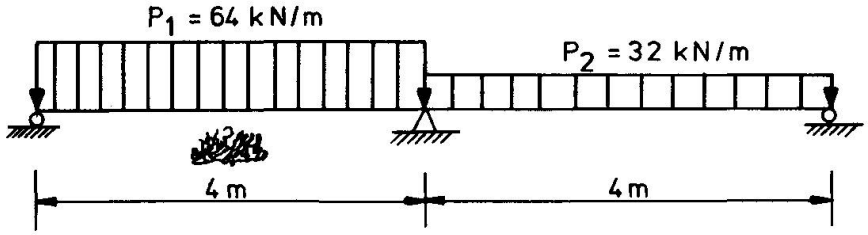

Figure 5: Fire test on continuous T beam loaded and heated unsymmetrically [9]

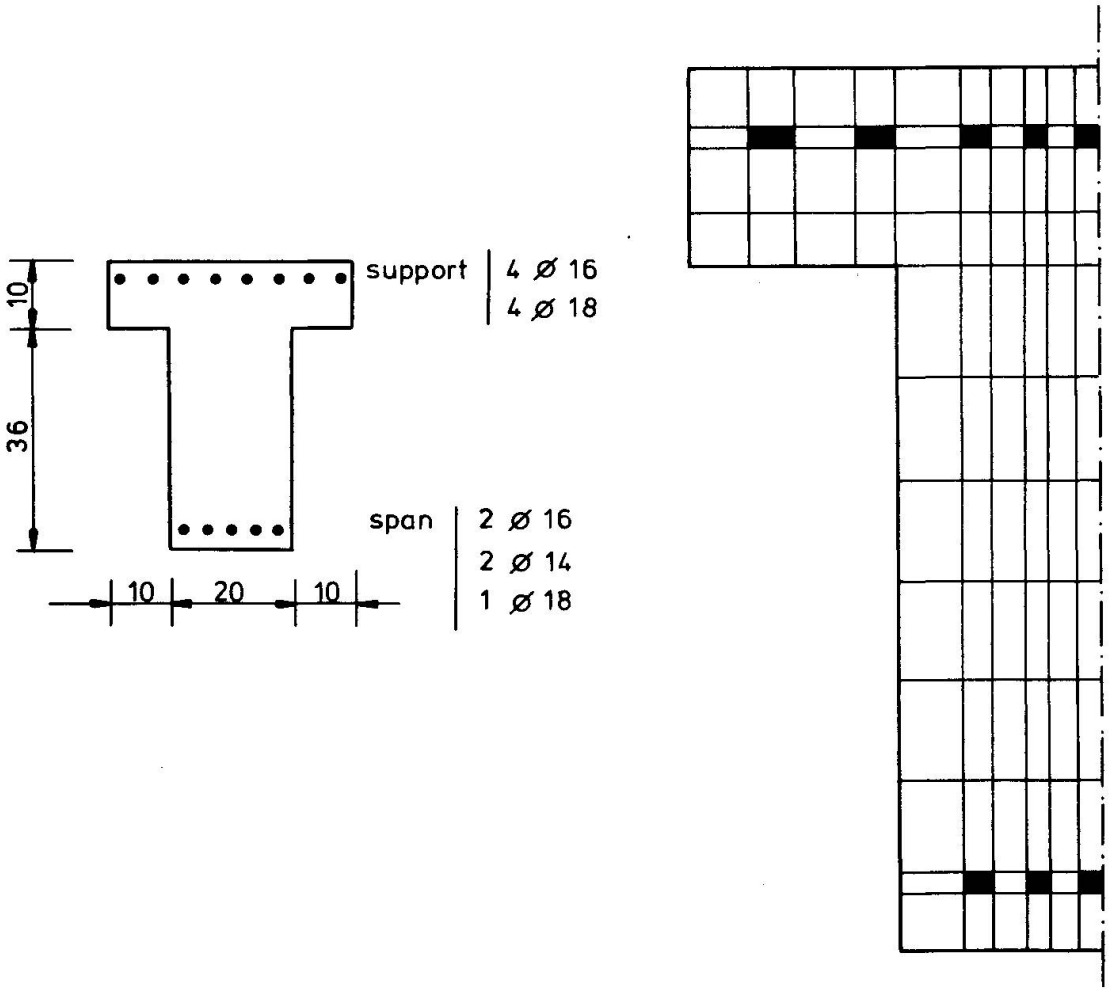

Figure 6: Cross section.
Reinforcement and subdivision in a rectangular mesh

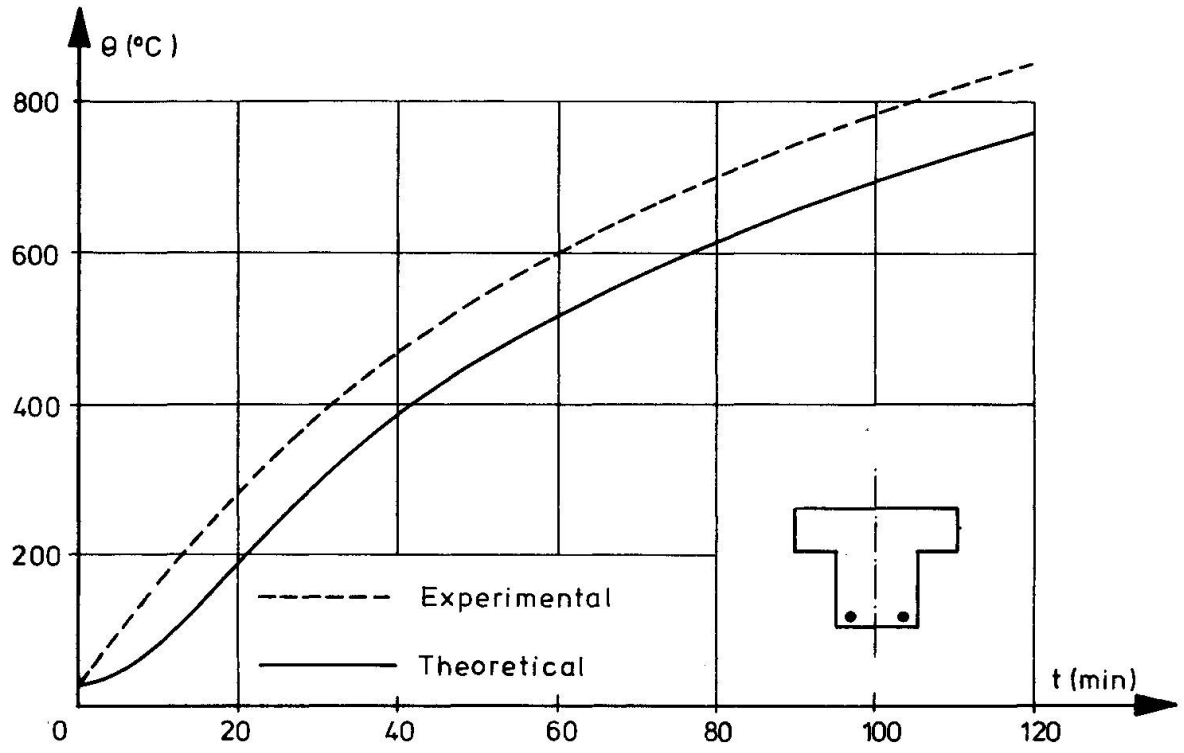

Figure 7: Temperature increase in the reinforcement

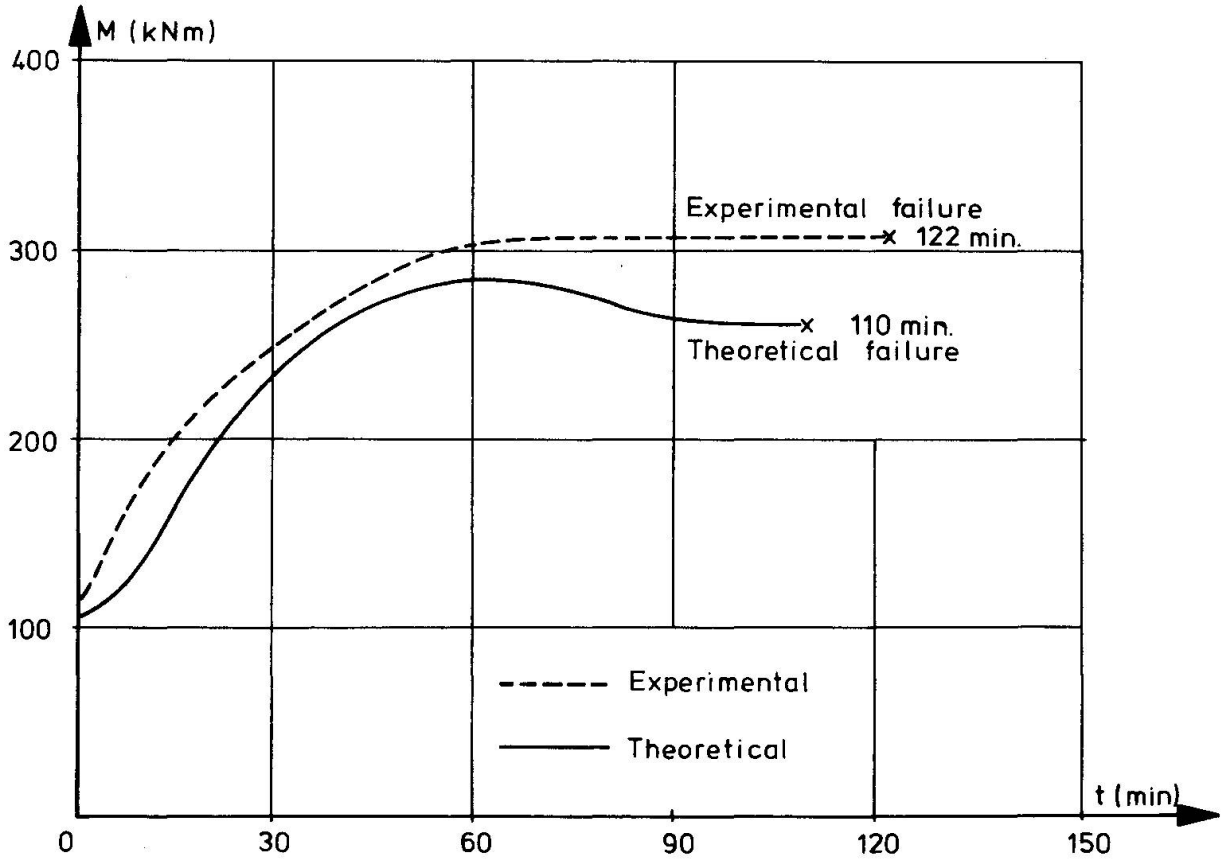

Figure 8 : Variation of the bending moment on the central support

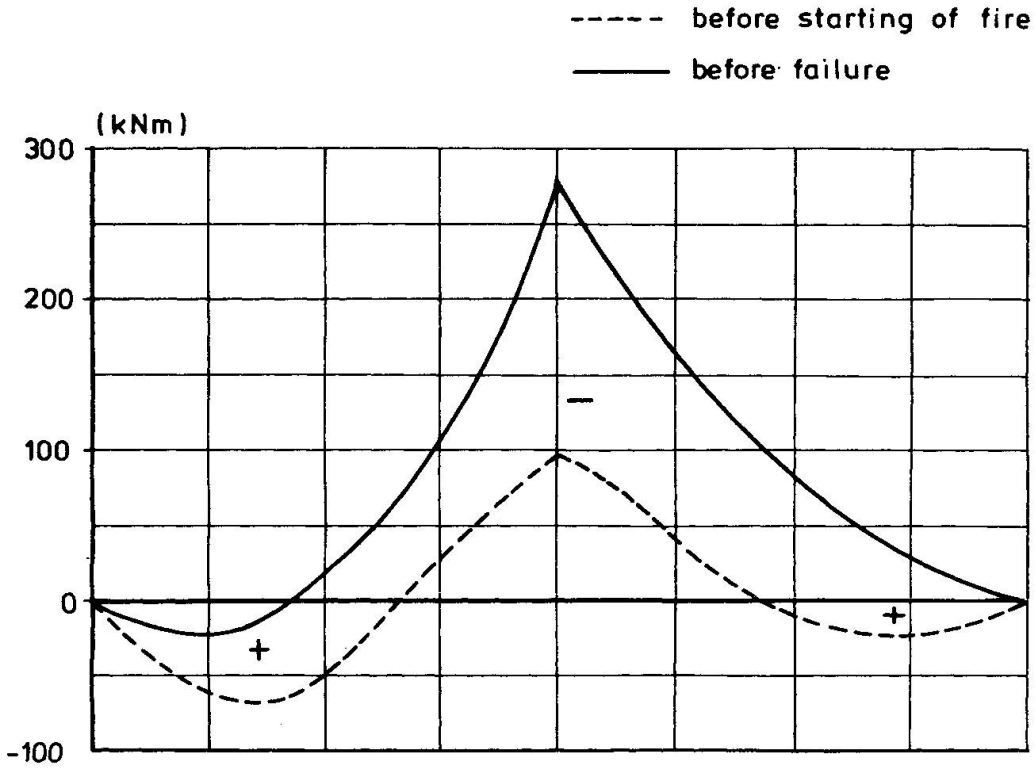

Figure 9 : Variation of the bending moment diagram in the beam

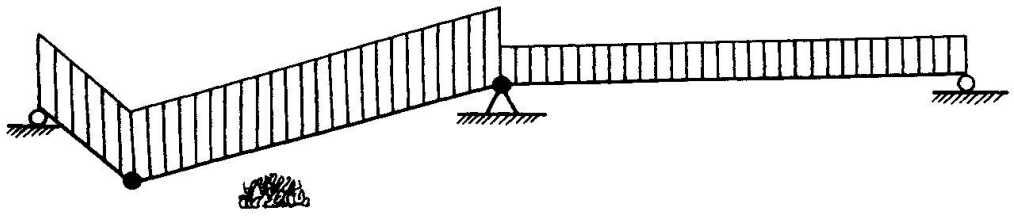

Figure 10 : Failure mechanism

The corresponding evolution of the bending moment diagram in the beam is represented on figure 9. This shows the important redistribution of internal forces in the element due to the thermal gradient. Before failure the diagram has only negative zones, except on the left hand side of the heated and most loaded span.

This explains the occurrence of failure after 2 hours. At this moment, the temperature in the tension reinforcement is greater than 700°C and the beam is no longer able to carry a small positive bending moment. For this reason a second plastic hinge forms where the positive moment is maximum and this leads to the failure mechanism represented on figure 10. The experimental observations confirm the formation of such a mechanism [5] [9].

6. CONCLUSIONS

A numerical procedure for the analysis of the structural behaviour of reinforced concrete structures under fire conditions has been presented. It is based on the finite element method with subdivision of the cross section in a rectangular mesh. A particular formulation has been used for the evaluation of thermal effects in a discretized structure and for the step-by-step structural analysis under increasing temperatures. A good agreement has been obtained between theoretical and experimental results.

There is a growing need of theoretical results to provide adequate structural integrity during fires. It is of course not possible, and even not desirable, to replace all laboratory tests by simulation programs or theoretical formulations. Experiment remains essential to understand structural behaviour and to observe almost unpredictable phenomena. Nevertheless numerical procedures such as the method presented in this paper, along with experimental studies, provide a powerful tool for a more thorough understanding of the fire endurance of structures.

REFERENCES

1. ANDERBERG, Y. : Fire Exposed Hyperstatic Concrete Structures - An Experimental and Theoretical Study. Division of Structural Mechanics and Concrete Construction, Lund Institute of Technology, Bulletin n° 55, Lund, 1976.

2. BAZANT, S.P., SCHNOBRICH, W.C., and SCORDELIS, A.C. : Analisi delle Strutture in Cemento Armato mediante il Metodo degli Elementi Finiti. Corso di Perfezionamento per le Costruzioni in Cemento Armato "Fratelli Pesenti", Politecnico di Milano, Milano,1978.

3. BRESLER, B. : Response of Reinforced Concrete Frames to Fire. Preliminary Report, 10 th IABSE Congress, Tokyo, 1976, pp. 273-280.

4. DOTREPPE, J-C., SCHNOBRICH, W.C., and PECKNOLD, D.A. : Layered Finite Element Procedure for Inelastic Analysis of Reinforced Concrete Slabs. IABSE Publications, Vol. 33-II, Zürich, 1973, pp. 53-68.

5. DOTREPPE, J-C.: Méthodes Numériques pour la Simulation du Comportement au Feu des Structures en Acier et en Béton Armé. Thèse d'Agrégation de l'Enseignement Supérieur, Université de Liège, Liège, 1980.

6. HAND, F.R., PECKNOLD, D.A., and SCHNOBRICH, W.C.: A Layered Finite Element Non Linear Analysis of Reinforced Concrete Plates and Shells. Civil Engineering Studies, Structural Research Series n° 389, University of Illinois, Urbana, Illinois, 1972.

7. ISO : Fire Resistance Tests - Elements of Building Construction. International Standard 834, 1975.

8. KORDINA, K., and KLINGSCH, W. : Tragverhalten Brandbeanspruchter Bauteile. Preliminary Report, 10 th IABSE Congress, Tokyo, 1976, pp. 287-292.

9. WESCHE, J. : Stahlbetondurchlaufkonstruktionen unter Feuerangriff. Institut für Baustoffkunde und Stahlbetonbau, Technische Universität Braunschweig, Braunschweig, 1974.

Computational Models for Reinforced Concrete Slab Systems

Modèles de calcul par ordinateur pour des systèmes de dalles en béton armé

Rechenmodelle für Stahlbetonplattensysteme

E. HINTON
Lecturer

H.H. ABDEL RAHMAN
Research Assistant

O.C. ZIENKIEWICZ
Professor

Department of Civil Engineering, University College of Swansea,
Swansea, Wales, United Kingdom.

SUMMARY
This paper discusses the finite element computational models used in program PLASAN for the nonlinear analysis of reinforced concrete slab systems. A layered Mindlin plate model is adopted and the discretisation is based on quadrilateral Mindlin elements. Some examples are presented and the relative efficiency of various nonlinear solution schemes is highlighted.

RÉSUMÉ
Dans cette publication on discute des modèles de calcul par la méthode des éléments finis, qui sont utilisés dans le programme PLASAN pour l'analyse non-linéaire des systèmes de dalles en béton armé. Un modèle de dalle multicouche MINDLIN est accepté et est basé sur des éléments MINDLIN quadrilatéraux. Certains exemples sont présentés et l'efficacité relative de différents schémes de solutions non-linéaires sont mises en valeur.

ZUSAMMENFASSUNG
Dieser Beitrag behandelt die Finite-Elemente-Rechenmodelle, die im Programm PLASAN für die nichtlineare Berechnung von Stahlbetonplatten verwendet werden. Ein Mindlin-Schichtplattenmodell wurde angenommen, während die Diskretisierung auf viereckigen Mindlin-Elementen beruht. Einige Beispiele werden gezeigt, und die relative Leistungsfähigkeit von verschiedenen nichtlinearen Lösungswegen wird beleuchtet.

1. INTRODUCTION

The present studies are motivated by the need to develop finite element computational models suitable for the accurate and efficient nonlinear analysis of reinforced concrete bridge decks and other flexural systems. Research work sponsored by the Highway Engineering Computer Branch (HECB) of the Department of Transport has resulted in the development of the computer program PLASAN [1]. This paper discusses the general approach in PLASAN and highlights the discretisation and equation solving techniques adopted therein. Results of some numerical experiments are also presented.

The present formulation is based on a layered reinforced concrete Mindlin plate model in which the plate is represented as a series of concrete and smeared unidirectional steel layers. Nonlinearities due to cracking, yielding and crushing of the concrete and yielding of the steel are taken into account. In PLASAN, the discretisation is based on a selectively integrated Heterosis quadrilateral plate element [2]. Experiments (not reported here) have been performed on other Mindlin elements. Two other useful elements emerge: a new 4-noded quadrilateral element developed recently by Hughes [3] and the 16-noded selectively integrated quadrilateral element [4]. Only the results obtained using the Heterosis element are discussed in this paper.

An accurate, reliable and efficient solution algorithm is of vital importance for the nonlinear analysis of reinforced concrete structures where cracking of the concrete forms a major problem. Although an elaborate modelling of the behaviour of the concrete and steel is essential, the solution algorithm plays an important role in the production of accurate results. In PLASAN, various incremental-iterative solution schemes are adopted. In the standard Newton-Raphson method (NR) the Jacobian (tangential stiffness matrix) is evaluated at each iteration. In the related methods various approximations to the Jacobian are used. In the Modified Newton-Raphson (MNR) methods, the approximation is updated only once for each increment and not for each iteration. Here the tangential stiffness matrix is formed and factored either at the beginning of each increment (KT1) or at the second iteration (KT2). Alternatively, the initial elastic stiffness matrix may be used throughout the entire analysis. This is known as the initial stress method (KO). Unfortunately NR and MNR methods have a tendency to diverge during elastic unloading and they sometimes lead to singular or ill-conditioned matrices near the limit load. The initial stress method provides a suitable solution to these problems but the convergence is slow particularly when fine convergence tolerances are used. The use of coarser tolerances with KO leads to faster convergence but at the expense of accuracy. Alternative computational strategies based on Quasi-Newton (QN) methods [5-7] offer a reasonable solution to this difficulty. In the present work, the BFGS Quasi-Newton updates are performed with the initial stiffness matrix (QNKO) and also in conjunction with MNR methods (QNKT1 and QNKT2). Line searches are also included in the MNR and QN methods. Various Secant Newton [8] and arc length methods [8-10] are also incorporated in PLASAN.

2. MINDLIN FORMULATION

In the usual Mindlin plate formulation the main assumption is that normals to the plate midsurface (xy-plane) before deformation remain straight but not necessarily normal to the midsurface after deformation. Thus the displacements u, v and w at any point with coordinates (x,y,z) can be expressed as

$$\begin{bmatrix} u(x,y,z) \\ v(x,y,z) \\ w(x,y,z) \end{bmatrix} = \begin{bmatrix} u_o(x,y) - z\theta_x(x,y) \\ v_o(x,y) - z\theta_y(x,y) \\ w_o(x,y) \end{bmatrix} \quad (1)$$

where u_o, v_o and w_o are the displacements at the plate midsurface in the x, y and z direction and θ_x and θ_y are the rotations of the normal in the xz and yz plane respectively. Table I shows the main features of the Mindlin formulation.

3. MATERIAL MODEL

3.1 Concrete in compression

When failure is dominated by concrete cracking and steel yielding, a relatively crude plasticity model suffices. In PLASAN, the concrete is treated as an elasto-plastic material. In biaxial compression the Von Mises ellipse is used to define the elastic limit and the flow function. After yielding, the concrete is assumed to be crushed and lose all of its strength when the failure envelope (in strain space) is exceeded.

3.2 Concrete in tension

Cracks are assumed to open perpendicular to the higher principal stress direction when the tensile strength of concrete is exceeded. The stress level in the cracked concrete is interpolated using a tension stiffening curve and depends on the degree of straining in the concrete. Concrete cracked in two directions is assumed to lose all of its strength.

3.3 Steel reinforcement representation

In the uniaxial stress-strain relationship for the reinforcement steel a plasticity formulation is adopted in which linear isotropic strain hardening is assumed after initial yielding. Elastic unloading is allowed.

4. DISCRETISATION

The selectively integrated, 8-9 noded Heterosis element is used in the discretisation. In PLASAN, a hierarchical formulation is adopted to represent all degrees of freedom. Thus for typical element e, $N_1^{(e)}$ to $N_8^{(e)}$ are the 8-node Serendipity shape functions and $N_9^{(e)}$ is the bubble function $(1-\xi^2)(1-\eta^2)$ associated with the ninth central node. Thus the hierarchical degrees of freedom at node 9 are perturbations from the associated Serendipity interpolants. The 8-node Serendipity representation can be obtained if all degrees of freedom at node 9 are constrained to zero. If they are left free then an element equivalent to the 9-node Lagrangian representation is obtained. For the Heterosis representation, only the hierarchical lateral displacement at node 9 is restrained to zero. In this element selective integration procedures are adopted [2]. Unlike most other Mindlin elements, the Heterosis element is free from major defects. It does not give overstiff solutions in limiting thin plate situations (lock) nor does it have any transmittable mechanisms. The only other Mindlin elements which are considered worthy of further attention are the recently developed 4-noded quadrilateral [3] and the 16-noded quadrilateral [4]. Both of these elements have been successfully implemented within the present

Table I Mindlin plate formulation

Virtual work equation

$$\int_V \delta \underline{\varepsilon}_1^T \underline{\sigma}_1 \, dV + \int_V \delta \underline{\varepsilon}_2^T \underline{\sigma}_2 \, dV - \int_V \delta \underline{u}^T \underline{b} \, dV - \int_{S_t} \delta \underline{u}^T \underline{t} \, dS = 0$$

where

displacements $\underline{u} = [u, v, w]^T$ virtual displacement $\delta\underline{u} = [\delta u, \delta v, dw]^T$

in-plane strains $\underline{\varepsilon}_1 = [u_{,x}, v_{,y}, u_{,y} + v_{,x}]^T$ $\delta\underline{\varepsilon}_1 = [\delta u_{,x}, dv_{,y}, du_{,y} + dv_{,x}]^T$

shear strains $\underline{\varepsilon}_2 = [w_{,x} - \theta_x, w_{,y} - \theta_y]^T$ $\delta\underline{\varepsilon}_2 = [\delta w_{,x} - \delta\theta_x, \delta w_{,y} - \delta\theta_y]^T$

in-plane stresses $\underline{\sigma}_1 = [\sigma_x, \sigma_y, \tau_{xy}]^T$ $\delta\underline{\sigma}_1 = [\delta\sigma_x, \delta\sigma_y, \delta\tau_{xy}]^T$

shear stresses $\underline{\sigma}_2 = [\tau_{xz}, \tau_{yz}]^T$ $\delta\underline{\sigma}_2 = [\delta\tau_{xz}, \delta\tau_{yz}]^T$

Incremental stress/strain relationships

$$d\underline{\sigma}_1 = \underline{D}_1 \, d\underline{\varepsilon}_1$$

$$d\underline{\sigma}_2 = \underline{D}_2 \, d\underline{\varepsilon}_2$$

Elastic

$$\underline{D}_1 = \underline{D} = \frac{E}{(1-\nu^2)} \begin{bmatrix} 1 & \nu & 0 \\ \nu & 1 & 0 \\ 0 & 0 & \frac{1-\nu}{2} \end{bmatrix}$$

$$\underline{D}_2 = \frac{E}{2(1+\nu)\alpha} \begin{bmatrix} 1 & 0 \\ 0 & 1 \end{bmatrix}$$

α is a modification factor (usually $\alpha = 1.2$)

Plastic

$$\underline{D}_1 = \underline{D} - \underline{D} \left[\frac{\partial F}{\partial \underline{\sigma}_1}\right] \left[\frac{\partial F}{\partial \underline{\sigma}_1}\right]^T \underline{D} \left[\bar{A} + \frac{\partial F}{\partial \underline{\sigma}_1} \underline{D} \frac{\partial F}{\partial \underline{\sigma}_1}\right]^{-1}$$

in which F is the yield function

$F = F(\underline{\sigma}_1, H)$, $\bar{A} = -\frac{1}{\lambda} \frac{\partial F}{\partial H} dH$

λ is the proportionality constraint

H is the hardening parameter

Finite element discretization

$$\underline{u} = \sum_i \underline{N}_i \, \underline{a}_i$$

$$\underline{\varepsilon}_1 = \sum_i \underline{B}_{1i} \, \underline{a}_i$$

$$\underline{\varepsilon}_2 = \sum_i \underline{B}_{2i} \, \underline{a}_i$$

where $\underline{N}_i = N_i \begin{bmatrix} 1 & 0 & 0 & -z & 0 \\ 0 & 1 & 0 & 0 & -z \\ 0 & 0 & 1 & 0 & 0 \end{bmatrix}$ $\underline{a}_i = [u_i, v_i, w_i, \theta_{xi}, \theta_{yi}]^T$

$$\underline{B}_{1i} = \begin{bmatrix} N_{i,x} & 0 & 0 & -zN_{i,x} & 0 \\ 0 & N_{i,y} & 0 & 0 & -zN_{i,y} \\ N_{i,y} & N_{i,x} & 0 & -zN_{i,y} & -zN_{i,x} \end{bmatrix} \qquad \underline{B}_{2i} = \begin{bmatrix} 0 & 0 & N_{i,x} & -N_i & 0 \\ 0 & 0 & N_{i,y} & 0 & -N_i \end{bmatrix}$$

Stiffness Matrices

$$\underline{K}_{ij} = \int_V \underline{B}_{1i}^T \underline{D}_1 \underline{B}_{1j} \, dV + \int_V \underline{B}_{2i}^T \underline{D}_2 \underline{B}_{2j} \, dV$$

Residual forces

$$\underline{\Psi}_i = \int_V \underline{B}_{1i}^T \underline{\sigma}_1 \, dV + \int_V \underline{B}_{2i}^T \underline{\sigma}_2 \, dV - \underline{f}_i$$

where the consistent nodal forces $\underline{f}_i = \int_V \underline{N}_i^T \underline{b} \, dV + \int_{S_t} \underline{N}_i^T \underline{\bar{t}} \, dS$

framework but results are not reported here.

5. SOLUTION SCHEMES

5.1 Standard and modified Newton-Raphson methods

Various incremental-iterative solution schemes are incorporated in PLASAN. In all of the methods the aim is to reduce the residual forces to small values. The residual force may be expressed as

$$\underline{\psi}(\underline{d}_i) = \int_V \underline{B}_{1i}^T \underline{\sigma}_{1i}\, dv + \int_V \underline{B}_{2i}^T \underline{\sigma}_{2i}\, dv - \underline{f}_i \tag{2}$$

where $\underline{f}_i = \lambda_i \underline{f}$ is the applied load vector and λ_i, $\underline{d}_i$, $\underline{B}_{1i}$, $\underline{B}_{2i}$, $\underline{\sigma}_{1i}$ and $\underline{\sigma}_{2i}$ are the loading parameter, displacement vector and strain-displacement matrices and stress vectors respectively. The vector $\underline{f}$ is a reference load vector and subscripts 1 and 2 refer to inplane and transverse shear quantities respectively.

In incremental-iterative solution schemes a sequence of corrections $\delta\underline{d}_i$ to the displacement vector are produced. Using the expression

$$\delta\underline{d}_i = - [\underline{K}_i]^{-1} \underline{\psi}_i \tag{3}$$

where $\underline{K}_i$ is an approximation to the Jacobian matrix which may be expressed as

$$\underline{J}(\underline{d}_i) = \left.\frac{\partial \underline{\psi}_i}{\partial \underline{d}}\right|_{d=\underline{d}_i} \tag{4}$$

The new estimate to the displacement vector is then given as

$$\underline{d}_{i+1} = \underline{d}_i + \eta_i \delta\underline{d}_i \tag{5}$$

where η_i may be found from a line search along direction $\delta\underline{d}_i$ which satisfies the condition

$$|[\delta\underline{d}_i]^T \underline{\psi}_{i+1}| \leq 0.5\, |[\delta\underline{d}_i]^T \underline{\psi}_i| \tag{6}$$

where $\underline{\psi}_{i+1}$ is found using the estimate $\underline{d}_{i+1}$. Often no line search is performed and η_i is taken as unity.

Various solution schemes are implemented in PLASAN using different approximation to the Jacobian matrix:

- KO $\quad \underline{K}_i$ is the initial elastic stiffness matrix
- NR $\quad \underline{K}_i = \underline{J}(\underline{d}_i)$
- KT1 $\quad \underline{K}_i = \underline{J}(\underline{d}_i)$
- KT2 for $i > 1$, $\underline{K}_i = J(\underline{d}_2)$

5.2 Quasi-Newton BFGS Methods

In PLASAN various Quasi-Newton BFGS methods are adopted in the form given by Matthies and Strang [5]. These methods seek to satisfy the secant condition

$$\underline{K}_i(\underline{d}_i - \underline{d}_{i-1}) = \underline{\psi}_i - \underline{\psi}_{i-1} \tag{7}$$

The BFGS update which does not destroy the banded nature of the stiffness matrix is given in the form

$$\underline{K}_i^{-1} = \{\underline{I} + \underline{w}_i \underline{v}_i^T\}[\underline{K}_{i-1}]^{-1} \{\underline{I} + \underline{v}_i \underline{w}_i^T\} \tag{8}$$

where

$$\underline{v}_i = \underline{\psi}_{i-1} \left\{1 + \left[\frac{\eta_{i-1}\, \delta\underline{d}_{i-1}^T \underline{\gamma}_i}{\delta\underline{d}_{i-1}^T \underline{\psi}_{i-1}}\right]^{\frac{1}{2}}\right\} - \underline{\psi}_i$$

$$\underline{w}_i = \delta\underline{d}_{i-1}/(\delta\underline{d}_{i-1}^T \underline{\gamma}_i)$$

and $$\underline{\gamma}_i = \underline{\psi}_i - \underline{\psi}_{i-1}$$

Equation (8) may be expanded and written in the form

$$\underline{K}_i^{-1} = \left[\prod_{j=i-1}^{1} \{\underline{I} + \underline{w}_j \underline{v}_j^T\}\right]\underline{K}_1^{-1} \left[\prod_{j=1}^{i-1} \{\underline{I} + \underline{v}_j \underline{w}_j^T\}\right] \tag{9}$$

In PLASAN the following variations are available

- QNKO $\underline{K}_1$ is the initial elastic stiffness matrix
- QNKT1 $\underline{K}_1 = \underline{J}(\underline{d}_1)$
- QNKT2 $\underline{K}_1 = \underline{J}(\underline{d}_2)$

Thus in QNKT2 the updates begin after the first iteration.

Crisfield [8] has suggested various Secant-Newton (SN) methods. In one of these equation (8) is used and $\underline{K}_{i-1}$ is always taken as $\underline{J}(\underline{d}_1)$. A major attraction of this method is that no previous values of $\underline{v}_i$ and $\underline{w}_i$ need be stored.

5.3 Arc length methods

Recently arc length methods have gained much popularity due to their ability to deal with geometrically nonlinear problems involving snap-through and snap-back behaviour [8-10]. The normal plane (NP) and spherical path (SP) variants are both implemented in PLASAN. In the normal plane method within a given increment the solution is constrained to lie in a plane normal to the tangent to the equilibrium curve at the beginning of the increment. In the spherical path method the solution is constrained to lie on a sphere of radius equal to the arc length which is defined as

$$\ell = [\Delta\underline{d}_1^T \Delta\underline{d}_1 + (\Delta\lambda_1)^2 \underline{f}^T \underline{f}]^{\frac{1}{2}} \tag{10}$$

In both the NP and SP methods it is necessary to evaluate updates $\delta\lambda_i$ which adjust the total load level for the increment. The arc length may be updated from increment to increment and Ramm [9] suggests the use of the equation in which the current arc length at load step n is given as

$$\ell^{(n)} = \ell^{(n-1)} (I_D/I^{(n-1)})^{\frac{1}{2}} \tag{11}$$

where I_D is the desired number of iterations per load step and $I^{(n-1)}$ is the actual number of iterations required in the previous load step. Further details of the methods are given elsewhere [8-10].

5.4 Convergence and final failure

Displacement, residual force and energy norms are used to check convergence in PLASAN. Final failure is assumed to occur when the current stiffness parameter [11] (which is a parameter that characterizes the overall stiffness of the slab) is less than some specified value.

Table II Solution time comparisons for Mueller slab

ALGORITHM	CPU		
	1.0%	0.1%	0.01%
K_O	41	123*	73*
NR	67	88✱	146✱
KT1	35	79*	101*
	(34)	(71)	(109)
KT2	30	37✱	46✱
	(35)	(45)	(61)
QNKO	29	49	64
QNKT1	32	37	44
	(35)	(52)	(66)
QNKT2	32	34	42
	(35)	(41)	(59)

* Failed to converge after 50 iterations

( ) Values with line search

✱ Premature structure failure

6. EXAMPLES

6.1 Mueller slab

This section is devoted to a comparison of different solution schemes for reinforced concrete plates. All methods are implemented in the same computer program so that all tasks - apart from those peculiar to the particular algorithm adopted - are accomplished in exactly the same way.

A corner supported doubly reinforced concrete slab tested by Mueller [12] is analysed using a 3x3 mesh in a symmetric quadrant. Numerical experiments are then carried out to test the accuracy and efficiency of the different solution algorithms suggested in this paper. Large load increments have been used and only 6 nonlinear increments are required. A summary of the results is given in Table II, while the load-central deflection curves of the slab are given in Figure 1. A study of the results shows that the use of KO with a coarse convergence tolerance (1.0%) results in over-stiff behaviour in the final stages of loading and an overestimation of the failure load. The rest of the algorithms, when they work, predict practically the same displacements regardless of the convergence tolerance used ($\leq$ 1.0%). However, it should be noticed that the convergence of the solution when KO is adopted is very slow and that the solution fails to converge within the specified number of iterations at a lower load level when a tighter convergence tolerance is used. Newton-Raphson and Modified Newton-Raphson - KT2 - methods indicate premature failure when fine convergence tolerances are used. The convergence of KT1 is also very slow at the later stages of loading. However when line searches are used with these methods reliable solutions are obtained. Methods based on BFGS updates always converge to the required convergence tolerance at a minimum cost. The use of BFGS updates with KO and a convergence tolerance of 1% renders the cheapest analysis for this slab and also retains all the advantages of using KO such as the possibility of elastic unloading, etc. If a finer convergence tolerance is required the BFGS - KT2 algorithm may be chosen. In the present example, the tension stiffening effect of reinforced concrete is exploited and on cracking the concrete is only allowed to release its tensile stresses gradually according to the tension stiffening curve shown in Figure 1. However, if the tension stiffening of reinforced concrete is not considered, or if only a small amount of stiffening is allowed, then the cracking of the concrete becomes severe resulting in large residual forces and the value under the square root in (8) may become negative preventing the use of the BFGS update. This situation occurred during another numerical experiment on a simply supported plate tested experimentally by Taylor et al [13]. Here a line search helps the BFGS updates to be applied and reduces the analysis cost considerably.

6.2 McNiece slab

Another numerical experiment is carried out using the well known corner supported McNiece slab [14] which has been tested numerically by many analysts. In this experiment a comparison is made between MNR, KT1 method and other methods used in conjunction with it, such as the Secant-Newton (SN2), the Quasi-Newton (QNKT1) and the spherical path (ARC-SP) methods. The automatic load incrementation is used first with the arc method, then the other techniques are used with the same prescribed increments. The displacement norm is used to check for convergence with a tolerance of 0.1%. The displacements predicted by the different techniques are almost identical and in good agreement with the experiment, see Figure 2. The cost of the analysis differs dramatically. In the KT1 method the solution fails to converge within the specified number of iterations and the Secant and Quasi-Newton methods do equally well. The superiority of the arc method in this problem is clear. However, it must be noted

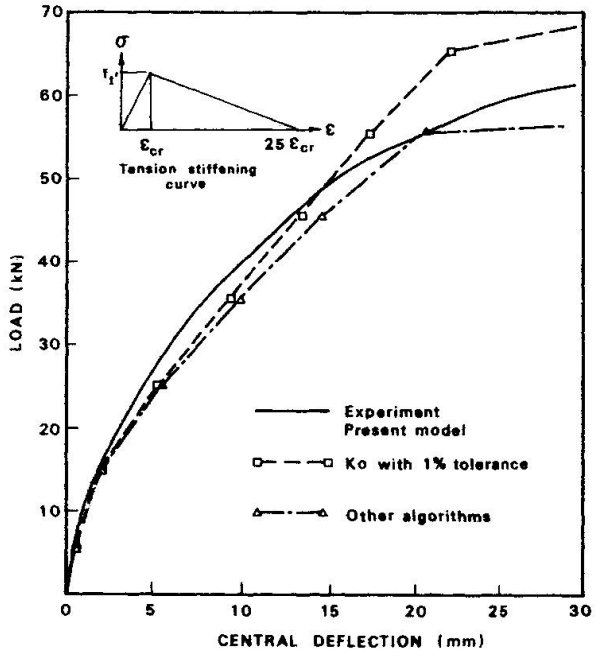

Figure 1 Load-central deflection curve for the Mueller slab

ALGORITHM	KT1	QNKT1	SN2	ARC-SP
CPU	> 146	108	102	72

CPU TIME FOR DIFFERENT ALGORITHMS

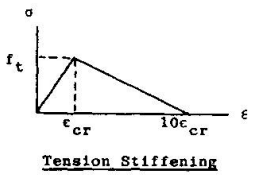

Tension Stiffening

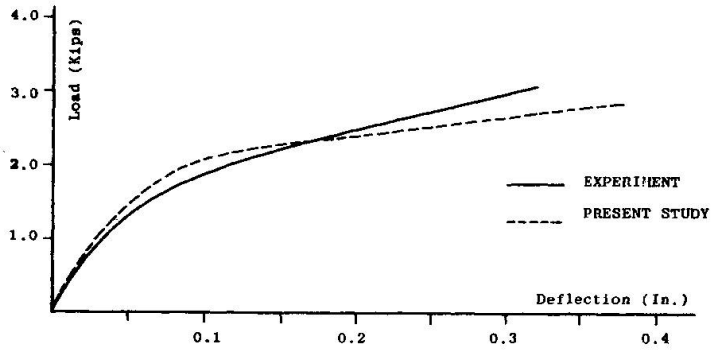

Figure 2 Load-central deflection curve for the McNeice slab and comparison of various algorithms

that when the tension stiffening effect of reinforced concrete after cracking is not fully exploited, and there is an instantaneous loss of strength, numerical difficulties may be anticipated. The use of line searches and relatively coarser convergence tolerances, together with some restart criteria to safeguard against divergence of solution, could be advantageous.

7. CONCLUSIONS

From the results discussed in the previous section and from other experience, it can be concluded that the use of the initial stress method in the nonlinear analysis of reinforced concrete plates with coarse convergence tolerances may result in an overestimation of the failure loads. The use of BFGS updates with the initial stiffness method, or Modified Newton-Raphson methods, is suggested for a reliable and relatively inexpensive nonlinear analysis of reinforced concrete plates if tension stiffening of concrete is considered. The use of line searches with methods based on BFGS updates is recommended if the tension stiffening of reinforced concrete is not considered. The arc length and Secant Newton methods also show promise.

REFERENCES

1. ABDEL RAHAMN, H. H. and HINTON, E.; "User manual for program - PLASAN", Report Dept. of Civil Eng., Swansea, June 1981.

2. HUGHES, T. J. R. and COHEN, M.; "The Heterosis finite element for plate bending", Computers and Structures, Vol. 9, 1978, pp.445-450.

3. HUGHES, T. J. R. and TEZDUYAR, T. E.; "Finite elements based upon Mindlin plate theory with particular reference to the four-node bilinear isoparametric element", to appear in J. Appl. Mech.

4. WONG, T. K.; "Nonlinear analysis of reinforced concrete slab systems using cubic Mindlin plate elements", M.Sc. Thesis, University College of Swansea, Jan. 1981.

5. MATTHIES, H. and STRANG, G.; "The solution of nonlinear finite element equations", Int. J. Num. Meth. in Engng., Vol. 14, 1979, pp.1613-1626.

6. BATHE, K. J. and CIMENTO, A.; "Some practical procedures for the solution of nonlinear finite element equations", Comp. Meth. in Appl. Mech. Eng., Vol. 22, 1979.

7. ENGELMAN, M. S., STRANG, G. and BATHE, K. J.; "An application of Quasi-Newton methods in fluid mechanics", to appear in Int. J. Num. Meth. in Engng., 1981.

8. CRISFIELD, M. A.; "Incremental/iterative solution procedures for nonlinear structural analysis", Proceedings of the Int. Conf. on Numerical Methods for Nonlinear Problems, University College of Swansea, Pineridge Press, 1980, pp.261-290.

9. RAMM, E.; "Strategies for tracing nonlinear response near limit points", Institut für Baustatik der Universität Stuttgart, W. Germany, 1980.

10. HINTON, E. and LO, C. S.; "Large deflection analysis of imperfect Mindlin plates using the modified Riks method", MAFELAP 1981, May, 1981. Proceedings to be published by Academic Press.

11. BERGAN, P. G.; "Solution algorithms for nonlinear structural problems", Computers and Structures, Vol. 12, 1980, pp.497-509.

12. MUELLER, G.; "Numerical problems in nonlinear analysis of reinforced concrete", UC-SESM Report No. 77-5, University of California, Sept. 1977.

13. TAYLOR, R., MAHER, D. R. H. and HAYES, B.; "Effect of the arrangement of reinforcement on the behaviour of reinforced concrete slabs", Magazine of Concrete Research, Vol. 18, No. 55, June 1966, pp.85-94.

14. JOFRIET, J. C. and McNIECE, G. M.; "Finite element analysis of reinforced concrete slabs", J. Struct. Division, ASCE, Vol. 97, No. ST3, 1971, pp.785-807.

Leere Seite
Blank page
Page vide

Modelling of the Cracked Elastic State of Reinforced Concrete

Modélisation de l'état fissuré élastique du béton armé

Modellierung von Stahlbeton im Zustand II.

GYÖRGY IVÁNYI
o. Prof. Dr.-Ing.
Universität Essen
Federal Republic of Gerrmany

SUMMARY
Based on observations of tests and analytical experiences, simple assumptions for a realistic description of the cracked elastic state of reinforced concrete are proposed.

RÉSUMÉ
A partir des observations expérimentelles et des expériences analytiques on propose des dispositions simples pour décrire le comportement réel du béton armé dans l'état fissuré élastique.

ZUSAMMENFASSUNG
Ausgehend von Versuchsbeobachtungen und rechnerischen Erfahrungen werden einfache Einsatze zur wirklichkeitsnation Erfassung des elastisch gerissenen Zustandes von Stahlbeton vorgeschlagen.

1. INTRODUCTION

Constitutive models of cracked reinforced concrete are numerously known. A survey of usual assumptions is found by Eibl and Iványi [6], Gerstle [8] , Argyris et al [1]. A special field of modeling is the phase of cracked elastic state with the following characteristics:

- progressive cracking, possibly perament change of crack orientation
- linear-elastic steel behavior
- significant effect of tension stiffening on the deformation behavior
- increasing non-linear behavior of concrete in compression.

In particular, the progressive cracking causes large changes of stiffnesses which requires an incremental load increase for numerical analysis to keep the stability of the solution. Additional difficulties are to note down at iteration processes relative to permanent changes of crack orientations and the appearance of secondary cracks. Often the appropriate realistic physical basis to judge these questions is missing, too. The consideration of bond between reinforcing bars and concrete for an analytical model needs special reflections because realistic physical assumptions, such as Ngo and Scordelis [14], go numerically to great expense. Just the same remark is valid for aspects of shear transfer through the crack due to aggregate interlock and dowel action.

In the following, some simplifying statements of the modeling of reinforced concrete constructions in the cracked elastic state are discussed, basing on the results of many tests on reinforced slabs of realistically dimensions and analytical experience with finite-element methods.

2. EXPERIMENTAL RESULTS

Tests on various two-way reinforced concrete slabs and panels are connected with numerous experimental problems. Most of the previous

results are faulty or useless as the profound analysis of Lenschow [13] has shown because the test rig restrains the deformation of the test slabs. The tests of Lenschow and the later ones of Clark [5], too, are mainly used for formulating yield criteria; the small scale of test specimens does not allow conclusions for the cracked elastic state. For answering the questions of

- primary and secondary crack formation
- crack orientation
- crack width

and solving the problem of section designing and analytical modeling, Kordina and Iványi have directed investigations in Braunschweig on uni- and biaxial bending tests on slabs ($M_2 = 0$ respectively $M_2/M_1 = -1$). The test specimens have a thickness of d = 14 cm and are two-way reinforced.

In the following only a few results concerning the cracking process and crack orientation are discussed.

The test specimen and the testing conditions for $M_2 = 0$ - developped by Lenschow - are shown in fig. 1. Torsional moments ($M_2/M_1 = -1{,}0$) are brought up in a similar way.

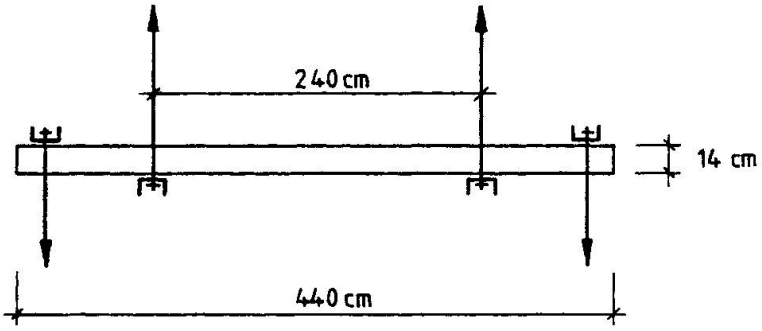

Fig. 1 Test slab

For various orientation of reinforcing steel to the principal moments with isotropic and orthotropic arrangement of reinforcement, strains of concrete and steel and crackwidth in several hundreds of places are measured. The load is brought up incrementally till yield state of reinforcement. The crack orientations are analysed by a stereometric method basing on Stroeven [17], for every load increment all together and also for every single one. Therefore, in Angle intervals of 10° a grid plan is revolved

round one point and the number of cuts along every line is summed up. The main crack orientation is to be found at the minimum number of cuts (fig. 2). This method is the only reliable one, the experience of the past has shown that many not serios estimations yield to faults.

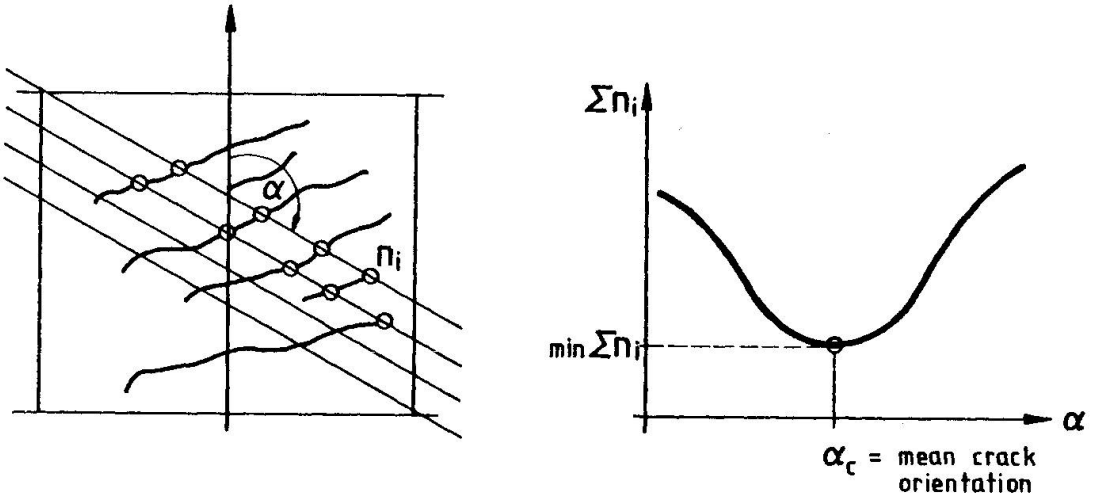

Fig. 2 Finding of crack orientation

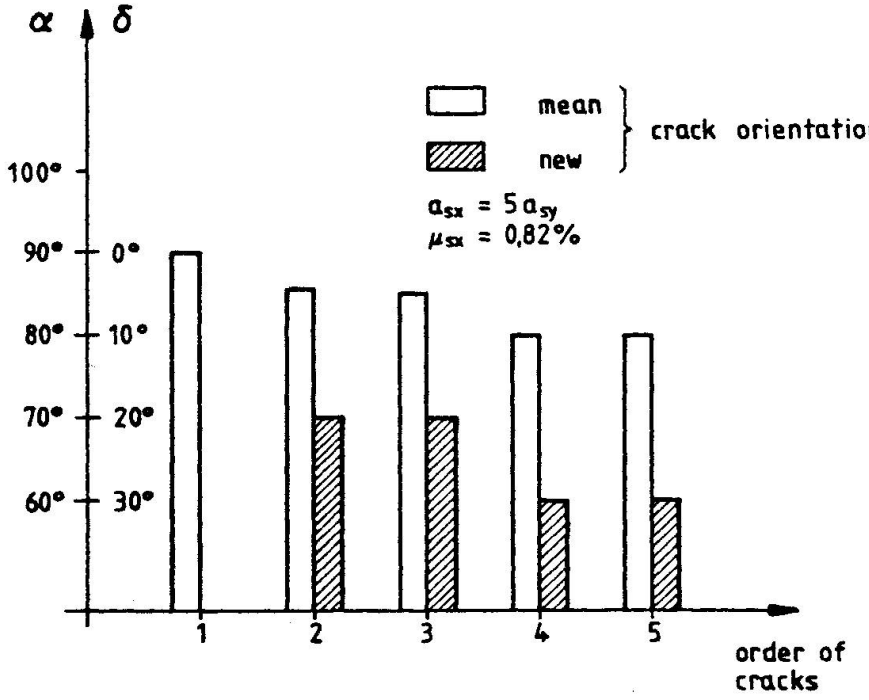

Fig. 3 Analyse of crack orientation (Test slab No.7, notations s. Fig. 6)

Fig. 3 shows the change of crack orientation of an anisotropic reinforced and uniaxial stressed slab ($M_2 = 0$) for every increment alone and the main crack orientation, too. The result shows that the secondary crack orientation causes only small changes concerning the main crack orientation, although the influence is most clear on that demonstrated marked anisotropy.

3. DISCUSSION OF TEST RESULTS

Baumann [2] takes the view that shear transfer along the primary cracks causes the development of secondary cracks with the result of a main crack orientation corresponding to H = O in the elastic cracked condition (fig. 4). This assumption is not realistic because shear forces along the crack can make only further cracks under very high reinforcing ratio.

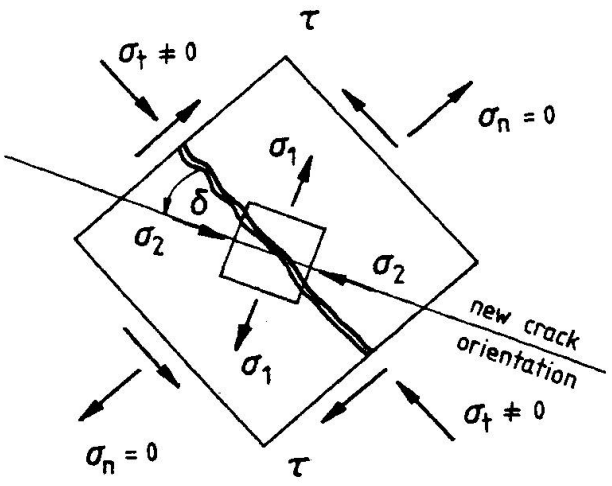

Fig. 4 Formation of secondary cracks according to Baumann [2]

To clarify the most important parameters concerning the secondary cracking, Fastabend [7] made investigations on a plain-stress model to define the state between two primary cracks. The reinforcing bars (truss elements) have been connected with nodal points of membrane elements by the aid of bond links (beam elements). Therefore, a linearizising bond law of Noakowski [15]was used. The edge forces have been developped on the equilibrium and compatibility conditions based on Baumann with the assumption of various shear stiffness for uniaxial tension. The model is shown in fig.5. Some analytical results are comparable with experiments. Table 1 shows the covering of both of them. The colums "main crack orientation" indicates that there is no fundamental change on the primary crack orientation caused by the development of secondary cracks. Analytical solutions for secondary crack orientations,

Table 1

Spec. No	$\frac{a_{sx}}{a_{sy}}$	α	cal δ	meas δ	mean δ	μ_{sx} [%]
7	5	30°	19°	20°	5°	
4	5	45°	11°	10°	0°	0,82
9	1	30°	11°	10°	5°	

(Notations see Fig. 6)

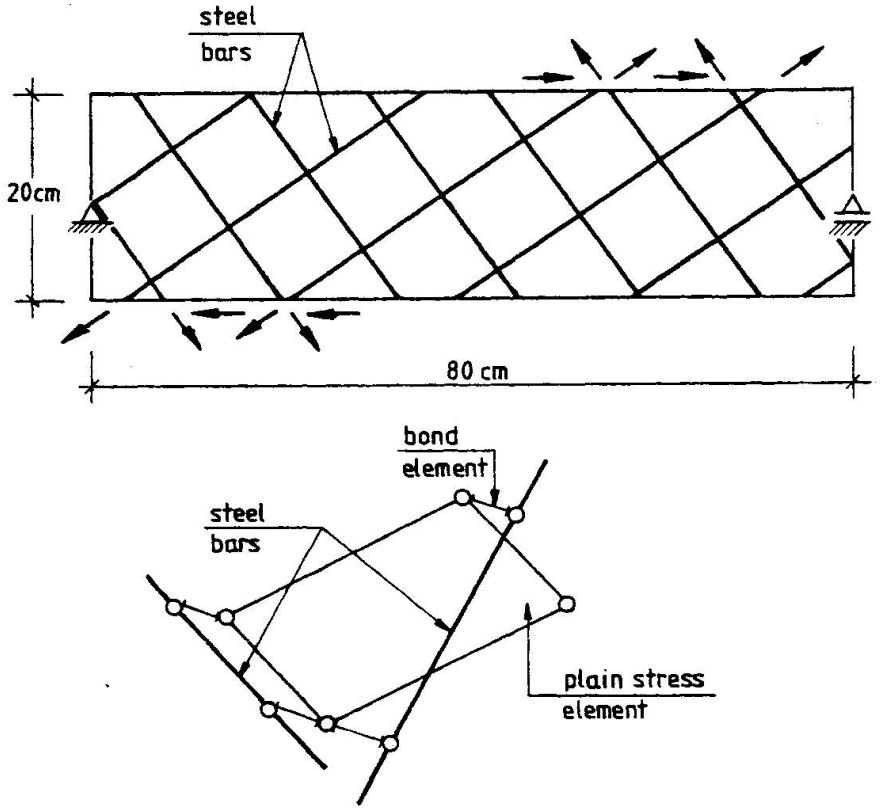

Fig. 5 Finite Element Model for analytical study of crack orientation [7]

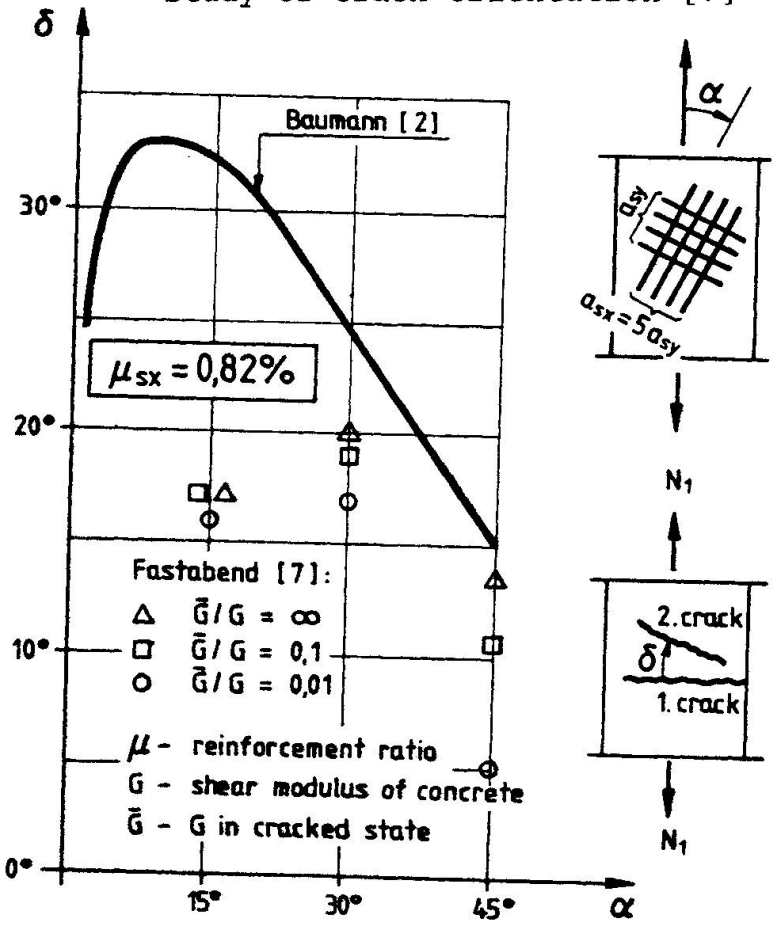

Fig. 6 Comparisation of the results according to [2] and [7]

according to [2] and [7], depend on the orientation of reinforcing steel to the principal moments for uniaxial bending are compared in fig. 6. The secondary crack orientation based on Baumanns solutions, as can be seen, indicate a fundamentally different development.

Similar results confirmed by Gilbert and Warner [9] show that secondary cracks with new orientations do not arise even throught assumption of any shear stiffness. Only a true modeling of bonding yields a physically correct behavior of the cracked elastic state (see 4.3).

4. PROPOSAL MODELING OF CRACKED ELASTIC STATE

4.1 Primary crack conditions

The tensile strength of concrete varies in dependence on special facts such as concrete quality (Rüsch [16]) and stress state (Kupfer et al [12]) statistic parameters as there are size effects (Bažant [3]) and last not least on the strain gradient (Iványi [10]). Most of these influence are not taken into consideration for numerical analysis because the detailed strength dates are missing. Even the check on a real experiment does not allow statements that the tensile strengthes found out on test specimens yield a realistic crack condition.

Another problem of numerical analysis is the fact that cracking in equally stressed fields begins nearly at the same time which may cause an instability of numerical analysis. In reality, these phenomena do not arise because the tensile strength of concrete is a stochastic variable.

Knowing these problems the following recommendation is made in order to describe the primary cracking on FEM analysis with "smeared" cracks.

- Proceeding from an ingeniously mean value of concrete tensile strength, there are to generate, e.g. according to the Gaussian distribution, individual tensile strengthes of elements or layers by the aid of a random generator in a very simple way.

Consequence of the different tensile strengths of each element is the development of cracks in the calculation only by degrees which does not mean instability for the analytical model.

Usually that order prevents that elements or layers appear cracked and uncracked by turns within the iteration cycles.

- The element tensile strengthes shall be valid irrespective of the stress state. Knowing the scatter of test results, too many specifications of dependences are superfluous.

- The primary crack orientation is to be chosen perpendicularly to the largest main strain of the element. Variability of primary crack orientations during iterations cycles are to be prevented.

- At stress states $\sigma_1/\sigma_2>0$ an orthogonal double cracked condition is to be supposed at the beginning of $\sigma_2>0{,}6\div0{,}8\cdot\sigma_1$ because this behavior is corresponding to the experiments (s. Lenschow's isotatic tests).

4.2 Secundary crack conditions

Following the results in part 2 of this paper it can be said that the development of new cracks in different direktions does not influence the behavior of the specimen fundamentally (Fig. 3). Numerically, this behavior is to be realized only in an insufficient way if smeared cracks are supposed because in an analytically double cracked state an unrealistic element behavior occurs. That does mean that at the numerical analysis the possibility of progressive cracking should be limited to prevent a physically wrong behavior. In the following some different ways are shown:

- a simple method to prevent "numerical" secondary cracks is to pull up the tensile strength of a primary cracked element, for example about 30 p.c.
- Another solution is to allow secondary cracks only above a divergence of 30° from primary crack orientation.

In both cases, a double cracked condition appears only if stronger emcompassments are caused as a result of the cracks occured or changing of the loading conditions. If such behavior is to be excluded at all (s. Jofried and McNeice [11]), it is also justified to renounce on further control concerning the tensile stress of primary cracked elements.

4.3 Consideration of bond

Usually, the calculation of complete constructions on micro-idealizing of bond (Ngo and Scordalis [14])must be resigned.

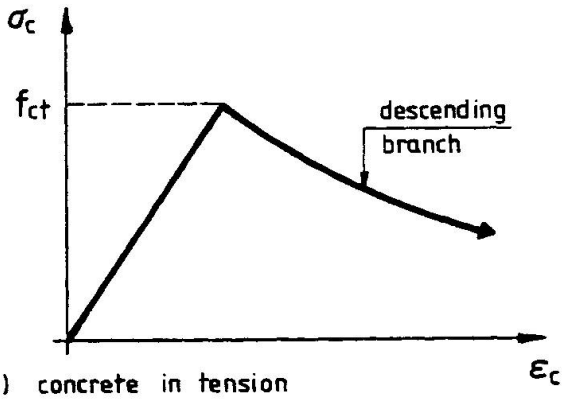

Fig. 7 Assumptions for tensile stiffening of reinforced concrete

A simple possibility is to consider tension stiffening

- to get a falling branch of the stress-strain-line of concrete intension

or

- to simulate the dependence of steel stress on average steel strains (fig. 7).

Physically, the consideration of bond at the reinforcing level is to be prefered: In multi-axial stress states the only way for describing the realistic concrete stress states is to do it that way. Gilbert and Warner [9] report moreover about the expectation of numerical advantages resulting from the restriction of the number of iterations on the steel layer concerning this method. In that way, stress transfer perpendicular to the crack orientation on the concrete elementis impossible.Nevertheless for the correct calculation of

the stresses in a cracked concrete element, it is necessary to add the strain differences of the steel layers $\Delta\varepsilon=\varepsilon_s-\varepsilon_m$ (fig. 7) as strain producer in direction of the reinforcing bars.

4.4 Shear stiffness in cracked state

The physical connection between crack width and crack shear stiffness is complicated and not exact definiable. Furthermore , numerous analytical results show no particular influence on the mechanical behavior of the varied shear stiffnesses with in far limits. Nevertheless, numerical reasons require a minimum of shear stiffness to avoid accidental instabilities of analysis.

With regard to these discussions very sofisticated assumptions concerning the shear stiffness are not recommendable. Basically in the analysis of once or double cracked elements $\beta=\bar{G}/G=0,2\div0,4$ has to be set.

REFERENCES

1. ARGYRIS, J.H., FAUST, G., WILLAM, K.J.: Finite element modeling of reinforced concrete structures, IABSE Colloquium, Delft 1981, Reports of the Working Commissions, Vol. 33, pp. 85-106
2. BAUMANN, T.: Tragwirkung orthogonaler Bewehrungsnetze beliebiger Richtung in Flächentragwerken aus Stahlbeton, Schriftenreihe des DAfStb., Heft 217, Berlin 1972
3. BAŽANT, Z.P.: Instability, ductility and size effect in strain-softening concrete, Journal of the Eng. Mech. Div., ASCE, Vol. 102, No. EM2, April 1976, pp. 331-344
4. BAŽANT, Z.P.: Advances in deformation and failure models for concrete, IABSE Colloquium, Delft 1981, Reports of the Working Commissions, Vol. 33, pp. 9-39
5. CLARK, L.A.: Tests on slab elements and skew slab bridges, Cement and Concrete Association London, Technical Report 42.474, Sept. 1972
6. EIBL, J., IVANYI, G.: Studie zum Trag und Verformungsverhalten von Stahlbeton, Schriftenreihe des DAfStb., Heft 260, Berlin 1976

7. FASTABEND, M.: Rißverhalten und Spannungsverlauf von schiefwinkelig zur Hauptnormalrichtung bewehrten Stahlbetonscheiben, Diplomarbeit an der Universität Essen, Februar 1981
8. GERSTLE, K.: Material modeling of reinforced concrete, IABSE Colloquium, Delft 1981, Reports of the Working Commissions, Vol. 33, pp. 41-61
9. GILBERT, R.I., WARNER, R.F.: Tension stiffening in reinforced concrete slabs, Journal of the Structural Division, ASCE, Vol. 104, No. ST12, Dec. 1978, pp. 1885-1900
10. IVANYI, G.: Effect of a strain-gradient on the tensile strength of concrete, Paper A 5-1, Second International Conference on "Mechanical Behavior of Materials", Boston 1976
11. JOFRIET, J.C., McNEICE, G.M.: Finite element analysis of reinforced concrete slabs, Journal of the Structural Division, ASCE, Vol. 97, No. ST3, March 1971, pp. 785-806
12. KUPFER, H., HILSDORF, H.K., RÜSCH, H.: Behavior of Concrete under biaxial stress, ACI Journal, Proc. Vol. 66, No. 8, Aug. 1969, pp. 656-666
13. LENSCHOW, R.J.: A yield criterion for reinforced concrete under biaxial moments and forces, Dissertation, University of Illinois, Urbana, Illinois, 1966
14. NGO, D., SCORDELIS, A.C.: Finite element analysis of reinforced concrete beams, ACI Journal, Proc. Vol. 64, No. 3, March 1967, pp. 152-163
15. NOAKOWSKI, P.: Die Bewehrung von Stahlbetonbauteilen bei Zwangbeanspruchung, Dissertation, Technische Universität München, 1977
16. RÜSCH, H.: Die Ableitung der charakteristischen Werte der Betonzugfestigkeit, beton, Heft 2, Febr. 1975, pp. 55-58
17. STROEVEN, P.: Some aspects of the micro-mechanics of concrete, Stevin Laboratory, Technologycal University of Delft, 1973

Leere Seite
Blank page
Page vide

Modelling of Viscoelastic Properties of Reinforced Concrete

Simulation des propriétes viscoélastiques du béton armé

Modellierung der viskoelastischen Eigenschaften des bewehrten Betons

LICHARDUS, S.,
Struct. Eng., C. Sc., Leading Research Worker, Institute of Construction and Architecture of Slovak Academy of Sciences,
Bratislava, Czechoslovakia.

SUMEC, J.,
Struct. Eng., RNDr., C. Sc., Senior Research Worker, Institute of Construction and Architecture of Slovak Academy of Sciences,
Bratislava, Czechoslovakia.

SUMMARY
The authors have developed a method of analysis allowing for the non-homogeneity of the structural material and the location of the reinforcement. It deals with the so-called Layer Finite Strip Method. The material characteristics of each strip are different and the material of the strips may even be anisotropic. The physical properties of the material are simulated on the basis of the linear theory of viscoelasticity and the theory of reinforcement. Using the method of identification, the influence of cracks was included in the material characteristics.

RÉSUMÉ
Les auteurs du mémoire ont élaboré une méthode de calcul permettant de prendre en considération la nonhomogénéité des matériaux et de l'armature. Il s'agit d'une méthode de bandes finies où les caractéristiques des bandes individuelles diffèrent et les matériaux peuvent être anisotropiques aussi. Les propriétes physiques des matériaux sont simulées selon la théorie linéaire de visco-élasticité et la théorie de l'armature. Les auteurs ont appliqués la méthode d'identification pour dériver les caractéristiques du matériau dans la zône sollicitée à la traction et à la compression en tenant compte de l'effect des fissures.

ZUSAMMENFASSUNG
Die Autoren entwickelten eine Berechnungsmethode, die die Nichthomogenität des Konstruktionsmaterials und der verwendeten Bewehrung berücksichtigt. Es handelt sich um die Methode der finiten geschichteten Streifen, wobei die Materialcharakteristiken in den einzelnen Streifen verschieden sind. Das Material kann in den Streifen auch anisotrop sein. Die physikalischen Eigenschaften des Materials sind auf Grund der linearen viskoelastischen Theorie und der Bewehrungstheorie modelliert.
Mittels der Methode wurden die Charakteristiken des Grundmaterials in der Zug- und Druckzone mit integraler Berücksichtigung des Einflusses von Rissen abgeleitet.

1. INTRODUCTION

We will analyse the state of stress and strain of layered two-dimensional structures. By deriving of the basic equations we considered the material viscoelastic and the displacements small and continues. The analysed structure is imaginary divided into finite number of layers. Each layer has different material properties, but constant within the region of particular layer.

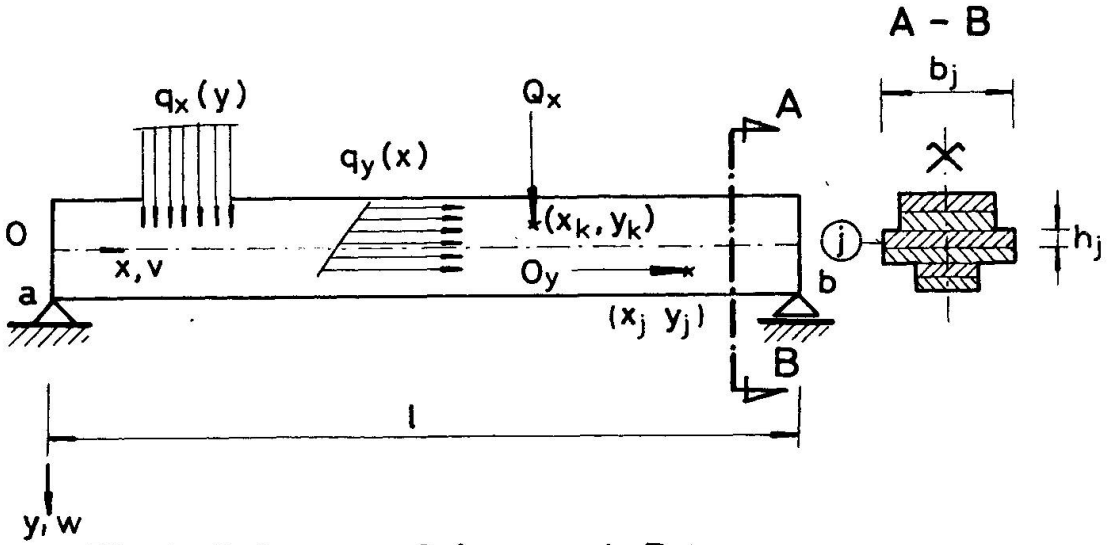

Fig.1. Scheme of Layered Beam

Material properties of each layer were simulated using the rheological models and the theory of reinforcement [1 - 3].

2. LAYER FINITE STRIP METHOD /LSFM/

From the mathematical point of view is our problem formulated as follows: We have to find the set of vector-functions $\{\tilde{\sigma}_m(x,y,t)\}$ for each $m = 1, 2, 3, \dots, \nu$, where ν is a total number of layers.

This set of vector functions $\{\tilde{\sigma}_m(x,y,t)\}$ and corresponding stress $\{\tilde{\sigma}_m(x,y,t)\}$ satisfies the equilibrium conditions and also given boundary conditions. The applied method is based on the well known idea, to minimize the energetical potencial of the associated problem $\tilde{\Phi}$ [4, 5] /tildas denote the Laplace transform/ over a finite space of functions $V_N \subset V$, where V is the infinite dimensional space. V will be the subspace of a Sobolev space $W_2^{(2)}(\Omega)$ generated by all functions from $W_2^{(2)}(\Omega)$, which satisfy the main /also stable/ boundary conditions for the associate elastic problem. Similar conditions are also for the Finite Element Method for viscoelastic structures [6, 7].

Necessary condition for the existence of the minimum of functional $\tilde{\Phi}$ of the given associated problem is

$$\frac{\partial \tilde{\Phi}}{\partial \tilde{\delta}} = 0 \qquad \tilde{\delta} = (\tilde{\delta}_1, \tilde{\delta}_2, \ldots, \tilde{\delta}_N)^T \tag{1}$$

where

$$\tilde{\Phi} = \frac{1}{2}\tilde{\delta}^T \tilde{K} \tilde{\delta} - \tilde{\delta}^T \tilde{F} = \tilde{W} + \tilde{U} \tag{2}$$

and

$\tilde{\Phi}$ - total potential energy
$\tilde{K}$ - stiffness matrix
$\tilde{F}$ - load vector
$\tilde{W}$ - potential energy due to external forces
$\tilde{U}$ - strain energy

Suitable set of displacement functions satisfy the given boundary conditions and also linear changes of displacements v and w across the thickness of the particular layers we will choose in the form [3]

$$\begin{Bmatrix} \tilde{v}_i \\ \tilde{w}_i \end{Bmatrix} = \sum_{n=1}^{s} \begin{bmatrix} 1-\bar{x}_i, \bar{x}_i, 0, 0 \\ 0, 0, 1-\bar{x}_i, \bar{x}_i \end{bmatrix} \begin{Bmatrix} \tilde{v}_{1i} \\ \tilde{v}_{2i} \\ \tilde{w}_{1i} \\ \tilde{w}_{2i} \end{Bmatrix} \times \begin{matrix} [Y_n(y)]' \\ [Y_n(y)] \end{matrix} \tag{3}$$

where

$\bar{x}_i = x/b_i$
b_i - is a width of the i - strip /layer/
s - is a number of members of trig. series

and $\tilde{v}_{1j}$, $\tilde{v}_{2j}$, $\tilde{w}_{1j}$, $\tilde{w}_{2j}$ are displacements parameters, location of which is indicated od Fig. 1.

$Y_n(y)$, $Y_n'(y)$, / $n = 1, 2, \ldots, s$ /are the basic functions and their first derivatives, and must a priori satisfy given boundary conditions for $y = 0$ and $y = l$. In our case

$$Y_n(y) = \sin(n\pi y/l).$$

The system of linear algebraic equations, derived on the above mentioned basic assumptions, solution of which is the set of vector functions $\{\tilde{\delta}\}$ ha formaly the same form for Finite Elements Method /FEM/ and also for Layer Finite Strip Method /LFSM/

$$[\tilde{K}]\{\tilde{\delta}\} = \{\tilde{F}\} \tag{4}$$

but stiffness matrix for FSM has the form

$$[\tilde{K}] = \int_{\Omega} [B]^* [\tilde{D}][B] \, d\Omega \tag{5}$$

and for LFSM

$$[\tilde{K}] = \sum_i \sum_k [\tilde{K}_{i(k)}] = \sum_i \sum_k \left(\sum_n [\tilde{K}_{i(k)n}] \right) \tag{6}$$

where

$$[\tilde{K}_{i\otimes n}] = \int_0^l \int_0^{b_i} \int_0^{h_k} [B_{i\otimes n}]^* [\tilde{D}_{i\otimes n}][B_{i\otimes n}]\, dx\, dy\, dz \qquad (7)$$

and $[B]$ is strain matrix.

In both cases the determination of property matrix is very important and requires adequate attention.

3, DERIVATION OF PROPERTY MATRIX

As a spatial case we consider standard linear viscoelastic material where

$E^{ijkl}_{(\alpha)}$ is a tensor of moduli of elasticity

$\eta^{ijkl}_{(\alpha)}$ is a tensor of moduli of viscosity

We assume, that the Maxwell element /of linear viscoelastic material, or called also Zener s material/ has a homogeneus relaxation spectrum and hence it holds

$$\eta^{ijkl}_{(\alpha)} = K E^{ijkl}_{(\alpha)} \qquad (8)$$

where K is the inverse value of relaxation time of the material of the structure. According to [8], this model is appropriate, under some simplifications, for the expression of concrete.

The differential equation describing this model is

$$K(E^{\alpha\beta\gamma\delta}_{(1)} + E^{\alpha\beta\gamma\delta}_{(2)})\dot{\varepsilon}_{\gamma\delta} + E^{\alpha\beta\gamma\delta}_{(1)}\varepsilon_{\gamma\delta} = K\dot{\sigma}^{\alpha\beta} + \sigma^{\alpha\beta} \qquad (9)$$

After Laplace transform of equation (9) where $p_i = 1/\tau_i$ is parameter of Laplace transform and tildas denote this transformation we obtain

$$(p + \frac{1}{K})\tilde{\sigma}^{ij} = [p(E^{ijkl}_{(1)} + E^{ijkl}_{(2)}) + \frac{1}{K}E^{ijkl}_{(1)}]\tilde{\varepsilon}_{kl} \qquad (10)$$

In contracted form, when we denote

$$E^{ij} = E^{ij}_{(1)} + E^{ij}_{(2)}$$

we obtain

$$\begin{aligned}
(p + \tfrac{1}{K})\tilde{\sigma}^{11} &= (pE^{11} + \tfrac{1}{K}E^{11}_{(1)})\tilde{\varepsilon}_{11} + (pE^{12} + \tfrac{1}{K}E^{12}_{(1)})\tilde{\varepsilon}_{22} \\
(p + \tfrac{1}{K})\tilde{\sigma}^{22} &= (pE^{12} + \tfrac{1}{K}E^{12}_{(1)})\tilde{\varepsilon}_{11} + (pE^{22} + \tfrac{1}{K}E^{22}_{(1)})\tilde{\varepsilon}_{22} \\
(p + \tfrac{1}{K})\tilde{\sigma}_{12} &= (pE^{66} + \tfrac{1}{K}E^{66}_{(1)})\tilde{\gamma}_{12}
\end{aligned} \qquad (11)$$

In the case of orthotropy and introducing a constracted form of E^{ij} we can rewrite equation (10)

$$[\tilde{\sigma}^{ij}] = (p + 1/K)^{-1} [d^{ij}][\tilde{\varepsilon}_{kl}] \tag{12}$$

where the matrix of viscoelastic coefficients is

$$d^{ij} = \begin{bmatrix} pE^{11} + \frac{1}{K}E^{11}_{(1)} & pE^{12} + \frac{1}{K}E^{12}_{(1)} & 0 \\ pE^{12} + \frac{1}{K}E^{12}_{(1)} & pE^{22} + \frac{1}{K}E^{22}_{(1)} & 0 \\ 0 & 0 & pE^{66} + \frac{1}{K}E^{66}_{(1)} \end{bmatrix} \tag{13}$$

The stresses in the elastic orthotropic two-dimensional structure we obtain from the known equation

$$[\sigma^{ij}] = [c^{ij}][\varepsilon_{kl}] \tag{14}$$

where the matrix $[c^{ij}]$ depends on the arrangement of reinforcing bars, or fibres. In the case, when the reinforced bars are arranged in two perpendicular directions, parallel with the directions of coordinate axes y and z, then the matrix $[c^{ij}]$ is in form (15). If we later suppose, that the standard linear viscoelastic model has isotropic material coefficients $E^{ijkl}_{(2)}$ and $\eta^{ijkl}_{(2)}$, /Maxwell element/ and coefficients $E^{ijkl}_{(1)}$ have orthotropic properties /elastic spring element/.

$$c^{ij} = \begin{bmatrix} \bar{E}^{11}A^{-1} & \bar{E}^{11}\mu_{21}A^{-1} & 0 \\ \bar{E}^{22}\mu_{21}A^{-1} & \bar{E}^{22}A^{-1} & 0 \\ 0 & 0 & G'_{12} \end{bmatrix}; \quad A = 1 - \mu_{12}\mu_{21} \tag{15}$$

If we introduce later

$$E^{ij}_{(1)} = \bar{E}^{ij}_{(1)} / (1 - \mu_{12}\mu_{21}) \tag{16}$$

where $\bar{E}^{ij}_{(1)}$ are moduli of elasticity calculated according to the theory of reinforcing [2] for the ideal structure made from the composite material, then we can easily determine the matrix $[d^{ij}]$, which fully describes the viscoelastic properties of the material considered.

4. NUMERICAL EXAMPLE

We investigated reinforcered concrete beams, simply supported and uniformly loaded with intensity $q = 3{,}43$ kN/m^2. The span of the beam was 3,60 m. Cross section 12 cm x 120 cm was divided

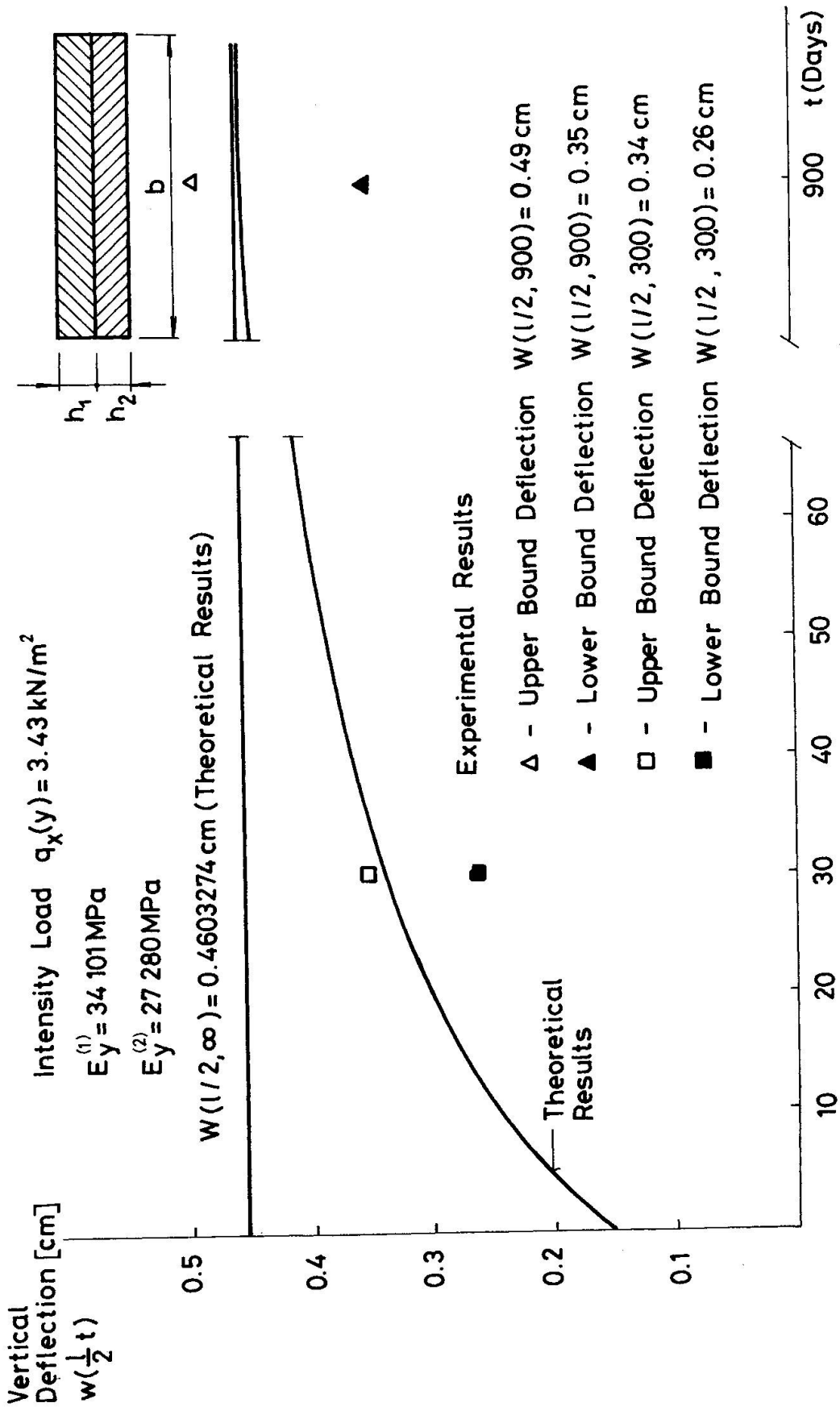

Fig.2. Vertical Time-dependend Deflection of Reinforced Concrete Beam

into two layers /Fig. 2/, where h_1 = 6,20 cm and h_2 = 5,80 cm.

The tension zone with depth h_2 bellow the neutral axes we considered weaken by cracks and microcracks. The material matrix was derived according to the method shown as above in part 3. Starting from the associated elastic problem to the viscoelastic one we used later in the inverse Laplace transform the displacement $w(x,y,t)$ from the experimental results [9]. Thus we could identify the modified stiffness of the layer in tension with cracks. From the Fig. 2 we can see that the theoretical solution of the deflection fits between upper and lower bound of experimental results for 30-days period, as well for 900-days period.

REFERENCES

1. LICHARDUS, S.: Modelling of viscoelastic properties of some composite materials /in Slovak/. Stavebnícky časopis, No. 26., VEDA Bratislava, 1978.
2. MALMEISTER, A.K., TAMUZ, V.P., TETERS, G.A.: Soprotivlenyje zostskych polimernych materialov. Izdat. Ziantne, Riga 1972
3. LICHARDUS, S., SUMEC, J.: Internal Research Report of ÚSTARCH SAV III-8-2/3.6 - 1980
4. BIOT, M.A.: Variational and Lagrangian Methods in Vicsoelasticity Deformation and Flow of Solids. IUTAM Coll. Madrid 1955, Springer Verlag, 1956
5. BRILLA, J.: Convolutional Variational Principles and Methods in Linear Viscoelasticity of Anisotropic Bodies. In: Proc.Int. Conf. Var. Method in Eng. Southampton 1972

Leere Seite
Blank page
Page vide

Man-Machine Interactive Analysis in Concrete Structures Using a Microcomputer

Une analyse interactive des structures en béton utilisant un micro-ordinateur

Mann-Maschine-Interaktionsanalyse von Stahlbeton mithilfe von Microcomputern

K. MAEKAWA
Graduate Student
University of Tokyo
Tokyo, Japan

J. YAMAZAKI
Associate Professor
Tokyo Metroplolitan University
Tokyo, Japan

T. SAKURAI
Advanced Numerical
Analysis Inc.
Tokyo, Japan

SUMMARY An interactive mode of operation using a microcomputer for nonlinear finite element analysis is presented. An example of how nonlinear phenomena can be analyzed using an interactive mode of computation is presented. The example predicts the nonlinear formation of cracks in a loaded concrete block. The calculated results closely resemble actual behaviour.

RÉSUMÉ
Cette étude présente une méthode d'opération interactive pour l'analyse non-lineaire par éléments finis au moyen d'un micro-ordinateur. L'exemple d'application prédit la formation de fissures dans un bloc en béton non-armé soumis à une charge uniaxiale. Les résultats calculés correspondent au comportement réel observé.

ZUSAMMENFASSUNG
Eine interaktive Methode für nichtlineare finite Elementeberechnungen mit einem Microcomputer ist gezeigt und auf das Beispiel der nichtlinearen Rissbildung in einem Betonblock angewandt. Die Rechenergebnisse stimmen mit dem wirklichen Verhalten gut überein.

1. INTRODUCTION

Recent and drastic developments of electronics have made inexpensive, but high performance, microprocessors available. This has made it possible for individuals to control the whole process of computer computation that previously could be handled only by large computers that were not readily accessible. This trend of using microcomputers for personal computation implies a possibility that the present inconvenient and cumbersome nature typical of analysis for concrete mechanics may become manageable and practicable. This paper discusses a "personal" method of analysis with reference to an example of numerical analysis. In the near future microcomputers will become a common tool for engineers. When compared to large computers, the microcomputers obviously suffer limitations in terms of computation abilities, various functions, and memory sizes. But on the other hand, because the individual users handle all-operations it might be more practical than present methods of analysis using large computers with the inconvenience of poor turn around time. The current limitation in computation ability of microcomputers will be reduced when the sixteen bit CPU that are already in existence become more generally available. The numerical computations described in this paper were performed on an 8-bit CPU microcomputer. The finite element program used is called FEMN (Finite Element Method of analysis for Nonlinear problems) and was developed by Sakurai as a part of the development work for NAPRA (Nonlinear Analysis Program Research Association). Several reports have been published on application of microcomputers for finite element methods of analysis, which include works by Wilson [1] and Yamada [2].

2. HARDWARE OF MICROCOMPUTER SYSTEM

A microcomputer system for analysis is shown in Fig.1. The basic requirements are a CPU with a memory unit, a display, a keyboard, an extended memory and a printer. A plotter or other graphics equipment is desirable. The memory required is about 64 k bytes of RAM and about 1 M bytes for the extended memory for finite element analyses. The capacity of this system can be expanded by connecting it to a large size computer through a sonic coupler and communication line.

3. CHARACTERISTICS OF MICROCOMPUTERS

The followings are meritorious features of microcomputers when compared to common usage of large computers.

3.1 Creation of algorithms

The personalized computers can be used exclusive by an individual or a small group of people. This makes it convenient and easy to develop programs, to debug, or to correct algorithms. The algorithms are portable when written in a common language such as FORTRAN and therefore can be run on large computers.

3.2 Economy

The major operating cost of microcomputers is for electricity. The initial cost for the system shown in Fig.1. is about 6,000 US dollars, which is affordable for a small group of people or an individual. This investment can be justified in the long term from a view point that most of the time for research work the microcomputers will be used for developing programs. The price trend is expected to continue to decrease thus further reducing the need to consider the hardware cost.

3.3 Interactive operation

The most obvious positive characteristic of computation by microcomputers is the possibility of interactive operation, which is particularly desirable, in nonlinear analysis. Interactive operation accomplished, when using microcomputers, can be by inputting various commands or data at intermediate stages of computation. By knowing the results of the previous step(s) of computation, intelligent modifications of boundary conditions or load increments for the next step(s) can be made for example, behavior of structure subject to hysteretic or time dependent loading. Thus feedback of the analyst judgement at various stages of the analysis process becomes very easy.

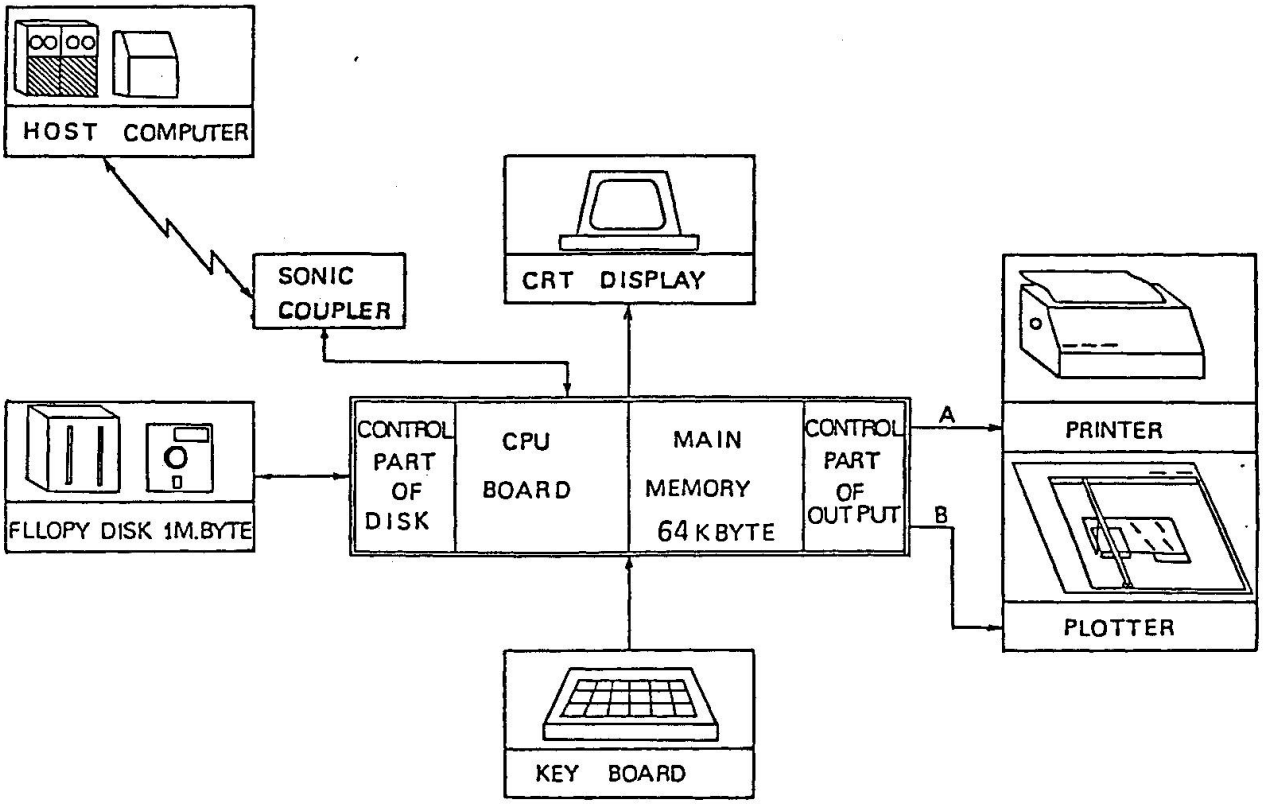

Fig.1 Microcomputer system

4. FINITE ELEMENT METHOD SOFTWARE PROGRAMMED FOR MICROCOMPUTERS

The limitation of 64 k byte of main memory dictates tight design of the main program and an efficient use of the areas for variables for computaion. Dynamic allocation of the area for variables is essential if large size problems are to be solved by the same program on large computers. A one dimensional common array called "POOL" is used to perform computation and thus just by changing the dimension of this array, programs of various sizes can be run on large computers.
The common array is controlled by three subprograms named OPEN, CLOSE and SEARCH. The data content in the POOL array is shown in Fig.2.

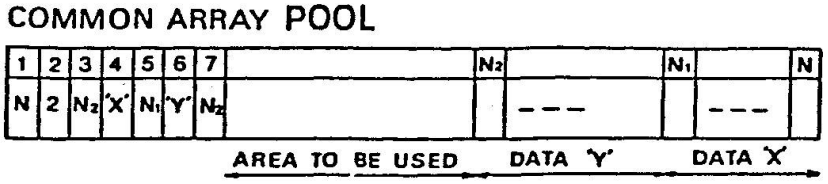

Fig.2 Constitution of common array POOL

The number of the dimension of POOL array is stored in POOL(1), and POOL(3) contains the top address of data sets which are inputed. The name and the address of each data set is stored starting at POOL(4) and continuing sequentially as requered. The corresponding data sets are stored from the bottom of POOL.
The OPEN subprogram writes the names of the arrays to be opened in the common data area, and reserves the memory area. Then the data are trasferred to this area and processed. The CLOSE subpogram deletes unoccupied variables area and packs the data of the POOL, and the indices are modified as indicated in Fig.3.

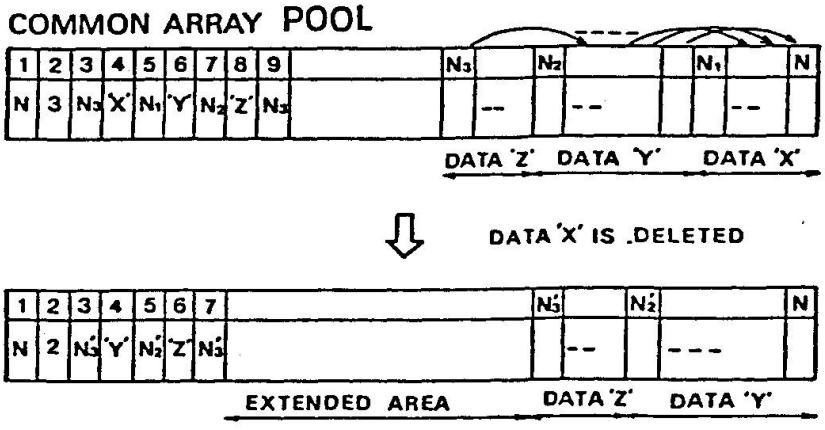

Fig.3 Function of subprogram CLOSE

The SEARCH subprogram searches to find certain data in the common area. Since the common area is controlled by these three subprograms, it is only necessary to change the array declaration of POOL to adjust for the various sizes of problems.

The solution of the equilibrium equations is by the Cholesky method incorporating the skyline technique and a modified Newton-Raphson iteration.
The stiffness matrix is processed in-core, because data transfer between the external files and core is time consuming.

5. MICROCOMPUTER CAPABILITY FOR NONLINEAR ANALYSIS OF CONCRETE MECHANICS

Utilizing the characteristics of microcomputers stated above, three capabilities were devised for analysis of concrete mechanics.
These are (1) Restart, (2) Split node, and (3) Relocatable node capabilities.

5.1 Restart

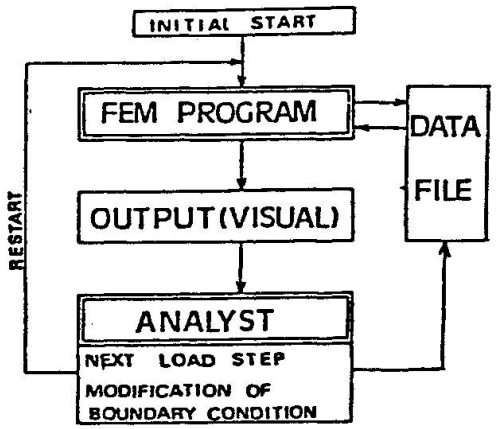

Fig.4 Flow chart of restart procedure

The "Restart" capability means the ability to suspend and restart a sequential computation, that is, the latest results of incremental computation are stored in the extended file and then the next increment of computation is started. Input is allowed at this stage for changing theboundary conditions and values and for incrementing the loads or displacements.The process is shown in Fig.4. Thus the intermediate results are preserved, at any stage and as many times as requied, until an appropriate load increment or other conditions are found by repetition of numerical simulation.
Such a process is useful and conveniently performed by the interactive handling as indicated above.

5.2 Split node

For a representation in analysis model of cracks in concrete, a formation of new surfaces or planes is more realistic than the frequently used smeared crack representation[4],[7] (altering the stiffness of a whole element) because the behavior of certain types of conc ete structures is significantly influenced by formation of isolated cracks. Several reports[3],[5] have been published on the analysis of concrete structures with cracked surfaces. In this case, the analysis with initially cracked element mesh can not calculate the inner stresses or strains when the constitutive equations have parameters influenced by the stress or strain history such as plastic strain. The following formulations try to make it possible using two dimensional 3 to 8 variable node isoparametric elements.

The nodes to be split in two to separate adjacent elements representing crack formation are specified initially, and only the locations in the stiffness matrices are reserved, see Fig.5. Then, the nodes to be split are specified at the Restart, and the B matrix and stiffness matrix are formed using the coordinates before the split.

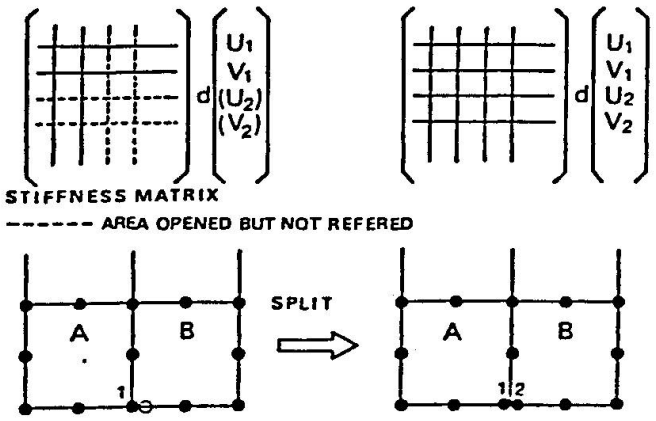

Fig.5 Split node

By this operation only the number of nodes is increased as shown in Fig.5 but not the number of elements. Then the computation is executed by letting the displacements for the split node (new node) equal to those for the node before splitting. When a crack is formed, the stresses and strains for all Gauss points in the involved elements use the values for the previous step. Hence, in general, the external and internal forces are not equilibrated and the difference will be,

$$V=F-\iiint B^T\sigma\,dv \qquad \text{--(eq.1)}$$

where. V= unbalanced nodal force vector
F= external nodal force vector
B= strain displacement matrix
σ= stress vector

The next correction of nodal displacements will be,

$$dU=K^{-1}V \qquad \text{--(eq.2)}$$

where dU= increment of nodal displacement vector
K= global stiffness matrix at each step

and so,

$$U=U+dU \qquad \text{--(eq.3)}$$
$$\varepsilon=\varepsilon+d\varepsilon \qquad \text{--(eq.4)}$$
$$\sigma=D(\varepsilon,d\varepsilon) \qquad \text{--(eq.5)}$$

where U= total nodal displacement vector
ε, $d\varepsilon$= total, and incremental strain vector
D= constitutive equations

The stresses (eq.5) are substituted into eq.1, and if the quantity V is not as small as required, the next iterative procedure must be executed using eq.2 through eq.5. Thus, computation is repeated until the value V becomes as small as required.

5.3 Relocation of nodes or modification of finite element mesh

When cracking is to be simulated in a model by release of connectivity of the variable node isopatametric elements, a necessity arises for the orientation of a side of elements to be altered tp align with the direction of the propagation of the cracks, or the mesh layout is to be modified each time when required. Here, only geometric alteration of node positions takes place but not the number of elements. When this procedure is used the B matrices for the elements are corrected at the Restart. Furthermore, since the Gauss points for evalution of stresses and strains are altered, these stresses and strains need to be corrected when moving the finite element mesh. Calculating the stresses and strains at the next step, these are calculated by use of the stresses and strains at the previous conditions. But, when the mesh of the finite elements are altered, there is no information at the new Gauss points so that the initial conditions of iterative procedure must be corrected.

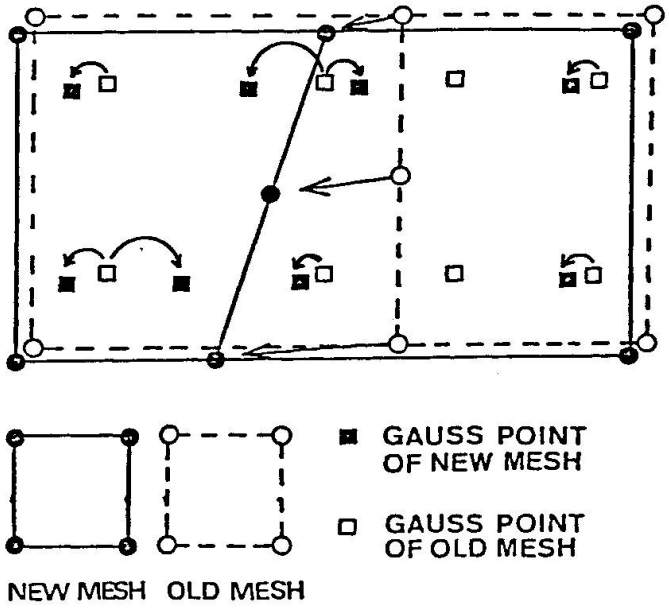

Fig.6 Correction of initial condition at each step due to relocation of finite element mesh

In this example as shown in Fig.6, correction is made by letting the nearest (in global coordinate system) Gauss points as an initial conditions based on the Gauss points in the previous computation step. Correction of nodal displacements is made by calculating the displacements at the new points of altered nodes with the interpolation founctions and nodal displacements of previous computation step. If a perfect correction is made, V in eq.1 is equal to zero. But in actual case, the unbalanced nodal force vector V appears by the modification of finite emement mesh, so the nonlinear trial and correction procedure (from eq.1 to eq.5) is executed, and the initial condition of iterative procedure is modified.

The flow charts in Figs. 7 and 8 indicate a method for an analysis including the relocation procedure and a method for correction of stresses and strains at Gauss points. The three procedures described above might appear cumbersome, but they can be handled because the process is sufficiently flexible and effective when installed on a personal computer systems. Such capabilities interacted with human decisions, and thus a synthesis of analyst and computer system enables a simulation of crack propagation in concrete structures which has been difficult to handle before.
The following is an analysis example.

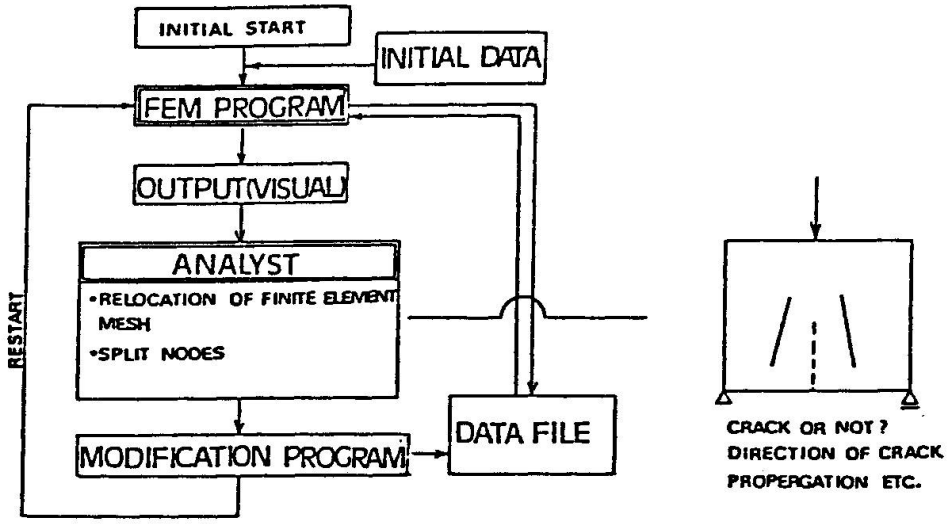

Fig.7 Flow chart of split node and relocation of finite element mesh

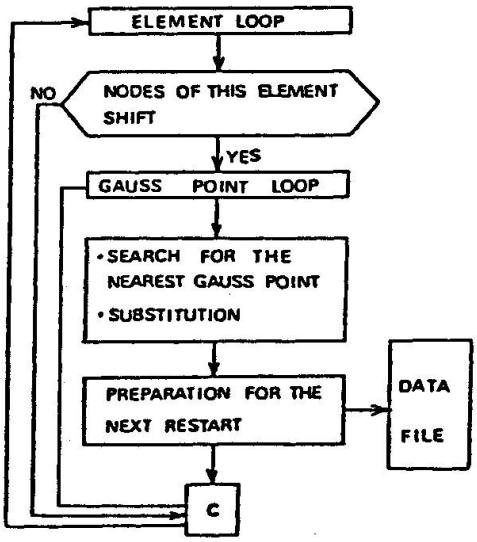

Fig.8 Modification of initial condition of iterative procedure for the next Restart

6. SAMPLE ANALYSIS

A simplified example, as reported in Ref.[6], was made that used the three computational capabilities stated above. A block of concrete was loaded at the center through a top and bottom steel plates as shown in Fig.9. The finite element mesh is shown in Fig.10. At the start of computation, all the nodes were specified to allow splitting at any node(s), and locations in the stiffness matrices were reserved in memory. The boundary conditions are indicated in Fig.10, and the top and bottom surfaces of the plate are considered to displace equally. The actual crack pattern is shown in Fig.11. The order for integration was made equal to 2. The concrete was assumed to be elastic, its modulus of elasticity E_0 was assumed to be $3.06*10^4$ N/mm^2, the poisson's ratio to be 0.2, and tensile strength F_t to be 2.55 N/mm^2. Other assumptions are a plane stress condition and perfect contact between the steel plates and the concrete block.

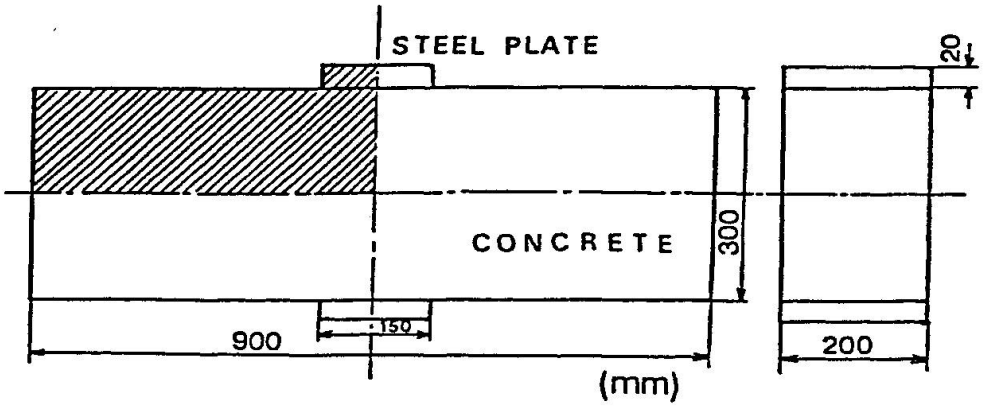

Fig.9 Concrete block

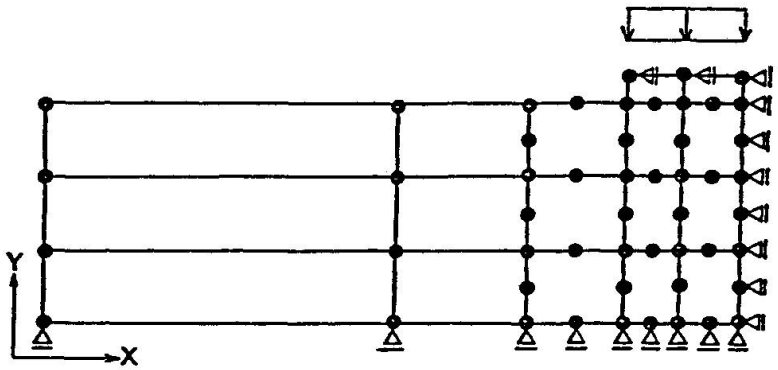

Fig.10 Initial mesh of Stage 1

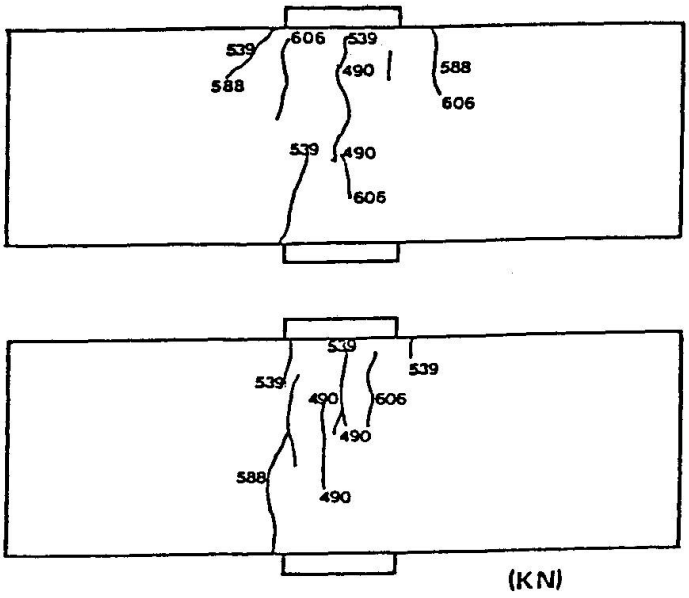

Fig.11 Actual crack pattern of a concrete block

Here, the decisions for the relocation of the mesh and the selection of nodes to be split were made at each step by the analyst interactively after a critical review of the intermediate results.
Cracking was assumed to occur at a node nearest to the point where the principal stress exceeded the tensile strength of concrete F_t. Then the node was split and the boundary condition was changed, and the mesh was altered so that the orientation was aligned to the direction of the principal stress.

Stage 1 - Stage 3 ; Fig.12-1, Fig.12-2
When the displacement of Node 100,101,102 =-0.06mm(Y-direction), the stress exceeded F_t at Gauss point A, and hence the boundary condtion restraints for the nearest Node 1 was released to represent cracking at restart(Stage 1). The restart resulted in excess of F_t for the major principal stress at t e point B, so that the Node 2 was made to be a free node(Stage 2). By the release of the boundary conditions a flexural crack propagated as shown in Fig.12-2.

Stage 3 - Stage 5 ; Fig.12-2, Fig.12-3
The restart resulted in excess of F_t for the major principal stress at the point C, (Stage 3) consequently, the boundary conditions for Node 3 was altered at restart(Stage 4). In the same procedure as the upper stage, the first crack was extended as shown in Fig.12-3(Stage 5).

Stage 5 -Stage 6 ; Fig.12-3, Fig.12-4
As a consequence of extension of crack, the principal stress exceeded F_t at the point D.(the increment for displacements is zero.)
Hence, Node 4 was split in Fig.12-4 and there a new node was created to indicate the second crack formation(Stage 6).

Stage 6 -Stage 7 ; Fig.12-4, Fig.12-5
With the condition of displacement increment being equal to zero, the unbalanced forces were distributed to the affected nodes. Due to the resulting stresses, the principal stress exceeded F_t at the point E(Stage 6). Hence Node 5 was split and node 6,7 and 8 were relocated as shown in Fig.12-4.

Stage 7 - Stage 8 ; Fig.12-5, Fig.12-6
The second crack extended, and the stresses were redistributed as shown in Fig.5(Stage 7). Only the stress of point F exceeded F_t, therefore, Node 9 was split and then all major principal stresses were lower than F_t. Hence, a new displacement increment = -0.0026mm(Y-direction) was imposed to Node 100,101,102.

Stage 8 - Stage 9 ; Fig.12-6, Fig.12-7
Imposing the new displacement the major principal stress at the point G exceeded F_t(Stage 8). This time, the direction of the major principal stress was approximately parallel to the X-axis, and therefore the node was split but the mesh was unchanged as shown in Fig.12-7.

Stage 9 - Stage 10 ; Fig.12-7, Fig.12-8
By the split of Node 10, a third crack was formed. This time, all principal stresses were lower than F_t so that the displacement increment = -0.0044(Y-direction) was imposed to Node 100,101 and 102. The resulting principal stress of points H and I exceeded F_t(Stage 9). Therefore, Node 11 was split by the same manner as Stage 8 and 9.

Stage 10 ; Fig.12-8
The third crack was made using the function of split node and the stresses were redistributed as shown in Fig.12-8, and the reaction at the plate was decresed(Stage 10). The relationship between the displacement at each stage and the reaction is shown in Fig.13.

STAGE 1
U=-0.06
R=496
where
U; DISPLACEMENT OF
NODE 100-102(MM)
R; LOAD(KN)

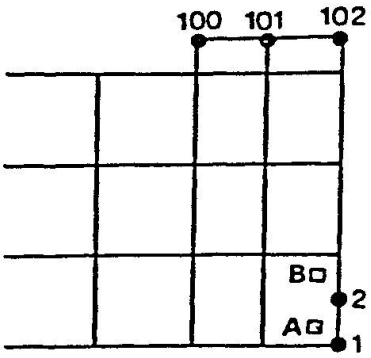

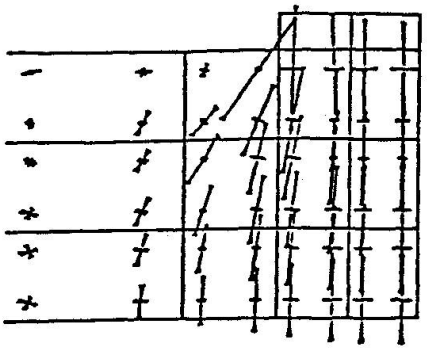

[Fig.12-1]

STAGE 3
U=-0.06
R=492

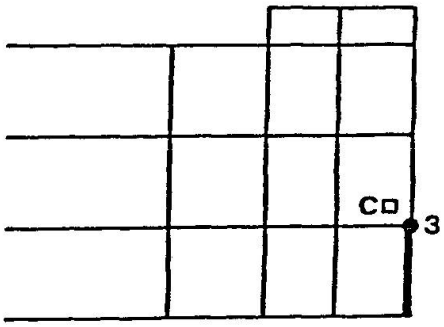

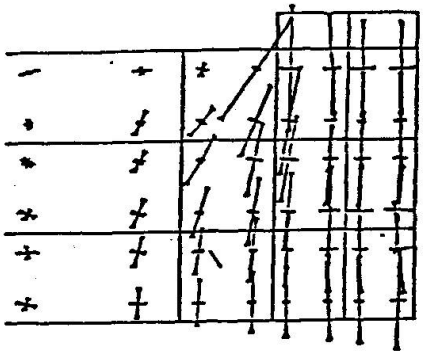

[Fig.12-2]

STAGE 5
U=-0.06
R=479

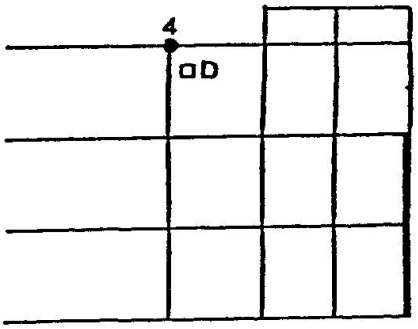

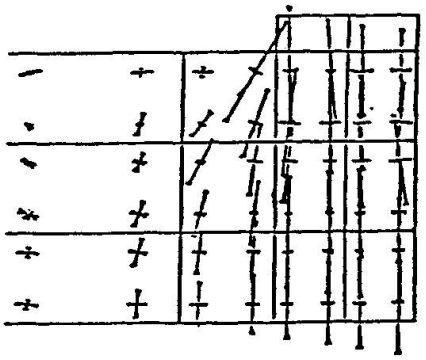

[Fig.12-3]

STAGE 6
U=-0.06
R=475

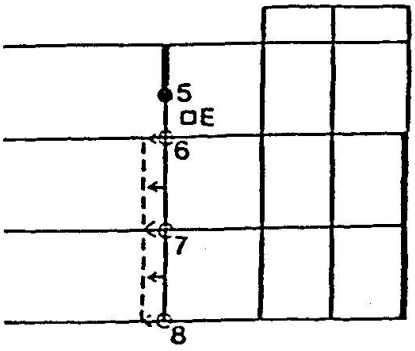

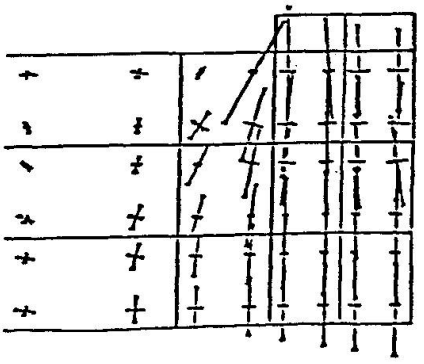

[Fig.12-4]

STAGE 7
U=-0.06
R=473
where
U; DISPLACEMENT OF
NODE 100-102(MM)
R; LOAD(KN)

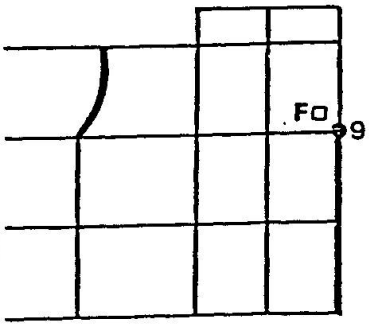

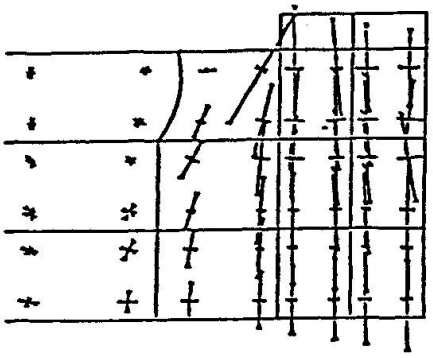

[Fig.12-5]

STAGE 8
U=-0.0626
R=487

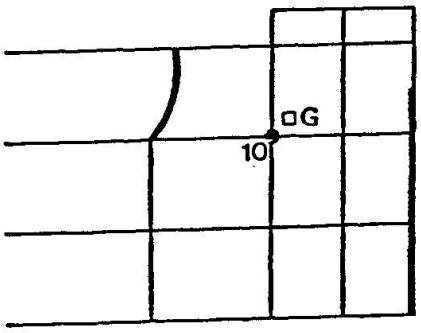

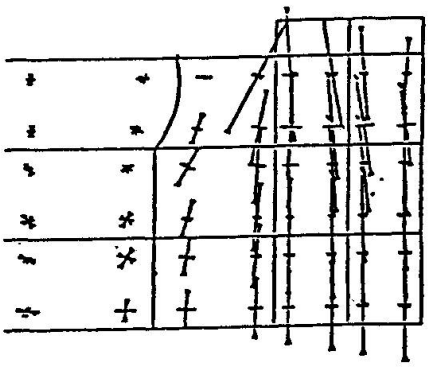

[Fig.12-6]

STAGE 9
U=-0.067
R=519

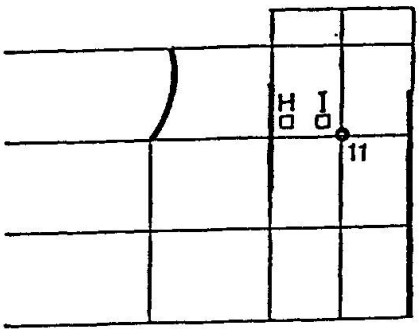

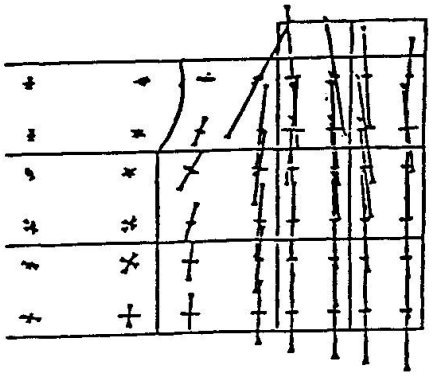

[Fig.12-7]

STAGE 10
U=-0.067
R=427

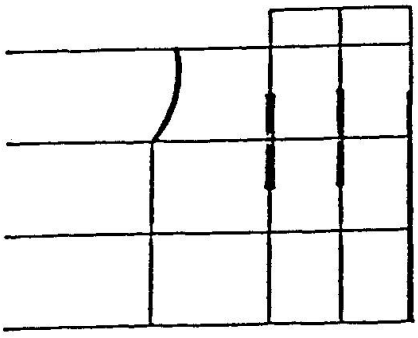

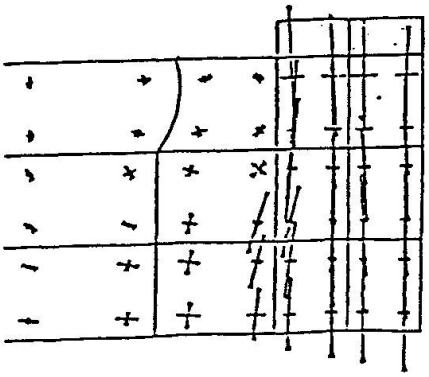

[Fig.12-8]

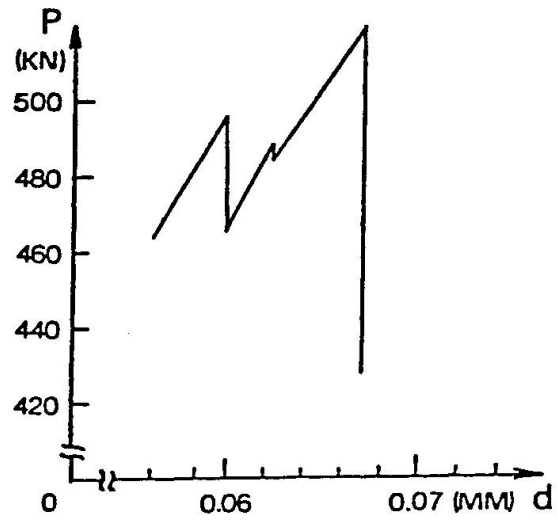

Fig.13 Calculated load-displacement relationship

7. CONCLUDING REMARKS

Because of the convenience of using microcomputers which are rapidly becoming available to all engineers, the methods of computation, which are different from those typically used for processing on large computers, appear to be undergoing change. In the near future it will be possible for engineers to analyze complex concrete mechanics problems at their convenience at their home or desk.
The possibility for improvement through new methods was demondstrated by an example of analysis and computer system presented in this paper. The improvement was made possible because the engineer was able to use the microcomputer in an interactive mode.

REFERENCES

1. E.L. Wilson, "SAP-80 Structural Analysis Programs for small or large Computer Systems"
2. Y.Yamada, H.Okumura and T.Sakurai, "System for Medium-Sized and Experimental Finite-Element Analysis" presented at Symposium of Computational Methods in Nonlinear Structural and Solid Mechanics, Oct. 6-8, 1980,NASA.
3. A.C.Scordelis, D.Ngo and H.A.Franklin, "F n'te Element Study of Reinforced Concrete Beams with Diagonal Tension Cracks" ACI SP 42-2.
4. D.Darwin and D.A.Pecknold, "Nonliner Biaxial Stress Strain Law for Concrete", ASCE Journal, Engineering Mechanics Division EM2 April 1977
5. A.H.Nilson, "Nonlinear Analysis of Reinforced Concrete by the Finite Element Method", ACI journal Sept. 1968.
6. A.C.T.Chen and W.Chen, "Constituteve Equations and Punch-Indentation of Concrete", ASCE Journal, Engineering Mechanics Division EM6 December 1975.
7. E.Raue, "Limit Analysis of Reinforced Concrete Shells of Revolution", IABSE Colloquium Copenhagen Final Report 1979

Leere Seite
Blank page
Page vide

Tension-Stiffening Concept for Reinforced Concrete Surface Structures

Tension-stiffening concept pour des constructions en surfaces porteuses en béton armé

Tension-Stiffening Konzept für Flächentragwerke aus Stahlbeton

H.A. MANG
Associate Professor

H. FLOEGL
Research Associate

Institut für Baustatik und Festigkeitslehre der TU-Wien
Wien, Österreich

SUMMARY

Disregard of the capacity of the concrete between neighboring cracks to carry tensile forces normal to the cracks - the so-called "tension-stiffening effect" - may result in underestimating member stiffnesses considerably. In this paper, a novel tension stiffening concept for reinforced concrete surface structures is presented. It is based on bond slip between the reinforcement and the surrounding concrete. Good agreement of results from geometrically and physically nonlinear finite-element-analyses with experimental results is demonstrated.

RÉSUMÉ

En négligeant la capacité du béton de transmettre des forces de traction perpendiculairement à la direction des fissures - qu'on appelle le "Tension-Stiffening Effect" - on sous-estime la rigidité des membres portants. Dans la publication qui suit on présente une nouvelle méthode de tenir compte du "Tension-Stiffening" pour des constructions en surfaces porteuses (dalles, coques, etc.) en béton armé. La méthode est basé sur les déformations relatives entre les barres d'acier et le béton. Les résultats des calculs non-linéaires (géometriquement et physiquement), faits avec l'aide de la méthode des éléments finis correspondent bien avec les résultats d'essais, connus d'autres publications.

ZUSAMMENFASSUNG

Die Nichtberücksichtigung der Kapazität des Betonzwischen benachbarten Rissen, Zugkräfte normal zu den Rissen aufzunehmen - des sogenannten "Tension-Stiffening Effekts" - kann zu einer beträchtlichen Unterschätzung der Steifigkeit von Traggliedern führen. In der vorliegenden Arbeit wird ein neuartiges Tension-Stiffening Konzept für Flächentragwerke aus Stahlbeton präsentiert. Es beruht auf Gleitverbund zwischen der Bewehrung und dem umgebenden Beton. Die Ergebnisse zufolge geometrisch und physikalisch nichtlinearer Berechnungen mittels der Methode der Finiten Elemente stimmen gut mit experimentellen Vergleichsresultaten aus der Literatur überein.

1. INTRODUCTION

The capacity of the concrete between neighboring cracks to carry tensile stresses, transferred from the reinforcement to the surrounding cracks is termed "tension-stiffening effect". The vehicle for this stress transfer is bond slip between the reinforcement and the surrounding concrete. If tension stiffening is disregarded, ultimate load analysis of reinforced concrete (RC) surface structures may result in average steel stresses between neighboring cracks which are too large. The ultimate load may be underestimated considerably.

In the course of the last years, a number of analytical models for consideration of tension stiffening have been proposed. With regard to thin slabs, more recently Gilbert and Warner [1] have reviewed some of these models which can be characterized as "strain-softening approaches". Fig.1, taken from [1], shows typical modified stress-strain diagrams for two different models for consideration of tension stiffening.

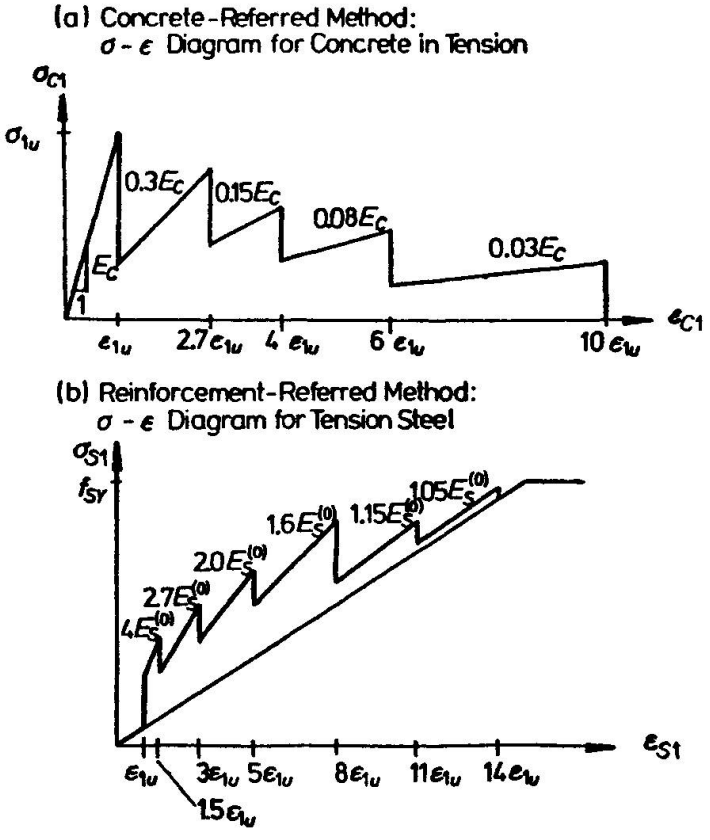

Fig.1 Modified Stress-Strain Diagrams for Consideration of Tension Stiffening (Ref.1)

Fig.1(a) illustrates the relationship between the average concrete tensile strain normal to neighboring parallel cracks, ε_{C1}, and the corresponding stress, σ_{C1}, for the so-called "concrete-referred method" [2], as proposed by Scanlon [3]. The quantities ε_{1u} and σ_{1u} denote the strain and the stress at initial cracking; E_C is the elastic modulus of concrete in uniaxial tension. Gilbert and Warner [1] have discussed modifications of this method.

Fig.1(b) shows a modified stress-strain diagram for steel in tension after cracking of concrete as used within the framework of the so-called "reinforcement-referred method" [2]. This method was proposed by Gilbert and Warner [1]. In Fig.1(b), ε_{S1}, $E_S^{(0)}$, σ_{S1} and f_{SY} denote the average steel strain between neighboring cracks, the elastic modulus of steel, the average steel stress and the yield stress of the reinforcement.

Both methods do not consider the influence of the angle between the crack and the intersecting reinforcement bar. Moreover, the influence of crack propagation through the thickness of slabs and shells on the tension-stiffening effect is not dealt with adequately, since it is not controlled by the coordinate normal to the middle surface of the shell.

The writers' purpose is to report on the essential features of a novel analytical concept within the framework of the Finite Element Method (FEM) for consideration of tension stiffening in thin RC surface structures, based on bond slip between the reinforcement and the surrounding concrete [2], [4]. It is characterized by approximate consideration of the influence of (a) the angle between the crack and the intersecting reinforcement bar, (b) crack propagation through the thickness of the shell, and (c) secondary cracks between neighboring primary cracks on the tension stiffening effect. Nonlinearity of concrete, strain-hardening plasticity of steel, geometric nonlinearity and the dependence of hydrostatic pressure on the state of deformation is taken into account.

The developed concept is applied to predict the short-term behavior of an RC panel and an RC shell, for both of which experi-

mental results are available in the literature.

2. THEORETICAL CONCEPT

2.1 Equilibrium Equations

Fig.2 shows the middle surface S of an undeformed RC shell with the boundary Γ. It also illustrates the deformed shell (middle surface S', boundary Γ'). The shell is subdivided into m C^o-conforming, curved, triangular finite elements each of which consists of n thin layers such that, approximately, a plane state of stress may be assumed in each layer. The thickness of layer ℓ is given

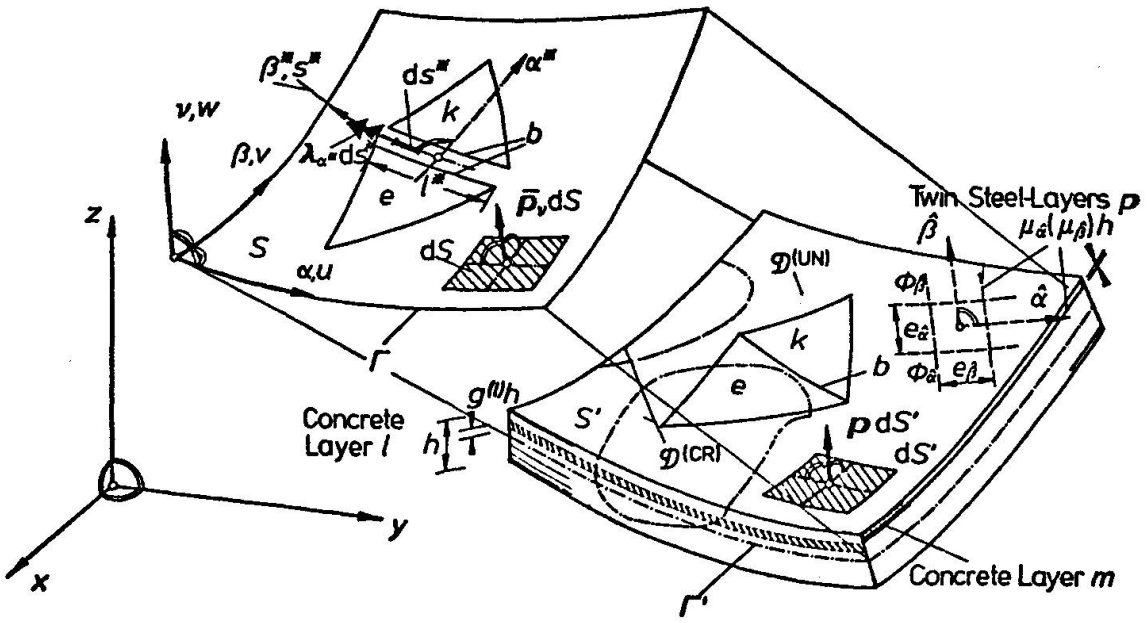

Fig.2 Middle Surface of Undeformed RC Shell; Layered Finite Element Model of Deformed, Partially Cracked Shell

as $g^{(\ell)}h$, where h is the thickness of the shell and $g^{(\ell)}$ is the weight coefficient for Gauss integration. Fig.2 contains global Cartesian coordinates, x,y,z, global surface coordinates, α,β,ν, local surface coordinates, α^*,β^*, referred to the common boundary

b of two neighboring elements, e and k, and local surface coordinates, $\hat{\alpha}$, $\hat{\beta}$, parallel to an orthogonal net of reinforcement bars with diameters $\hat{\phi}_\alpha$, $\hat{\phi}_\beta$. The bars are "smeared" to "twin steel-layers" with thicknesses $\mu_{\hat{\alpha}}(\mu_{\hat{\beta}})h$, where $\mu_{\hat{\alpha}}(\mu_{\hat{\beta}})$ are the degrees of reinforcement. In addition to dead load, the shell is assumed to be loaded by hydrostatic pressure (undeformed configuration: $\bar{p}_\nu dS$, deformed configuration: $p\,dS'$); $\lambda_{\alpha^*} ds^*$ is an unknown distributed bending moment, required for enforcing C^1-continuity at b; u, v, w are components of the displacement vector parallel to α, β, ν. The symbols $\mathcal{D}^{(UN)}$ and $\mathcal{D}^{(CR)}$ denote the entirety of uncracked and cracked subregions of the shell. To talk of such subregions is only meaningful if a "smeared-crack concept" is applied as is done in the given case.

The equations of equilibrium are given as [4]

$$\sum_{e=1}^{m}\Big[\sum_{\ell=1}^{n} g^{(\ell)}\Big(\int_{S_C^{(e,\ell;UN)}} \sigma_{i''}\,\delta\varepsilon_{i''}\,h\,dS + \int_{S_C^{(e,\ell;CR)}} \sigma^{(a)}_{i'j'}\,\delta\varepsilon^{(a)}_{i'j'}\,h\,dS\Big) +$$

$$+\sum_{p=1}^{r}\Big(\int_{S_{S\hat{\imath}}^{(e,p;UN)}} \sigma_{\hat{\imath}}\,\delta\varepsilon_{\hat{\imath}}\,\mu_{\hat{\imath}}\,h\,dS + \int_{S_{S\hat{\imath}}^{(e,p;CR)}} \sigma^{(a)}_{\hat{\imath}}\,\delta\varepsilon^{(a)}_{\hat{\imath}}\,\mu_{\hat{\imath}}\,h\,dS - \int_{\sum \ell_{\hat{\imath}}^{(e,p;CR)}} t^{(a)}_{B\hat{\imath}}\,\delta u^{(a)}_{R\hat{\imath}}\,ds_{\hat{\imath}}\Big) -$$

$$-\int_{V^{(e)}} \bar{p}_g\,\delta u_g\,dV - \int_{S_p^{(e)}} p_g\,\delta u_g\,dS\Big] - \sum_{b=1}^{q}\int_{\ell^*(b)}\left(\lambda_{1^*}\,\delta\vartheta_{1^*} + \vartheta_{1^*}\,\delta\lambda_{1^*}\right)ds^* = 0,$$

$$g = 1, 2, 3;\quad i,j = 1,2;\quad 1\equiv\alpha,\ 2\equiv\beta,\ 3\equiv\nu. \qquad (1)$$

The first integral in (1) represents the virtual work of the internal forces acting in the part of concrete layer ℓ of element e which belongs to $\mathcal{D}^{(UN)}$. The respective part of the middle surface of layer ℓ is denoted as $S_C^{(e,\ell;UN)}$; $\varepsilon_{i''}$ and $\sigma_{i''}$ are the strains and stresses in the principal directions, α'', β''. The transfer from displacements to strains is accomplished by means of a theory of small strains but moderately large rotations, developed by Koiter [5]. Biaxial stress-strain relations, proposed by Liu, Nilson and Slate [6] on the basis of experiments of Kupfer [7] are used.

The second integral in (1) extends over $S_C^{(e,\ell;CR)}$, which is part of $\mathcal{D}^{(CR)}$; $\varepsilon^{(a)}_{i'j'}$ and $\sigma^{(a)}_{i'j'}$ are average strains and stresses

normal and parallel to cracks. Within tributary domains of Gauss points for numerical integration, the cracks are assumed to be parallel and equidistant. Only two crack bands are taken into account. For reasons of simplicity, the second crack band is assumed to be normal to the first one. The directions of the normals to the two crack bands are denoted as α' , β' .

The third and the fourth integral in (1) refer to the reinforcement steel in "twin steel-layers" p ; $S_{S\hat{\imath}}^{(e,p;UN)}$ ($S_{S\hat{\imath}}^{(e,p;CR)}$) denotes the part(s) of the middle surface(s) p which are located in $\mathcal{D}^{(UN)}$ ($\mathcal{D}^{(CR)}$); $\varepsilon_{\hat{\imath}}^{(a)}$ and $\sigma_{\hat{\imath}}^{(a)}$ are average strains and stresses in the directions of the reinforcement bars, $\hat{\alpha}$, $\hat{\beta}$.

The integrand of the fifth integral in (1) represents the virtual work done by average bond forces $t_{B\hat{\imath}}^{(a)}$, given as

$$t_{B\hat{\imath}}^{(a)} = \tau_{B\hat{\imath}}^{(a)} \phi_{\hat{\imath}} \pi , \qquad \hat{\imath} = \hat{1},\hat{2} \text{ (no summation)}; \hat{1} \equiv \hat{\alpha}, \hat{2} \equiv \hat{\beta}, \quad (2)$$

where $\tau_{B\hat{\imath}}^{(a)}$ are average bond stresses, on virtual average bond slips, $\delta u_{R\hat{\imath}}^{(a)}$. In the context of concrete-frame analysis, Åldstedt and Bergan [16] have considered an analogous virtual-work term.

Assuming full bond in $\mathcal{D}^{(UN)}$, the aforementioned integral stretches only over those parts of the reinforcement bars which are located in $S_{S\hat{\imath}}^{(e,p;CR)}$. The domain of integration is written symbolically as $\sum \ell_{\hat{\imath}}^{(e,p;CR)}$, where $\ell_{\hat{\imath}}^{(e,p;CR)} \equiv \ell_{\hat{\imath}}$ are lengths of reinforcement bars between neighboring cracks in $S_{S\hat{\imath}}^{(e,p;CR)}$ [4].

Fig.3 contains a comparison of "actual" stress distributions between neighboring parallel cracks with idealized stress distributions employed for the analysis; $\tau_{B\hat{\imath}}^{(a)}$ represents the average value of $\tau_{B\hat{\imath}}$. Note that $\sigma_{C\hat{\imath}\hat{\imath}}^{(a)}$ and $\sigma_{S\hat{\imath}}^{(a)}$ are not average values of $\sigma_{C\hat{\imath}\hat{\imath}}$ and $\sigma_{S\hat{\imath}}$.

On the basis of Fig.3, the average bond slip between neighboring cracks, $u_{R\hat{\imath}}^{(a)}$, is obtained as

$$u_{R\hat{\imath}}^{(a)} = \Delta_{S\hat{\imath}}^{(a)} - \Delta_{C\hat{\imath}}^{(a)} = \left(\varepsilon_{S\hat{\imath}}^{(a)} - \varepsilon_{C\hat{\imath}\hat{\imath}}^{(a)}\right) \frac{\ell_{\hat{\imath}}}{4} \quad (3)$$

where

$$\Delta_{S\hat{\imath}}^{(a)} = \frac{1}{2}\left[u_{S\hat{\imath}}(s_{\hat{\imath}} = \ell_{\hat{\imath}}/2) - u_{S\hat{\imath}}(s_{\hat{\imath}} = 0)\right] \quad (4.1)$$

and

$$\Delta_{C\hat{i}}^{(\sigma)} = \frac{1}{2}\left[u_{C\hat{i}}(s_{\hat{i}} = \ell_{\hat{i}}/2) - u_{C\hat{i}}(s_{\hat{i}} = 0)\right] \tag{4.2}$$

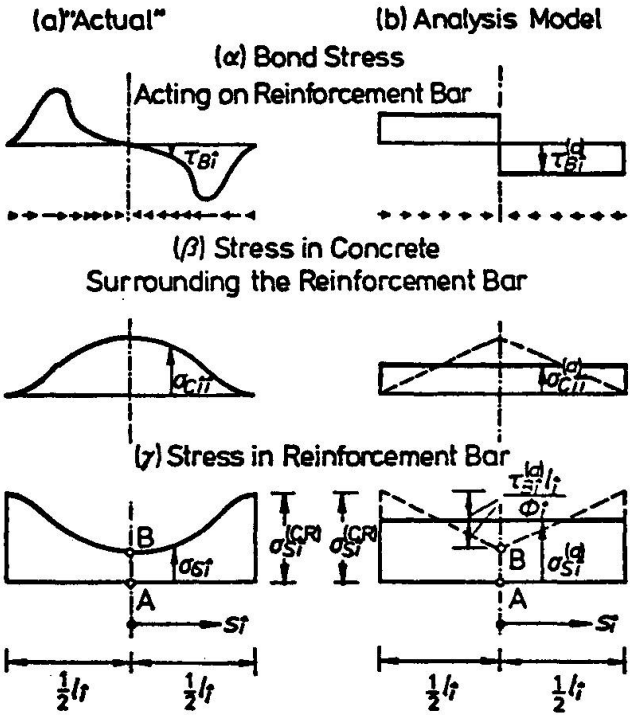

Fig.3 "Actual" and Idealized Stress Distributions

In case of cracks which are non-orthogonal to the reinforcement bars, $\ell_{\hat{i}}$ may exceed the boundaries of the tributary domain of the considered integration point. In case of such cracks, kinking of the reinforcement will occur at cracks, resulting in a reduction of bond slip. This suggests replacing (3) by

$$u_{R\hat{i}}^{(\sigma)} = \Delta_{S\hat{i}}^{(\sigma)} - \Delta_{C\hat{i}}^{(\sigma)} \tag{5}$$

where $|\Delta_{S\hat{i}}^{(\sigma)}| \leq |\Delta_{S\hat{i}}^{(\sigma)}|$ and $|\Delta_{C\hat{i}}^{(\sigma)}| \leq |\Delta_{C\hat{i}}^{(\sigma)}|$ and where $\Delta_{S\hat{i}}^{(\sigma)}$ is estimated as follows:

$$\Delta_{S\hat{i}}^{(\sigma)} = \begin{Bmatrix} n_{1'\hat{i}}^2 \\ 1 \end{Bmatrix} \left[\sum_{\ell=1}^{n} g^{(\ell)} \left(1 + \frac{12\,\nu_{S\hat{i}}}{h^2} \nu_C^{(\ell)} \right) \frac{\ell_{\hat{i}}}{\ell_{\hat{i}}^{(\ell)}} \right] \varepsilon_{S\hat{i}}^{(\sigma)} \frac{\ell_{\hat{i}}}{4} . \tag{6}$$

For parallel cracks in one direction (see Fig.4),

$$\ell_{\hat{i}} = \frac{b_{1'}}{|n_{1'\hat{i}}|} , \qquad \ell_{\hat{i}}^{(\ell)} = \frac{b_{1'}^{(\ell)}}{|n_{1'\hat{i}}^{(\ell)}|} , \tag{7.1}$$

and for parallel cracks in two directions (see Fig.4),

$$\ell_{\hat{\imath}} = \frac{b_{1'} b_{2'}}{b_{1'} |n_{2'\hat{\imath}}| + b_{2'} |n_{1'\hat{\imath}}|}, \qquad \ell_{\hat{\imath}}^{(\ell)} = \frac{b_{1'}^{(\ell)} b_{2'}^{(\ell)}}{b_{1'}^{(\ell)} |n_{2'\hat{\imath}}^{(\ell)}| + b_{2'}^{(\ell)} |n_{1'\hat{\imath}}^{(\ell)}|} \,. \tag{7.2}$$

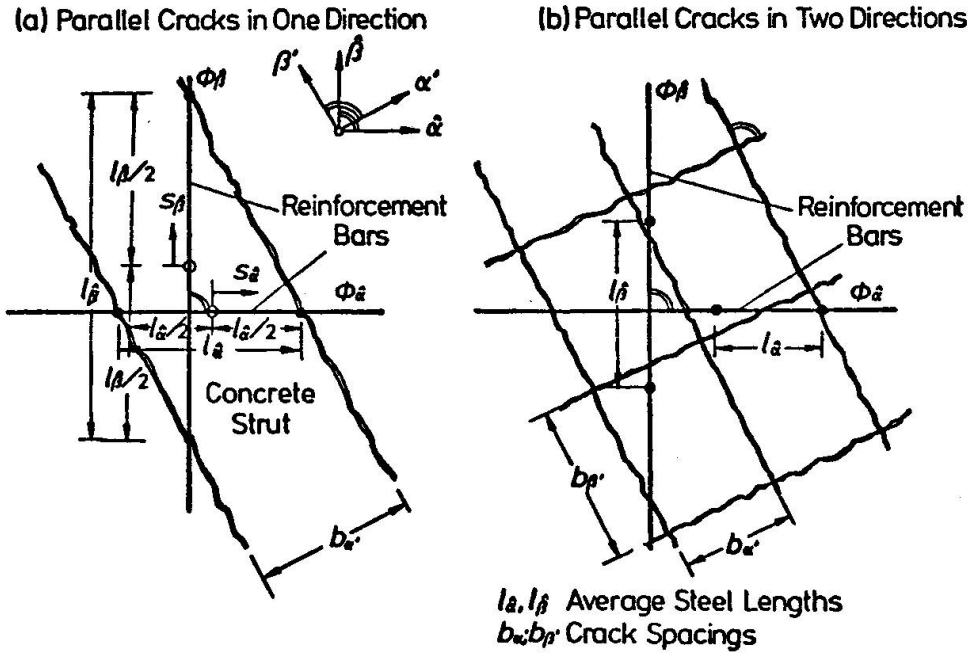

Fig.4 Reinforcement Bars Intersecting Crack Bands in One or Two Directions

Note that for parallel cracks in two directions, $\ell_{\hat{\imath}}$ ($\ell_{\hat{\imath}}^{(\ell)}$) are average quantities. In (7.2), $b_{1'}$ and $b_{2'}$ denote crack spacings in the concrete layer containing the considered steel layer; $n_{1'\hat{\imath}}$ and $n_{2'\hat{\imath}}$ are the direction cosines of angles enclosed by the normals to the cracks and the reinforcement bars in the mentioned concrete layer. The quantities $b_{1'}^{(\ell)}$, $b_{2'}^{(\ell)}$, $n_{1'\hat{\imath}}^{(\ell)}$ and $n_{2'\hat{\imath}}^{(\ell)}$ refer to concrete layer ℓ; $z_{S\hat{\imath}}$ ($z_C^{(\ell)}$) is the distance of the considered steel layer (concrete layer ℓ) from the middle surface of the shell. The upper (lower) quantity in the factor $\begin{Bmatrix} n_{1'\hat{\imath}}^2 \\ 1 \end{Bmatrix}$ in (5) refers to parallel cracks in one (two) direction(s).

The crack spacings $b_{\hat{\imath}'}$, are influenced, to a different degree, by various physical parameters of which the concrete strain normal to the crack, $\varepsilon_{C\hat{\imath}'}$, is believed to be the most important one. For the present investigation, according to [2], [4],

$$b_{i'} = 1{,}5\, b_{i'}^{(1)} \left(\frac{\varepsilon_{Ci'i'}}{\varepsilon_{Ctu}}\right)^{-\left(\frac{\log 2}{\log \varrho}\right)} \tag{8}$$

where

$$\varrho = \frac{\varepsilon_{Ci'i'}^{(r+1;a)}}{\varepsilon_{Ci'i'}^{(r;a)}} = \left(\frac{\bar{\varepsilon}_{SY}}{\varepsilon_{Ctu}}\right)^{\frac{1}{s-1}} \qquad j \tag{9}$$

$\varepsilon_{Ci'i'}^{(r;a)}$, r=1,2,...s, denotes average concrete strains at the formation of cracks of order r. In this terminology, r=1 refers to primary cracks; s is the order of cracks assumed to open at initial yield of the reinforcement steel, $\bar{\varepsilon}_{SY}$ is the strain at incipient yield of the reinforcement steel; ε_{Ctu} stands for the uniaxial ultimate tensile strain. Fig.5 shows a plot of $b_{i'}^{(1)}$ versus $\varepsilon_{Ci'i'}^{(a)} \equiv \varepsilon_{i'i'}^{(a)}$.

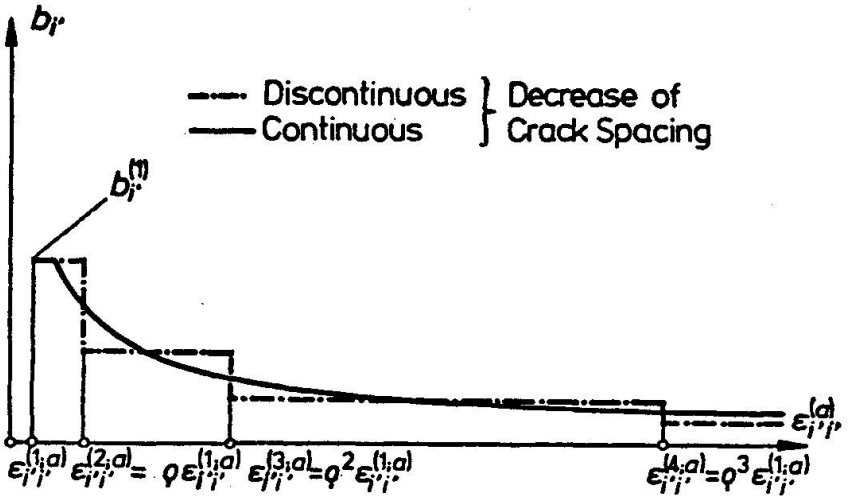

Fig.5 Crack Spacing as a Function of Average Strain Normal to Crack

Substituting (6) into (5), permits writing the integrand of the fifth integral in (1) as follows:

$$t_{B\hat{i}}^{(a)}\,\delta u_{R\hat{i}}^{(a)} = -\Bigg[\frac{|\tau_{B\hat{i}}^{(a)}|}{\sigma_{S\hat{i}}^{(a)}}\frac{\left\{\frac{b_{i'}}{\ell_{\hat{i}}}\right\}}{\phi_{\hat{i}}}\sum_{\ell=1}^{n} g^{(\ell)}\left(1+\frac{12\,\nu_{S\hat{i}}}{h^2}\,\nu_C^{(\ell)}\right)\frac{\left\{\frac{b_{i'}}{\ell_{\hat{i}}}\right\}}{\ell_{\hat{i}}^{(\ell)}}\Bigg]\sigma_{S\hat{i}}^{(a)}\,\delta c_{S\hat{i}}^{(a)}\,\frac{\phi_{\hat{i}}\,\pi}{4} + \\ + |\,t_{B\hat{i}}^{(a)}|\;\delta|\Delta_{C\hat{i}}^{(a)}|\,, \tag{10}$$

$-\ell_{\hat{i}}/2 \le s_{\hat{i}} \le \ell_{\hat{i}}/2$; $\hat{i}=\hat{1},\hat{2}$ (no summation); $\hat{1}\equiv\hat{\alpha}$, $\hat{2}\equiv\hat{\beta}$, $i'\equiv\alpha'$,

where

$$|\tau_{B\hat{i}}^{(a)}| = \left[0{,}07 + 0{,}16\left(\frac{\varepsilon_{S\hat{i}}^{(a)}\left\{\frac{b_{i'}}{\ell_{\hat{i}}}\right\}}{2}\right)^{0.3}\right]|f_{cu}| + 0{,}2\,|\sigma_{C\hat{j}\hat{j}}|, \quad \hat{i}\neq\hat{j}, \tag{11}$$

$\hat{i},\hat{j} = \hat{1},\hat{2}$ (no summation); $\hat{1}\equiv\hat{\alpha}$, $\hat{2}\equiv\hat{\beta}$.

The right side of (11) is an approximation to $|\tau_{B\hat{\imath}}^{(a)}|$. The original expression for $|\tau_{B\hat{\imath}}^{(a)}|$ was derived by Grelat and Potucek [8]. In (10) and (11), upper (lower) quantities refer to parallel cracks in one (two) direction(s). In (11), the dimension of $b_{1'}$ and $\ell_{\hat{\imath}}$, respectively, is [mm]; f_{cu} is the uniaxial compressive strength (prism strength) of concrete.

A few words remain to be said about the last three integrals in (1). The sixth integral represents the virtual work of volume forces $\bar{p}_g$. The integral extends over the volume of finite element e, $V^{(e)}$. The seventh integral expresses the virtual work of hydrostatic pressure $p_g(u_i)$ [9]. It stretches over the loaded part of the surface of element e, $S_p^{(e)}$. The last integral in (1) represents the variation of a load potential with $\lambda_{1*}^{(b)} \equiv \lambda_{1*}$ as the load and with $\vartheta_{1*}^{(b)} \equiv \vartheta_{1*}$ as the corresponding "displacement" in the form of the difference of normal slopes of elements e and k at b. The integral extends over the length of b, $l^{*(b)}$.

2.2. Tension Stiffening Factor

In the following, local groups of equilibrating "external" and internal forces in the concrete surrounding two orthogonal reinforcement bars between neighboring cracks will be identified. For a typical group of such equilibrating forces, the equilibrium equations are obtained as

$$\Big[\sum_{\ell=1}^{n} g^{(\ell)}\left(\sigma_{i'j'}^{(a)} - \tilde{\sigma}_{i'j'}^{(a)}\right)\delta\varepsilon_{i'j'}^{(a)} S_C^{*(e,\ell,r;CR)}\Big] h = \left|t_{B\hat{\imath}}^{(a)}\right| \delta\left|\underset{\sim}{\Delta}_{C\hat{\imath}}^{(a)}\right| \ell_{\hat{\imath}} ,$$

$$i,j = 1,2; \quad 1 \equiv \alpha, 2 \equiv \beta, \tag{12}$$

where $\tilde{\sigma}_{i'j'}^{(a)}$ represent average values of residual stresses which would act in the concrete between neighboring cracks if no stress transfer from the two orthogonal reinforcement bars to the surrounding concrete took place between neighboring cracks.

For one crack band only,

$$\begin{Bmatrix} \tilde{\sigma}_{1'1'}^{(a)} \\ \tilde{\sigma}_{2'2'}^{(a)} \\ \tilde{\sigma}_{1'2'}^{(a)} \end{Bmatrix} \equiv \begin{Bmatrix} \tilde{\sigma}_{\alpha'\alpha'}^{(a)} \\ \tilde{\sigma}_{\beta'\beta'}^{(a)} \\ \tilde{\sigma}_{\alpha'\beta'}^{(a)} \end{Bmatrix} = \begin{Bmatrix} 0 \\ \sigma_{\beta'\beta'}^{(a)}\left(\sigma_{\alpha'\alpha'}^{(a)} = 0\right) \\ 2\bar{G}\varepsilon_{\alpha'\beta'}^{(a)} \end{Bmatrix} \tag{13}$$

where $\bar{G}$ is taken from [10]. For two crack bands, also $\tilde{\sigma}^{(\sigma)}_{\beta'\beta'} = 0$. $S_C^{*(e,\ell,r;CR)}$ refers to integration point r.

Substitution of (10) into (1), considering (12), results in

$$\sum_{e=1}^{m}\Big[\sum_{\ell=1}^{n} g^{(\ell)}\Big(\int_{S_C^{(e,\ell;UN)}} \sigma_{l''}\,\delta\varepsilon_{i''}\,h\,dS + \int_{S_C^{(e,\ell;CR)}} \tilde{\sigma}^{(\sigma)}_{i'j'}\,\delta\varepsilon^{(\sigma)}_{i'j'}\,h\,dS\Big) + \sum_{r=1}^{r}\Big(\int_{S_{S\hat{\imath}}^{(e,r;UN)}} \sigma_{\hat{\imath}}\,\delta\varepsilon_{\hat{\imath}}\,\mu_{\hat{\imath}}\,h\,dS +$$

$$+\int_{S_{S\hat{\imath}}^{(e,r;CR)}} f_{\hat{\imath}}\,\sigma^{(\sigma)}_{\hat{\imath}}\,\delta\varepsilon^{(\sigma)}_{\hat{\imath}}\,\mu_{\hat{\imath}}\,h\,dS\Big) - \int_{V^{(e)}} \bar{\rho}g\,\delta u_g\,dV - \int_{S_p^{(e)}} \rho g\,\delta u_g\,dS\Big] - \sum_{b=1}^{a}\int_{S^{*(\ell)}} \big(\lambda_{1*}\,\delta\vartheta_{1*} + \vartheta_{1*}\,\delta\lambda_{1*}\big)\,ds^* = 0, \tag{14}$$

$$g = 1,2,3; \quad i,j = 1,2; \quad 1\equiv\alpha,\ 2\equiv\beta,\ 3\equiv\nu,$$

where

$$f_{\hat{\imath}} = 1 + \frac{|\tau^{(\sigma)}_{B\hat{\imath}}|}{\sigma^{(\sigma)}_{S\hat{\imath}}}\,\frac{\{b_{1'}\}}{\{\ell_{\hat{\imath}}\}}\,\frac{}{\phi_{\hat{\imath}}}\sum_{\ell=1}^{n} g^{(\ell)}\Big(1 + \frac{12\,\nu_{S\hat{\imath}}}{h^2}\,\nu_C^{(\ell)}\Big)\,\frac{\{b_{1'}\}}{\ell_{\hat{\imath}}^{(\ell)}} \tag{15}$$

is termed tension-stiffening factor. Upper (lower) quantities in brackets refer to parallel cracks in one (two) directions.

For the limiting case of zero steel stress at $s_{\hat{\imath}} = 0$, that is, for point B in the plot at the bottom right of Fig.3 coinciding with point A, $\sigma^{(CR)}_{S\hat{\imath}} = 2\sigma^{(\sigma)}_{S\hat{\imath}}$. Thus,

$$1 \le \frac{\sigma^{(CR)}_{S\hat{\imath}}}{\sigma_{S\hat{\imath}^{(\sigma)}}} \le 2, \tag{16}$$

resulting in the following bounds for $f_{\hat{\imath}}$ [4]:

$$1 \le f_{\hat{\imath}} \le 1 + \begin{Bmatrix} |n_{1'\hat{\imath}}| \\ 1 \end{Bmatrix}\sum_{\ell=1}^{n} g^{(\ell)}\Big(1 + \frac{12\,\nu_{S\hat{\imath}}}{h^2}\,\nu_C^{(\ell)}\Big)\,\frac{\{b_{\nu}\}}{\ell_{\hat{\imath}}^{(\ell)}}\ . \tag{17}$$

2.3. Incremental-Iterative FE Analysis

For ultimate load analysis of RC surface structures, the load must be applied incrementally. The resulting incremental internal forces are computed with the help of incremental equations of equilibrium, following from (14). In order to reduce the unbalance between external and internal forces, equilibrium iterations are performed at each load increment. Details of the incremental-iterative FE analysis are given in [4]. Details of the employed finite element may be found in [11].

3. NUMERICAL INVESTIGATION

The developed concept for consideration of tension stiffening is applied to an experimental RC panel and an experimental RC shell within the framework of ultimate load analyses.

3.1. RC Panel

The experimental panel shown in Fig.6 is considered. This panel was tested by Leonhardt and Walther [12] and analyzed by Cedolin and Dei Poli [13]. For the present analysis the panel is divided into three subregions of different material properties (subregions 1, 2, 3 in the right half of Fig.6). Material properties are listed in Table 1. The increase of the value for f_{cu} in the vicinity of the supports (subregion 3) should account for the local increase of panel strength, resulting from steel wires of 2mm diameter, helically wrapped round each pair of horizontal hooks at both ends of the main reinforcement [2]. Because of symmetry, only one half of the panel needs to be considered for the analysis. The FE model consists of 72 triangular elements. Cubic interpolation polynomials are chosen as mode shapes for the element displacement functions [11].

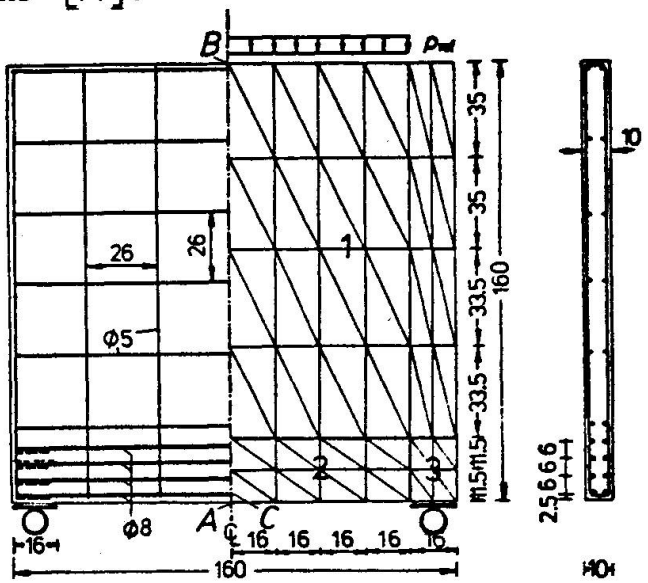

φ5(8) ≙ diameter of reinforcement steel: 5 (8) mm
dimensions of panel in cm
p_{ref} = 1.6406 kN/cm

Fig.6 Experimental RC Panel (Ref. 12) - Finite Element Model

Table 1 Material Properties for Panel

Concrete			Steel		
$E_C^{(0)}$	3200	kN/cm²	$E_S^{(0)}$	2100	kN/cm²
ν_C	0.20	—	$E_S^{(h)}$	0	kN/cm²
$f_{cu}^{(1,2)}$	-3000	N/cm²	$\phi_x^{(1)} = \phi_y$	0,5	cm
$f_{tu}^{(1,2)}$	300	N/cm²	$f_{SY}^{(I)}$	±24000	N/cm²
$f_{cu}^{(3)}$	-4000	N/cm²	$\phi_x^{(2,3)}$	0.8	cm
$f_{tu}^{(3)}$	400	N/cm²	$f_{SY}^{(II)}$	±54700	N/cm²

Arabic Superscripts Denote Subregions of Panel (See Fig.6)
Roman Superscript Indicates Steel Quality for Above Listed Bars

Fig.7 contains diagrams of the vertical displacement v at point A (see Fig.6) as a function of the load intensity factor $\chi = P/P_{ref}$, where Pref = $p$ref • 128cm = 210 kN is the resultant of $p$ref (see Fig.6). The diagram resulting from the experiment seems to indicate that the failure load is lower than the analytically obtained failure load in case of consideration of tension stiffening. In this context it should be mentioned that after initial failure at $\chi = 4.5$ in the vicinity of the left support, caused by improper consolidation of concrete, steel bandages were pressed sideways against the damaged part of the panel and the experiment was continued. At $\chi = 6.0$, failure also occurred in the vicinity of the right support, caused by fracturing of concrete [12]. Unfortunately, the continuation of the load-displacement diagram beyond initial failure is not reported in [12].

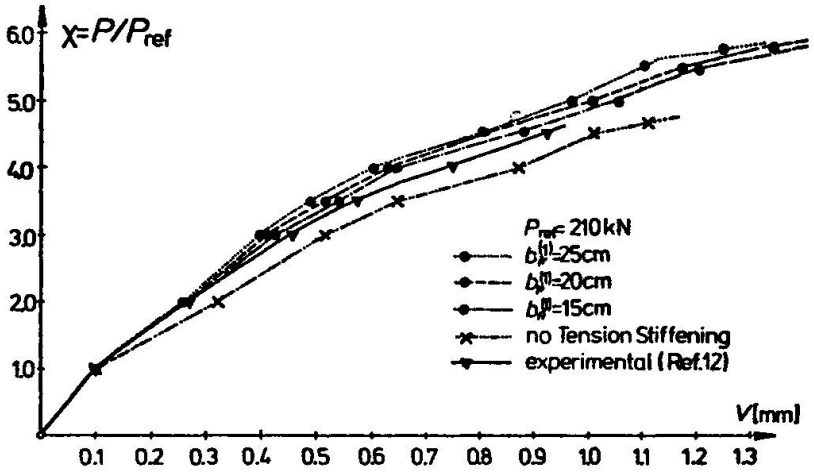

Fig.7 Vertical Displacement v of Point A versus load Intensity Factor χ

It is seen that the experimental failure load is reproduced by the analysis in case tension stiffening is considered. The load-displacement diagrams are found to be relatively insensitive to variations of the free parameter $b_f'^{(1)}$. If the tension-stiffening effect is disregarded, the failure load is underestimated by approximately 25 %.

Fig.8 shows a comparison of concrete stresses σ_{Cxx} along center line $\overline{AB}$ for three different material models at three different load intensities. The plot for $\chi = 3.0$ illustrates that, as a consequence of the tension-stiffening effect, the neutral axis experiences a shift towards the neutral axis that would be obtained in case concrete was treated in the analysis as a linear elastic, uncracked material.

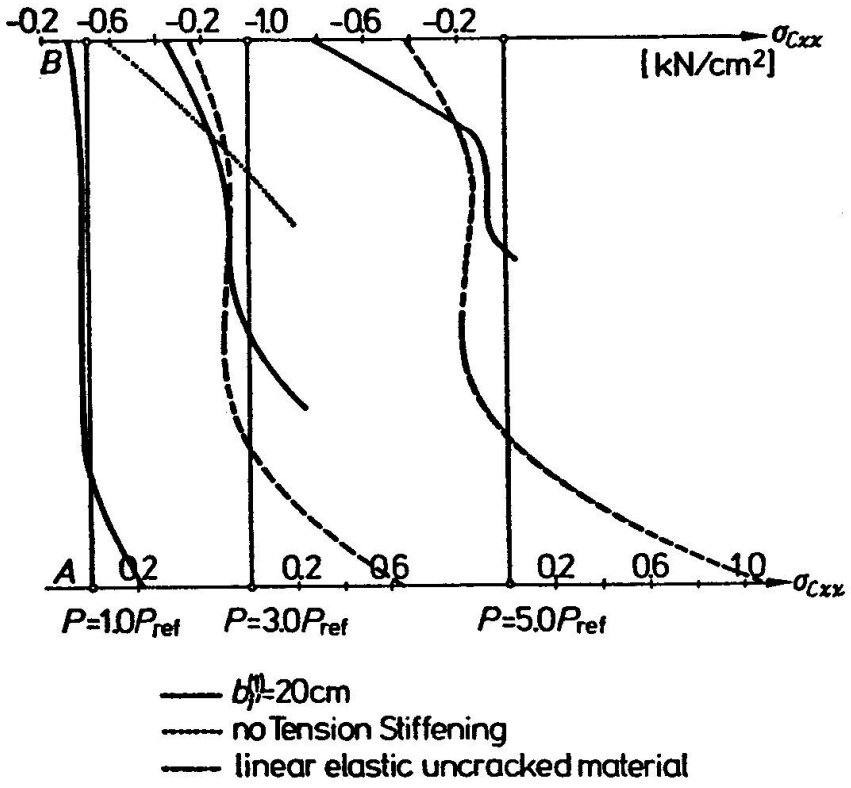

Fig.8 Comparison of Concrete Stresses σ_{Cxx} Along Center Line $\overline{AB}$ for Three Different Load Intensities

Fig.9 shows diagrams of the steel stress σ_{Sx} in the bottom main reinforcement at point C versus the load intensity factor χ . In case of consideration of the tension-stiffening effect, the results

of the writers agree well with the experimental results. This follows from consideration of average stresses in the experiment as well as in the analysis.

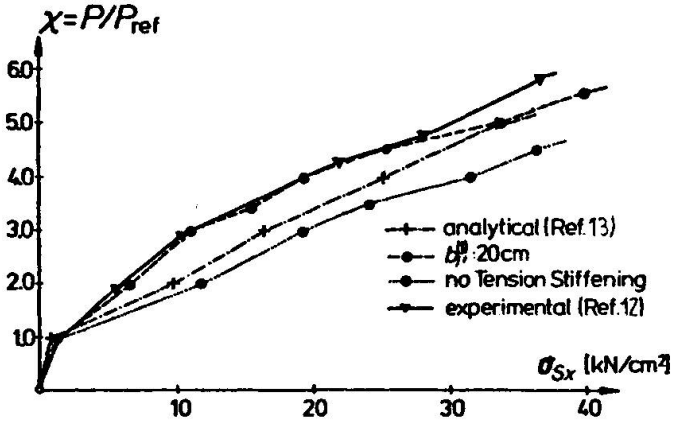

Fig.9 Stress σ_{Sx} in Main Reinforcement at Point C versus Load Intensity Factor χ

3.2. Parabolically - Cylindrical RC Shell

A 1: 8 model of a built barrel vault, tested by Hedgren [14] and analyzed by Lin [15], is re-analyzed by the writers. Because of

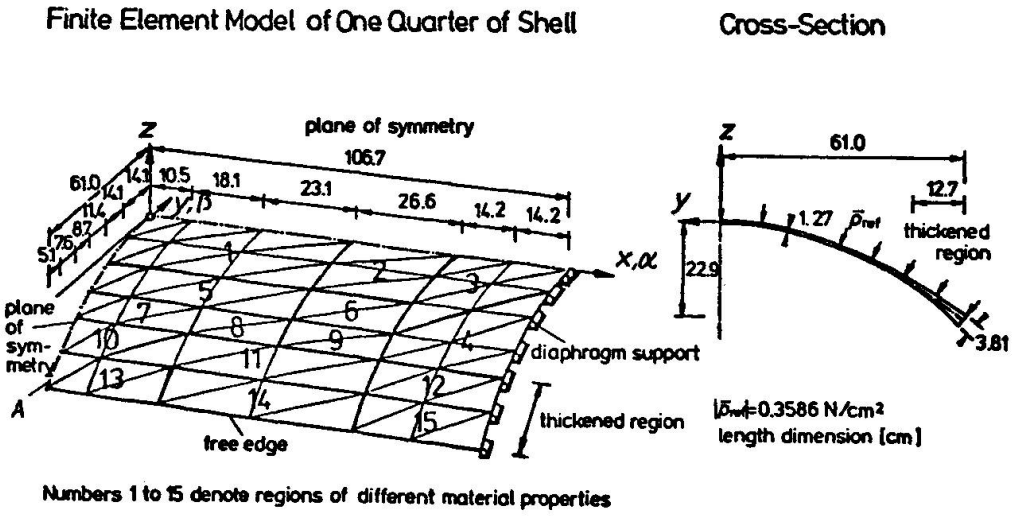

Fig.10 Experimental Parabolically - Cylindrical RC Shell (Ref.14)- Finite Element Model

symmetry, only one quarter of the shell needs to be considered for the analysis. Fig.10 shows the FE model as well as the cross section of the shell. The shell is subjected to constant hydrostatic pressure, representing a so-called "follower load".

Table 2 contains material properties. The numbers 1-15 in Fig.10 permit identification of subregions of the shell, characterized by constant material properties. Table 3 contains distances of steel layers from the middle surface of the shell, ν, referred to the thickness of the shell, h, as well as thicknesses of steel layers. For the analysis, the shell is divided into 9 concrete layers.

Table 2 Material Properties for Shell

Concrete			
$E_C^{(0)}$	2069.1		kN/cm²
ν_c	0.145		-
f_{cu}	-3027.8		N/cm²
f_{tu}	480.0		N/cm²
Steel			
Designation	Diameter [cm]	$\lvert\sigma_y\rvert$ [kN/cm²]	$\lvert\sigma_u\rvert$ [kN/cm²]
#3	0.122	25.3	36.4
#4	0.157	21.9	34.5
#9	0.343	30.7	42.0
$E_S^{(0)}$	20001.6		kN/cm²
$E_S^{(h)}$	2000.2		kN/cm²

Table 3 Steel Layers in Shell

Mat #	Bottom Longitudinal (φ=0°) ν/h	$\mu\cdot h$*	#	Bottom Circumferential (φ=90°) ν/h	$\mu\cdot h$	#	Bottom Free Edge (φ=0°) ν/h	$\mu\cdot h$	#	Middle Surface Diagonal (φ=45°) ν/h	$\mu\cdot h$	#	Top Free Edge (φ=0°) ν/h	$\mu\cdot h$	#	Top Longitudinal (φ=0°) ν/h	$\mu\cdot h$	#	Top Circumferential (φ=90°) ν/h	$\mu\cdot h$	#
1					0.014007															0.011684	
2					0.003064					-	θ	-								0.010225	
3					0.003828															0.006135	
4										0.000	0.007668	4									
5	-0.250	0.003064		-0.154	0.014007											0.140			0.250	0.005842	
6					0.003064		-	θ	-	-	θ	-	-	θ	-					0.005112	
7			3																		
8					0.007008	3				0.000	0.007668	4					0.003064	3		0.005842	4
9					0.006128															0.005112	
10										-	θ										
11	-0.312	0.006128		-0.239	0.007008					0.000	0.007668	4				0.229			0.312	0.005842	
12					0.003678						0.005112									0.006135	
13								0.058141		-	θ			0.058141							
14	-0.397	0.010225	4	-0.352	0.007008		-0.231	0.054322	9	0.000	0.007668	4	0.231	0.054322	9	0.352			0.397	0.005842	
15					0.003678			0.036215			0.005112			0.036215						0.006135	

*dimension $\mu\cdot h$ [cm]

Fig.11 shows the influence of tension stiffening on the transverse displacement w at point A (midspan of the free edge). The horizontal hatching in this figure indicates the "band width" within which the load-displacement curve obtained from the experiment is located. This band width was introduced by the writers in [4] because of the uncertainty concerning the exact location of this curve. Note that Lin [15] obtained this curve from extrapolation of Hedgren's experimental results [14]. Fig.11 illustrates that the load-displacement curve is significantly "softer" if tension stiffening is disregarded (f_t=1). In this case the failure load of the shell is underestimated.

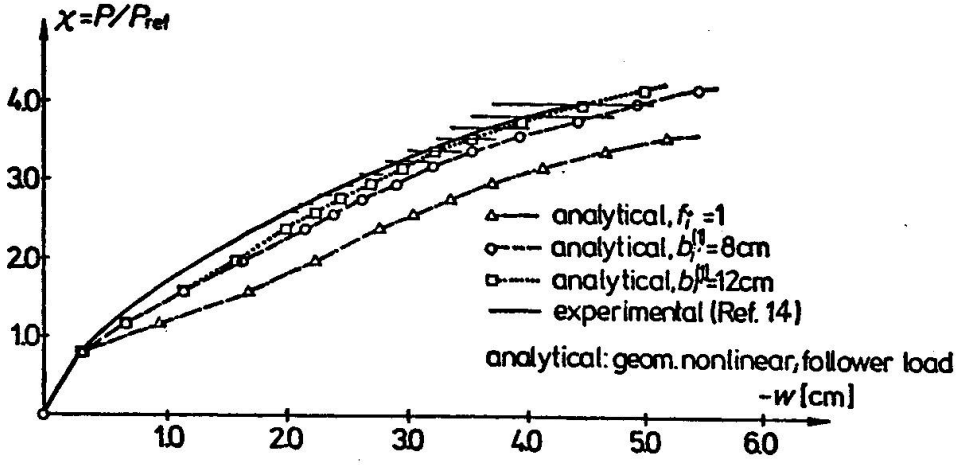

Fig.11 Transverse Displacement w at Point A versus Load Intensity Factor χ - Influence of Tension-Stiffening

Fig.12 shows the stress $\sigma_{S\alpha}$ in the bottom main reinforcement at point A as a function of the load intensity factor χ. At low load levels, the tension-stiffening effect results in a significant reduction of the steel stress.

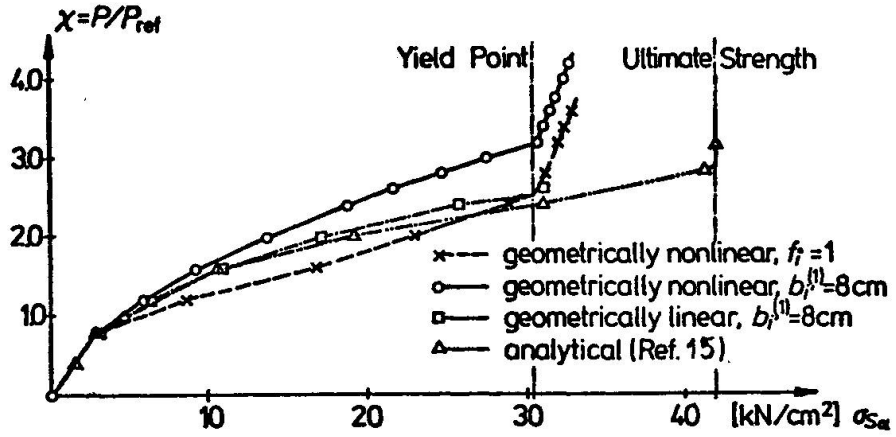

Fig.12 Stress in Bottom Main Reinforcement at Point A versus Load-Intensity Factor χ

4. CONCLUSIONS

The tension-stiffening effect is considered by means of tension-stiffening factors, representing multipliers for average values of steel stress between neighboring cracks in the equations of equilibrium. The tension-stiffening factor depends on (a) the average bond stress between neighboring cracks, (b) the angle between the normal to the crack and the intersecting reinforcement bar, (c) the degree of crack propagation through the thickness of the shell and (d) the extent of formation of secondary cracks between neighboring primary cracks. In spite of the fact that bond slip is the basis for the proposed concept, relative displacements between the reinforcement and the surrounding concrete need not be employed for the numerical analysis. Disregard of the tension-stiffening effect may result in a significant underestimation of the ultimate load. At intermediate load levels the steel stresses may be overestimated considerably. Provided a reasonable assumption is made for the initial crack spacing, results are insensitive to variation of this value.

ACKNOWLEDGEMENTS

The writers are indebted to L. Cedolin of Politecnico di Milano who devoted much of his time for introducing them to the theoretical concept and to computational details of his research on RC panels. He also made available a computer program for iterative determination of stress in the intact concrete. Many helpful discussions with W. Mudrak of Technische Universität Wien and W. Potucek of Österreichische Bundesbahn are thankfully acknowledged. Financial support of the Fonds zur Förderung der wissenschaftlichen Forschung der Republik Österreich is gratefully acknowledged.

REFERENCES

1. GILBERT, R.I.; WARNER, R.F.: Tension Stiffening in Reinforced Concrete Slabs. Proc. ASCE, J.Struct.Div. 104, 1978, 1885-1899
2. FLOEGL, H.; MANG, H.A.: Tension Stiffening Concept for RC Panels Based on Bond Slip. Manuscript Submitted for Publication in Proc. ASCE, J.Struct.Div.

3. SCANLON, A.: Time Dependent Deflections of Reinforced Concrete Slabs. Dissertation, University of Alberta, Edmonton, Canada, 1971

4. FLOEGL, H.; MANG, H.A.: On Tension Stiffening in Cracked Reinforced Concrete Slabs and Shells Considering Geometric and Physical Nonlinearity. Ing.-Arch., in print

5. KOITER, W.T.: General Equations of Elastic Stability for Thin Shells. Proc.Symp. on the Theory of Shells to Honor Lloyd Hamilton Donell, University of Houston, 1967

6. LIU, T.C.Y.; NILSON, A.H.; SLATE, F.O.: Biaxial Stress-Strain Relations for Concrete. Proc. ASCE, J.Struct.Div. 98, 1972, 1025-1034

7. KUPFER, H.: Das Verhalten des Betons unter mehrachsiger Kurzzeitbelastung unter besonderer Berücksichtigung der zweiachsigen Beanspruchung. Report, Deutscher Ausschuß für Stahlbeton, Vol. 229, Berlin, 1973

8. GRELAT, A.; POTUCEK, W.: Comportement de Panneaux en Béton précontraint soumis au Cisaillement. Report, CEBTP Paris, St. Rémy-lés-Chevr, 1978

9. FLOEGL, H.; MANG, H.: Zum Einfluß der Verschiebungsabhängigkeit ungleichförmigen hydrostatischen Drucks auf das Ausbeulen dünner Schalen allgemeiner Form. Ing.-Arch. 50, 1981, 15-30

10. CEDOLIN, L; DEI POLI,S.: Finite Element Nonlinear Plane Stress Analysis of Reinforced Concrete. Report, Costruzioni in Cemento Armato, Studi e Rendiconti, Vol. 13, Politecnico di Milano, 1976

11. MANG, H.; GALLAGHER, R.H.; CEDOLIN, L.; TORZICKY, P.: Deformation und Stabilität windbeanspruchter Kühlturmschalen. Ing.-Arch. 47, 1978, 391-410

12. LEONHARDT, F.; WALTHER, R.: Wandartige Träger. Report, Deutscher Ausschuß für Stahlbeton, Vol.178, Berlin, 1963

13. CEDOLIN,L.; DEI POLI, S.: Berechnung wandartiger Stahlbetonträger mit dem Verfahren der finiten Elemente. Beton- und Stahlbetonbau 73, 1978, 226-230

14. HEDGREN, A.W., JR.: A Numerical and Experimental Study of Translational Shell Roofs. Dissertation, Princeton University, 1965

15. LIN, C.S.: Nonlinear Analysis of RC Shells of General Form. Report, Dept. of Civ.Engng., University of California at Berkeley, 1973

16. ÅLDSTEDT, E.; BERGAN, P.G.: Nonlinear Time-Dependent Concrete-Frame Analysis. Proc. ASCE, J.Struct.Div. 104, 1978, 1077-1092

Leere Seite
Blank page
Page vide

Ellipses of Inertia for Nonlinear Analysis of Structures

Ellipses d'inertie pour l'analyse non-linéaire des structures

Trägheitsellipsen für die nichtlineare Berechnung von Konstruktionen

M. MENEGOTTO
Professor of Structural Engineering
Faculty of Architecture, University of Rome
Rome, Italy

SUMMARY
A general procedure is presented for the analysis of concrete structures composed of linear members, which is based on a particular definition of the structural stiffness. This is derived from a linearization of the paths, run by all the points of the materials, on their respective constitutive law for a given loading step.
Modified Culmann's ellipses of inertia of the corss sections allow exact incorporation of this idealization into the stiffness matrix of the structure.
The method is well suited for taking into account the interaction of the internal forces correctly.
Examples of applications are shown, including monotonic and cyclic loadings.

RÉSUMÉ
Une procédure générale est présentée pour l'analyse de structures en béton composées d'éléments monodimensionnels, basée sur une définition particulière de la rigidité de la structure. Cette rigidité est derivée d'une linéarisation des chemins, parcourus par tous les points des matériaux sur leurs propres lois tension-déformation, pour un incrément donné des charges.
Des ellipses de Culmann modifiées des sections droites permettent d'introduire exactement ce schéma dans la matrice de rigidité de la structure.
La méthode est très apte à prendre en compte correctement l'intéraction des efforts. Des exemples d'application sont présentés, comprenant charges monotones et cycliques.

ZUSAMMENFASSUNG
Ein allgemeines Verfahren für die Analyse von aus Stabelementen bestehenden Konstruktionen wird erläutert, das auf einer besonderen Definition der Steifigkeit beruht. Diese wird abgeleitet aus einer Linearisierung der Wege aller Punkte der Materialen in Bezug auf ihr Spannungs-Dehnungsverhältnis für eine gewisse Belastungsstufe.
Modifizierte Culmann's Trägheitsellipsen der Querschnitte gestatten, dieses Schema in die Steifigkeits-Matrix der Konstruktionen einzuführen.
Diese Methode eignet sich besonders, um die Interaktion innerer Kräfte korrekt in Betracht zu nehmen; Anwendungsbeispiele werden gezeigt, monotone und zyklische Belastungen inbegriffen.

1. INTRODUCTION

The basic factors generating an overall nonlinear response of the structure are geometric factors, important for slender compressed members, and mechanical factors.

Due to them, the stiffness (or the deformability) of the structure is altered following the gradual application of the loadings, and all the internal forces redistribute continuously. An accurate description of the varying stiffness of the structure is essential for the correct solution of the problem.

The numerical reproduction by matrix analysis of the behavior of structures requires a linearization of the stiffness corresponding to a given increment of the loadings or of the deformations.

The ways of performing the linearization, i.e. of defining the stiffness coefficients satisfying the correct relationships of nodal forces and displacements, are infinity; thus the actual selection is arbitrary. Among all the possible ways, the one is assumed here corresponding to a particular pseudo--elastic criterion which is deemed to be the most valuable, and conceptually correct.

In case of beam flexural elements, this criterion leads to a synthetic and easy procedure for building up the stiffness matrix, taking advantage of Culmann's theory of the ellipse of inertia.

2. IDEALIZATION OF THE STRUCTURAL PROBLEM

A set of idealizations, including a discretization of the structure into elements, is necessary in order to establish the model for the analysis.

The analysis of concrete beam elements is generally performed by first considering several representative cross sections, an then working out the characteristics of the whole element.

For the cross section, usually the linear distribution of strains is assumed, including the bond between concrete and steel. Various models of stress-strain relationships are used for the materials, either holonomic or including stress reversal paths.

For the element, the distribution of the deformabilities, within the segment connecting the analyzed sections, may be assumed as varying linearly, or with different laws. A proper selection of the spacing of sections must be made, in order to realize a suitable equivalent length of plastic rotation zones, according to empirical formulas.

The effects of cracking and tension stiffening of concrete is often accounted for approximately, through a conventional constitutive law. Shear deformations are disregarded, in dealing with flexural structures.

Once a consistent idealization is set down for the structure and for the external actions, the analytical problem is defined.

The solution may be obtained by various procedures, that will be generally iterative, due to the nonlinearity. The stiffness or the deformability method may be employed. The forces may be applied either at once or step by step.

Taking for instance the most general case of a stiffness method step by step procedure, the solution of a set of equations like

$$\mathbf{K}_{st} \cdot \Delta\mathbf{U} = \Delta\mathbf{P} \tag{1}$$

is to be performed at each step; where

$\mathbf{K}_{st}$ is a stiffness matrix of the structure

$\Delta\mathbf{U}$ is the vector of nodal displacements

$\Delta\mathbf{P}$ is the vector of applied nodal forces;

all being referred to the actual step.

$\mathbf{K}_{st}$ is only valid for the particular step and for the particular set of loads, as it represents a linearization of a nonlinear relationship.

The criterion of linearization is deemed to be of major importance for finding the comprehensive

correct solution, and for a speedy convergence.

The criterion is arbitrary. In fact, the matrix $\mathbf{K}_{st}$ is n x n (n being the number of components of $\Delta\mathbf{U}$), so that infinite combinations of its coefficients satisfy eqn. (1), given $\Delta\mathbf{U}$ and $\Delta\mathbf{P}$.

The criterion presented in the following has been employed for numerous applications and allows for a detailed analysis of the behavior of any structure idealized as above.

3. STIFFNESS CRITERION

The stiffness matrix of the structure will be derived from a secant linearization of the paths run by "every" point of material in the structure on its own constitutive law, during the considered step.

Selected representative cross sections are suitably discretized into a finite number of areolas of the different materials (Fig. 1).

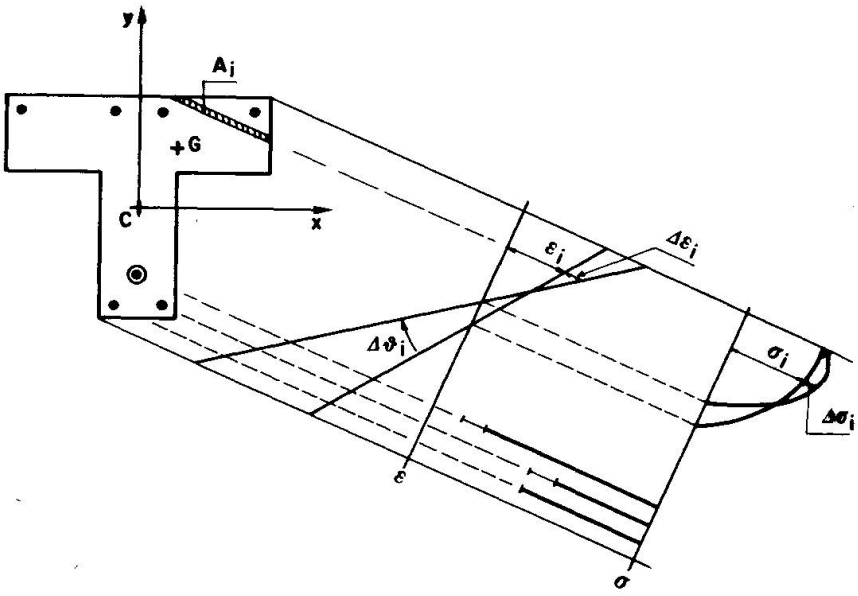

Fig. 1

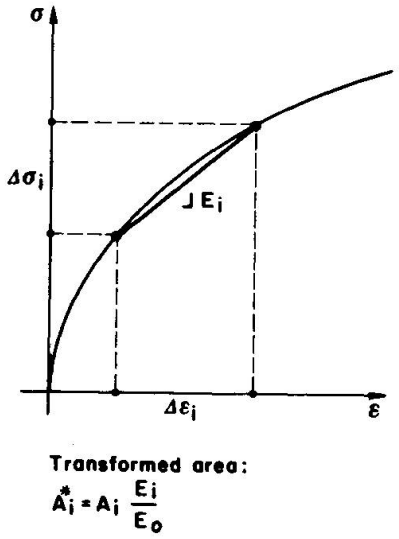

Fig. 2

If $\Delta\epsilon_i$ and $\Delta\sigma_i$ are the strain and the stress variations undergone by the i-th areola during the step (Fig. 2), a pseudo-elastic modulus is defined as:

$$E_i = \frac{\Delta\sigma_i}{\Delta\epsilon_i} \tag{2}$$

Then the areola is assigned a transformed area:

$$A_i^* = A_i \frac{E_i}{E_0} \tag{3}$$

A_i being its geometric area, and E_0 an arbitrary reference modulus, which can be taken as $E_0 = 1$.

This operation has the most general application: the stress-strain state of the areolas may run on strain-softening branches (E_i negative) or rest on a cracked part ($E_i = 0$, if the crack remains opened for the step) or run on strain reversal paths of any shape.

Extending the calculation of A_i^* to all the areolas of the section, a whole transformed section is obtained. This can be handled as a homogeneous linear elastic section, having a modulus of elasticity E_0.

Namely, all the typical characteristics of the homogeneous sections, as Centroid G, Area A, Static Moments S, Moments of Inertia J, etc, may be easily calculated. Indeed, the well known Culmann's ellipse of inertia [1] may be built up, which summarizes all these characteristics and relates the internal forces N M_x M_y with the strain state (except for the E modulus).

When putting $E_0 = 1$, such a modified ellipse not only relates the load center with the neutral axis, but it completely represents the secant stiffness or deformability of the cross section for the step.

Of course, it is meaningful for the original section, only when referring to the particular forces applied at the particular step, due to eqn (2), and it may be called the "step secant" ellipse of the section.

But its usefulness is twofold. First, the ellipse is very helpful in finding the stress-strain state on the section itself, corresponding to a given internal forces variation. Then, it is necessary for the construction of the structure's stiffness relationships according to the criterion adopted.

4. CROSS SECTION ANALYSIS

During the iterative procedure for solving the structure's problem (eqn. 1), at each cycle all the cross sections must be analyzed to find their stress strain variation, as well as the corresponding secant deformability, expressed by the relationship

$$\Delta\mathfrak{E} = \mathbf{K}_{cs}^{-1} \cdot \Delta\mathbf{S} \tag{4}$$

where:

$\Delta\mathfrak{E} \equiv \{\Delta\epsilon_c, \Delta\theta_x, \Delta\theta_y\}$ is the vector of deformation variations: strain of reference point C, and curvatures about the fixed axes x, y, (Fig. 1);

$\Delta\mathbf{S} \equiv \{\Delta N, \Delta M_x, \Delta M_y\}$ is the vector of force variations; and

$\mathbf{K}_{cs}^{-1}$ is the deformability matrix of the cross section, that is to be found together with $\Delta\mathfrak{E}$; it will be defined as follows:

$$\mathbf{K}_{cs}^{-1} \equiv \begin{vmatrix} \left(\frac{\partial\epsilon_c}{\partial N}\right)^* & \left(\frac{\partial\epsilon_c}{\partial M_x}\right)^* & \left(\frac{\partial\epsilon_c}{\partial M_y}\right)^* \\ \left(\frac{\partial\theta_x}{\partial N}\right)^* & \left(\frac{\partial\theta_x}{\partial M_x}\right)^* & \left(\frac{\partial\theta_x}{\partial M_y}\right)^* \\ \left(\frac{\partial\theta_y}{\partial N}\right)^* & \left(\frac{\partial\theta_y}{\partial M_x}\right)^* & \left(\frac{\partial\theta_y}{\partial M_y}\right)^* \end{vmatrix} \tag{5}$$

and directly written down throughout the parameters of the modified ellipse of inertia of the section (Fig. 3).

$$\begin{aligned}
&\left(\frac{\partial\epsilon_c}{\partial N}\right)^* = \frac{1}{A} + \frac{\xi_c^2}{J_\xi} + \frac{\eta_c^2}{J_\eta} \\
&\left(\frac{\partial\epsilon_c}{\partial M_x}\right)^* = \frac{\xi_c}{J_\xi}\cos\tau + \frac{\eta_c}{J_\eta}\sin\tau = \left(\frac{\partial\theta_x}{\partial N}\right)^* \\
&\left(\frac{\partial\epsilon_c}{\partial M_y}\right)^* = \frac{\xi_c}{J_\xi}\sin\tau + \frac{\eta_c}{J_\eta}\cos\tau = \left(\frac{\partial\theta_y}{\partial N}\right)^* \\
&\left(\frac{\partial\theta_x}{\partial M_x}\right)^* = \frac{1}{J_\xi}\cos^2\tau + \frac{1}{J_\eta}\sin^2\tau \\
&\left(\frac{\partial\theta_x}{\partial M_y}\right)^* = \left(\frac{1}{J_\eta} - \frac{1}{J_\xi}\right)\sin\tau\cos\tau = \left(\frac{\partial\theta_y}{\partial M_x}\right)^* \\
&\left(\frac{\partial\theta_y}{\partial M_y}\right)^* = \frac{1}{J_\xi}\sin^2\tau + \frac{1}{J_\eta}\cos^2\tau
\end{aligned} \tag{6}$$

The expressions of the above coefficients require some observations.

The areas and moments of inertia in eqns. (6) are not only geometric, but contain the moduli of elasticity too, having put $E_0 = 1$ in eqn. (3).

The partial derivatives appearing in eqns. (5) and (6) are marked with a star (*), meaning that they are calculated on the pseudo-elastic secant scheme: for instance, $(\partial\epsilon_c/\partial N)^*$ is not calculated as variation of ϵ_c for a variation of N alone, but for a variation of N on the transformed section, which accounts for the actual interaction of ΔM_x and ΔM_y with ΔN for that step.

The matrix appears symmetric, due to the pseudo-elastic homogenization.

The way of calculating the coefficients (eqns. 6) corresponds to the particular definition given for the secant deformability.

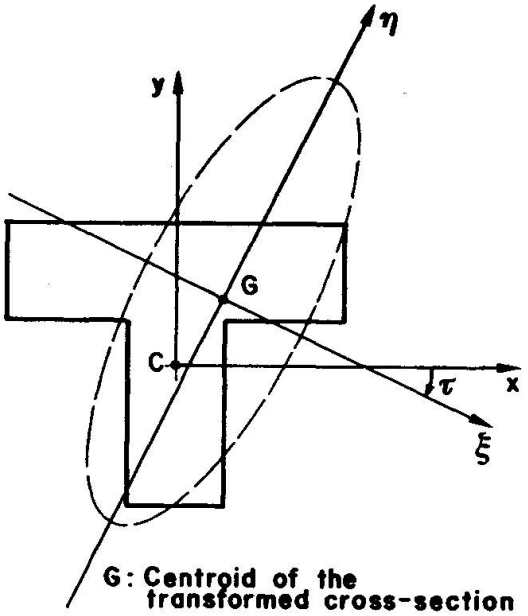

Fig. 3 — Ellipse of inertia of the transformed section.

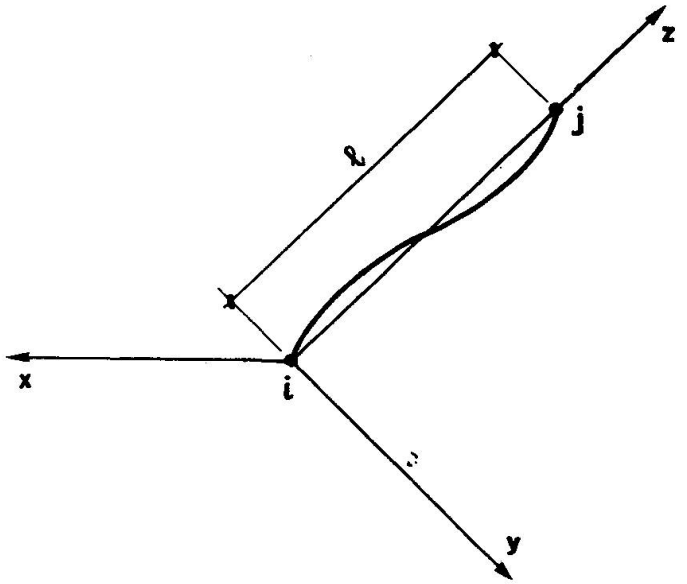

Fig. 4 — Intrinsic coordinates of the element i - j.

During the iterative solution of eqn. (4), the matrix $\mathbf{K}_{cs}^{-1}$, i.e., the modified ellipse of inertia of the cross section, is easily built up at every cycle, as follows.

The section is discretized into a large number of areolas of concrete, of ordinary and of prestressing steel (initial prestress is accounted for on all the materials). From a first tentative strain variation, all the transformed areas A_i^* are calculated by means of eqns. (2) and (3), as well as all the characteristics A, J etc of the transformed section. These, introduced into $\mathbf{K}_{cs}^{-1}$ through eqns. (6), allow for a new vector $\Delta\mathfrak{E}$ being calculated, as function of the given $\Delta\mathbf{S}$ (eqn. 4). The cycle is repeated up to convergence.

This is sped up substantially by the step secant ellipse, which provides immediately good orientation toward the state of stress produced by the combined internal forces $\Delta\mathbf{S}$.

On the other hand, it must be said that this procedure is comparatively less effective when considering only the gradual softening of the material for increasing stress. In fact, in cases of single or independent variables, as for pure compression or pure uniaxial bending, procedures like Newton-Raphson are faster in converging.

But, when concrete sections are subject to combined forces, the ordinary partial derivatives would be extremely (and uncorrectly) sensitive to the position of the neutral axis and, specially, to its deviation induced by finite variations of internal forces. Then, the much better orientation of the derivatives defined as in eqns. (6) becomes the decisive factor.

Furthermore, it was shown that this procedure offers the simultaneous finding of the correct secant deformability itself of the cross section, $\mathbf{K}_{cs}^{-1}$, which represents the best basis for the definition of the stiffness of the element and of the whole structure.

5. ELEMENT AND STRUCTURE STIFFNESS

The problem of selecting a proper linearization of the stiffness is quite the same as for the cross section; only there are more interacting forces.

To define the mechanic stiffness of an element i-j in its intrinsic coordinate system (Fig. 4), five components are to be related:

$$\Delta \mathbf{F} = \mathbf{K}_{el} \cdot \Delta \Phi \tag{7}$$

where:

$$\Delta \mathbf{F} \equiv \{\Delta N, \Delta M_{xi}, \Delta M_{xj}, \Delta M_{yi}, \Delta M_{yj}\}$$

$$\Delta \Phi \equiv \{\Delta\Delta l, \Delta\phi_{xi}, \Delta\phi_{xj}, \Delta\phi_{yi}, \Delta\phi_{yj}\}$$

$\mathbf{K}_{el}$ is the stiffness matrix of the element, yet to be defined.

As, for the section, the deformability was worked out by considering the areolas of material as linear elastic consistently with the secant moduli; thus, for the element, the cross section will be considered linear elastic consistently with the secant ellipses.

Thus, the definition of $\mathbf{K}_{el}$ consists in expressing the stiffness of an elastic beam with variable cross section, which can be done by means of well known procedures.

First, the deformability matrix is built up:

$$\mathbf{K}_{el}^{-1} \equiv \begin{vmatrix} \left(\frac{\partial \Delta l}{\partial N}\right)^* & \left(\frac{\partial \Delta l}{\partial M_{xi}}\right)^* & \left(\frac{\partial \Delta l}{\partial M_{xj}}\right)^* & \left(\frac{\partial \Delta l}{\partial M_{yi}}\right)^* & \left(\frac{\partial \Delta l}{\partial M_{yj}}\right)^* \\ & \left(\frac{\partial \phi_{xi}}{\partial M_{xi}}\right)^* & \left(\frac{\partial \phi_{xi}}{\partial M_{xj}}\right)^* & \left(\frac{\partial \phi_{xi}}{\partial M_{yi}}\right)^* & \left(\frac{\partial \phi_{xi}}{\partial M_{yj}}\right)^* \\ & & \left(\frac{\partial \phi_{xj}}{\partial M_{xj}}\right)^* & \left(\frac{\partial \phi_{xj}}{\partial M_{yi}}\right)^* & \left(\frac{\partial \phi_{xj}}{\partial M_{yj}}\right)^* \\ & \text{(Symm)} & & \left(\frac{\partial \phi_{yi}}{\partial M_{yi}}\right)^* & \left(\frac{\partial \phi_{yi}}{\partial M_{yj}}\right)^* \\ & & & & \left(\frac{\partial \phi_{yj}}{\partial M_{yj}}\right)^* \end{vmatrix} \tag{8}$$

The starred derivatives have the same meaning as in cross section analysis, i.e., they are calculated on the secant pseudo-elastic scheme; therefore, the matrix in eqn. (8) is also symmetric.

The coefficients are calculated by numerical integration of the deformed axis line, through the coefficients of the matrixes $\mathbf{K}_{cs}^{-1}$ of the selected cross sections in the element, according to the distribution assumed for the deformabilities between two of them.

$$\left(\frac{\partial \Delta l}{\partial N}\right)^* = \int_0^l \left(\frac{\partial \epsilon_c}{\partial N}\right)^* dz$$

$$\left(\frac{\partial \Delta l}{\partial M_{xi}}\right)^* = \int_0^l \left(\frac{\partial \epsilon_c}{\partial M_x}\right)^* \left(\frac{z}{l} - 1\right) dz \tag{9}$$

$$\left(\frac{\partial \Delta l}{\partial M_{xj}}\right)^* = \int_0^l \left(\frac{\partial \epsilon_c}{\partial M_x}\right)^* \frac{z}{l}\, dz$$

. . . . . .

. . . . . .

Finally, by inverting the matrix $\mathbf{K}_{el}^{-1}$, the stiffness matrix of the element, $\mathbf{K}_{el}$, is obtained.

Then, the stiffness matrix $\mathbf{K}_{st}$ of the structure is built up, as for a linear elastic structure: i.e. the intrinsic stiffness matrixes $\mathbf{K}_{el}$ are projected onto the global coordinate system — eventually being added "geometric matrixes" — and are assembled to form $\mathbf{K}_{st}$.

This matrix is adjusted iteratively during a step, up to convergence of eqn. (1).

It has the property, like the section and the element matrixes seen above, of incorporating exactly the secant stress-strain paths of all the considered points. Therefore it offers a very accurate relationship between the set of external forces and the displacements.

Indeed, all its coefficients represent partial derivatives calculated on the secant elasticity resulting from the combined acting of all the components of $\Delta\mathbf{P}$ (eqn. 1); the meaning of the generic coefficient of $\mathbf{K}_{st}$ is in fact:

$$k_{mn} = \left(\frac{\partial P_m}{\partial U_n}\right)^* \tag{10}$$

(where the asterisk is to be understood as before).

As a consequence, the internal forces distribution rapidly assumes the correct trim in the iterations. Whereas the calculation of derivatives from the separate application of the loading components, i.e.,

$$k_{mn} = \frac{\partial P_m}{\partial U_n} \tag{11}$$

would yield very dispersive iterations, particularly when the degrees of freedom are numerous, and the mutual orientation of the displacements is much affected by the simultaneous action of various forces.

6. TYPICAL APPLICATIONS

The described ellipse was called "step-secant", being referred to the secant elasticity of the structure during a step of an incremental analysis.

Incremental analysis is convenient in several cases, as for example in highly hyperstatic structures showing subsequent formations of "plastic hinges"; while it necessary in cases of loading reversals, or even of monotonic loadings inducing significant stress reversals. Some applications have been done, with computer programs using this type of analysis [2, 4].

Figures 5, 6, 7 illustrate the results of the analysis of a micro-concrete multistory frame for reproducing an experimental test. The calculated load-deflection cyclic curve matched the test result very well. Moreover, the moment-curvature history under variable normal force was recorded in all the sections as shown in Fig. 6.

In other cases, the use of different types of linearization may be suitable: the "full-secant" linearization and the "tangent" linearization, which are limit cases of the previous one and require the same sequence of calculation.

An example is the case of slender bridge piers in biaxial bending [3]. These structures are generally statically determinate or lowly indeterminate, and do not undergo extended plasticizations. On the other hand, the variability of the cross section and the presence of distributed normal and lateral forces produce important relative deviations of the neutral axis along the height of the structure (Fig. 9).

Then, the design loads may be applied in a single step, the pseudo-elastic model resulting full--secant. Eqn. (2) becomes

$$E_i = \frac{\sigma_i}{\epsilon_i} \tag{12}$$

The deformed axis line is numerically integrated along the height, and compatibility conditions are imposed at the top, if the structure is hyperstatic.

In the latter case, the deformability corresponding to small variations of the stress strain state, around the calculated state, must be defined. Therefore a "tangent" ellipse is built up at every cross

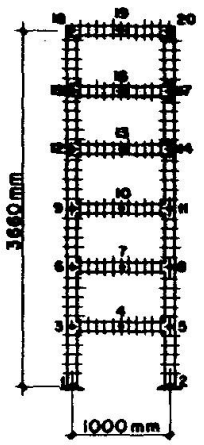

GIRDERS

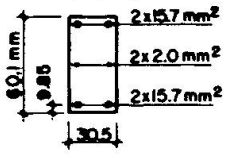

COLUMNS

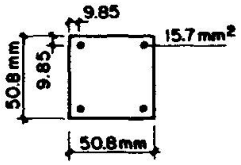

CONCRETE
f_c = 33 MPa
E = 38000 MPa

STEEL
f_y = 300 MPa
E = 210000 MPa
b = 0.0125
R = 20

5

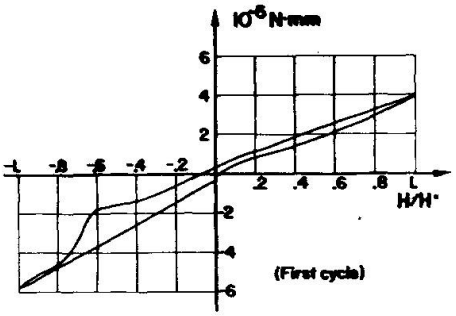

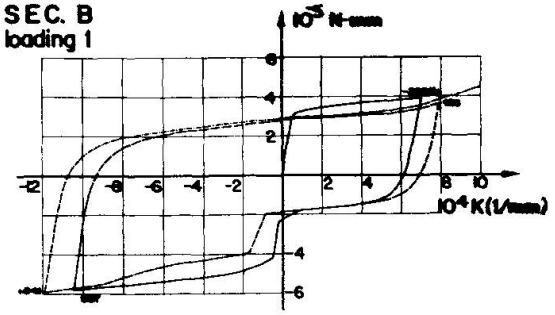

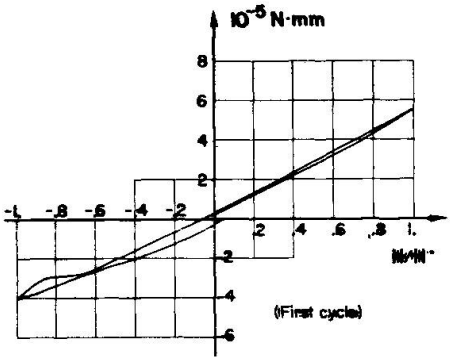

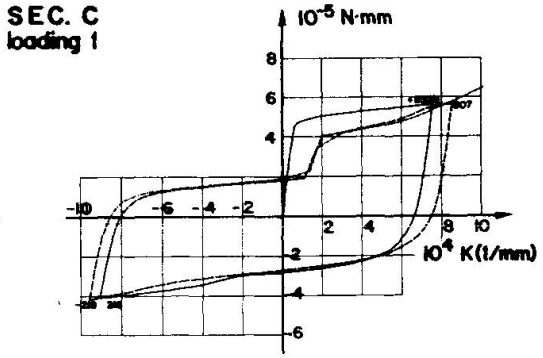

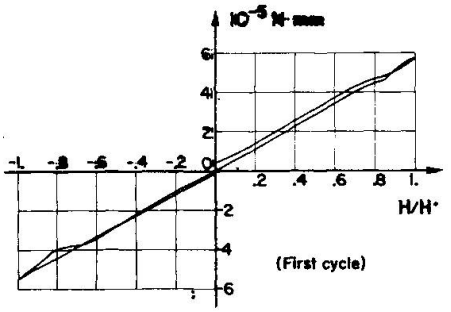

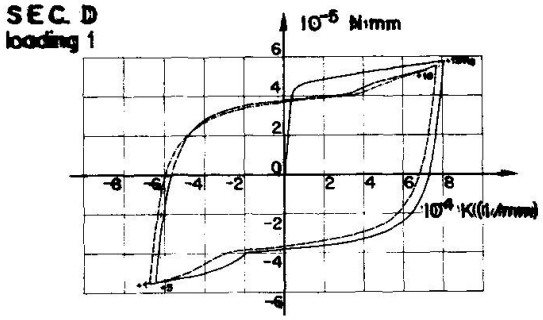

6

7

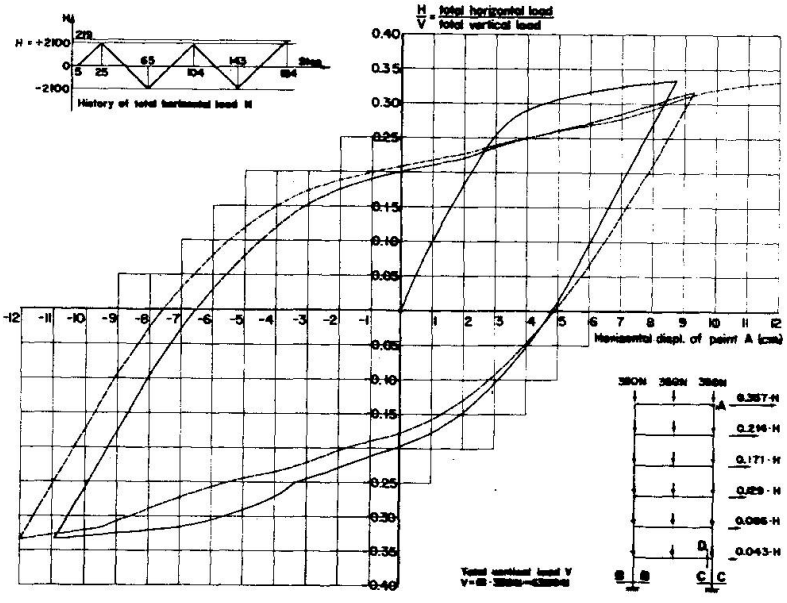

Fig. 5 — Multistory microconcrete frame as described for the analysis [2].

Fig. 6 — Moment-External Load Diagrams and Moment-Curvature Diagrams.

Fig. 7 — Load-displacement diagram obtained analytically.

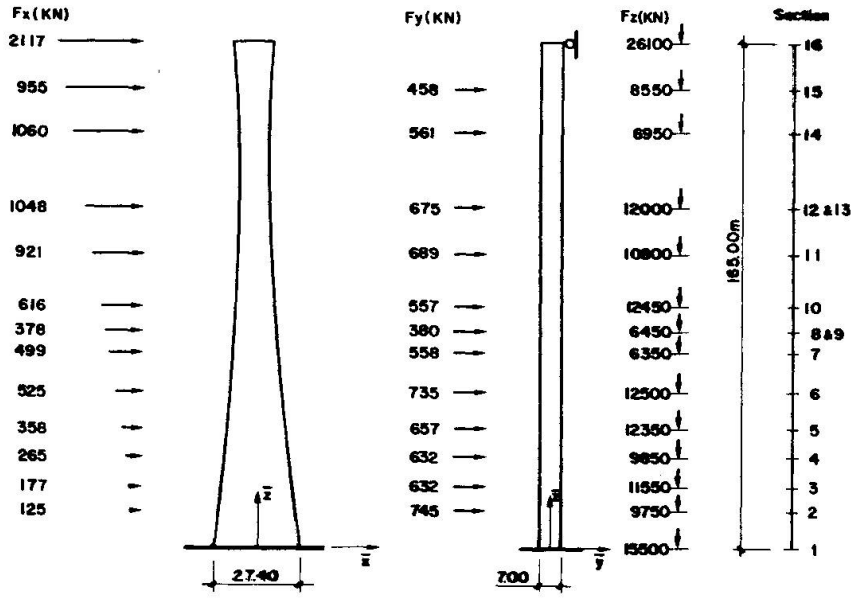

Fig. 8 – Prestressed tall bridge pier, with discretized design loads and cross-sections [3].

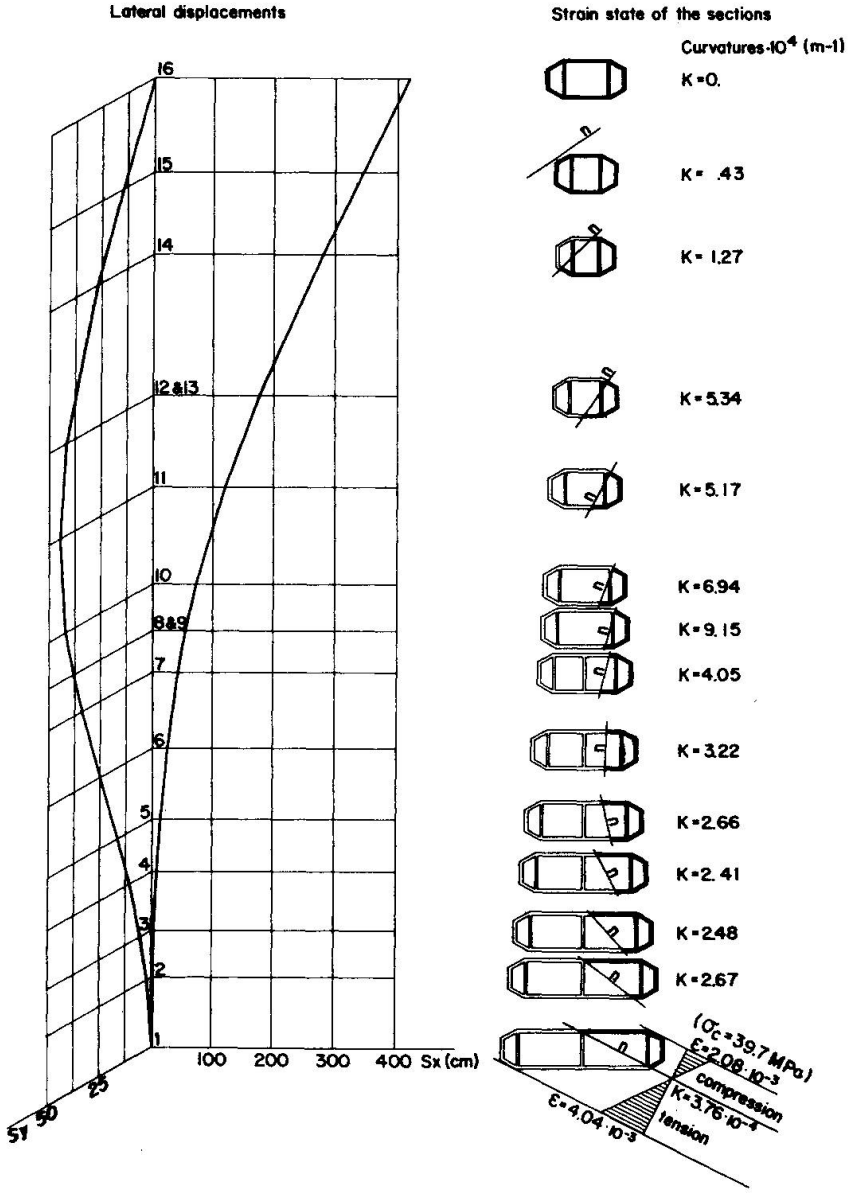

Fig. 9 – Deformation and strain state of the pier in fig. 8 at collapse.

section, using, as pseudo-elastic moduli E_i, the tangent values

$$E_i = \left(\frac{d\sigma_i}{d\epsilon_i}\right)_{S_i} \tag{13}$$

calculated at the strain states S_i of the respective areolas.

These ellipses are used to make up, by integration along the axis of the structure (similar to that of eqn. 9), the flexibility matrix referred to the displacements at the top.

Fig. 8 shows the problem of a prestressed concrete tall bridge pier under triaxial loadings [3]. In Fig. 9 the complete state of stress at collapse is illustrated, as furnished by the analysis.

7. CONCLUSION

The nonlinear behavior of concrete structures is strongly affected by the interaction of and the continuous redistribution of the internal forces.

A general procedure for structural analysis has been presented, based on a particular definition of the linearized stiffness of a structure.

The stiffness matrix of the structure is worked out on the assumption that the materials in every point of the structure — instead of describing the actual curved paths on the respective constitutive laws — describe the corresponding secant segments.

Such a matrix obviously yields, for the whole step of calculation, the same results that would be obtained following the actual nonlinear paths, thus being a correct linearization, as well as any arbitrary *a posteriori* linearization fulfilling the true solution. But it is the only one that would yield exact solutions for any fraction of the step, if the local secant paths were true.

Therefore it should be acknowledged as the only true secant linearization for the structural stiffness.

The construction of such a matrix is possible by the use of modified ellipses of inertia of the cross sections, which are the means of incorporating the *spot* secant stiffness of the material into the global stiffness relationship. By that means, the local phenomena contributing to the deformation (cracking, yielding, degradation) can be exactly related with all the individual displacement components — provided that they are suitably incorporated in the constitutive laws — theoretically with any degree of precision, if the geometric discretization and the loading steps are fine enough.

The method proved itself to be very effective in the analysis of nonlinear problems of structures, subject to monotonic or cyclic loadings.

Several computer programs have been prepared following it, and many applications have been performed like in the examples sketched in this paper.

REFERENCES

[1] CULMANN, K. — ***Die graphische Statik*** — Meyer - Zeller, Zürich, 1875.

[2] MENEGOTTO, M. and PINTO, P.E. — ***Exact Analysis of Reinforced Concrete Building Frames. Cyclic Loadings and Stability Problems*** — C.E.B. Bulletin n.101 - Paris, 1974.

[3] MENEGOTTO, M. and PINTO, P.E. — ***Slender R.C. Compressed Members in Biaxial Bending*** — A.S.C.E. Jnl of Struct. Div. Vol. 103, New York, March 1977.

[4] MENEGOTTO, M. — ***Analisi Non Lineare di Strutture a Telaio in Cemento Armato*** — L'Industria delle Costruzioni, n. 7, Rome, July 1978.

3-Dimensional Nonlinear Analysis of Reinforced Concrete Columns

Analyse 3-dimensionnelle non-linéaire de colonnes en béton armé

3-Dimensionale nichtlineare Berechnung von Stahlbetonstützen

KIYOSHI MUTO
Professor Emeritus
University of Tokyo
Tokyo, Japan

TADASHI SUGANO
Dr. Eng., Senior Research Eng.
Muto Institute of Kajima Corp.
Tokyo, Japan

TAKASHI MIYASHITA
Senior Research Eng.

NORIO INOUE
Senior Research Eng.

SUMMARY
Experimental and analytical studies are presented on the nonlinear behavior of reinforced concrete columns under earthquake loads. The analytical method is based on the 3-dimensional Finite Element Method which enables dealing with repeated load reversals. To establish the nonlinear parameters of concrete, experiments and their simulation analyses of columns under axial force only were conducted with attention given to the confinement effect of hoops (ties). Finally a simulation analysis of a hooped column under repeated lateral forces and axial forces was conducted.

RÉSUMÉ
Le comportement non-linéaire des colonnnes en béton armé pour des charges sismiques est étudié au moyen de la Méthode des Eléments Finis Tri-dimensionnels, qui peut également être utilisée pour des charges répétées réversibles. Dans la première partie, des expériences et des analyses de simulation des colonnes portant uniquement la force axiale se sont conduit pour déterminer le paramètre non-linéaire du béton en tenant compte du faible effet des étriers. Ensuite l'analyse de simulation de la colonne avec étriers portant les forces latérales et axiales est faite.

ZUSAMMENFASSUNG
Das nichtlineare Verhalten von Stahlbetonstützen unter Erdbebenbelastung ist mit 3-dimensionaler Finite-Elemente-Methode untersucht, die eine Behandlung der Wechselbelastung ermöglicht.
Am Anfang wurden Versuch und simulierende Analysis der Stützen nur mit der Axialkraft durchgeführt, um die nichtlinearen Parameter des Betons unter Berücksichtigung der Umschliessungswirkung der Bügel festzusetzen.
Dann wurde die simulierende Analysis von Stützen mit Bügelbewehrung unter Wechselbelastung und Axialkraft durchgeführt.

1. INTRODUCTION

When a reinforced concrete column is subjected to repeated lateral forces, such as earthquake loads, its plastic behavior is considerably influenced not only by longitudinal reinforcement but also by lateral reinforcement, which confines core concrete. This paper presents a study of the three dimensional nonlinear behavior of reinforced concrete columns by experiments and analyses, with attention given to afore-mentioned confining effect (1).

In the proposed method of analysis a reinforced concrete column is considered to be composed of core concrete, cover concrete, reinforcing bars and bonds with appropriate nonlinearity of each element. For core concrete the plasticity theory assuming Drucker-Prager's yield function is adopted as it is a simple formula which can introduce the volume dilatancy caused by the plastic deformation of concrete. Further hysteretic loops are assumed for each element so that the reversal of loading can be analyzed.

In the beginning experiments and their simulation analyses of columns subjected to axial force only were conducted to establish the nonlinearity parameter with attention given to the confinement effect of hoops.

Then the proposed method was applied to a column subjected to repeated lateral forces and axial force. This pursued the reversal of loading from the positive to the negative region.

2. METHOD OF ANALYSIS

2.1 Modeling of column

A reinforced concrete column is considered to be composed of core concrete, cover concrete, longitudinal and lateral reinforcing bars, and bond between concrete and reinforcing bars as shown in Fig. 1 (2,3,4). Here core concrete and cover concrete are modeled separately because the former shows improvement of strength and ductility compared with the latter. Such behavior is caused by the confinement effect of lateral reinforcement, which can be investigated only by these three dimensional studies.

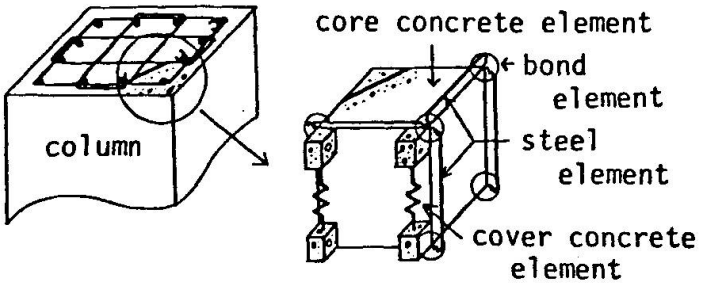

Fig. 1 Modeling of Column

2.2 Core concrete element

2.2.1 Modeling of core concrete

Core concrete is represented by a hexahedral isoparametric element (5). For numerical integration two integrating points are assumed in each direction and Gaussian Quadrature Formula is adopted. The nonlinearity of concrete is judged by the stress and strain at eight Gauss points respectively.

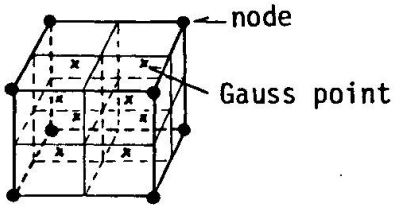

Fig. 2 Core Concrete Element

2.2.2 Nonlinearity in compressive side

The constitutive equation of concrete in plastic range is defined by several theories, such as plasticity [6,7], nonlinear elasticity [8,9,10,11], orthotropic model [12,13,14], Endochronic theory [15] and others [16,17]. Among them the plasticity theory is adopted in this analysis. Then the nonlinearity of concrete is defined by the initial yield condition, flow rule and hardening rule as indicated below. The constants adopted in their rules are established to be adequate to uniaxial condition. Next the first yield surface and the second one are considered homologous and the ultimate strain is replaced with the ultimate equivalent plastic strain.

Initial yield condition: For the yielding criteria of concrete, several functions are proposed [18,19,20,21]. As a matter of course, if more parameters are assumed, better coincidence will be obtained. In this analysis the following Drucker-Prager's function is adopted as it is the simplest formula which can introduce the volume dilatancy caused by the plastic deformation of concrete. Then only one parameter α is assumed for representing the nonlinearity of concrete.

$$f = \frac{3}{2}\alpha(\sigma_x+\sigma_y+\sigma_z)+f_0 = k \tag{1}$$

$$f_0^2 = \frac{1}{2}\{(\sigma_y-\sigma_z)^2+(\sigma_z-\sigma_x)^2+(\sigma_x-\sigma_y)^2+6(\tau_{yz}^2+\tau_{zx}^2+\tau_{xy}^2)\} \tag{2}$$

Where k is a constant representing strength of concrete, which is obtained by the uniaxial test. This yield function can be shown by principal stress field as in Fig. 3.

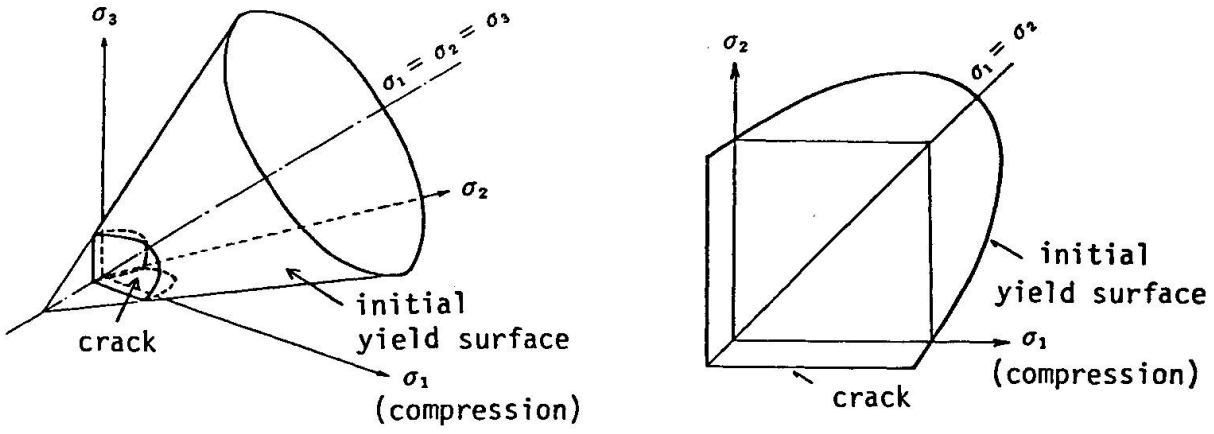

(A) 3 Dimension (B) 2 Dimension

Fig. 3 Initial Yield Condition

Flow rule: Due to v. Mises the plastic strain increment vector $\{d\varepsilon^p\}$ lies in the exterior normal of the yield surface at the stress point (Fig. 4).

$$\{d\varepsilon^p\} = \left\{\frac{\partial f}{\partial \sigma}\right\} d\lambda \qquad d\lambda > 0 \tag{3}$$

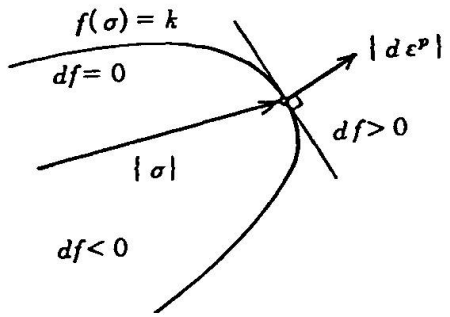

Fig. 4 Flow Rule

Hardening rule: Prager's kinematic hardening rule modified by Ziegler [22] is used (Fig. 5). The incremental translation of the center of the yield surface $\{d\sigma_0\}$ is defined by

$$\{d\sigma_0\} = \{\sigma - \sigma_0\}\, d\mu \qquad d\mu > 0 \tag{4}$$

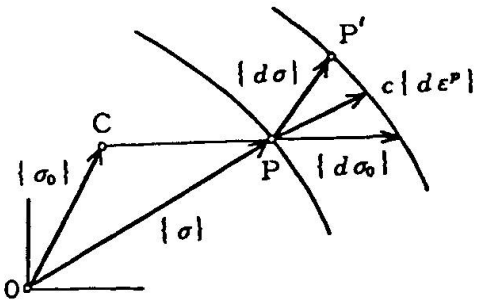

Fig. 5 Hardening Rule

Here the yield surface moves in the direction of the vector CP connecting the center of the yield surface with the stress point. The scalar $d\mu$ in Eq. 4 is determined by the condition that P remains on the yield surface in plastic flow. This condition is

$$\{d\sigma - d\sigma_0\}^T \left\{\frac{\partial f}{\partial \sigma}\right\} = 0 \tag{5}$$

and from Eq. 4 and Eq. 5 the following is obtained.

$$d\mu = \frac{\left\{\frac{\partial f}{\partial \sigma}\right\}^T \{d\sigma\}}{\{\sigma - \sigma_0\}^T \left\{\frac{\partial f}{\partial \sigma}\right\}} \tag{6}$$

If it is assumed that the vector $c\{d\varepsilon^p\}$ is the projection of $\{d\sigma\}$ (and thus of $\{d\sigma_0\}$) on the exterior normal of the yield surface, this condition is

$$\{d\sigma - c\, d\varepsilon^p\}^T \left\{\frac{\partial f}{\partial \sigma}\right\} = 0 \tag{7}$$

then from Eq. 3 and Eq.7 the following is obtained.

$$d\lambda = \frac{1}{c} \frac{\left\{\frac{\partial f}{\partial \sigma}\right\}^T \{d\sigma\}}{\left\{\frac{\partial f}{\partial \sigma}\right\}^T \left\{\frac{\partial f}{\partial \sigma}\right\}} \tag{8}$$

Constitutive equation of concrete: The stress vs. strain relation in elastic range is represented incrementally by the Hooke's law.

$$\{d\sigma\} = [D^e]\{d\varepsilon^e\} \tag{9}$$

The total strain is obtained by the summation of elastic strain and plastic strain.

$$\{d\varepsilon\} = \{d\varepsilon^e\} + \{d\varepsilon^p\} \tag{10}$$

Then from Eq. 3 through Eq. 10 the constitutive equation in plastic range is represented by

$$\{d\sigma\} = [D^p]\{d\varepsilon\}$$

$$= \left[[D^e] - \frac{[D^e]\left\{\frac{\partial f}{\partial \sigma}\right\}\left\{\frac{\partial f}{\partial \sigma}\right\}^T [D^e]}{c\left\{\frac{\partial f}{\partial \sigma}\right\}^T \left\{\frac{\partial f}{\partial \sigma}\right\} + \left\{\frac{\partial f}{\partial \sigma}\right\}^T [D^e] \left\{\frac{\partial f}{\partial \sigma}\right\}} \right] \{d\varepsilon\} \tag{11}$$

Crush: When the equivalent plastic strain $\bar{\varepsilon}^p$ reaches the limited value, crush is considered to occur. After that all stresses sustained by concrete are released.

$$\bar{\varepsilon}^p = -\frac{\sqrt{2}}{3}\{(\varepsilon_y^p - \varepsilon_z^p)^2 + (\varepsilon_z^p - \varepsilon_x^p)^2 + (\varepsilon_x^p - \varepsilon_y^p)^2 + 1.5(\gamma_{yz}^{p2} + \gamma_{zx}^{p2} + \gamma_{xy}^{p2})\}^{\frac{1}{2}} \tag{12}$$

If crush occurs at the j Gauss point in i concrete element, stresses $\{\sigma_i^j\}$ are transformed into equivalent nodal forces $\{F_i^j\}$.

$$\{\varepsilon_i\} = [B_i]\{\delta_i\} \tag{13}$$

$$\{F_i^j\} = \iiint [B_i]^T \{\sigma_i^j\} dV \tag{14}$$

Where $\{\varepsilon_i\}$ and $\{\delta_i\}$ are strain and nodal displacement of i element respectively.

2.2.3 Nonlinearity in tensile side

When the maximum principal stress reaches the tensile strength, the cracking is assumed to occur along a plane normal to the principal stress direction. Accordingly, the stresses in the direction are released and transformed into equivalent nodal forces just as in the method described above. Cracking is judged at each Gauss point, where three cracks can occur and they are mutually orthogonal. After cracking the shear transfer factor along the

cracked surface is reduced to β. This reducing factor should be a function of the gap between crack surfaces, but in this analysis it is assumed to be a constant value from 0 to 1.

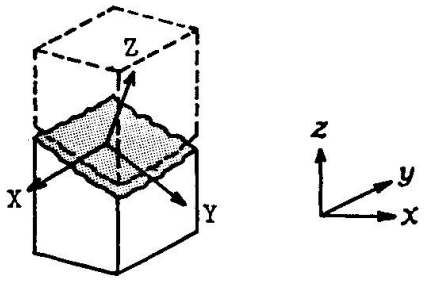

Fig. 6 Concrete Element after Cracking

After cracking, if the local co-ordinates X-Y-Z are defined according to the crack surface, the constitutive equation is represented as the following in local co-ordinates. Here the elements d_{ij}^{p} are calculated by solving a two dimensional problem in X-Y co-ordinates just like three dimensional one. This stiffness matrix is transformed by rotation matrix into the matrix defined in global co-ordinates.

$$\begin{Bmatrix} d\sigma_X \\ d\sigma_Y \\ d\sigma_Z \\ d\tau_{YZ} \\ d\tau_{ZX} \\ d\tau_{XY} \end{Bmatrix} = \begin{bmatrix} d_{11}^{p} & d_{12}^{p} & 0 & 0 & 0 & d_{13}^{p} \\ d_{21}^{p} & d_{22}^{p} & 0 & 0 & 0 & d_{23}^{p} \\ 0 & 0 & 0 & 0 & 0 & 0 \\ 0 & 0 & 0 & \beta G & 0 & 0 \\ 0 & 0 & 0 & 0 & \beta G & 0 \\ d_{31}^{p} & d_{32}^{p} & 0 & 0 & 0 & d_{33}^{p} \end{bmatrix} \begin{Bmatrix} d\varepsilon_X \\ d\varepsilon_Y \\ d\varepsilon_Z \\ d\gamma_{YZ} \\ d\gamma_{ZX} \\ d\gamma_{XY} \end{Bmatrix} \tag{15}$$

2.2.4 Hysteretic loop

The hysteretic loop of concrete is defined as the tri-linear curve which is expressed under uniaxial force (Fig. 7). Below the first yielding point the concrete remains elastic and after that it is semi-elastic up to the second yielding point. After the second point the tangent stiffness modulus is assumed very small and crush occurs when the strain reaches the limited value. In reversal region the usual tri-linear one is adopted.

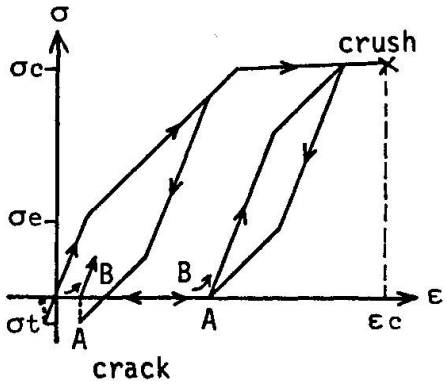

Fig. 7 Hysteretic Loop of Core Concrete

When the stress reaches the tensile strength, cracking occurs at point A. Thereafter if the strain returns to point B (where the cracking occurred in the former stage), the concrete revives elasticity. But the tensile stress normal to cracking surface is assumed not to be sustained.

2.3 Cover concrete, steel and bond elements

2.3.1 Cover concrete

This is represented by a rod element possessing only longitudinal stiffness. The stress vs. strain relation is characterized by the uniaxial state of concrete. The reduction of strength after the peak stress is considered as shown in Fig. 9. The hysteretic rule is assumed to be the same as core concrete.

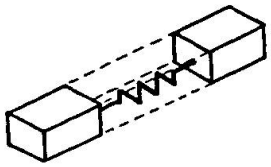

Fig. 8 Cover Concrete Element

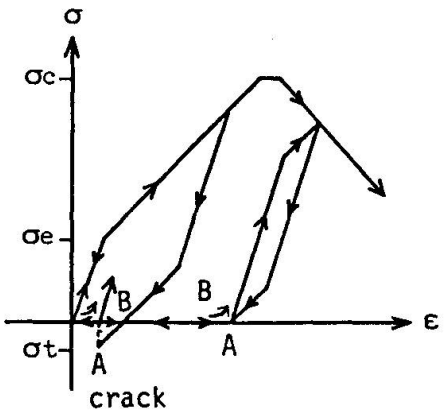

Fig. 9 Hysteretic Loop of Cover Concrete

2.3.2 Steel reinforcement

This is represented by a rod element possessing only axial stiffness. The stress vs. strain relation is assumed to be a bi-linear loop (Fig. 11).

Fig. 10 Steel Element

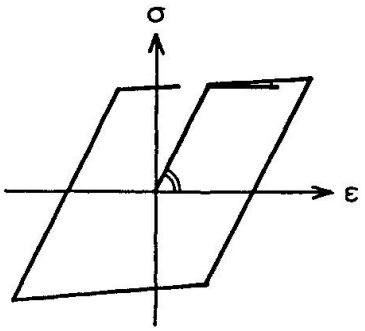

Fig. 11 Hysteretic Loop of Steel

2.3.3 Bonds

They are modeled as a set of link elements connecting steel elements and concrete elements. For bond force vs. relative displacement between steel and concrete elements, a slip-type bi-linear loop is assumed (Fig. 13).

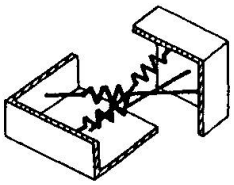

Fig. 12 Bond Element

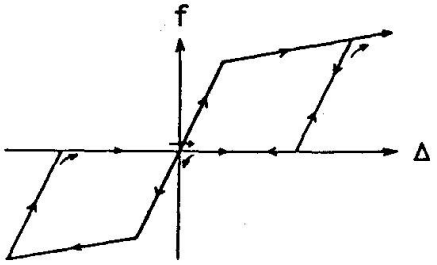

Fig. 13 Hysteretic Loop of Bond

3. PROCEDURE OF CALCULATION

The equilibrium equation is solved incrementally by step by step method. Nonlinearity or revival of elasticity is checked by obtained stress and strain in each element, and the alteration of stiffness is executed if necessary. The procedure is shown in Fig. 14.

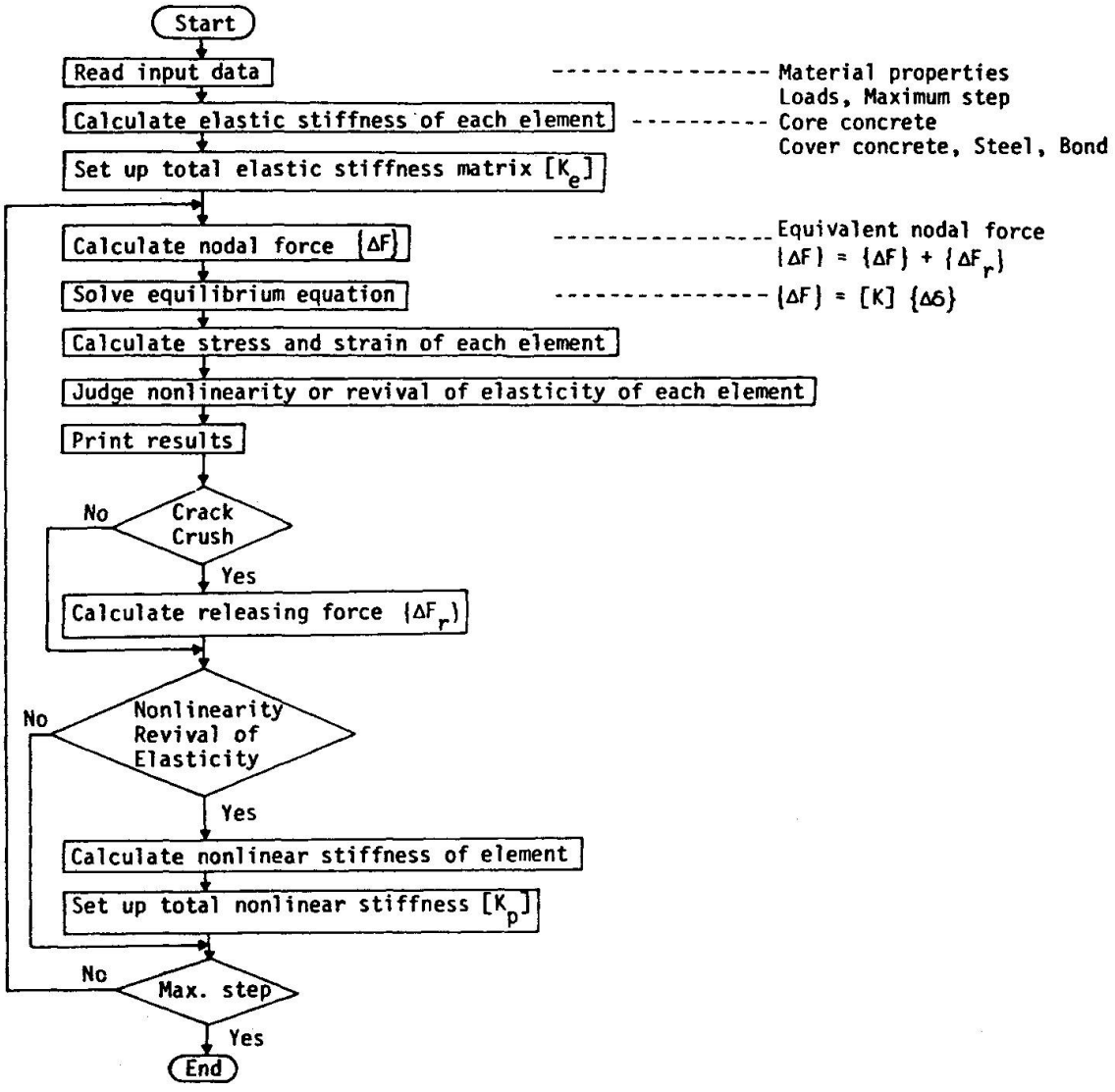

Fig. 14 Flow Chart of Calculation

4. EXPERIMENT AND ANALYSIS TO DETERMINE α

4.1 Purpose

Experiments and their simulation analyses of columns subjected to axial force only were conducted to establish the nonlinear parameter α of concrete in the Drucker-Prager's function. This is the simplest application model for a reinforced concrete column, which can be said to mean the compressive side of a column subjected to earthquake loads.

Many researchers have conducted these experiments and have pointed out the improvement of strength and ductility of confined concrete [23,24,25,26,27]. The authors investigated this confinement effect and determined α.

4.2 Outline of experiment

The test specimen is a column with square hoops which is 45 cm long and cross sectional dimensions of 18 cm x 18 cm (Fig. 15, Photo. 1). The diameter of hoops is 6 mm and their spacing is 20 mm. So the ratio of lateral reinforcement is 1.57%. Normal concrete is used and its compressive strength obtained by the cylinder test is 200 kg/cm^2.

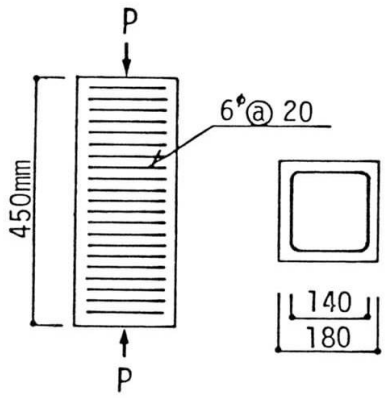

Fig. 15 Section of Test Specimen

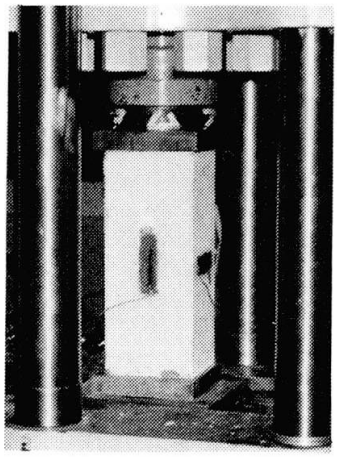

Photo. 1 Test Specimen

The vertical and lateral strain of concrete were measured at the surface in the middle of the specimen to exclude confining effect caused by the loading boundary. The strain of a hoop located in the middle of the column was measured at its center and end portion. These strains were measured at inside and outside surface to exclude bending component (Fig. 16).

Loading cycles are as follows. First axial loads were gradually increased up to 60 ton and then reversed to zero. Next they were increased up to the first peak value 77.9 ton and decreased to 50 ton. Finally they were increased up to the next peak value 80.3 ton, when the forces were sustained only by core concrete as the cover concrete broke away.

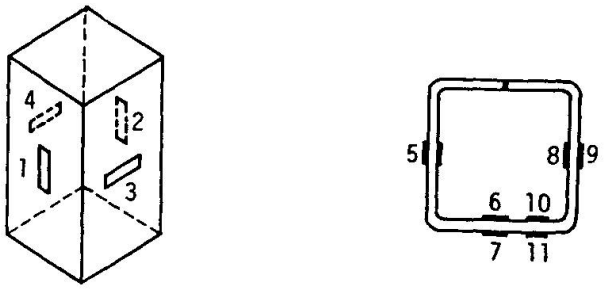

(A) Concrete (B) Hoop

Fig. 16 Measurement of Strain

4.3 Results of experiment

The observed vertical strain of concrete and strain of hoops are shown in Fig. 17 (A) and (B) respectively. In these figures the solid lines are observed results at inside and outside, and the broken lines are their mean values excluding bending component.

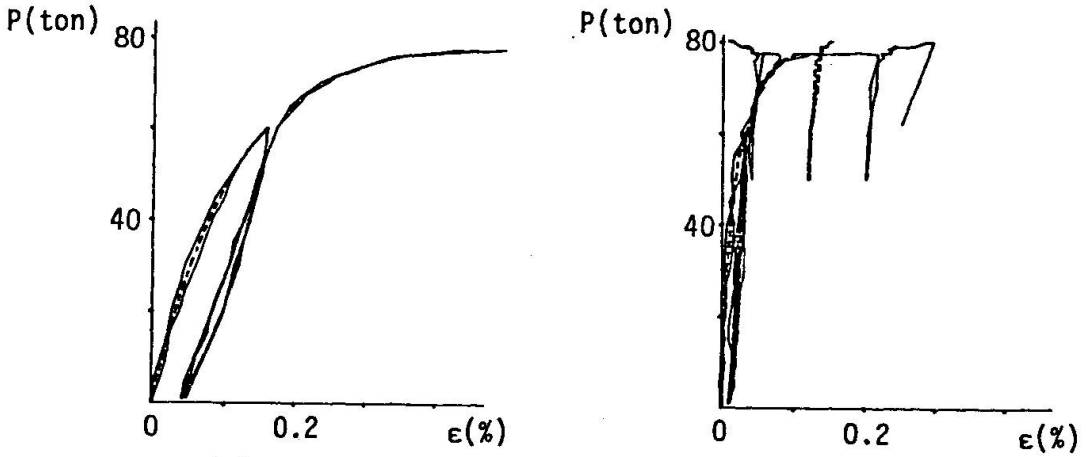

(A) Concrete (B) Hoop

Fig. 17 Observed Strain

4.4 Model for analysis

In Fig. 18 the model of core concrete for analysis is presented. Taking

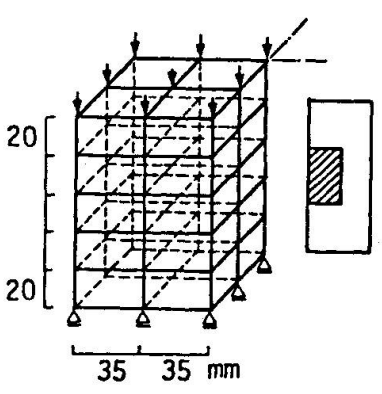

Fig. 18 Mesh Layout of Core Concrete

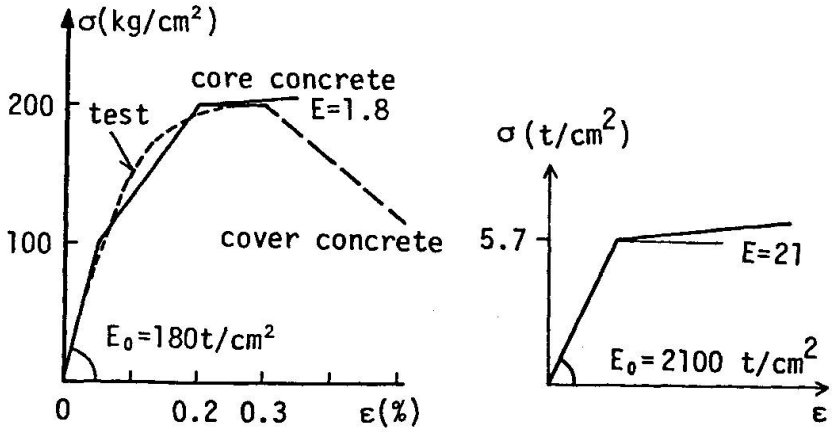

(A) Concrete (B) Steel

Fig. 19 Material Properties

advantage of the symmetrical condition one quarter portion was considered horizontally. Vertically five layers were adopted to decrease the influence of boundary conditions. The hoops were assumed to be anchored to concrete at the corner and center of core concrete. Material properties used in this analysis are presented in Fig. 19. The parameter $3/2\,\alpha$ of concrete is assumed to be 0, 0.1, 0.2, 0.3 and 0.4.

4.5 Results of analysis

Loads vs. vertical strain of concrete is presented in Fig. 20. Here (A) shows the bearing forces of core concrete and cover concrete respectively. From this it is recognized that core concrete can sustain further force after the force of cover concrete has decreased as α increases due to the confinement effect of the hoops. In (B) the sum of the two values are compared with observed results. This shows that the maximum strength of a column is decided according to the sum of the ascending gradient of core concrete and the descending gradient of cover concrete. Among the calculated results the value obtained by assuming $3/2\,\alpha = 0.2$ shows best agreement.

Loads vs. strain of hoop is presented in Fig. 21. From this the effectiveness of hoops is recognized distinctly after the stress of concrete has reached the vicinity of compressive strength of plain concrete. In the case of hoops the best result is obtained also by assuming $3/2\,\alpha = 0.2$. Here it is noticeable that the hoops remain elastic when the column reaches the maximum value.

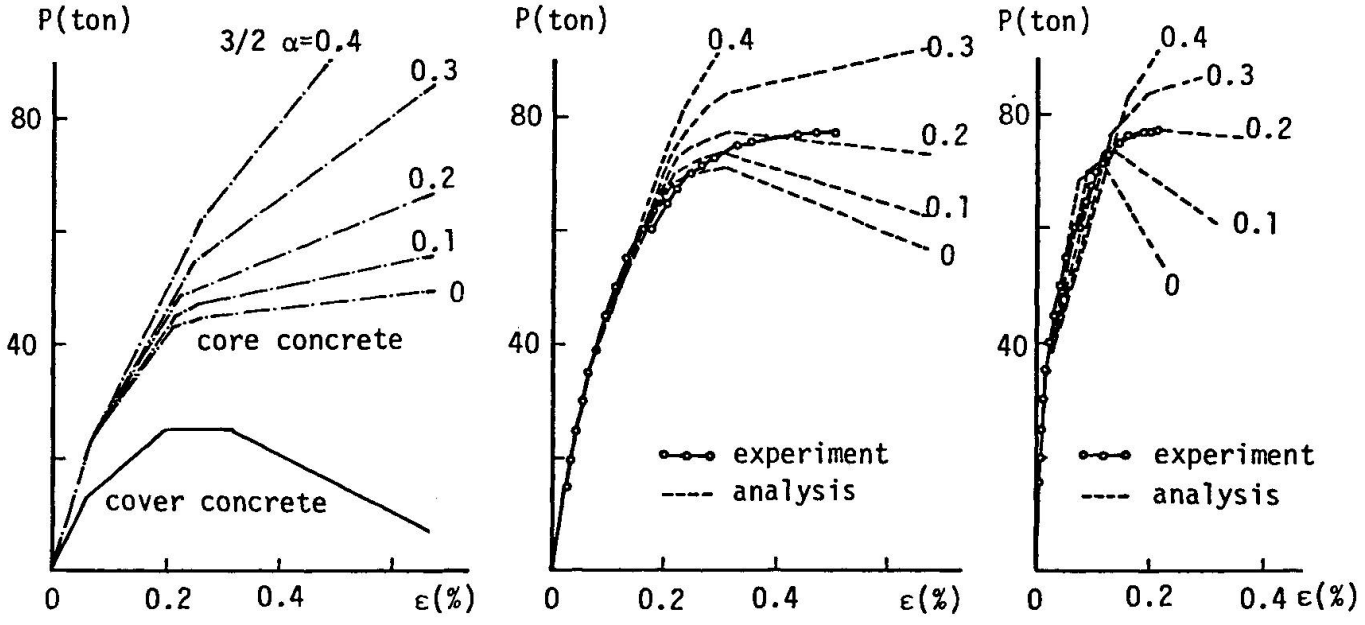

(A) Core and Cover Concrete (B) Total

Fig. 20 Loads vs. Vertical Strain of Concrete

Fig. 21 Loads vs. Strain of Hoop

5. ANALYSIS OF COLUMN UNDER REPEATED LATERAL FORCES

5.1 Outline of experiment

The test specimen is a 1/2 scaled column subjected to repeated lateral forces with a constant axial force which is equal to one third of compressive strength as shown in Fig. 22 (28). During the first and second cycles, the loading was gradually increased up to 30 tons and 60 tons respectively. Then 30 cycles of loading were applied to the specimen, keeping the maximum deflection constant at a relative deflection angle R of 1/100 rad. Finally, the relative deflection angle of the specimen was increased to 1/50 rad. In Fig. 23 and Fig. 24 the observed relative deflection and strain of longitudinal reinforcement are presented respectively.

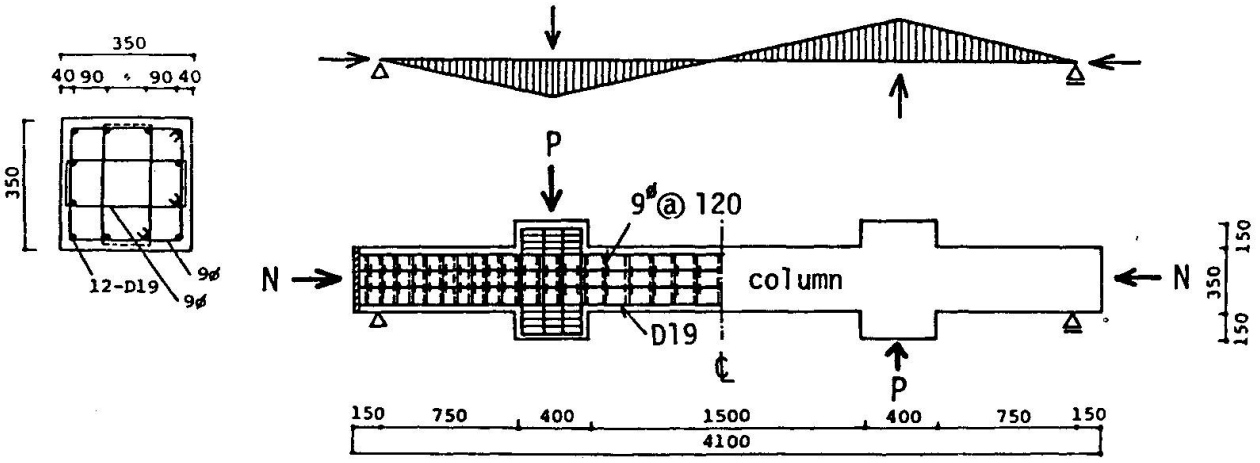

Fig. 22 Test Column (by Hisada, Ohmori and Bessho)

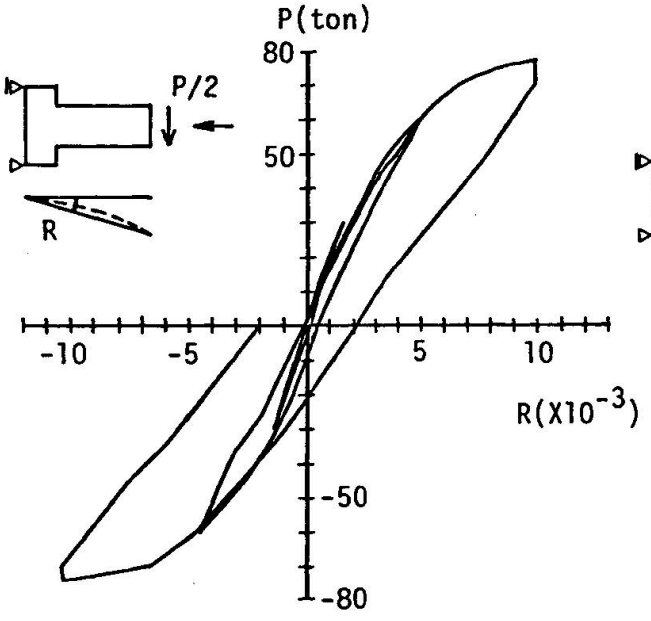

Fig. 23 Observed Relative Deflection

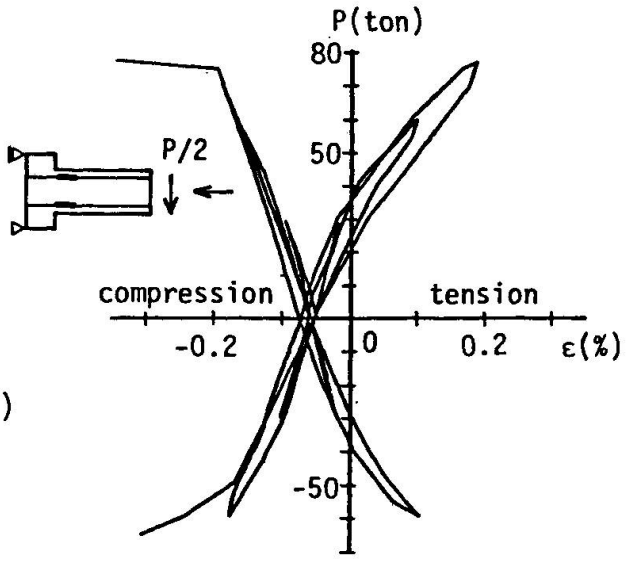

Fig. 24 Observed Strain of Longitudinal Reinforcement

5.2 Model for analysis

Analysis was performed on a half model by considering its antisymmetry (Fig. 25). The assumed material properties are shown in Tab. 1. Here, $3/2\,\alpha = 0.2$ is assumed from the result of the afore-mentioned preliminary study. The second and third loading cycles were simulated because the first one is considered elastic.

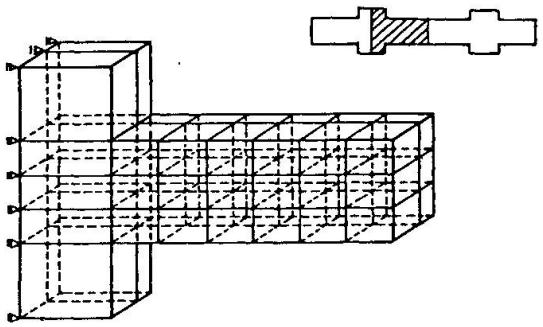

Fig. 25 Mesh Layout of Core Concrete

Tab. 1 Material Properties

Concrete

compressive strength	370 kg/cm²
elastic limit	133 kg/cm²
tensile strength	28 kg/cm²
elastic modulus	180 t/cm²
semi-elastic modulus	136 t/cm²
$3/2\alpha$	0.2
Poisson's ratio	0.2
limiting comp. strain	0.0035

Steel

yield stress	
longitudinal bar	3.7 t/cm²
transverse bar	3.6 t/cm²
Young's modulus	2100 t/cm²

Bond

yield stress	
longitudinal bar	50 kg/cm³
transverse bar	30 kg/cm³
first stiffness	25 t/cm³
second stiffness	0.84 t/cm³

5.3 Results of analysis

Among obtained results deflection and strain of longitudinal reinforcement are shown in Fig. 26 and Fig. 27 respectively. Here the second and third cycle are separately shown. The observed results are well simulated by this analysis from the positive to the negative region on the deflection and strain of longitudinal reinforcement. Especially, it is very important that the behavior while unloading is obtained by this incremental analysis method.

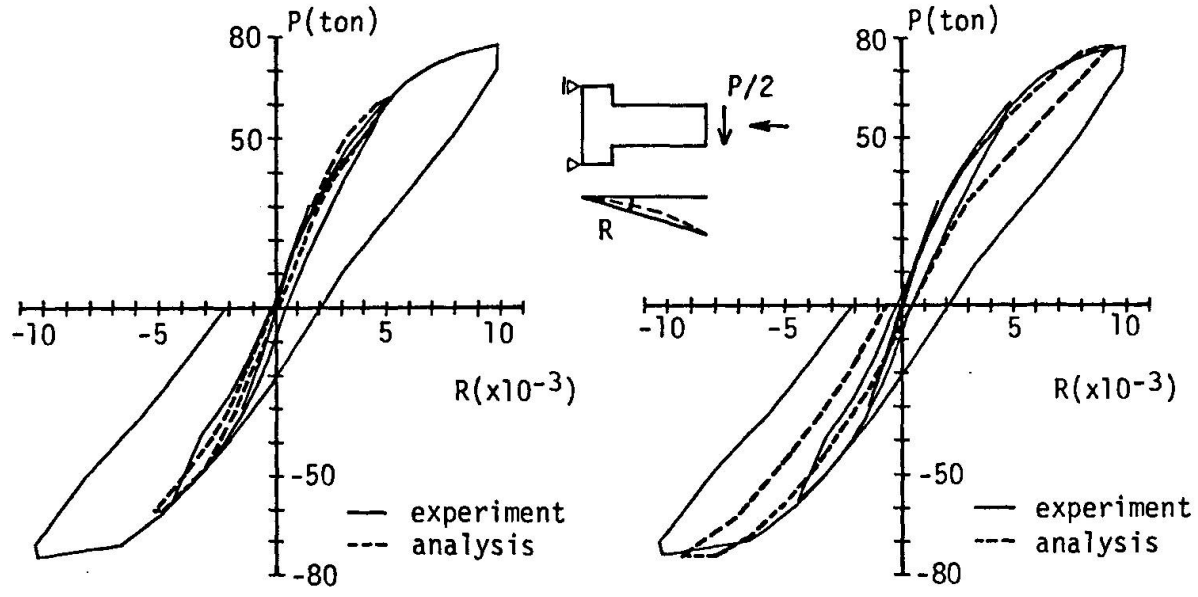

(A) 2nd Cycle (B) 3rd Cycle

Fig. 26 Relative Deflection

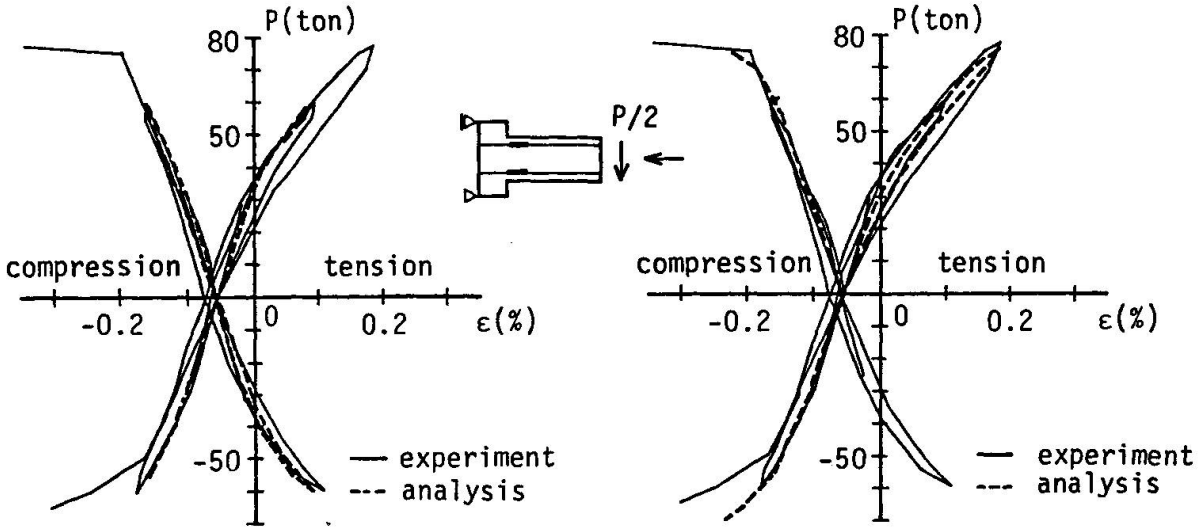

(A) 2nd Cycle (B) 3rd Cycle

Fig. 27 Strain of Longitudinal Reinforcement

Finally in Fig. 28 (A) and (B), the calculated axial stresses at the critical cross section are presented at the stage when the load is 70 and 76 ton respectively. Here the arrow marks mean forces of longitudinal bars and shaded zones mean axial stress distribution of concrete. It is noticeable in Fig. (B) that the maximum compressive stress of concrete occurs in core concrete by the confining effect of hoops.

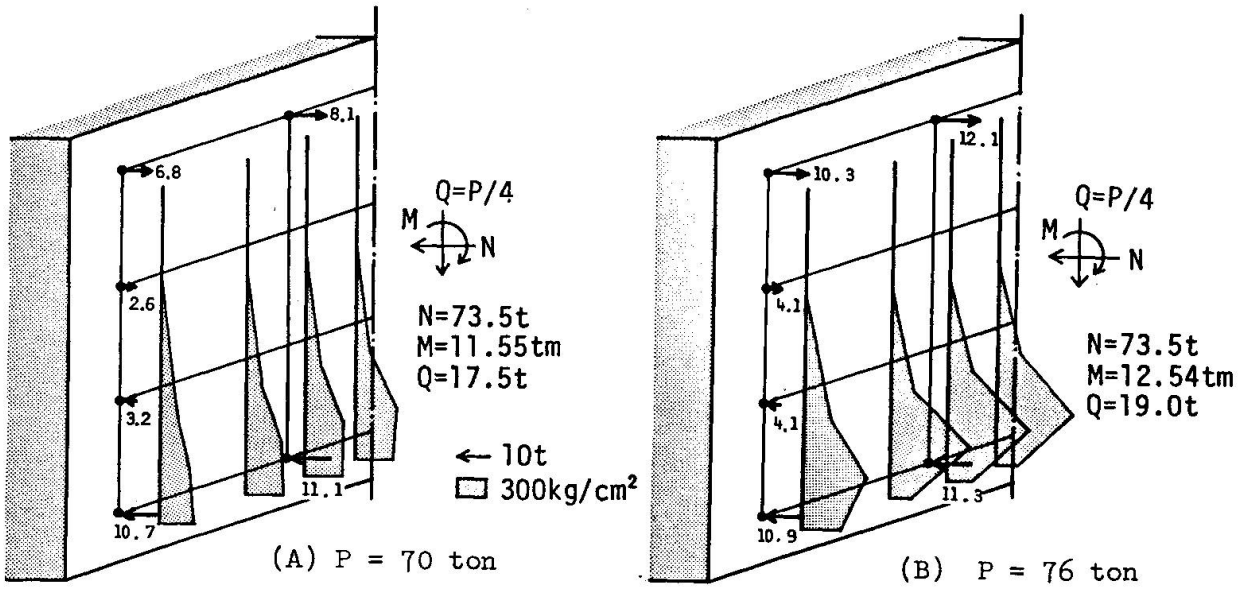

Fig. 28 Calculated Axial Stresses

6. CONCLUSION

The nonlinear behavior of reinforced concrete columns were studied by 3-dimensional Finite Element Method developed by the authors. First the preliminary study determined the parameter α used in plastic condition of concrete. Then, on the basis of these results, a simulation analysis of a hooped column under repeated lateral forces was performed from the positive to the negative region and good agreement was obtained.

7. ACKNOWLEDGMENTS

Y. Abe conducted the uniaxial test and S. Bessho provided the results of a hooped column subjected to repeated lateral forces. They are acknowledged with gratitude.

8. REFERENCES

1. Sugano, T., Miyashita, T., and Inoue, N., " 3-dimensional Study of Nonlinear Behavior of Reinforced Concrete Column under Repeated Lateral Forces," Proceedings of 7th World Conference on Earthquake Engineering, Vol.5, 1980, pp. 497-504
2. Ngo, D., and Scordelis, A.C., "Finite Element Analysis of Reinforced Concrete Beams," ACI Journal, Vol. 64, No. 3, March, 1967, pp. 152-163
3. Franklin, H.A., "Nonlinear Analysis of Reinforced Concrete Frames and Panels," Structures and Materials Research Department of Civil Engineering, University of California
4. Valliappan, S., and Doolan, T.F., "Nonlinear Stress Analysis of Reinforced Concrete," Journal of the Structural Division, ASCE, Vol. 98, No. ST4, 1972 pp. 885-897
5. Zienkiewicz, O.C., "The Finite Element Method in Engineering Science," McGraw-Hill, 1971.
6. Chen, A.C.T., and Chen, W.F., "Constitutive Equations and Punch-Indentation of Concrete," Journal of the Engineering Mechanics Division, ASCE, Vol.101, No. EM6, Dec., 1975, pp. 889-906
7. Suidan, M., and Schnobrich, W.C., "Finite Element Analysis of Reinforced Concrete," Journal of the Structural Division, ASCE, Vol. 99, No. ST10,

Oct., 1973, pp. 2109-2122
8. Kupfer, H., and Gerstle, K., "Behavior of Concrete Under Biaxial Stress," Journal of the Engineering Mechanics Division, ASCE, Vol. 99, No. EM4, Aug., 1973, pp. 852-866
9. Cedolin, L., Crutzen, R.J., and Poli, S.D., "Triaxial Stress-Strain Relationship for Concrete," Journal of the Engineering Mechanics Division, ASCE, Vol. 103, No. EM3, June, 1977, pp. 423-439
10. Palaniswamy, R., and Shah, S.P., "Fracture and Stress-Strain of Concrete Under Triaxial Compression," Journal of the Structural Division, ASCE, Vol. 100, No. ST5, May, 1974, pp. 901-916
11. Kotsovos, M.D., and Newman, J.B., "Generalized Stress-Strain Relations for Concrete," Journal of the Engineering Mechanics Division, ASCE, Vol. 104, No. EM4, Aug., 1978, pp. 845-856
12. Darwin, D., and Pecknold, D.A., "Inelastic Model for Cyclic Biaxial Loading of Reinforced Concrete," University of Illinois, UILU-ENG-74-2018, 1974
13. Elwi, A.A., and Murray, D.W., "A 3D Hypoelastic Concrete Constitutive Relationship," Journal of the Engineering Mechanics Division, ASCE, Vol. 105, No. EM4, Aug., 1979, pp. 623-641
14. Liu, T.C.Y., Nilson, A.H., and Slate, F.O., "Biaxial Stress-Strain Relations for Concrete," Journal of the Structural Division, ASCE, Vol. 98, No. ST5, May, 1972, pp. 1025-1034
15. Bažant, Z.P., Bhat, P.D., and Shieh, C.L., "Endochronic Theory for Inelasticity and Failure Analysis of Concrete Structures," Northwestern University, Structural Engineering Report, No. 1976-12/259, Dec., 1976
16. Romstad, K.M., Taylor, M.A., and Hermann, L.R., "Numerical Biaxial Characterization for Concrete," Journal of the Engineering Mechanics Division, ASCE, Vol. 100, No. EM5, Oct., 1974, pp. 935-948
17. Ottosen, N.S., "Constitutive Model for Short-Time Loading of Concrete," Journal of the Engineering Mechanics Division,ASCE, Vol. 105, No. EM1, Feb., 1979, pp. 127-141
18. Hobbs, D.W., Pomeroy, C.D., and Newman, J.B., "Design Stresses for Concrete Structures Subject to Multi-axial Stresses," The Structural Engineer, Vol. 55, No. 4, Apr., 1977
19. Kotsovos, M.D., "Effect of Stress Path on the Behavior of Concrete Under Triaxial Stress States," ACI Journal, Feb., 1979
20. Andenaes, E., Gerstle, K., and Ko, H.Y., "Response of Mortar and Concrete to Biaxial Compression," Journal of the Engineering Mechanics Division, ASCE, Vol. 103, No. EM4, Aug., 1977, pp. 515-526
21. Ottosen, N.S., "A Failure Criterion for Concrete," Journal of the Engineering Mechanics Division, ASCE, Vol. 103, No. EM4, Aug., 1977, pp. 527-535
22. Ziegler, H., "Modification of Prager's Hardening Rule", Quart., Appl. Math., Vol. 17, No. 1, 1959, pp. 56-65
23. Kent, D.C., and Park, R., "Flexural Members with Confined Concrete," Journal of the Structural Division, ASCE, Vol. 97, No. ST7, July, 1971, pp. 1969-1990
24. Sheikh, S.A., "Effectiveness of Rectangular Ties as Confinement Steel in Reinforced Concrete Columns," Department of Civil Engineering, University of Toronto, June, 1978
25. Manrique, M.A., Bertero, V.V., and Popov, E.P., "Mechanical Behavior of Lightweight Concrete Confined by Different Types of Lateral Reinforcement," University of California, Report No. UCB/EERC-79/05, May, 1979
26. Sargin, M., Ghosh, S.K., and Handa, V.K., "Effects of Lateral Reinforcement upon the Strength and Deformation Properties of Concrete," Magazine of Concrete Research, Vol. 23, No. 75-76, June-Sept., 1971, pp. 99-110
27. Burdette, E.G., and Hilsdorf, H.K., "Behavior of Laterally Reinforced Concrete Columns," ASCE, Vol. 97, No. ST2, Feb., 1971, pp. 587-602
28. Hisada, T., Ohmori, N., and Bessho, S., "Earthquake Design Considerations in Reinforced Concrete Columns," The Journal of the International Association for Earthquake Engineering, Vol. 1, No. 1, 1972, pp. 79-91

Two Simple Reinforced Concrete Beam Elements for Static and Dynamic Analysis

Deux éléments simples pour l'analyse statique et dynamique des structures porteuses en béton armé

Zwei einfache Balkenelement für die statische und dynamische Berechnung von Stahlbetontragwerken

M. ROSSI
Researche Associate
Swiss Federal Institute of Technology
Zurich, Switzerland

G. BAZZI
Research Associate
Swiss Federal Institute of Technology
Zurich, Switzerland

SUMMARY
Two simple beam elements for static and dynamic analysis of reinforced concrete members under bending, shear and normal forces are proposed. Basic assumptions are stated. The applicability is discussed making comparisons of computed and analytical or experimental results.

RÉSUMÉ
On presente deux éléments simples qui permettent le calcul statique et dynamique de structures porteuses en béton armé qui sont soumises à des sollicitations de flexion, d'effort tranchant et d'effort axial. On mentionne également les hypothèses qui sont à la base du calcul. Le champ d'application est illustré à l'aide de quelques exemples. On a fait une comparaison entre les résultats obtenus numériquement et ceux déterminés à l'aide d'essais ou de modèles analytiques.

ZUSAMMENFASSUNG
Zwei einfache Balkenelemente für die statische und dynamische Berechnung von Stahlbetonbauteilen unter Biegung, Schub und Normalkraft werden dargestellt und die zugrundegelegten Annhamen angegeben. Durch den Vergleich von numerischen mit analytischen und experimentellen Resultaten wird die Anwendbarkeit der Modelle aufgezeigt.

1. INTRODUCTION

Theoretical investigations of statically and dynamically loaded structures are based on a variety of diverse mathematical models, which - corresponding to their complexity - allow a more or less accurate idealization of real structural behavior. In order to make a critical examination of these models feasible and to differentiate possible fields of application, essentially two basic model types are distinguished.

On the one hand, local phenomena of structural components are frequently studied with microelements, based on continuum mechanics. The range of possible utilization, however, is narrowly restricted by the often prohibitive computing time and by the excessive storage capacity required. Moreover in many cases this type of model leads to an overestimation of the accuracy of results, because the effects of the basic assumptions on the global behavior are often difficult to estimate.

On the other hand, when using macromodels, the knowledge of the physical phenomena at the level of the structural component is essentially. The simplicity and economy of these models are sometimes offset by severe restrictions on its applicability.

As part of a research project at the Swiss Federal Institute of Technology Zurich on the dynamic behavior of structures in the inelastic range a finite element (FE) computer program (PIFF) has been developed which enables the implementation of different FE-formulations. The application of the program to the analysis of real structures has been the objective from the beginning, so that computational efficiency and physical reliability have been equal criteria in the development of the models. The result of this concept has been the decision, neither to strive for refinements of sophisticated micromodels nor to search for modifications of existing macromodels, but to develop models, which make understandable the inelastic dynamic behavior of structures in their fundamental characteristics.

A first limitation has been adopted in the choice of types of structures: for the present only plane systems are considered, since many structures may be idealized very well by plane frames, trusses and/or shear walls. The development of models therefore has been undertaken for plane structural components, which usually are loaded with moments, normal and shear forces. According to the above specified objective of research, beam finite elements are able to fulfill these requirements.

As theoretical and experimental investigations show, the hysteretic behavior of cyclically deformed reinforced concrete structural components can be very complex. To formulate the relationship between forces and deformations two notions have been widely used:

- Stiffness-Degradation
- Strength-Degradation

Hence, practical requirements for FE-formulations result from the fact that they should idealize stiffness and strength behavior without a full knowledge of the occurring phenomena at the level of structural components. This behavior is mainly influenced by:

- Properties of steel and concrete
- Bond behavior
- Loading combinations
- Loading history

The present elements idealize the interaction between steel and concrete assuming rigid bond, because in many cases bond properties can be neglected and moreover the exact treatment of the problem requires a three-dimensional analysis.

In chapter 3 a simple beam element for bending and normal forces is described, while in chapter 4 a model is presented which includes also shear effects. A few FE-concepts are summarized, as far as they are indispensable in explaining the beam elements.

2. FINITE ELEMENT CONCEPTS

2.1 Fundamentals

To study complex physical problems, the three-dimensional continuum generally is transformed into a discrete system and then solved with numerical methods. In most cases in structural engineering today, this space discretization is performed with the well-known finite element method. Therein, the behavior of a single finite element can be described using the concepts of equilibrium loads and tangential stiffness matrix.

On the element level (subscript e) the equilibrium load vector is given by

$$\{F\}_e = \int_{V_e} [B]^T \{\sigma\}\, dV \qquad (1)$$

where $[B]$ relates the increments of strains $\{\varepsilon\}$ and nodal displacements $\{w\}_e$: $d\{\varepsilon\} = [B]\, d\{w\}_e$. The coefficients B_{ij} are easily derived from the underlying element shape functions. The stress vector $\{\sigma\}$ in cyclic loading depends not only on the strain vector $\{\varepsilon\}$, but also on the entire stress-strain history. It must be mentioned that strains and stresses may also be interpreted as generalized quantities.

The corresponding tangential stiffness matrix can be evaluated by a similar integration (e.g. geometric linear, first order analysis)

$$[K_T]_e = \int_{V_e} [B]^T [D_T][B]\, dV \qquad (2)$$

where $[D_T]$ symbolizes the incremental constitutive law of the material: $d\{\sigma\} = [D_T]\, d\{\varepsilon\}$. If a geometrical nonlinear formulation is required, both initial displacements and stress parts have to be taken into account [1].

2.2 Beam Theory

A special case of the above-sketched discretization is obtained if the three-dimensional displacements of a single element are reduced to shape functions, valid for a line element only. This so-called beam theory will be reviewed shortly. The simplifications of the continuum causes a loss of information, which consequently has to be replaced by a set of appropriate assumptions.

For instance, the commonly used classical beam theory postulates:

- Cross sections maintain their shape
- Cross sections remain plane and perpendicular to the beam axis (hypothesis of Navier-Bernoulli)

These assumptions yield the strains in any point of the element. It is easily shown that only longitudinal strains occur. Hence, no strains perpendicular to the

axis and no shearing deformations are permitted. This implies the violation of the equilibrium conditions within the element and on its boundary and, even more important, allows for no interaction between the shear and the other section forces: the shear force, therefore, is to be perceived as a reaction. Furthermore, directly from the assumption of plane cross sections follows the concept of a rigid bond between steel and concrete. Within the framework of this theory, no other bond law can be specified.

An extension of this classical theory can be obtained by abandoning the assumption cross sections remain perpendicular to the deformed axis. An additional shape function for the angle between the perpendicular and the beam axis leads, in contrast to the above remarks, to shear strains within the element. Using this extension to the classical theory, the interaction between the three section forces can be taken into account in some cases. For reinforced concrete beam elements, however, this approach has to be completed by an additional mode shape, as will be shown in chapter 4.

3. BEAM ELEMENT FOR BENDING AND NORMAL FORCES

Prior to describing the new element, a few notes on customary idealizations will be helpful for the classification of the element and for the subsequent comparisons.

The direct relationship between generalized strains and stresses (e.g. moment-curvature) is usually taken for granted in the derivation of the relatively simple macroelements. Provided that the occurring physical phenomena are well-known and simple enough to formulate, this method of solving engineering problems is advantageous and reasonable. Unfortunately, the inelastic cyclic behavior rarely can be modeled realistically with an elementary stress-strain relationship such as the bilinear law, the Ramberg-Osgood-function or more sophisticated hysteresis laws. In many cases, the properties and the amount of steel and concrete, the level of normal forces (also changing normal force) and the deformation history complicate the structural behavior, so that a generally applicable element formulation is very difficult to realize.

Another often used idealization is the layer-model. In this model the concrete cross section is subdivided into small layers over the height. These individual layers then contribute to the behavior of the element by summation. The steel is treated separately in the same way. This procedure is straightforward and correct within the framework of the classical beam theory, but one can easily imagine, that for practical applications the computational efforts and storage requirements will become prohibitive.

3.1 Model Assumptions

In contrast to the layer-model the proposed element idealizes the concrete contribution to both the equilibrium load vector and the stiffness matrix with only two layers. Obviously, this would be a very crude approximation of the cross section if these layers, here denoted as stringers, were constant in area and position. Thus, the concept of variable stringers has been introduced, observing the classical beam theory. This means that the stringer areas are directly dependent on the position of the neutral axis or, in other words, on the generalized strains of the considered cross section.

The idealizations of the actual stress and stiffness distributions are shown in Fig. 1. The reference points for which the stringer areas (F_t, F_b) and the per-

tinent stresses (σ_t, σ_b) are to be evaluated are assumed to lie in the middle of the stringer areas. Within a stringer the stress distribution is assumed constant, since in general further information is lacking. The same assumptions are made for the stringer stiffnesses (E_t, E_b) and also the lever arms (z_t, z_b) are defined by these reference points. This implies that the concrete strain histories refer to points, varying over the beam height. Fig. 2 shows all strain and one possible appertaining stress distribution, which have to be distinguished.

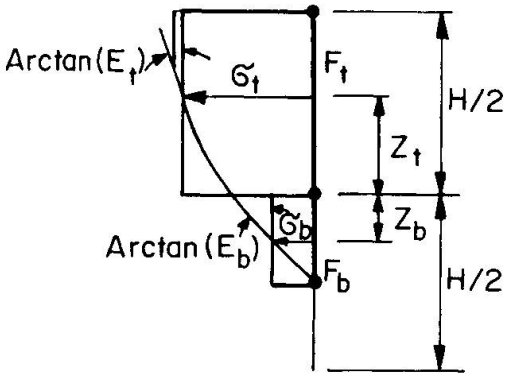

Fig. 1 Idealizations

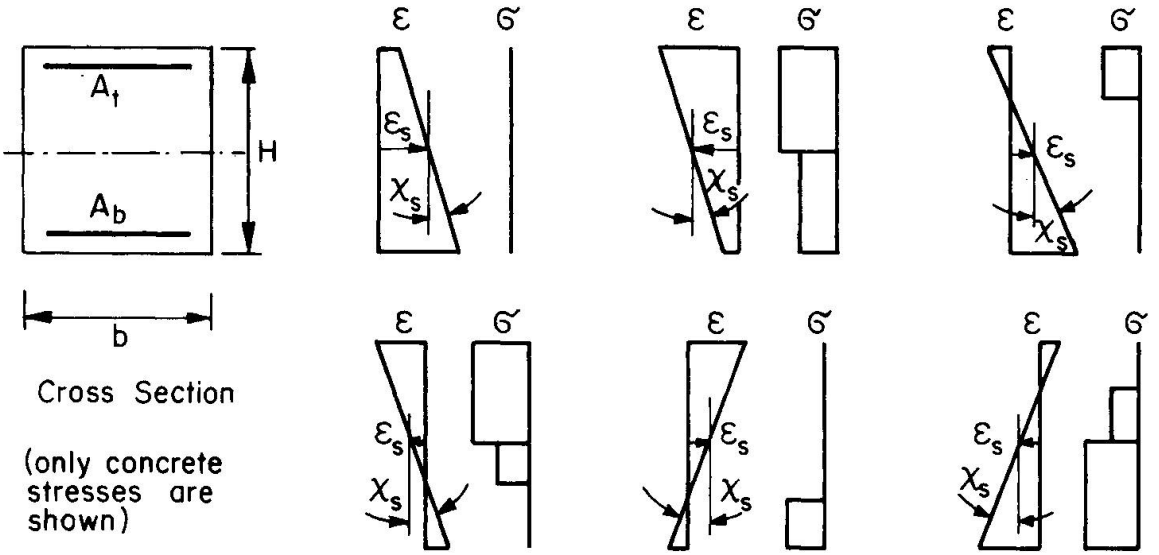

Fig. 2 Strain and Stress Distributions

Mathematically, the previously explained idealizations can be quickly realized. Starting with Eq. 1 for the equilibrium load vector, a numerical integration can be performed, if the generalized section forces $\{\sigma\} = \{N,M\}$ and the kinematical matrix $[B]$ are known. In the discussed element, the matrix $[B]$ has been derived from the commonly-used hermitian polynoms, while the concrete contribution of $\{\sigma\}$ is calculated directly by summing the expressions for the bottom (b) and top (t) stringer. Steel behavior is treated in an analogous manner. In order to keep the mathematical expressions as clear as possible, in this paper these additional terms are not listed.

With the symbols of Fig. 1, it follows:

normal force $$N = \sum_{b}^{t} \sigma F \qquad (3)$$

bending moment $$M = \sum_{b}^{t} \sigma z F \qquad (4)$$

According to the model concept, the three terms σ, z and F are functions of the

generalized strains ε_s and χ_s.

For the evaluation of the tangential stiffness matrix (Eq. 2), in addition to the matrix [B] the knowledge of the constitutive law $[D_T]$ in generalized quantities is required. The coefficients of this matrix are given by the partial derivatives of the section forces with respect to the axial strain ε_s and the curvature χ_s.

$$\frac{\partial N}{\partial \varepsilon_s} = \sum_b^t \left(\frac{\partial \sigma}{\partial \varepsilon_s} F + \sigma \frac{\partial F}{\partial \varepsilon_s}\right) \tag{5}$$

$$\frac{\partial N}{\partial \chi_s} = \sum_b^t \left(\frac{\partial \sigma}{\partial \chi_s} F + \sigma \frac{\partial F}{\partial \chi_s}\right) \tag{6}$$

$$\frac{\partial M}{\partial \varepsilon_s} = \sum_b^t \left(\frac{\partial \sigma}{\partial \varepsilon_s} z F + \sigma \frac{\partial z}{\partial \varepsilon_s} F + \sigma z \frac{\partial F}{\partial \varepsilon_s}\right) \tag{7}$$

$$\frac{\partial M}{\partial \chi_s} = \sum_b^t \left(\frac{\partial \sigma}{\partial \chi_s} z F + \sigma \frac{\partial z}{\partial \chi_s} F + \sigma z \frac{\partial F}{\partial \chi_s}\right) \tag{8}$$

It should be mentioned that the resulting stiffness matrix is no longer symmetric due to the geometrically changing terms $\partial F/\partial \varepsilon_s$, $\partial F/\partial \chi_s$, $\partial z/\partial \varepsilon_s$ and $\partial z/\partial \chi_s$. In order to incorporate this finite element into a customary FE program, it is necessary to neglect the nonsymmetric parts. Nevertheless, for algorithms with equilibrium iterations convergence can be reached with a reasonable tangential stiffness approximation.

3.2 Applications

So far, nothing has been assumed for the steel and concrete properties. In order to estimate the accuracy of the model the behavior of a cross section predicted by this model will be compared with the exact solutions.

First, linear behavior of steel and concrete is considered. The tensile strength of concrete is neglected. Obviously, the normal force N is modeled exactly for all possible strain distributions, while the moment M is only an approximation due to the fact that the lever arm in general is underestimated. In Fig. 3 the relative error of the moment is shown as a function of the neutral axis. As can be seen, for $\xi \leq 0.25$ the relative error is very small, while for $\xi \geq 0.5$ the relative error is up to 25%. The presence of reinforcement improves the solution.

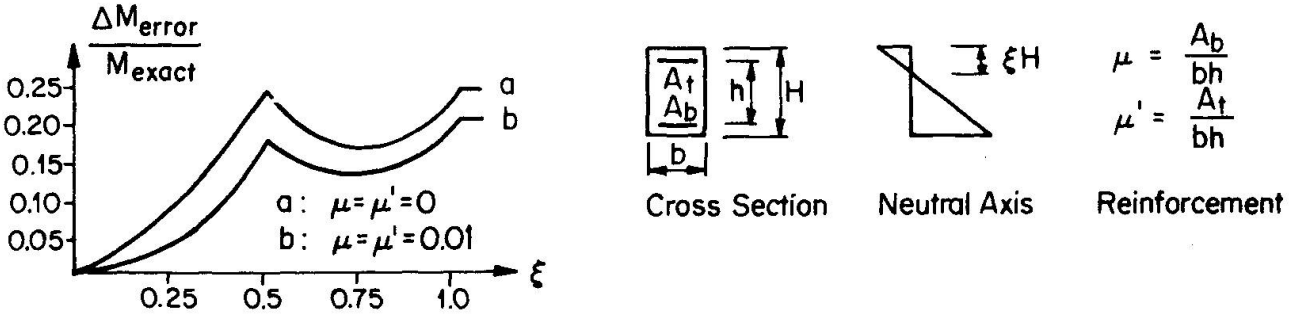

Fig. 3 Accuracy for the Stringer Model (linear elastic material)

As second example rigid-plastic material behavior is taken, neglecting again the tensile strength of the concrete. In this case only a prediction of strength is obtained. The idealization gives the exact solution since not only the stress distribution, but also the lever arm is correct. Fig. 4 shows the interaction curves for two different parameters.

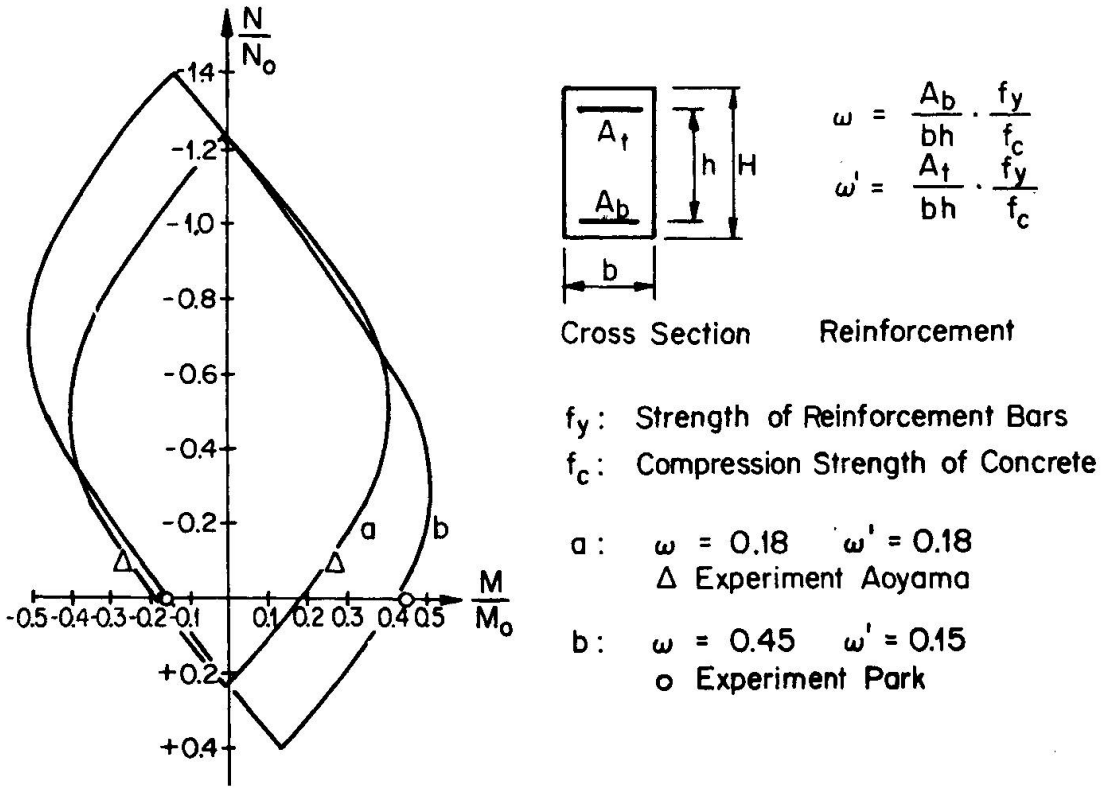

Fig. 4 Interaction Curves (rigid plastic material)

The preceding examples have been used to qualitatively show the accuracy of the proposed model. In the following, more realistic material behavior will be considered.

The steel properties are modeled with the well-known Ramberg-Osgood-function, adopting the procedures and the empirical data proposed by Park [2].

For cyclic one-dimensional concrete behavior, three different concrete models are implemented in the FE program and may be used alternatively, depending on the problem. Typical cyclic behavior of the three models is sketched in Fig. 5.

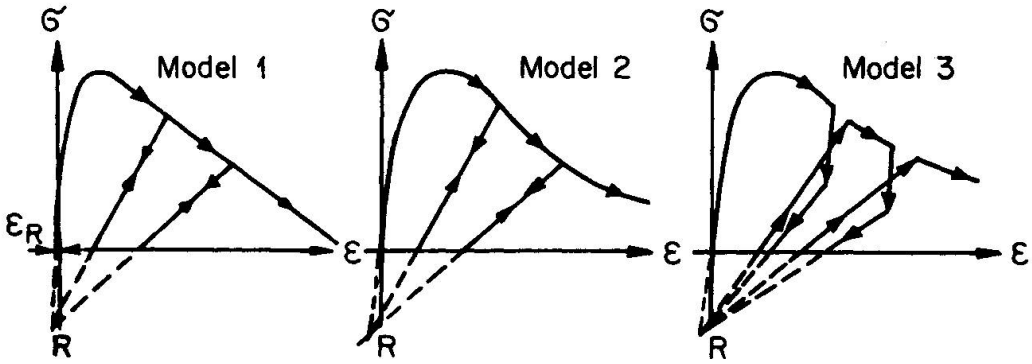

Fig. 5 Typical Stress-Strain-Relationship of Concrete Models

Models 1 and 2 differ only in the descending branch of the stress-strain relationship. In both models, the unloading path is directed towards an appropriately selected point R and therefore the unloading stiffness becomes dependent on the maximum of the compression strain.

Model 3 additionally allows for plastic strain increments by applying constant stress amplitudes. By deforming the concrete with constant strain amplitudes a reduction of the stress amplitude will result.

Following are several comparisons between experimental results and theoretical values using the above mentioned stress-strain relationships for steel and concrete.

First, a few cycles from experiments performed in Zurich [3] are compared with the FE calculations. The statical system and the loading are shown together with the pertinent FE idealization in Fig. 6. As can be seen, the FE solution is always too stiff. The main reasons for this observation is found in the very rough FE mesh. Since a displacement based model is used, the calculated response of the beam must be expected to be too stiff. Comparing the same results for the moment-curvature relationship, the agreement between experiment and the FE calculation is more satisfying.

The next example illustrates the influence of a constant compression force on a symmetrically reinforced concrete cross section, loaded with bending moments according to a given curvature history [2].

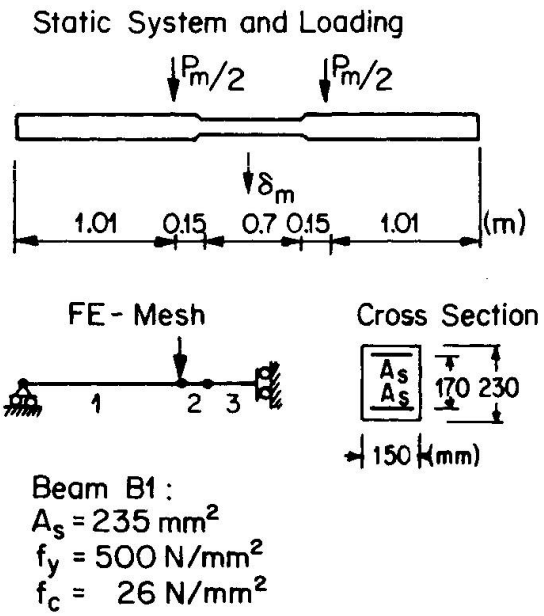

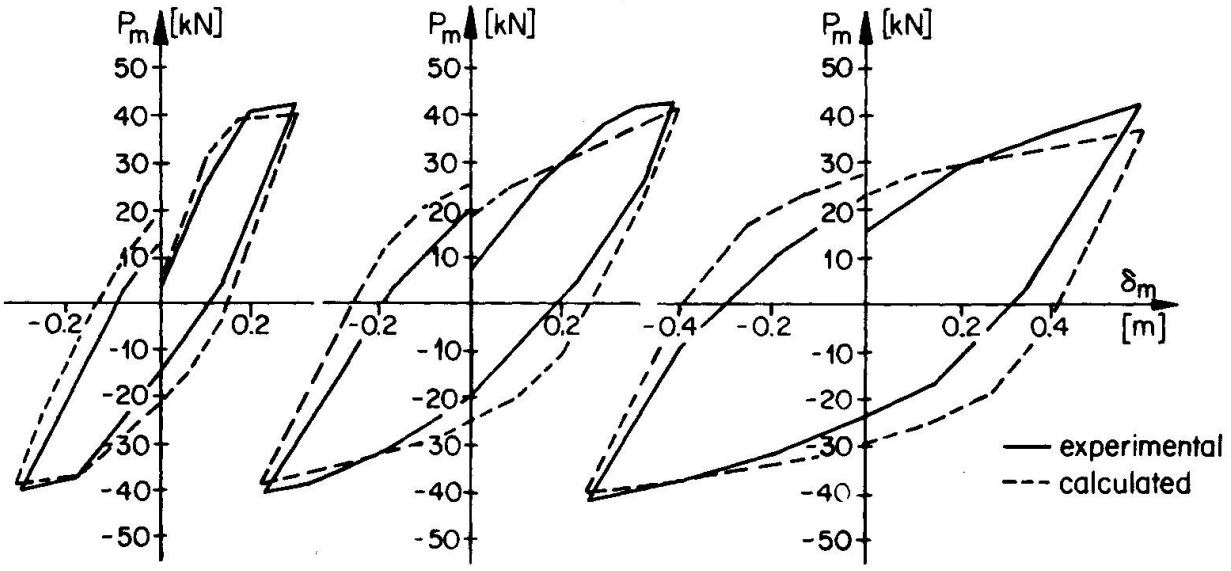

Fig. 6 Comparison I between FE-Calculation and Experiment [3]

Again the agreement between the experimental and computed values is good (Fig.7). The yielding of the reinforcing bars in compression and the subsequent closing of the cracks - the cause of the pinched form of the hysteresis - can be modeled

quite well with the proposed model. A complementary comparison can be performed by plotting the positive and negative extreme moments M_{ult} into the corresponding nondimensional interaction curve (Fig.4).

The last example shows the hysteretic behavior (moment-curvature) of a reinforced concrete cross section with different top and bottom reinforcement [2]. The imposed curvature history is typical for earthquake-loaded structures. Once more the strength in both directions is simulated very well, while the stiffness shows more deviation. In Fig. 4 the positive and the negative extreme moments M_{ult} are plotted on the interaction curve.

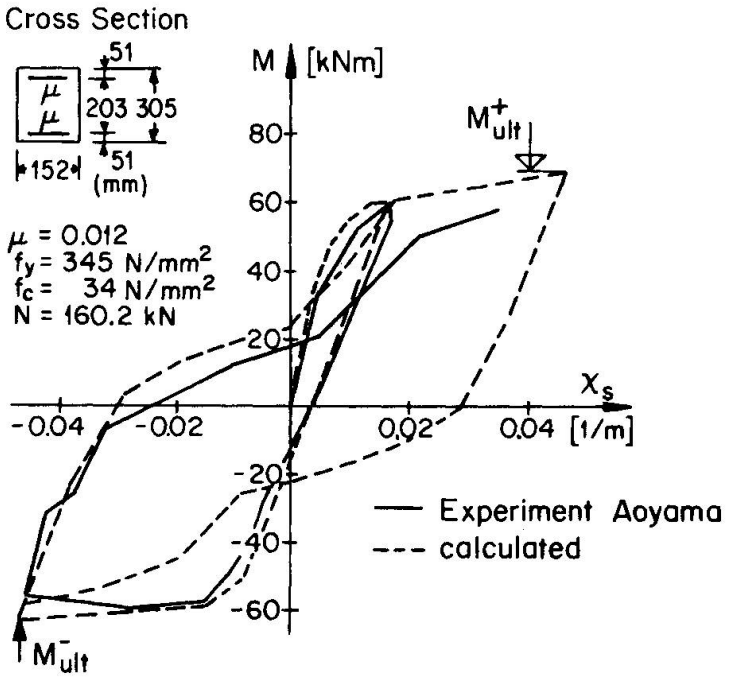

Fig. 7 Comparison II between FE-Calcultation and Experiment [2]

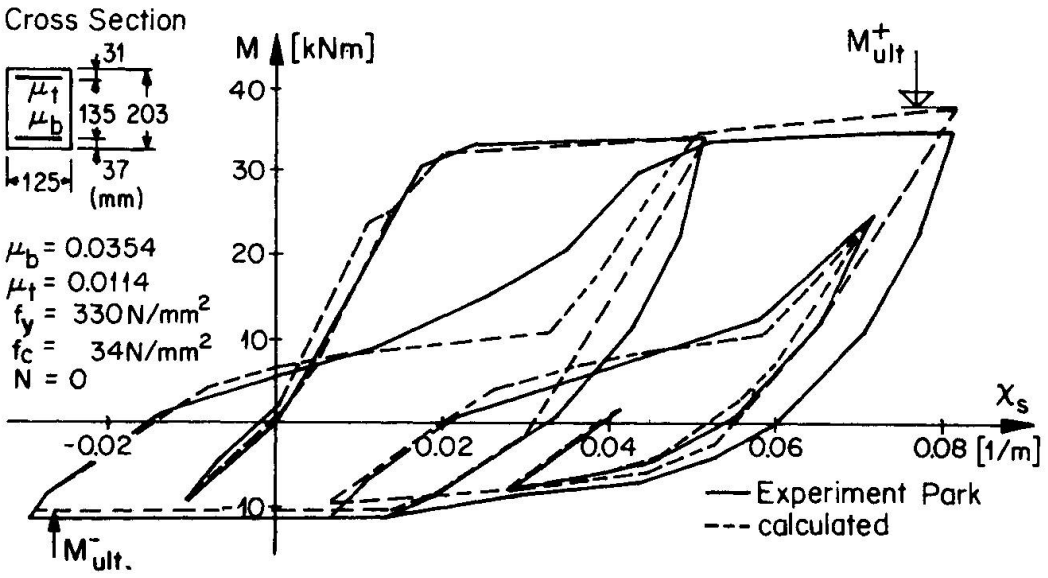

Fig. 8 Comparison III between FE-Calculation and Experiment [2]

In order to show the field of application of the proposed element, a brief estimation is carried out. As has been demonstrated in Fig. 3 accurate solutions may be expected if the compression portion of the cross section is relatively small. Since in cyclic loading the yielding of the reinforcement causes an opening of the cracks, the behavior of the reinforcement plays a major role in most cases. Only for high normal forces larger parts of the concrete cross section will contribute considerably to the section forces, and thus influence the behavior significantly. Hence, the limited reliability for high normal forces must be kept in mind. However, as can be seen in Fig. 1, the more the concrete is strained, the better the stress idealization coincides with the actual stress distribution. Hence, improved accuracy will result for such cases.

4. BEAM ELEMENT FOR BENDING, SHEAR AND NORMAL FORCE

4.1 FE Models for Shear Problems

If in addition to bending and normal forces, shear forces must also be taken into account, the idealization of structural members with two- or three-dimensional FE is commonly accepted. This means that the concrete is modeled with multidimensional isoparametric FE, whereas a uniaxial discretization for the reinforcing bars is chosen. The simulation of bond effects can be performed with additional spring elements.

This procedure is conceptually straightforward but, as mentioned earlier, for actual structures becomes impracticable. Furthermore, from an engineering point of view, the enormous flow of local stress-strain histories is not very meaningful and complicates control and judgement of the results.

In the following, attention will be focused on structural members which are significantly influenced by shear forces, although geometrically they are idealized as beam elements. The proposed generalized new beam element seems to be of interest since - compared to multidimensional FE - the computational efficiency, the facility of the specified input and the critical estimation of results are improved. The development starts from the extended beam theory including shear deformations. For both steel and reinforced concrete members this theory will be generalized in this paper. The cross sectional shape is restricted to rectangular, T- and I-sections. Flange bending is neglected since the flanges and the longitudinal reinforcing bars are idealized as one-dimensional stringers.

4.2 Assumed Shape Functions

In order to allow for shear displacements it is convenient to formulate the shape functions in natural modes, as shown in Fig. 9.

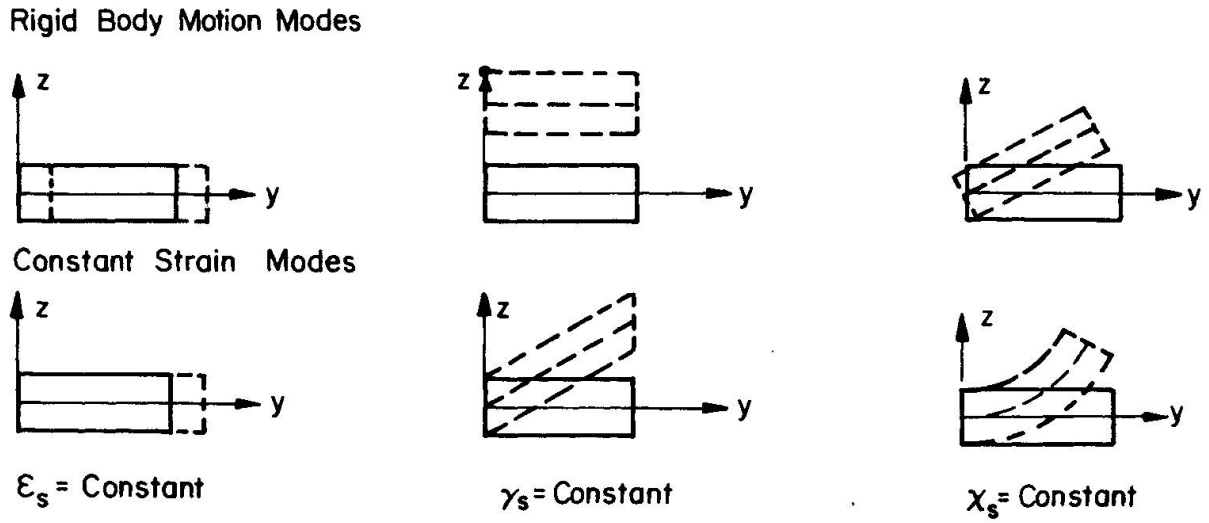

Fig. 9 Modal Shapes

The given modes correspond to constant section forces over the element length, which permits the use of a single integration point in the longitudinal direction for the evaluation of the equilibrium loads and the tangential stiffness matrix. The simultaneous assumption of constant shear force and bending moment

are inconsistent, but for displacement FE models this inconsistency is not important. Therefore a stepwise approximation results in the actual moment distribution.

Blaauwendraad et al. [4] proposed a model, which shows similarities to the present one. In the following sections, some differences will be discussed.

4.3 Nodal Displacements, Strains and Stress-Strain Properties

As noted earlier, the incremental relationship between the generalized element strains and the nodal displacements is given by

$$\begin{Bmatrix} d\varepsilon_s \\ d\gamma_s \\ d\chi_s \end{Bmatrix} = [B]\, d\{w\}_s \tag{9}$$

By applying the concept of the extended beam theory, the uniaxial longitudinal strains ε_{st} in the stringers as well as the longitudinal strain ε_y and the shearing strain γ_{yz} over the cross section height are found.

For the web section, an isotropic two-dimensional incremental material law is adopted

$$\begin{Bmatrix} d\sigma_y \\ d\sigma_z \\ d\tau_{yz} \end{Bmatrix} = [D_T] \begin{Bmatrix} d\varepsilon_y \\ d\varepsilon_z \\ d\gamma_{yz} \end{Bmatrix} \tag{10}$$

So far, no information on the actual vertical strain ε_z can be gathered from the chosen mode shape. Two extreme cases are conceivable:

$\sigma_z = 0$ i.e. completely unrestrained boundary condition in the z-direction

$\varepsilon_z = 0$ i.e. rigid boundary condition in the z-direction

To judge the reliability of these assumptions, different material properties will be discussed.

Steel Members

The hypothesis of unrestrained vertical boundary condition ($\sigma_z = 0$) is usually reasonable for steel beam elements; computed and experimental results are well in agreement (see chapter 4.5). Steel generally is idealized with homogeneous and isotropic material behavior. For the element under consideration the well-known Von Mises yield criterion with a kinematic hardening rule has been implemented into the program.

Reinforced Concrete Members

In the case of elements composed of concrete and steel, the boundary conditions $\sigma_z = 0$ as well as $\varepsilon_z = 0$ do not reflect the actual behavior of reinforced concrete members at all. Rather, the constraining influence of the stirrups on the concrete plays a major role in the mechanism of shear transfer; that is, the stirrups act as an elastic-plastic support for the concrete web. In the proposed model the influence of the stirrups is "smeared" over the element length.

In order to show the consequences of typical multiaxial yield conditions - sensitive to the hydrostatic pressure - on the behavior of reinforced concrete members, the Drucker-Prager yield criterion (Fig. 10) is used to idealize the

strength behavior of concrete. It is a rather crude approximation for the actual concrete behavior. For problems where concrete fails predominantly in multiaxial compression, a refined material formulation with at least three parameters must be used. Otherwise, the strength is strongly overestimated. Furthermore, for cyclic behavior an even more sophisticated formulation has to be adopted. However, the chosen yield criterion will suffice to explain the element.

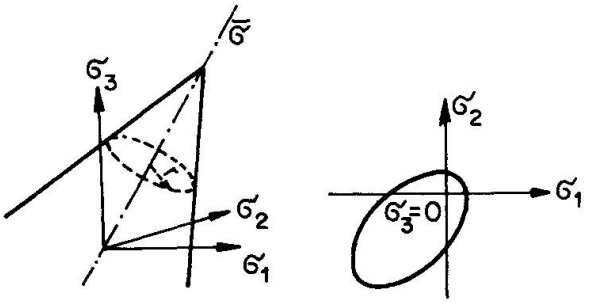

Fig. 10 Drucker-Prager (extended v. Mises) Yield Criterion

4.4 Additional Degree of Freedom

In order to complete the missing information about the strain component ε_z additional mode shapes are considered. This can be realized in two different manners, by introducing either internal or external degrees of freedom.

Internal, Element-Related Degree of Freedom

The additional mode shape is shown in Fig. 11. It corresponds to a constant strain state ε_z in the entire element. As can be seen the element is kinematically noncompatible, as at the element boundaries displacement continuity may be violated.

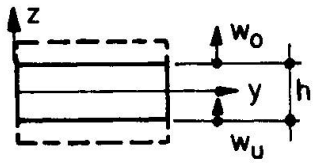

$$w_7 = w_0 - w_u \qquad \varepsilon_z = \frac{w_7}{h}$$

Fig. 11 Additional Internal Mode

Using the notions of Fig. 11 the incremental relationship between the generalized strains and the nodal displacements can be written

$$\begin{Bmatrix} d\varepsilon_s \\ d\gamma_s \\ d\chi_s \\ d\varepsilon_z \end{Bmatrix} = \begin{bmatrix} [B] & \cdot \\ \cdot & \frac{1}{h} \end{bmatrix} \begin{Bmatrix} d\{w\}_e \\ dw_7 \end{Bmatrix} \tag{11}$$

The contributions to the equilibrium load vector and to the stiffness matrix can be taken into account by adding the parts of the concrete web and the "smeared" stirrups.

First, the actual stiffness matrix (6x6) is derived from the original element stiffness matrix (7x7) by a standard condensation procedure. This derivation results in the relationship between the 6 external and the internal parameters as well. In order to achieve global equilibrium, element internal iterations in the added degree of freedom (dw_7) are performed first and then the equilibrium loads are evaluated by numerical integration. This redistribution of the unbalanced forces has to be performed for each time or load step so that accuracy and convergence is guaranteed. The setting up of the tolerance parameters requires good engineering judgement and experience. Otherwise this iteration procedure may become too time-consuming for practical analysis.

External, Global Degree of Freedom

The strain state ε_z alternatively can be realized by adding a global nodal parameter to the three commonly-used joint parameters.

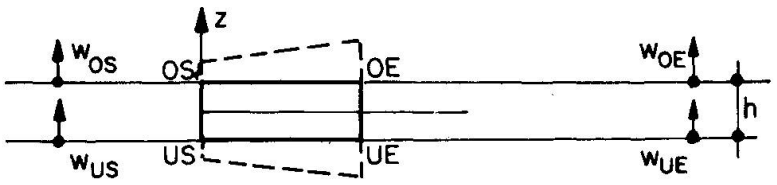

Fig. 12 Additional Internal Mode

Keeping one integration point in the middle of the element, the additional degrees of freedom correspond to a constant strain state $\varepsilon_z = 1/2h\ (w_7+w_8)$. This formulation introduces one kinematical mode at element level; in order to prevent the resulting instabilities in the global system, adequate boundary conditions must be specified.

This procedure (not yet implemented) seems to be more efficient than the one previously explained since unbalanced load components can be redistributed simultaneously. On the other hand, a larger number of degrees of freedom is involved and difficulties may arise in defining boundary conditions (e.g. joints with more than two incidences). Furthermore, flexible problem-dependent convergence criteria will become complicated.

The approach presented by Blaauwendraad et al. [4] shows some similarities with the present model. However, in contrast to the proposed element, layer techniques, linear generalized strain states and a different material formulation are used.

4.5 Numerical Investigation

Simply-supported Steel Beam

Experimental results of simply-supported steel beams have been reported by K. Brandt et al. [5]. The plastic irreversible deformation pattern of one of these beams (Fig. 13) is characterized by the shear yielding of the web. For analysis, one-half of the beam was idealized with three elements. Predicted and experimental responses are shown in Fig. 14.

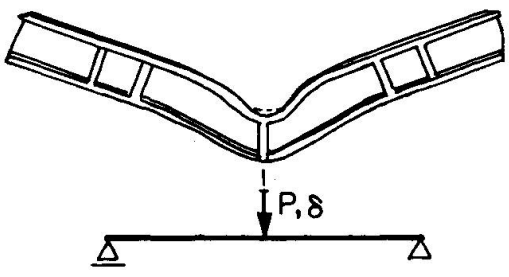

Fig. 13 HEM-160, Beam A3 [5]
$f_y = 360\ N/mm^2$
$f_u = 540\ N/mm^2$

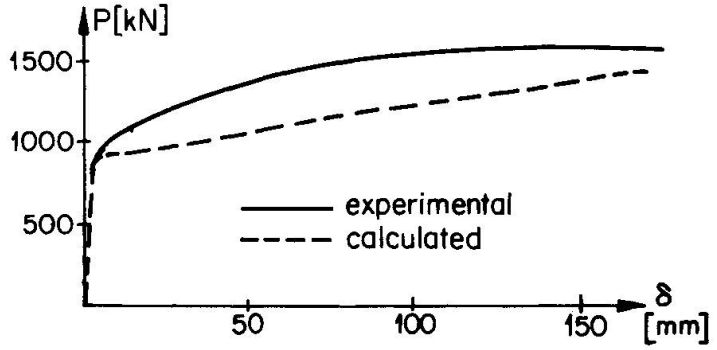

Fig. 14 Load-Displacement Diagrams

Steel Frame

The response of a plane steel frame (Fig. 15) was expected to be governed by shear and large-displacement effects. Hence, for a first idealization 25 two-dimensional isoparametric elements for the webs and 100 truss elements for the flanges were

used. Geometrical and material nonlinearities (von Mises yield criterion, kinematical hardening) were taken into account. The analysis was stopped prematurely since the load increment required for convergence had become extremely small and the costs unreasonable high.

Using the above-explained shear beam element for the same problem, the calculation was performed successfully with a computing time of about 10% of that required for the two-dimensional isoparametric element analysis.

A comparison calculation was carried out with a simple moment-curvature element. Since it accounts for bending effects only, the strength of the beam is strongly overestimated as can be seen in Fig. 16.

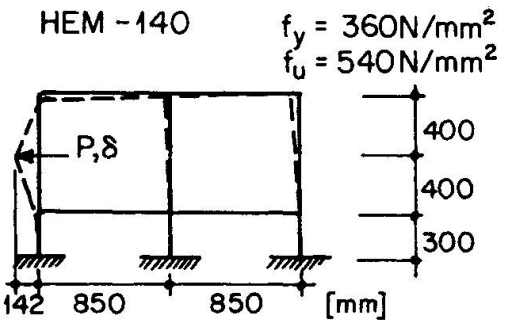

Fig. 15 Frame Displacements at Failure

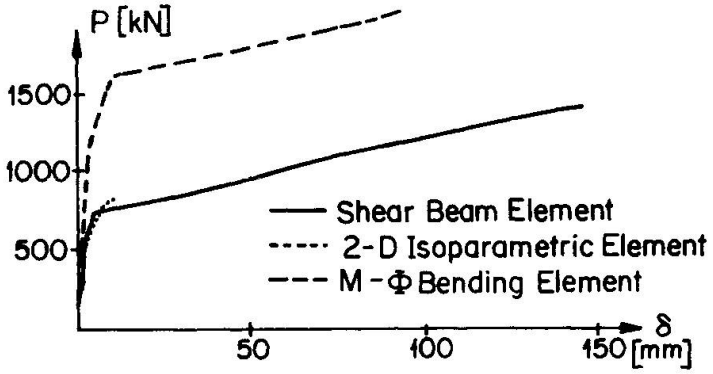

Fig. 16 Load-Displacement Diagrams

Reinforced Concrete Beam Subjected to Pure Shear

The web of a reinforced concrete beam can be idealized as a shear wall subjected to pure shear. To describe this behavior analytically truss models with inclined compression struts (Fig. 17) have been applied widely [6] and constitute the theoretical background of the Directive 34 of the Swiss Code 162.

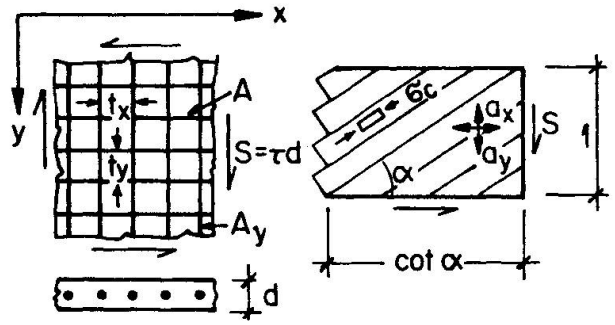

$$a_x = \frac{A_x}{t_y} \qquad p_x = a_x f_{sx}$$

$$a_y = \frac{A_y}{t_x} \qquad p_y = a_y f_{sy}$$

f_{sx}, f_{sy} : Yield Stresses

Fig. 17 Shear Web Model [6]

In order to compare the FE-idealization with the analytical model, the expected inclination of the compression struts are plotted in Fig. 18. Five different reinforcement ratios p_y/p_x are considered. In the present example the amount of reinforcement was chosen small enough, so that failure was reached after yielding of both longitudinal and vertical reinforcement.

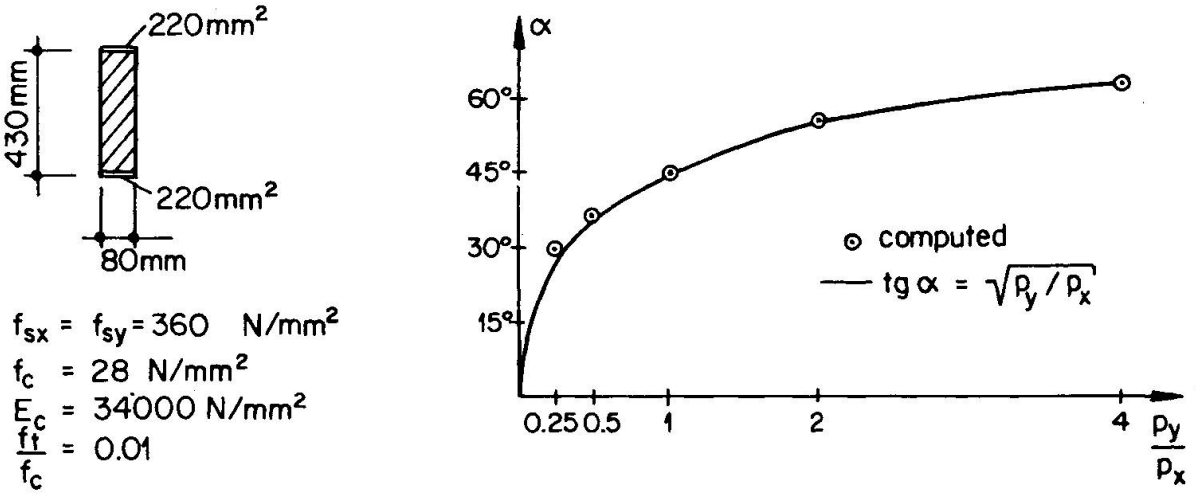

Fig. 18 Analytical and Computed Values of α

A comparison of computed and tested response is presented in Fig. 19. The experimental results have been gathered from the measurements on a box girder subjected to pure torsion [7]. The investigated shear web is shown in Fig.18 (Beam T2: shear reinforcement 1000 mm²/m')

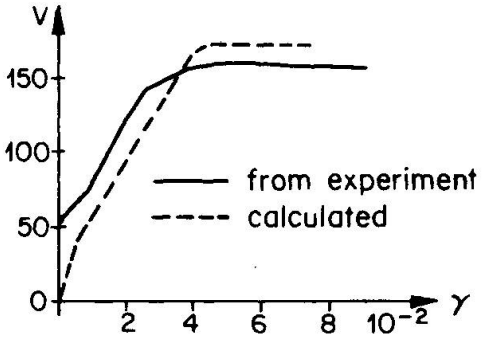

Fig. 19 Shear Force - Shear Strain

Reinforced Concrete Beam Subjected to Bending and Shear

With the above mentioned truss model, bending moment (M) - shear force (V) interaction curves for ultimate strength can be derived [6]. In Fig. 20 a M-V-interaction curve is plotted. The analogous computer analysis has been performed on a single element. In order to obtain some points of the interaction curve the ratio between the applied shear force and resulting bending moment has been varied.

The actual beam cross section is shown in Fig. 18 with a shear reinforcement of 1000 mm²/m' and in accordance with [6] the stringers were assumed very stiff in compression.

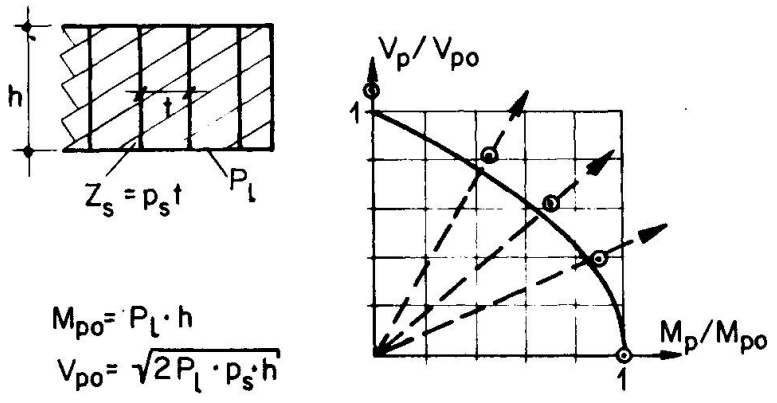

Fig. 20 Bending Moment - Shear Force Interaction Diagram

Considering that numerical computation was performed with $f_t = 0.01\ f_c$ while zero tensile strength is assumed in [6], acceptable agreement is found.

If the bending strength of the web is taken into account for cross sections such as rectangular ones additional shear strength due to the bending compression zone can be expected and was also observed in a numerical investigation. However, the presented - displacement based - FE model fulfills in this case equilibrium within a single element only in a global sense. A trend to overestimate the strength is therefore inherent. Additional research work is needed for definitive conclusions.

A comparison of calculated and measured bending and shear response will be illustrated with a last example. A serie of two span reinforced concrete beams has been tested and reported by Leonhardt et al. [8]. The behavior of beam HH5 was strongly governed by shear effects and the ductile failure of the beam was reached after yielding of bending and shear reinforcement.

In Fig. 22 the computed load-displacement diagram is compared with the experimental curve and in Fig. 21 both the calculated and measured displacement shapes at a load level of 140 kN are plotted. The agreement between experiment and theory is satisfying.

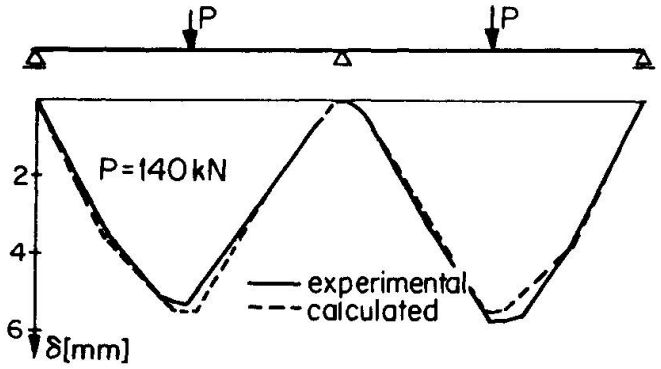

Fig. 21 Displacements of Beam HH5 [8]

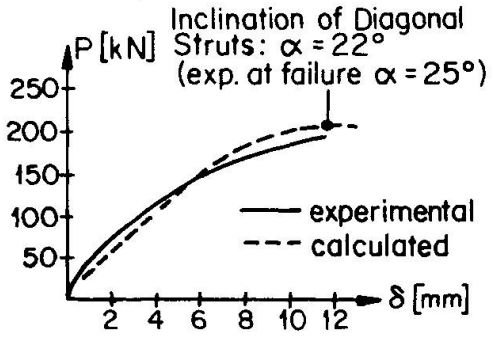

Fig. 22 Load-Displacement Diagram

Summarizing the previous remarks the discussed element models seem to describe adequately the nonlinear behavior of steel and reinforced concrete beams under combined bending and shear. Applicability is limited by the assumed simple constitutive laws for concrete and steel and by possible stiffening effects due to local equilibrium violations as explained above. While the first restriction is not inherent to the model itself, further studies are under way in order to improve equilibrium fulfillment within the element.

REFERENCES

[1] O.C. Zienkiewicz, "The Finite Element Method in Engineering Science", McGraw Hill, 1971
[2] R. Park, T. Paulay, "Reinforced Concrete Structures", John Wiley & Sons, Inc., 1975
[3] M. Rossi, B. Thürlimann, "Das Verhalten von Stahlbeton-Balken bei wiederholter Belastung", Institut für Baustatik und Konstruktion, ETH Zürich, Bericht Nr. 7503-1, Mai 1981
[4] J. Blaauwendraad,S.F.C.H. Leijten, J.G.M. van Mier, "Comparison of Plastic Prediction with STANIL/1 Analysis", IABSE, Vol. 29, Copenhagen 1979
[5] K. Brandt, S. Klee, "Traglastversuche an gewalzten Breitflanschprofilträgern", Der Stahlbau, 7/1979
[6] B. Thürlimann, "Plastic Analysis of Reinforced Concrete Beams", IABSE, Vol. 28, Copenhagen 1979
[7] P. Lampert, B. Thürlimann, "Torsionsversuche an Stahlbetonbalken", Institut für Baustatik und Konstruktion, ETH Zürich, Bericht Nr. 6506-2, Juni 1968
[8] F. Leonhardt, R. Walther, W. Dilger, "Schubversuche an Durchlaufträgern", DAfSt, Heft 163, Berlin 1964

Fracture Mechanics Analysis of Discrete Cracking

Analyse par la mécanique de rupture de la propagation des fissures distinctes

Bruchmechanische Behandlung diskreter Rissausbreitung

VICTOR E. SAOUMA
Post-Doctoral Research Associate
Dept. of Civil Engineering
Princeton University
Princeton, NJ, USA

ANTHONY R. INGRAFFEA
Assistant Professor and Manager
of Structural Research
Dept. of Structural Engineering
Cornell University
Ithaca, NY, USA

SUMMARY
A completely new and comprehensive solution to the problem of discrete crack m@delling using fracture mechanics concepts is described. The solution predicts the trajectory and stability of any number of cracks propagating in mixed-mode. Remeshing and renumbering are done automatically. Analysis is performed in an interactive computer graphics environment. Example problems are presented.

RÉSUMÉ
Une solution exhaustive et nouvelle de la modélisation des fissures distinctes employant la mécanique de rupture est présentée. La solution prédit la trajectoire et la stabilité de plusieures fissures se propageant suivant une direction arbitraire. Le maillage du réseau est ajusté automatiquement.
L'analyse est accomplie au moyen d'un traitement interactif et graphique. Des exemples sont présentés.

ZUSAMMENFASSUNG
Eine ganz neue, wie auch umfassende Lösung des Problems des diskreten Bruchmodellierens mittels bruchmechanischer Begriffe wird beschrieben. Die Lösung beschreibt Richtung und Stabilität von Rissen, die bei gemischten Brucharten auftreten. Neueinteilung und Neunummerierung der Elementeneinteilung wird automatisch ausgeführt. Die Behandlung geschieht in einem dialogfähigen Graphikcomputer. Probleme werden exemplarisch behandelt.

1. INTRODUCTION

In two of the introductory reports presented at this colloquium, the increasing importance of applying fracture mechanics to the study of cracking in reinforced concrete is emphasized. Bazant [1] shows that objectivity in predicting fracture initiation is satisfied if fracture toughness, rather than the currently employed tensile strength, is used as a measure of resistance to crack growth. On the issue of discrete versus smeared crack modelling, Bazant [1] argues for the smeared approach. He states that a numerically smeared representation is more realistic, and, moreover, precludes the need to update mesh topology and connectivity with each increment of cracking.

Argyris, Faust, and Willam [2] concur with Bazant's [3] findings on the objectivity of fracture toughness as a cracking criterion. They, like Bazant [1], list the relative merits of discrete versus smeared crack representations but appear to favor the former approach [4].

Together, the two papers highlight the pressing need for research into the following areas of application of fracture mechanics to reinforced concrete:

1. Topology: If a discrete crack model is to be used, a method of regeneration of the finite element mesh to accommodate incrementally changing crack trajectories must be found. This method must introduce the appropriate displacement and traction discontinuities across the crack, must properly account for required meshing near the crack tips, and, ideally, should minimally disturb the bandedness of the system stiffness matrix in accounting for element connectivity changes. Moreover, the method must be fast and user-friendly.

2. Singularity: A linear elastic fracture mechanics approach to discrete cracking requires recognition of the theoretically singular nature of the crack tip stress field. If fracture toughness, K_{Ic}, is to be the controlling material parameter, stress intensity factors K_I, K_{II}, K_{III}, the coefficients of the singular stress terms, must be found for a given crack configuration and loading. In the finite element context, this implies the ability to compute accurately and efficiently the stress intensity factors through proper near-tip meshing.

3. Stability: Cracking in reinforced concrete is not always catastrophic because stable growth always occurs before global instability as a result of the crack arresting effect of the steel. Neither is it always in pure Mode I, since cracking is generally curvilinear due to mixed-mode action. For a given load increment on a structure with multiple cracks, methods must be available for predicting the length and direction of the corresponding crack increments.

In response to this call for research this paper presents, for the first time to the authors' best knowledge, a comprehensive solution to the problem of discrete crack modelling using fracture mechanics concepts. It will be shown that the solution is comprehensive in the sense that it satisfies all of the requirements listed above under topology, singularity, and stability for problems which can be modelled as two-dimensional or axisymmetric.

In solving the problems of topology, the present method employs automatic mesh regeneration and bandwidth minimization algorithms. The developed code operates in a medium-level, i.e. storage-tube, interactive computer graphics environment. The primary objective here is to completely eliminate the strongest drawback to discrete crack modelling: manual remeshing and renumbering. An equally important objective, however, is to take advantage of the rapidly developing techniques and hardware of computer graphics to put the engineer back into

structural analysis. Analyses which involve physically complex processes such as crack propagation are least effectively done in a "black-box" environment. The user should be allowed to observe the analysis and inject his judgment into it as appropriate while it is in progress. Examples of automatic remeshing and other aspects of the interactive nature of the present program are contained in this paper.

The present solution is predicated on the applicability of linear elastic fracture mechanics to concrete cracking. Consequently, a key aspect of the analysis process is automatic computation of mixed-mode stress intensity factors, K_I and K_{II}, at the tip of each crack. The method used has been shown to be highly accurate and efficient in other areas of fracture.

The questions of stability and crack increment direction are answered in the present approach by use of recent developments in mixed-mode crack initiation theory. The length of a crack increment is computed through a recently developed energy balance algorithm. When the length and direction of each crack increment is computed, the necessary topology changes are known and the automatic mesh generator and bandwidth minimizers are invoked for the next cycle of loading. Again, details of these methods, as well as results of example problems are presented in this paper.

It will be shown that a thoroughly new and comprehensive tool for analysis of certain classes of reinforced concrete structures has been created. In comparison with currently popular analysis programs, the present one is as efficient and accurate, but much more friendly and appealing to the analyst.

2. THEORETICAL BACKGROUND

2.1 Crack Stability

The question of applicability of a single-parameter, K_{Ic}, to the onset of Mode I crack propagation in concrete has had a checkered history. Reference to many publications addressing this question was made in a recent report by the authors [5] in which they concluded that a classical fracture mechanics approach can indeed be valid if, as in testing of metals, certain geometrical conditions are met. It is the authors' contention that for materials in which a microcracking process zone is created at the crack tip:

1. A valid K_{Ic} can be measured using standard techniques such as ASTM E 399-80 [5,6,7,8].

2. Of the geometrical conditions to be met in such testing, the most important is that crack length, a, be large compared to maximum, aggregate size, d_{max} [7,8].

3. The ratio a/d_{max} can be as small as four or five in tests which would yield a K_{Ic} valid for structural engineering purposes.

4. Contrary to Bazant's [1] blunt crack band approach, the observed [8,9] process zone size is a small percentage of crack length at crack tip instability. In tests on concrete [9], the process zone size has been observed to be only a few millimeters in length.

Consequently, a classical linear elastic fracture mechanics approach to crack instability in Mode I is taken in the present model. That is, when the computed stress intensity factor, K_I, reaches the value of the concrete fracture toughness, K_{Ic}, a necessary and sufficient condition for local instability is met.

It should be recalled, however, that cracks rarely propagate in concrete structures in pure Mode I. In the present model the local stability of a crack loaded in mixed-mode is approached through substitution of the computed K_I and K_{II} into a theoretical interaction formula. The formula used in the analysis of the problems presented in this paper was developed by Erdogan and Sih [10]. It states that fracture initiation is dependent on the circumferential tensile stress, $\sigma(\theta)$, (Fig. 1) near the crack tip and that fracture initiates from the crack tip in a direction normal to $\sigma(\theta)_{max}$. The $\sigma(\theta)_{max}$ theory predicts an interaction in the K_{Ic}-normalized K_I-K_{II} plane according to,

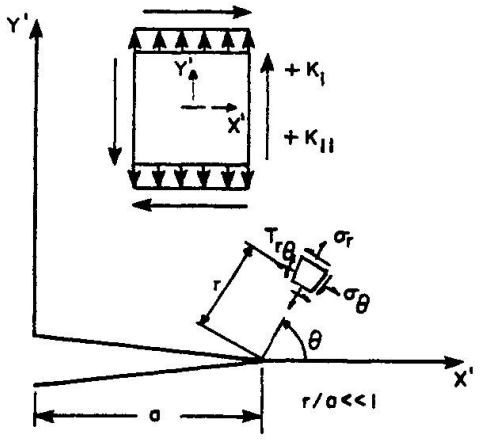

Fig. 1 Crack-Tip Stress Notation

$$\cos\frac{\theta_o}{2}\left[\frac{K_I}{K_{Ic}}\cos^2\frac{\theta_o}{2} - \frac{3}{2}\frac{K_{II}}{K_{Ic}}\sin\theta_o\right] = 1 \qquad (1)$$

The fracture angle, θ , is found by maximizing the expression for the circumferential stress around a crack tip, yielding:

$$\cos\frac{\theta_o}{2}\left[K_I\sin\theta_o + K_{II}(3\cos\theta_o - 1)\right] = 0 \qquad (2)$$

Many mixed-mode fracture initiation theories have been proposed recently and three of the most widely accepted theories have been made available in the code: 1) the maximum circumferential stress theory, 2) the maximum energy release rate theory ($G(\theta_{max})$) [11], which states that the crack will grow in the direction along which the elastic energy release rate will be maximum, and the crack will start to grow when this energy release rate reaches a critical value, and 3) the minimum strain energy density theory ($S(\theta_{min})$) [12] which states that the crack will extend in the direction along which the strain energy density at a critical distance is a minimum when this minimum reaches a critical value.

2.2 Crack Increment Length

Thus far, only the problem of local stability has been considered. That is, the substitution of K_I, K_{II} and K_{Ic} into any of the three mentioned theories will indicate whether a crack will extend, and its angle of propagation.

It is important to realize that a crack extension, or local instability, is not synonymous with failure or with global instability. This is because a crack may be unstable only for a certain crack extension length. Due to the stress redistribution accompanying the crack propagation (a form of geometric non-linearity), its stress intensity factors may decrease resulting in an eventual crack arrest. Alternatively, as a crack crosses reinforcement, the steel acts as a crack arrestor and decreases the stress intensity factors.

An algorithm for computing the length of each increment of cracking caused by an increase in load was first proposed by Ingraffea [15]. In the present case, the problem was addressed from a different point of view; the load increase which forces a crack to extend a given distance in a quasi-stable way was computed. The scheme is based on the release of potential energy to form surface energy. The energy required to create a new unit of surface area is a material constant

related to its fracture toughness by:

$$R = \frac{K_{Ic}^2}{E'}$$

$$\text{where } E' = E \qquad \text{for plane stress} \qquad (3)$$

$$E' = \frac{E}{(1-\nu^2)} \qquad \text{for plane strain}$$

The direct determination of the energy released, $G(\theta)$, during the propagation of a crack at an arbitrary angle had been a mathematical challenge for many years. Of the many solutions now becoming available, that of Hussain et al. [11] is employed in the present analysis.

If for a given crack configuration G is greater than R, a local instability occurs and the crack will extend. As the crack propagates, G may increase, resulting in an unstable crack growth or global instability. Alternatively, G may decrease and lead to stable crack growth.

For stable crack growth, the question is then how far the crack extends under a given fixed load before it stops. It is clear that an equilibrium state will be reached when a balanced energy transfer occurs from G to R, as shown in Fig. 2, in the following form.

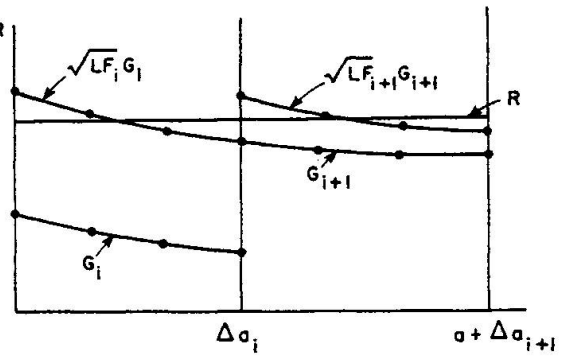

Fig. 2 Graphical Form of Energy Balance Algorithm for Crack Length Prediction

$$\int_o^{\Delta a^*} G(a,\theta,K_I,K_{II})\, d\Delta a = \int_o^{\Delta a^*} R(K_{Ic})\, d\Delta a \qquad (4)$$

where Δa^* represents the point of crack arrest.

In the present investigation, the problem consists in determining the load amplification factor which will cause the initial crack to extend by a predefined increment, Δa^*.

Given a structure, analyzed for four crack positions all with the same load P_i, a curve through the four corresponding values of G can be defined. The area under the G-curve, A_G, is the amount of energy released, and the area under the R-curve, A_R, is the amount of energy needed to create a new surface area corresponding to the crack increment Δ^*.

If A_G is greater than A_R, then a form of instability occurs. It will be a local instability if G decreases with crack length and the energy balance transfer will be satisfied before the crack reaches a free surface. Alternatively, if G increases with crack extension, then a global instability and failure take place.

If A_G is smaller than A_R, then to satisfy the energy balance transfer, A_G should be increased by appropriately shifting the G-curve upward. Since G is proportional to the square of stress intensity which in turn is directly proportional

to the load, the load amplification factor for the current increment will be:

$$LF = \sqrt{\frac{A_R}{A_G}} \tag{5}$$

The determination of A_G is accomplished by dividing each crack increment into three sub-increments, each with its own direction and value of G, fitting a curve through the four G-values, and integrating the resulting expression over the crack increment length. This is done automatically for each crack increment.

2.3 Stress Intensity Factor Calculations

To ascertain the stability, direction, and length of a crack increment, the stress intensity factors must be known. The problem here is twofold: (a) modelling the appropriate form of singularity by special elements, and (b) the extraction of the stress intensity factors from the near-tip displacement field.

The development of a reliable, simple and "cost effective" singular element had to wait until 1975 when, concurrently, Barsoum [13] and Henshall and Shaw [14] discovered the fortuitously singular nature of the quarter-point, quadratic, isoparametric quadrilateral and triangle.

Since the quadratic displacement interpolation functions are not in any way altered in creating the $r^{-1/2}$ stress singularity in the element, use of this offset-node geometry does not change the element convergence characteristics. Moreover, the element stiffness matrix is formulated by the same subroutine as usual; only the nodal coordinate input data are altered.

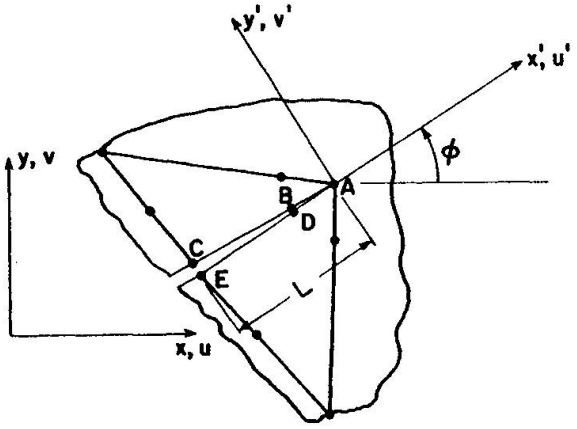

Fig. 3 Crack-Tip Element Nodal Lettering Scheme

The displacement correlation method [15,16] is employed for determination of stress-intensity factors from the nodal displacements of the singular elements. Denoting the local displacements along the crack axis as U' (crack sliding displacement, CSD) and the displacement normal to the crack axis as V' (crack opening displacement, COD) the stress intensity factors can be directly evaluated from:

$$K_I = \frac{G}{\kappa+1}\sqrt{\frac{2\pi}{L}}\left[4(V'_B - V'_D) + (V'_E - V'_C)\right]$$

$$K_{II} = \frac{G}{\kappa+1}\sqrt{\frac{2\pi}{L}}\left[4(U'_B - U'_D) + (U'_E - U'_C)\right] \tag{6}$$

where $\kappa = \frac{(3-\nu)}{1+\nu}$ plane stress

$\kappa = 3 - 4\nu$ plane strain

with reference to Fig. 3. Examples of the accuracy and simplicity of this method can be found in References 17 and 18.

3. PROGRAM DESCRIPTION

With the objective of modelling discrete crack propagation in reinforced concrete, the theoretical developments outlined above were incorporated into a program entitled FEFAP (Finite Element Fracture Analysis Program). Its general capabilities are described in this section.

3.1 Element Library

Concrete is modelled by quadrilateral or triangular quadratic isoparametric elements. Main steel reinforcement is modelled by quadrilateral elements which provide both axial and bending stiffness. Three-noded linear elements are used for shear reinforcement. Bond between the concrete and steel and aggregate interlock along cracks are modelled by an isoparametric version of the interface element developed by Goodman et al. [19,20].

3.2 Constitutive Models

While the initial objective of this investigation was restricted to a linear elastic concrete model, it was found from test problems that the response under high loads was too stiff. This was attributed to the constant value assigned to the concrete Young's modulus.

The code was extended to account for material softening as dictated by an appropriate model. A simple model which would encompass both the biaxial and triaxial state of stress (for plane strain and axisymmetric analyses) for the failure criterion and the prediction of the secant Young's modulus and Poisson's ratio was selected and implemented. The secant values are needed because load is always applied in a single increment, as will be indicated below. The selected failure criterion, proposed by Ottosen [21,22], is based on a four-parameter equation containing explicitly all the three stress invariants.

The steel model is currently linear elastic.

Steel-concrete bond was governed by the equation developed by Nilson [23].

Finally, the aggregate interlock model requires special comment. It has been recognized that the shear modulus along a crack is a portion, α, of the inital uncracked modulus. Theoretically, α should be inversely proportional to the crack opening, but such a relative displacement is not directly derived in the general smeared cracked model. The present model takes advantage of the discrete nature of the crack to directly compute the crack opening and accurately evaluate the shear stiffness along the crack using the empirical equation derived by Fenwick and Paulay [24].

3.3 Program Capabilities

To model discrete crack propagation, in plane and axisymmetric structures, the following capabilities were implemented:

1. An automatic element and node generation capability for regular meshes.

2. An automatic nodal adjustment for the singular elements, and direct extraction of the stress intensity factors.

3. A graphical display capability on a TEKTRONIX 4013 or 4014 terminal.

4. Forms of loading: a) nodal, b) edge, c) initial nodal displacement, d) gravity, and e) thermal.

5. A mesh optimizer for bandwidth minimization and direct nodal renumbering [25,26].

6. A highly efficient In/Out of core skyline-banded equation solver [27].

7. Graphical display of the deformed mesh, the principal stresses, and the cracking pattern.

8. A completely interactive means of operation within the program.

9. Automatic, discrete crack nucleation at arbitrary points, on an edge or in the interior of a domain, and angles as specified by the analysis.

10. Automatic, discrete crack propagation capability with mesh adjustment along the propagating crack.

11. User interaction with the code to perform interactively final minor adjustments to each regenerated mesh.

These capabilities required about 9000 FORTRAN statements grouped in 80 subroutines.

A detailed scenario of the analysis procedure is too long to include in this paper. It can be found in Reference 28. Some further details of the mesh regeneration accompanying crack propagation are, however, included in the next section.

4. DISCRETE CRACK PROPAGATION MODELLING

The essential requirement of the present model is the availability of a set of routines which will control the mesh modification caused by an arbitrary extension of an interelement crack.

4.1 General Strategy

The general strategy followed for the crack extension through a finite element mesh is as follows:

1. From the initial direction of the crack axis, and the predicted angle of crack extension with respect to the crack direction, determine the angle of crack propagation in global coordinates.

2. Replace the quarter-point nodes to their initial midside position, to remove the local singularity.

3. Define a new crack tip node whose coordinates are determined from the length and angle of crack extension.

4. Define a new node adjacent to the old crack tip node.

5 Search the previous singular elements, to determine which one is going to be crossed by the crack.

6. If the new crack tip node falls inside this element, extend the crack to it and go to 8, otherwise simply extend the crack through the entire length.

7. Locate the next element to be crossed by the crack and go to 6.

8. Define the new nodes from which the stress intensity factors will be evaluated.

9. Adjust the midside nodes to the quarter-point position, where needed.

10. Display the modified mesh, to allow the user to interactively perform final adjustments.

11. Evaluate the stiffness matrices of those elements perturbed or newly created by the mesh modification.

4.2 Actual Implementation

The actual implementation of the above mentioned strategy rests on three main requirements:

1. To handle a discrete crack crossing an element.

2. Once a crack emerges from an element, to find out which element is the next to be entered.

3. Check if the crack will stop in the next element to be entered.

In the most general case, the crack may cross a triangular or a quadrilateral element in different ways. The crack may enter from a node or a side, leave from another node or another side or simply stop inside it. Thus a number of different situations may arise where some adjustments are required, and all possible combinations have to be accounted for.

The 25 possible cases are schematically shown in Fig. 4.

Once a crack has emerged from an element side or node, a search is performed to locate which of the elements is going to be entered next, and (if so) whether the crack is going to stop in it.

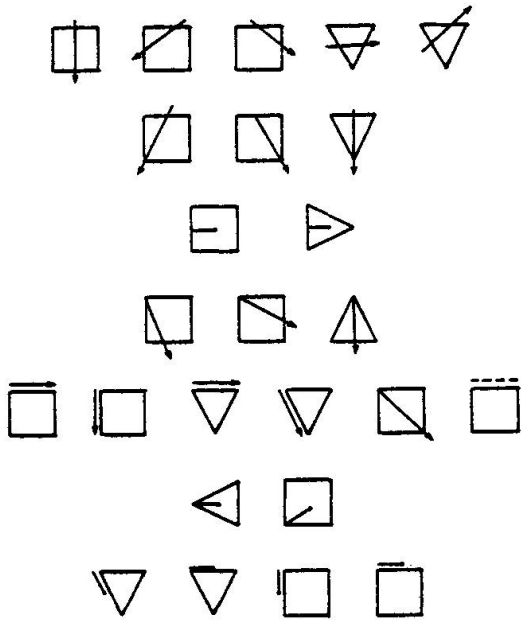

Fig. 4 Possible Crack Paths Across, Into, and Around Elements

4.3 Corrective Measures

A number of pathological situations may arise, and if properly diagnosed, special corrective measures will automatically be taken by the code. Those corrections occur:

1. When a crack is about to cross a bond or steel element. Since steel elements can obviously not be broken by the crack, special modifications which will ensure subsequent displacement continuity will be performed (see Fig. 5).

2. When a crack extends through an element by breaking it in two (the most general case), and one of the resulting elements has a very large aspect ratio, then one of the sides of the original element will be shifted. This will allow the crack to propagate between two adjacent elements and will further require the adjustment of some of the midside nodal coordinates and the reevaluation of the stiffness matrices of the elements sharing the shifted side.

3. When a crack tip stops close to a side or to a node, then elements with a poor aspect ratio will be generated and some modification will be necessary.

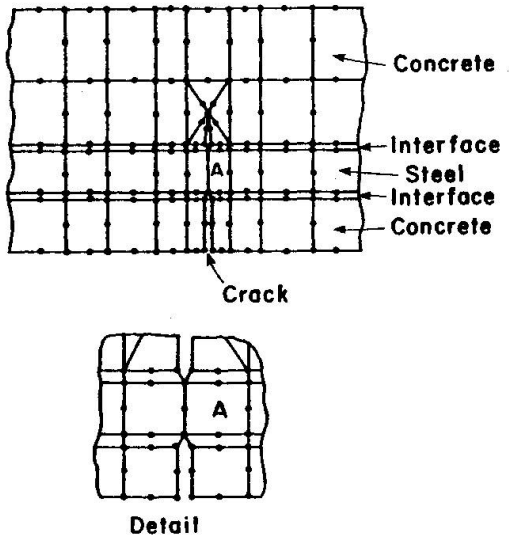

Fig. 5 Topology Around Crack Which Crosses Main Reinforcement. Interface Elements Model Bond.

Even though much effort has been made to automate the progressive crack growth and nucleation procedure, no claim can be made that the method will cover every possible cracking condition encountered in every analysis. In fact engineering judgment should remain an essential and ultimate part of the analysis. To this end, the user, based on a picture display of the modified mesh, can interactively take appropriate corrective measures. These include the dragging of a node from one position to another, or changing a diagonal common to two triangular elements, to improve their aspect ratios.

4.4 Discrete Crack Nucleation

If a crack is to nucleate at a certain Gauss point of a particular element, the following steps will be performed:

1. The direction of the new crack is displayed on the screen for approval by the user who may reverse its direction by 180 degrees.

2. The user is prompted to locate the node where the crack is to nucleate.

3. The program will generate a new node adjacent to the indicated one.

4. From that point on, the code will treat the problem as if it were asked to propagate a crack emanating from a node. This process will be applied once (if the crack nucleates from a free surface), or twice (if the crack nucleates from the interior). The initial crack size is arbitrary; the crack tip is located in such a way that its distance from the nucleating node is equal to half the closest element side length.

5. Singular element angles are checked and adjusted if necessary.

6. Once the crack has been nucleated, the user can either reduce its length by shifting the crack tip node, or extend it by asking for a complete crack extension run.

5. EXAMPLE PROBLEMS

As an integral part of their research program on the shear strength of reinforced concrete beams, Bresler and Scordelis performed a number of experimental tests. Those tests were so accurately performed and so thoroughly recorded [29,30] that their primary objective has been overshadowed by their use as a yardstick to evaluate many, if not most, finite element reinforced concrete codes. Beam OA-1 of their test series is here analyzed as an example of the capabilities of FEFAP.

5.1 Problem Description

The experimental setup of the beam and its dimensions are shown in Fig. 6. The beam was reported to have:

Thickness: 12 in. (305 mm)
Concrete compressive strength: 3.27 ksi (22.6 MN/m^2)
Concrete secant modulus: 3,470 ksi (23.9 GN/m^2)
Concrete modulus of rupture: .575 ksi (3.96 MN/m^2)
Concrete Poisson's ratio: .15
Steel yield stress: 82 ksi (566 MN/m^2)
Longitudinal reinforcement: 4 #9 bars
Vertical reinforcement: None

The steel bars were bolted to a plate at each end of the beam to prevent bond failure due to possible insufficient anchorage after the formation of diagonal tension cracks.

The beam was reported to have failed in a diagonal tension failure mode at a load of 58 kips (258 KN). The final observed crack pattern, Fig. 7, indicates that five major cracks had developed on each side of the center line. It should be noted that the beam had a steel ratio of 1.8 percent, well above the balanced one of 1.4 percent.

5.2 FEFAP Analysis

Four different analyses of this problem have been performed. The varying parameters were: 1) concrete material model, 2) fracture toughness, 3) shear transfer along the crack. Since the beam was overreinforced, and the steel bars were bolted at each extreme, bond was not expected to play a major role and was not considered as a variable in the present investigation. Descriptions of the four analyses are summarized in Table 1.

TABLE 1. Description of Analyses Performed

	Concrete Model	Shear Transfer Along Crack	Fracture Toughness ($lb\text{-}in^{-3/2}$)	Fracture Toughness ($MNm^{-3/2}$)
L-AI-600	Linear	Yes	600.	0.66
L-NAI-600	Linear	No	600.	0.66
L-AI-1200	Linear	Yes	1200.	1.32
NL-AI-600	Non-linear	Yes	600.	0.66

After a description of the finite element idealization, the results of each analysis will be presented, discussed, and compared with other results.

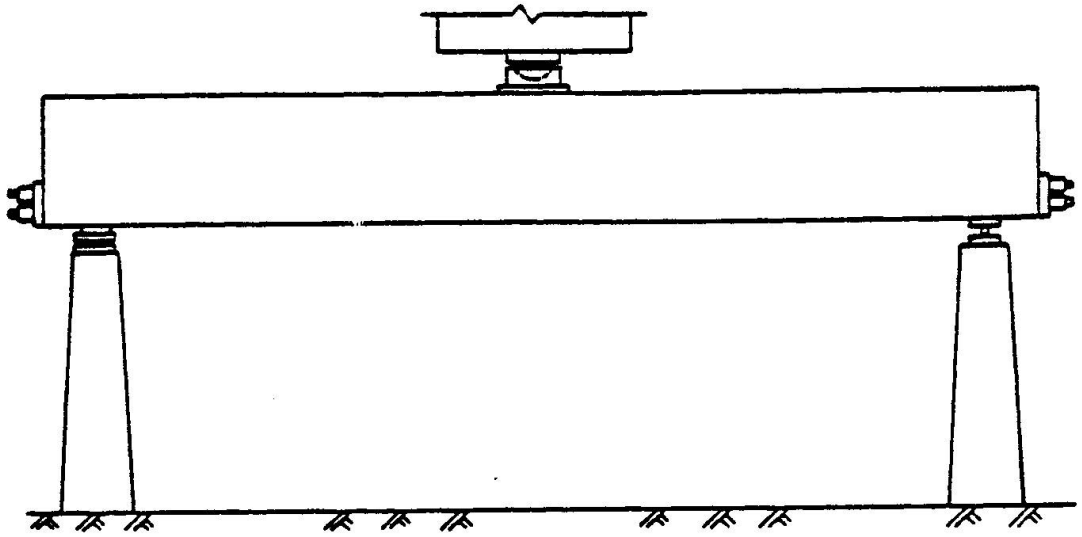

Fig. 6 Testing Configuration of Beam OA-1 [29,30]

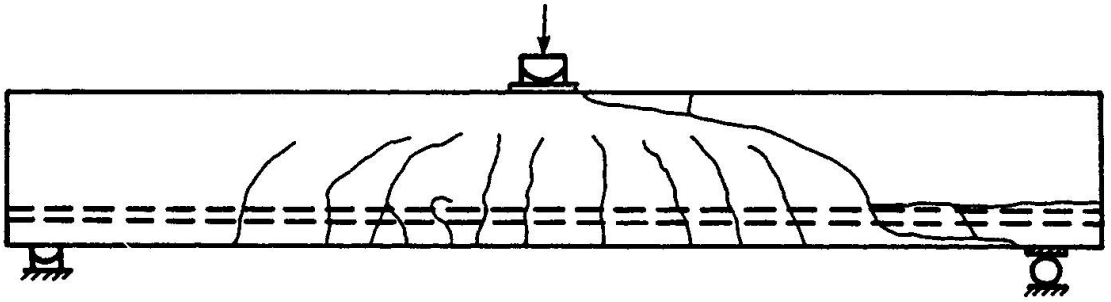

Fig. 7 Observed Crack Pattern on Beam OA-1 [29,30]

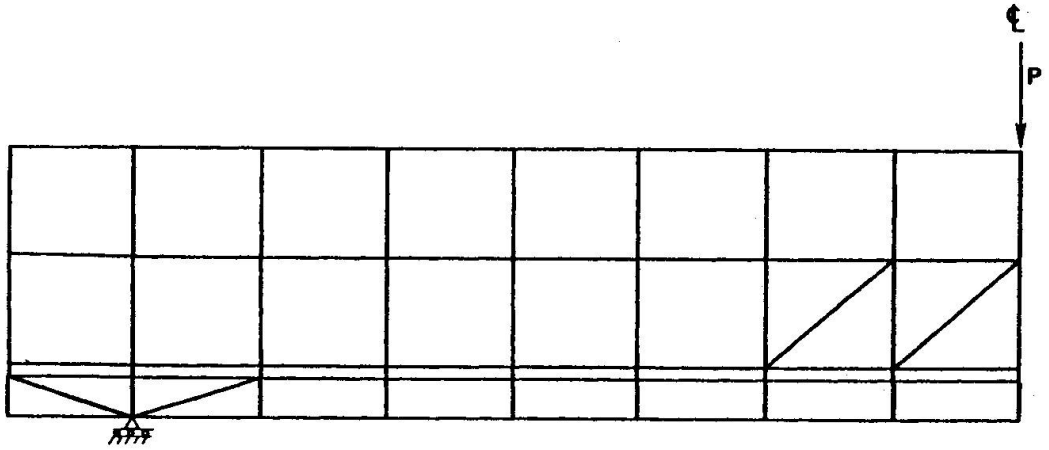

Fig. 8 Initial FEFAP Finite Element Idealization of Beam OA-1

5.2.1 Finite Element Idealization

The smooth stress gradients in an uncracked beam, the accuracy provided by the isoparametric quadratic elements, and the obvious objective of minimizing the initial number of nodes, allowed the selection of the initial mesh shown in Fig. 8. Interface elements are spread along both sides of the steel layer except for the last steel element next to the anchorage.

The only restriction imposed by the selection of an initial mesh is the minimum distance between two adjacent cracks [approximately 10 inches (254 mm)]. This is imposed by the present code limitation to nucleate a crack from an element corner node only. The local mesh refinement below the load point was initially implemented to allow the simultaneous occurrence of two adjacent cracks with the same initial length without their having a common singular element.

The $\sigma(\theta)_{max}$ theory [10] was used throughout the analyses as the mixed-mode fracture criterion.

5.2.2 Finite Element Results

Results of each analysis will be individually reported as follows:

1. A plot of the final deformed mesh.
2. A plot outlining the final crack pattern.
3. A figure of the final load-displacement curve.

These results are shown in Figures 9 through 12. With reference to those figures, the following general comments may be made:

1. The simple linear model with aggregate interlock, Fig. 9 is satisfactory up to a load of about 40 kips (178 KN) [where the maximum computed compressive stress reaches a value of 1900 psi (13.1 MN/m^2)]. The discrepancy above this load is attributed to the constant elastic modulus assigned to the concrete.

2. The second analysis, Fig. 10, differing from the first only in the value of K_{Ic}, shows a definitely stiffer response than the previous one.

This difference can easily be explained by recalling that the load forcing a crack to extend is directly proportional to fracture toughness. If two identical structures are subjected to similar loads, the one with the lower fracture toughness will be more extensively cracked and thus exhibit a softer response than the other. This is reflected by the larger load (84.5 kip vs 64.5 kip, 376 KN vs 287 KN) required to crack this beam less extensively than L-AI-600.

It is important, however, to note the relatively low sensitivity of the load-displacement curve to a large change in the value of the fracture toughness. One may conclude that a realistic value is really all that is needed. Of course, if prediction of a crack tip location as a function of the load is required, then great care should be exercised in selecting a proper value for the fracture toughness.

3. The third analysis, Fig. 11, produced, initially, a good load displacement correlation with the experimental results. However, it became apparent from the evolving crack configuration that unrealistic crack paths were being followed. The analysis was interrupted when it became clear that two cracks were about to intersect with each other; this could not have been modelled by the present version of FEFAP.

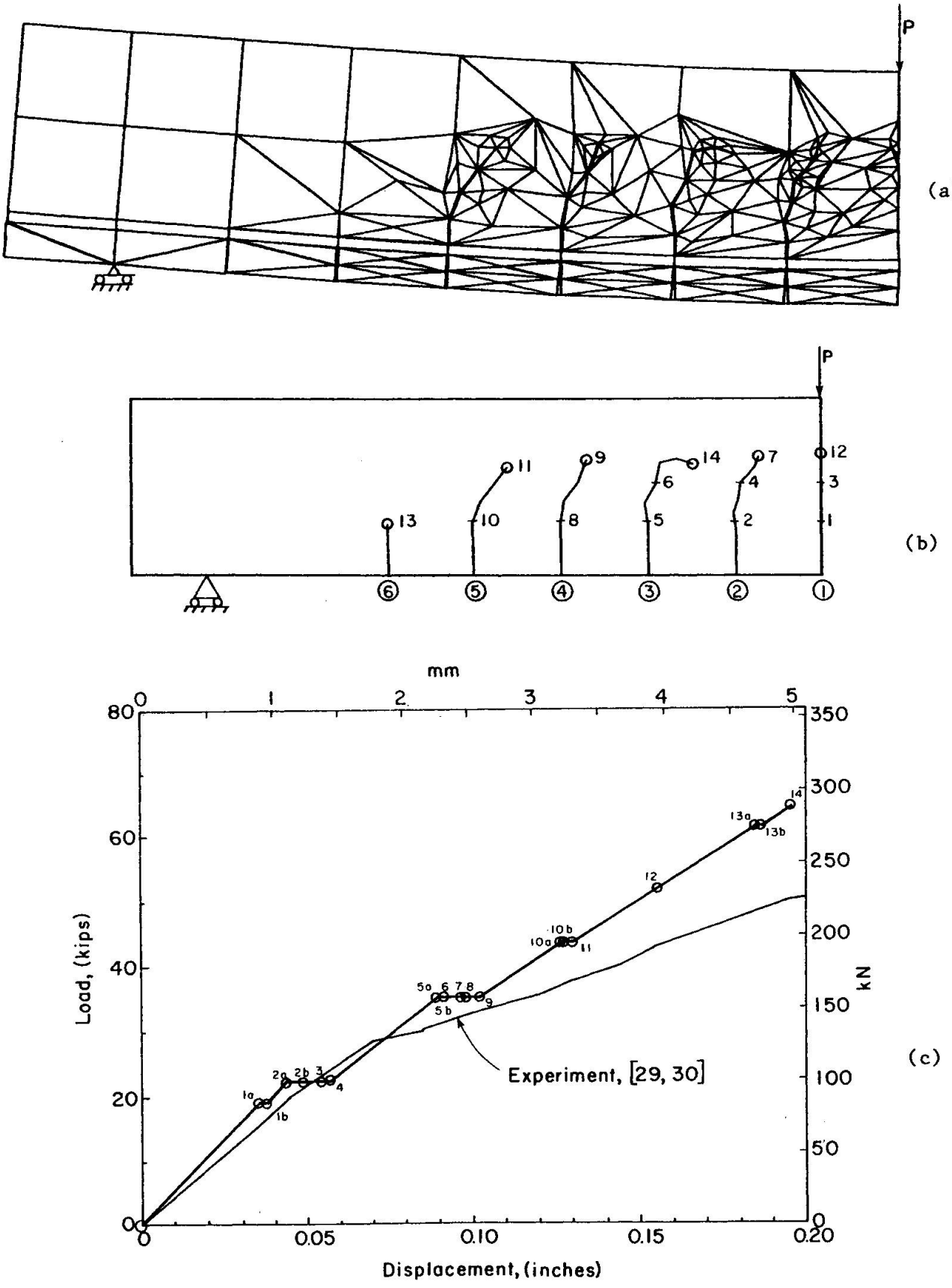

Fig. 9 Results of Analysis L-AI-600. a) Final Mesh on Deflected Shape b) Final Crack Pattern c) Comparison of Calculated and Observed Load-Displacement Curves.

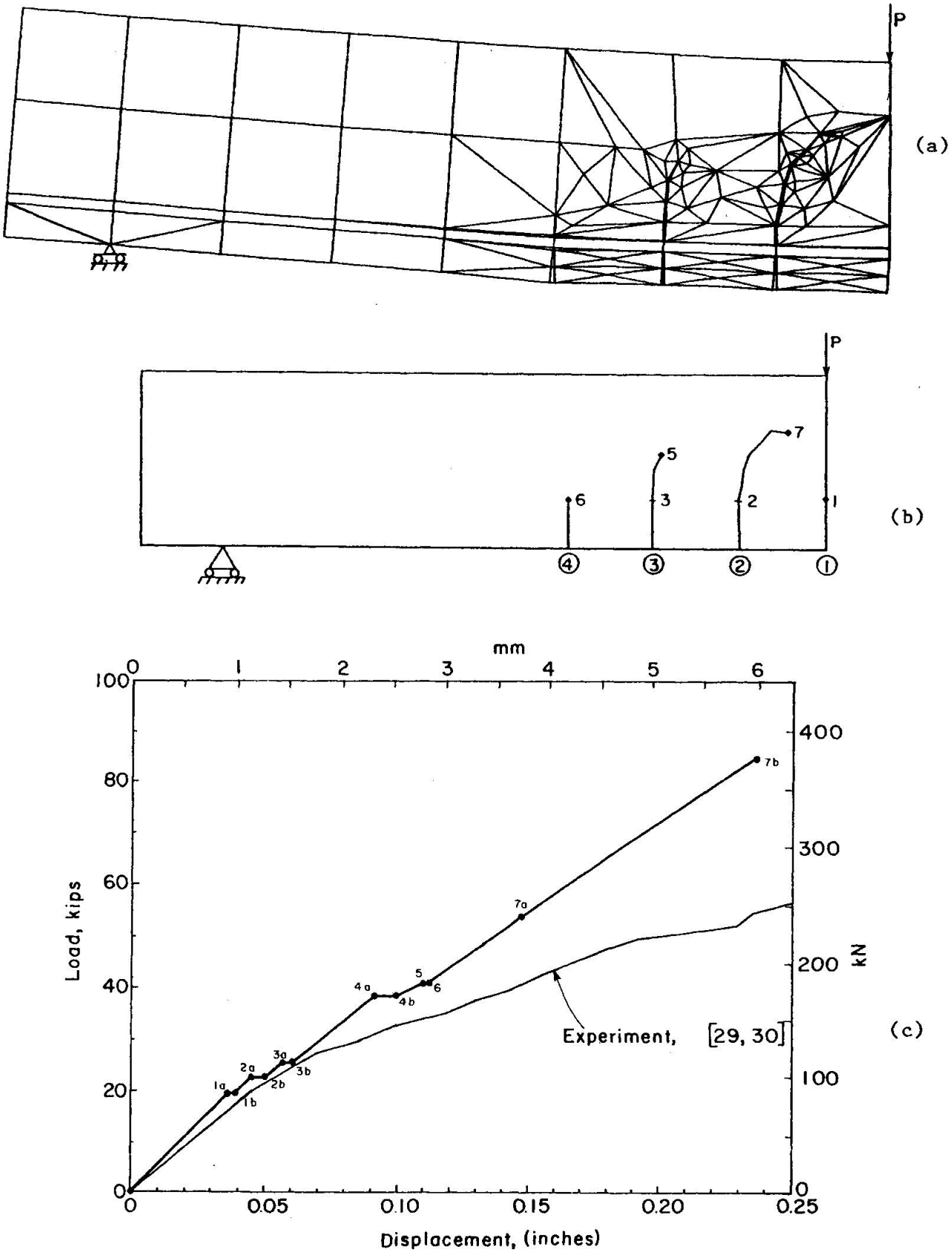

Fig. 10 Results of Analysis L-AI-1200. a) Final Mesh on Deflected Shape b) Final Crack Pattern c) Comparison of Calculated and Observed Load-Displacement Curves.

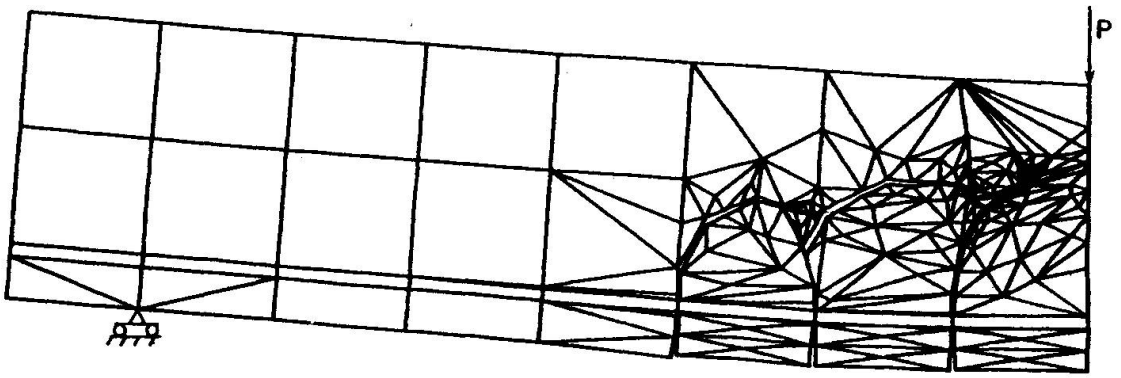

(a)

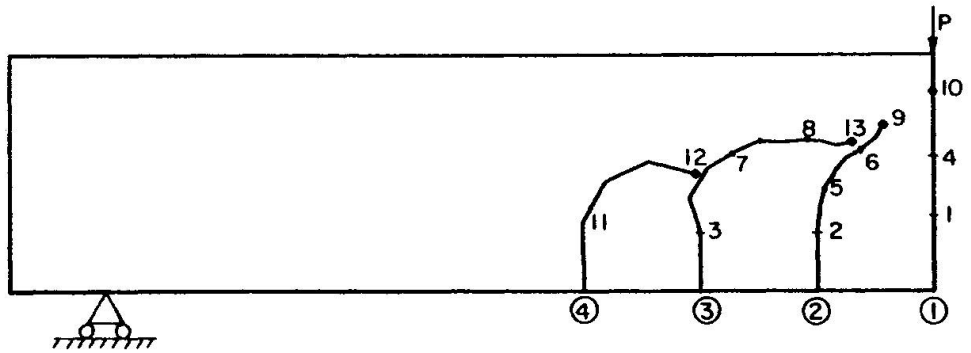

(b)

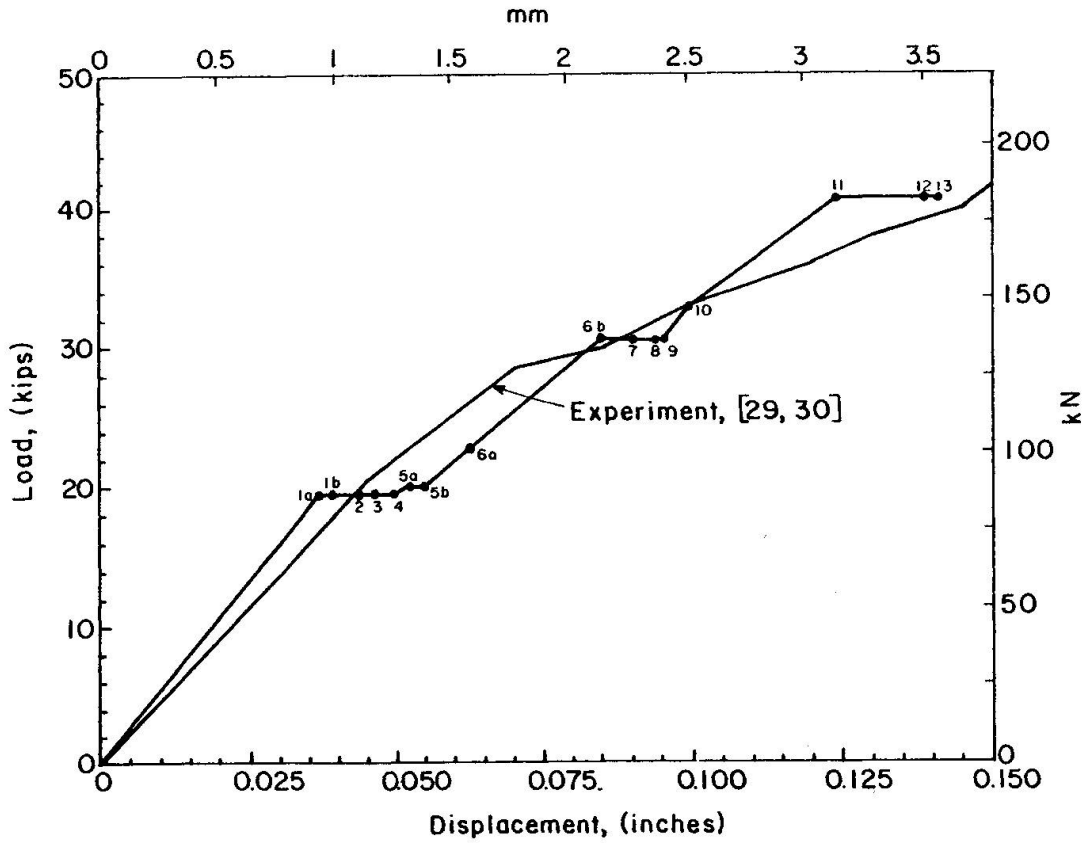

(c)

Fig. 11 Results of Analysis L-NAI-600. a) Final Mesh on Deflected Shape b) Final Crack Pattern c) Comparison of Calculated and Observed Load-Displacement Curves.

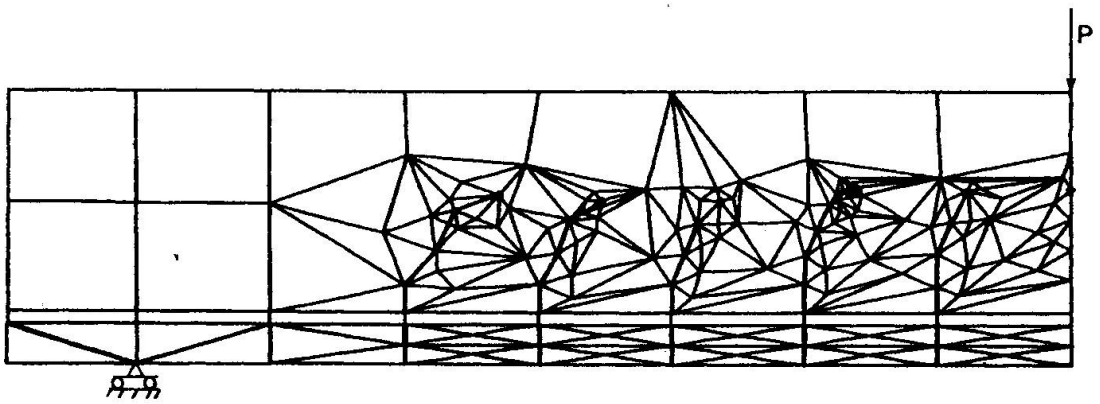

(a)

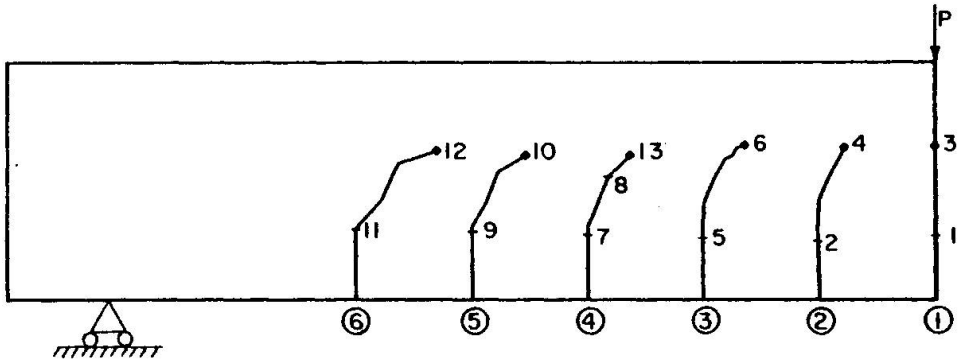

(b)

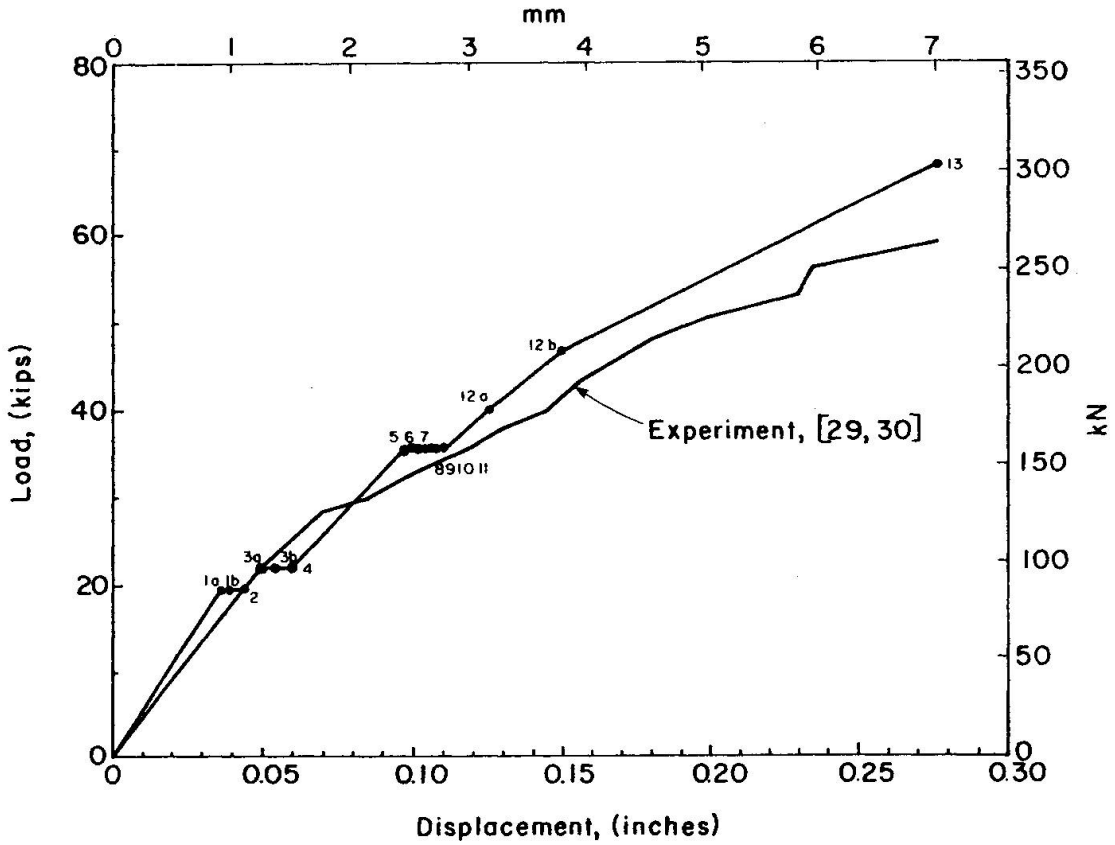

(c)

Fig. 12 Results of Analysis NL-AI-600. a) Final Mesh b) Final Crack Pattern c) Comparison of Calculated and Observed Load-Displacement Curves.

It appears that the absence of interface elements along a crack, modelling the aggregate interlock shear transfer, increases both K_I and K_{II} (as reflected by the large amount of cracking for a comparatively low load), and the ratio of K_{II}/K_I (as reflected by the large curvature of the cracks).

The softer response exhibited by this analysis is not surprising since no stiffness was present along the cracks to reduce the shear displacements.

Based on the final crack configuration, it seems reasonable to conclude that modelling of the shear transfer along cracks is an important factor. This conclusion agrees with Cedolin [31], who reached it based on a different criterion. He found substantial differences in the load displacement curves obtained through a parametric study of the shear modulus along a smeared crack.

4. The last, non-linear analysis, Fig. 12, is certainly the most accurate and satisfactory one. Good correlation between the experimental and numerical results is achieved all along the load path. The approach followed by the code to determine the load at the end of an increment makes it difficult to accurately predict the failure load (assumed to occur whenever a Gauss point will have its Young's modulus equal to zero) which can explain some of the small error in its predicted value. In fact, recalling that the code computes the load causing a crack to extend a certain predetermined length, one should select progressively smaller crack increments as the crack tips approach the compressive region. A selected length which may be too large will force the crack to enter the compressive region resulting in an unrealistically large load increase.

5. It is interesting to compare the relative contributions to the overall nonlinearity due to cracking (geometrical) and concrete softening (material), since no such comparison could be performed in a smeared crack approach.

To achieve such a comparison, for different load values, it has been assumed that the total displacement is a linear function of the 1) elastic response, 2) cracking and 3) concrete softening. The first contribution is obtained by extrapolating the initial stiffness of the uncracked beam in analysis L-AI-600. The second one is determined by subtracting the results of L-AI-600 from the first one,,and the last component by subtracting results of L-AI-600 from those of NL-AI-600. A normalized plot of the three contributions is shown in

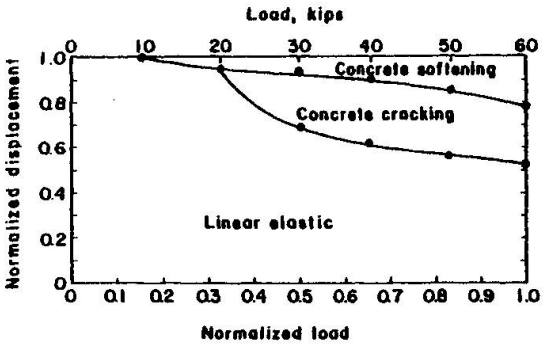

Fig. 13 Relative Contributions to Displacement Under the Load on Beam OA-1

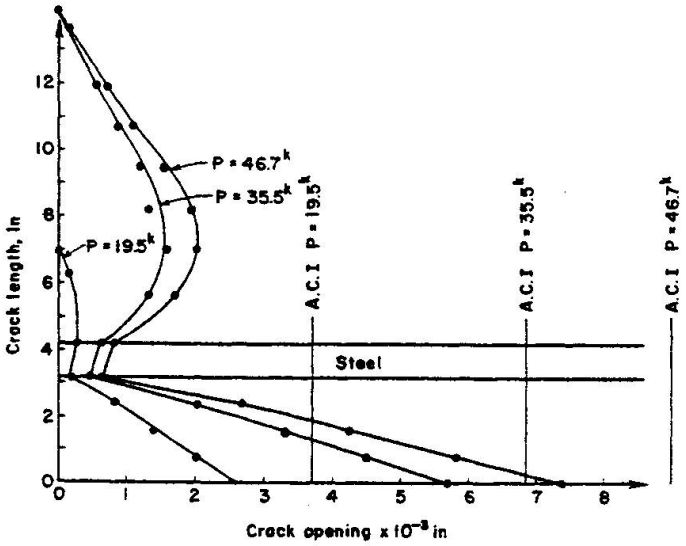

Fig. 14 Comparison Between Empirical and Calculated COD for Center Crack of Beam OA-1

Fig. 13. The most important observation indicated by this diagram is that once a crack has formed [at a load of about 20 kips (89 KN)], the cracking contribution throughout the whole range of loading is about 27 percent. It is not until about 70 percent of the failure load has been reached that concrete non-linearity starts to account for more than 10 percent, and at no time does the material non-linearity contribution exceed the geometrical one (22 percent as opposed to 26 percent at failure).

Of course no generalization could be made from this particular analysis, but the trend is a clear indication of the primary sources of non-linearity in a reinforced-concrete structure, and what their relative contributions are.

6. Another comparison which the smeared crack approach cannot perform is the measurement of the crack opening displacements. While those values were not reported in [29,30], a comparison with the ACI 318-77 Code [32] equation for crack opening is possible.

The center crack of NL-AI-600 has been selected, and its opening at three different load stages compared with the empirical ACI equation based on the experimental work of Gergely and Lutz, [33] Fig. 14.

The empirical equation overestimated the maximum crack opening at the lower fibers of the beam by 42, 19 and 21 percent under loads of 19.5, 35.5 and 46.7 kips (87, 158, and 208 KN), respectively. This percentage of error is certainly small in terms of engineering accuracy for an empirically derived formula for reinforced concrete.

Another interesting observation, which again could be done only through a discrete crack finite element analysis, is the shape of the crack opening. While the actual opening at the level of the steel bar is very much dependent upon the bond stiffness, it is nevertheless an order of magnitude smaller than the one occurring at the free surface.

7. Finally, it should be mentioned that the execution time of FEFAP is not prohibitively expensive as compared to the currently available codes using the smeared crack approach. Cedolin [31], reported a total CPU time of 1120 sec. on a UNIVAC 1108 for an analysis of the same beam problem, while the CPU time of the NL-AI-600 analysis was 460 sec. on an IBM 370/168 model 3 (estimated to be six times faster than the UNIVAC 1108).

6. DISCUSSION

Certain characteristics of FEFAP, positive and negative, merit discussion. On the positive side, it needs to be emphasized that the initial data set for the above example problem consisted of 30 card images, and that was all the data ever generated and entered into the computer by the analyst. All remeshing and renumbering was done automatically, quickly, cheaply, and without the possibility of human error.

Secondly, the interactive nature of FEFAP puts the analyst back into the analysis. With each increment of loading, the analyst is informed graphically of resultant changes in material properties and mesh topology, and immediately sees their effect on the load-displacement response of the structure. Moreover, since the program can be restarted from a previous crack increment at any time, parametric studies which highlight the effect of change in a particular variable on structural response can be easily performed.

Finally, it is clear that progressive cracking and material nonlinearity make a reinforced concrete structure increasingly difficult to analyze; the structure

is much more complex, topologically and constitutively, near failure than when unloaded. Yet, in the standard smeared crack approach to analysis, the initial mesh is the final mesh. This forces the analyst either to compromise accuracy at later stages of loading for cost-effectiveness at the initial stages when a complex mesh is unnecessary, or to carry a very fine mesh all the way through the analysis thereby incurring an initial inefficiency. The present approach is a natural one from the point of view of accuracy, as well as rigor. As the topology becomes more complex more elements are added as needed, yet no sacrifice in the rational fracture mechanics approach to crack propagation is made.

There are, however, some significant drawbacks in the operation of the current version of FEFAP. These fall into two general categories, topology and material modelling. Figs. 9 through 12 show that cracks currently can nucleate only from corner nodes of elements. This is an artificial and inaccurate constraint on crack modelling. These figures also show that a burden of many unnecessary elements behind the crack tip area is carried through the analysis. As mentioned above, the number of elements should increase with cracking, but not to the unnecessary degree presently seen.

As mentioned in Section 5.2.2, the current algorithm for modelling of material non-linearity is basically purely incremental, with no iteration capability to reduce unbalanced nodal loads. The inaccuracy introduced by this shortcoming is especially evident in the last load increment of analysis NL-AI-600, Fig. 12.

These and other minor drawbacks in the current version of FEFAP are the subject of ongoing improvement of the code. Example problems evincing their solution will be detailed during the oral presentation of this paper.

Finally, the authors would like to offer some philosophical comments concerning objectivity and the need for a rigorous, fracture mechanics approach to cracking. There are clearly, many classes of problems in reinforced concrete in which a tensile-strength-controlled, smeared crack approach to analysis is sufficiently accurate. It is also likely that there are some in which it is not. There can be no doubt that problems involving crack propagation in plain concrete structures, such as dams [34], must be approached with the objective tool of fracture mechanics. The key element in this issue is the crack arresting character of the reinforcement; in a given structure, if the layout and strength of the reinforcement, and the capacity of bond to transmit stress to it, are sufficient to arrest cracks and maintain their local stability throughout the course of loading, then it is likely that the currently popular approach is sufficiently accurate. If not, then the proposed approach is necessary.

In light of these final comments, the authors suggest that an international "Blind Round-Robin" testing analysis program be formed. A series of well controlled and documented laboratory or field tsts on various types of structures would be performed in Europe and the United States. Concurrently, various research groups will analyze the same structures using the approach of their choice. An international symposium would then bring together experimentalists, analysts, and their results for comparison and discussion.

This initiative would give new impetus to a field with rapidly expanding applications, but in which significant new development has not occurred for nearly a decade.

7. CONCLUSIONS

A completely new and comprehensive solution methodology to the problem of modelling discrete crack propagation in reinforced concrete was presented. An interactive computer code, FEFAP, was developed which uses linear elastic

fracture mechanics principles to govern mixed-mode crack propagation. A new mesh is generated and renumbered automatically, quickly, and cheaply, after each topology change. The following conclusions concerning FEFAP and its bases are drawn:

1. The example reinforced concrete problem analyzed shows that:

   i) Concrete fracture toughness value does not play a dominant role in the load displacement response.

   ii) Aggregate interlock must be modelled.

   iii) Most of the overall structural non-linearity stems from concrete cracking, and only toward failure does concrete softening play a substantial role.

   iv) FEFAP costs about the same to run on a given problem as codes using a smeared crack approach.

2. The most important advantages that the discrete-crack, fracture mechanics model has over the smeared crack model are:

   i) Rational and rigorous criteria for stability, direction, and length of a crack increment.

   ii) Accurate determination of crack tip location.

   iii) Evaluation of crack opening displacements.

   iv) Breakdown of nonlinearity into its two components, cracking and softening.

   v) Control of the strain energy gradient within each element throughout the analysis due to the local remeshing along the crack and around its tip.

   vi) Capability of using rational models for aggregate interlock along the cracks.

3. Interactive mode of analysis through a storage tube display device (medium level computer graphics) is found to be a very efficient mode of operation. Information which would otherwise require pages of output and hours of study of printed forms is displayed continuously and quickly. Furthermore, the analyst can inject his engineering judgment into the analysis within a "friendly" working environment.

It is hoped that the initial success of the fracture-mechanics, discrete crack approach will stimulate more research and applications not only in reinforced concrete but in other structural materials as well.

8. ACKNOWLEDGMENTS

The authors would like to thank Professors Peter Gergely and Richard White for their assistance and encouragement in this research. The financial support of the National Science Foundation under Grant PFR7900711 to Cornell University is gratefully acknowledged. The first author also extends thanks to the Interactive Computer Graphics Laboratory of Princeton University for their technical support in some parts of the program development.

9. REFERENCES

1. Bazant, Z.P., "Advances in Deformation and Failure Models of Concrete," Introductory Report, IABSE Colloquium on Advanced Mechanics of Reinforced Concrete, Delft, 1981, pp. 9-37.

2. Argyris, J.H., Faust, G., and Willam, K.J., "Finite Element Modelling of Reinforced Concrete Structures," Introductory Report IABSE Colloquium on Advanced Mechanics of Reinforced Concrete, Delft, 1981, pp. 85-106.

3. Bazant, Z.P., Cedolin, L., "Blunt Crack Band Propagation in Finite Element Analysis," J. of the Engineering Mechanics Div., Proc. ASCE, Vol. 105, No. EM2, April 1979, pp. 297-315.

4. Argyris, J.H., Faust, G., and Willam, K.J., "Finite Element Analysis of Concrete Cracking," ISD-Report No. 254, Stuttgart, 1979.

5. Saouma, V., Ingraffea, A.R., Catalano, D., "Fracture Toughness of Concrete - K_{Ic} Revisited," Dept. of Structural Engineering Report 80-9, Cornell University, 1980.

6. Ingraffea, A.R., and Schmidt, R.A., "Experimental Verification of a Fracture Mechanics Model for Tensile Strength of Indiana Limestone," Proc. 19th U.S. Symposium on Rock Mechanaics, Stateline, Nevada, 1978, pp. 247-253.

7. Schmidt, R.A., and Lutz, T.J., "K_{Ic} and J_{Ic} of Westerly Granite--Effect of Thickness and In-Plane Dimensions," ASTM STP678, 1979, pp. 166-182.

8. Catalano, D., "A Linear Elastic Fracture Mechanics Approach to Toughness of Concrete," M.S. Thesis, Dept. of Structual Engineering, Cornell University, 1981.

9. Schmidt, R.A., "A Microcrack Model and Its Significance to Hydraulic Fracturing and Fracture Toughness Testing," Proc. 21st U.S. Symposium on Rock Mechanics, Rolla, Missouri, 1980.

10. Erdogan, F., and Sih, G.C., "On the Crack Extension in Plates Under Plane Loading and Transverse Shear," ASME J. Basic Engineering, V. 85, 1963, pp. 519-527.

11. Hussain, M.A., Pu, S.L., and Underwood, J.H., "Strain Energy Release Rate for a Crack Under Combined Mode I and Mode II," Fracture Analysis, ASTM, STP560, 1974, pp. 2-28.

12. Sih, G.C., "Strain-Energy-Density Factor Applied to Mixed-Mode Crack Problems," Int. J. of Fracture Mechanics, V. 10, No. 3, 1974, pp. 305-321.

13. Barsoum, R.S., "On the Use of Isoparametric Finite Elements in Linear Fracture Mechanics," Int. J. of Numerical Methods in Engineering, V. 10, No. 1, 1976, pp. 25-37.

14. Henshall, R.D., and Shaw, K.G., "Crack Tip Elements are Unnecessary," Int. J. of Numerical Methods in Engineering, V. 9, 1975, pp. 495-509.

15. Ingraffea, A.R., Heuze, F.E., "Finite Element Models for Rock Fracture Mechanics," Int. J. for Numerical and Analytical Methods in Geomechanics, V. 4, 1980, pp. 25-43.

16. Shih, C.F., de Lorenzi, H.G., and German, M.D., "Crack Extension Modeling with Singular Quadratic Isoparametric Elements," Int. J. of Fracture, V. 12, 1976, pp. 647-651.

17. Lynn, P.P., and Ingraffea, A.R., "Transition Element to be Used With Quarter-Point Crack Tip Elements," Int. J. of Numerical Methods in Engineering, Vol. 12, No. 6, 1978, pp. 235-248.

18. Ingraffea, A.R., and Manu, C., "Stress-Intensity Factor Computation in Three Dimensions With Quarter-Point Elements," Int. J. for Numerical Methods in Engineering, Vol. 15, No. 10, 1980, pp. 1427-1445.

19. Goodman, R.E., Taylor, R.L., and Brekke, T.L., "A Model for the Mechanics of Jointed Rock," J. of the Soil Mechanics Div., ASCE, SM3, 1968, pp. 637-659.

20. Ngo, D., "A Network-Topological Approach for the Finite Element Analysis of Progressive Crack Growth in Concrete Members," Ph.D. Dissertation, Div. of Structural Engineering and Structural Mechanics, University of California, Berkeley, UC-SESM 75-6, 1975.

21. Ottosen, N.S., "A Failure Criterion for Concrete," J. of the Engineering Mechanics Div., ASCE, Vol. 103, No. EM4, 1977, pp. 527-535.

22. Ottosen, N.S., "Constitutive Model for Short-Time Loading of Concrete," J. of the Engineering Mechanics Div., ASCE, Vol. 105, No. EM1, 1979, pp. 127-141.

23. Nilson, A.H., "Bond Stress-Slip Relations in Reinforced Concrete," Report No. 345, Dept. of Structural Engineering, Cornell University, 1971.

24. Fenwick, R.C., and Paulay, T., "Mechanics of Shear Resistance of Concrete Beams," J. of the Structural Div., ASCE, V. 94, No. ST10, 1968, pp. 2325-2350.

25. Everstine, G., "A Comparison of Three Resequencing Algorithms for the Reduction of Matrix Profile and Wavefront," Int. J. of Numerical Methods in Engineering, V. 14, 1979, pp. 837-853.

26. Gibbs, N.E., Poole, W.J., and Stockmeyer, P.K., "An Algorithm for Reducing the Bandwidth and Profile of a Sparse Matrix," SIAM J. of Numerical Analysis, V. 13, 1976, pp. 236-250.

27. Chang, S.C., "An Integrated Finite Element Nonlinear Shell Analyusis System with Interactive Computer Graphics," Ph.D. Dissertation, School of Civil and Environmental Engineering, Cornell University, 1981.

28. Saouma, V.E., "Finite Element Analysis of Reinforced Concrete: A Fracture Mechanics Approach," Ph.D. Disseration, School of Civil and Environmental Engineering, Cornell University, 1981.

29. Bresler, B., and Scordelis, A.C., "Shear Strength of Reiforced Concrete Beams," Structures and Materials Research Department of Civil Engineering, Series 100, Issue 13 (SESM 61-13), Institute of Engineering Research, University of California, Berkeley, 1961.

30. Bresler, B., and Scordelis, A.C., "Shear Strength of Reinforced Concrete Beams," J. of the American Concrete Institute, V. 60, No. 1, 1963, pp. 51-74.

31. Cedolin, L., and Dei Poli, S., "Finite Element Studies of Shear Critical R/C Beams," J. of the Engineering Mechanics, Div., ASCE, Vol. 103, No. EM3, 1977, pp. 395-410.

32. ----, "Building Code Requirements for Reinforced Concrete (ACI 318-77)", American Concrete Institute, Detroit, 1977.

33. Gergely, P., and Lutz, L., "Maximum Crack Width in Reinforced Concrete Flexural Members," Causes, Mechanisms and Control of Cracking in Concrete, ACI Publ. SP-20, 1968, pp. 1-17.

34. Chappell, J., "A Fracture Mechanics Investigation of the Cracking of Fontana Dam," Report No. 81-7, Dept. of Structural Engineering, Cornell University, 1981.

Nonlinear Analysis of Reinforced Concrete as a Minimization Problem, by a Finite Element Representation of the Stress Field

Analyse non-linéaire du béton armé comme problème varationnel, pour les éléments finis qui définissent le champ des contraintes.

Nichtlineare Berechnung von Stahlbeton als Minimierungsproblem, mit Finite-Elemente-Darstellung des Spannungsfeldes

GIANFRANCO VALENTE
Prof. Ing.
University of Rome
Rome, Italy

SUMMARY

In previously published papers [4], [7], [8], [9], the approach to the limit analysis of reinforced concrete bodies was formulated as a minimax problem, whose solution could be achieved by means of an appropriate algorithm based on the discretization of the structure into finite elements. This algorithm was implemented in a computer program including an incremental method, where the steps amplitude is defined by crack development. In this paper, the problems connected with the numerical performance of that procedure are taken into account. Finally, the experimental data on concrete rings for determining tensile strength of concrete obtained by Malhotra [5] are compared with numerical results of the proposed method.

RÉSUMÉ

Dans les publications précédentes [4], [7], [8], [9], l'approche des états-limites de béton armé était formulée sous forme d'un problème variationnel, dont la solution pouvait être approximée par éléments finis. La discrétisation dans le temps était definie par le développement successif des fissures. Cette publication-ci prend la performance numérique de cette procédure sous la loupe. Ensuite la méthode proposée est appliquée à la détermination de la résistance à la traction de béton non-armé. Les résultats numériques correspondent aux données expérimentales de Malhotra [5].

ZUSAMMENFASSUNG

Grenztragfähigkeitsanalyse von Stahlbeton wurde als Minimaxproblem behandelt auf der Grundlage finiter Elemente. Diese Methode wurde in ein Computerprogramm implementiert, wobei die Inkremente durch die Rissentwicklung bestimmt sind. In diesem Bericht wird die numerische Behandlung beschrieben und auf das Beispiel der Betonringzugprüfung angewandt.

1. SYMBOLS

They are as follows:

NC number of concrete nodes,
NS number of steel nodes,
NEC number of concrete elements,
NES number of steel elements,
NVS number of aligned bars couples,
KK total number of equilibrium equations,
NN number of linearly independent equations,
number of kynematic independent parameters,
LL number of static independent parameters,
MM total number of static parameters,
NF total number of failure functions.

2. INTRODUCTION

The author have developed a finite element method for finding lower bounds on the limit load for reinforced concrete with perfectly plastic steel and perfectly brittle concrete. Let the two dimensional domain R be subdivided into elements triangular for concrete and linear for steel bars.
Stress and velocity components relevant to the problem under consideration are assumed to have linear distribution within each element, and to be continuous across the elements boundaries. In this way a family of stress fields is considered, whose generic member is identified by the values that the stress components assume at the nodal points. The bound stresses between steel and concrete and the dowel effect are taken into account. Let the stress values be collected in a vector $\underset{\sim}{\sigma}$.
Vector σ has MM = 3 NC + 5 NES components
(plane stress components σ_x, σ_y and τ_{xy} for concrete nodes; normal, shear and bond stresses σ_i, σ_j, τ_i, τ_j and τ_d for steel bars).
A family of velocity fields is also considered whose generic member is identified by the values of the velocity components at the nodal point; values collected in a vector $\underset{\sim}{u}$. The total number of equilibrium equations is KK = 2 NC + NVS + NES and the dimension of vector u is NN = KK - NV.
Now a somewhat restricted equilibrium condition is imposed to the stress fields previously defined, by means of the virtual work theorem, taking as a virtual kinematic field any member of the family of velocity fields previously defined, together with the strain rate field kinematically consistent with it.
The virtual work equation may then be written as

$$\underset{\sim}{u}^T \underset{\sim}{Q}\, \underset{\sim}{\sigma} - \rho\, \underset{\sim}{u}^T \underset{\sim}{p}_2 = 0 \qquad (1)$$

The first term in Eq. (1) is the internal virtual work, $\underset{\sim}{Q}$ being the equilibrium matrix, assembled as shown in Fig. 1, depending upon the assumed stress and velocity distribution. The second and the third terms are the external virtual work due to external load p_1 and to prestressing loads $\underset{\sim}{p}_2$, ρ is the multiplier of external load $\underset{\sim}{p}_1$ alone.

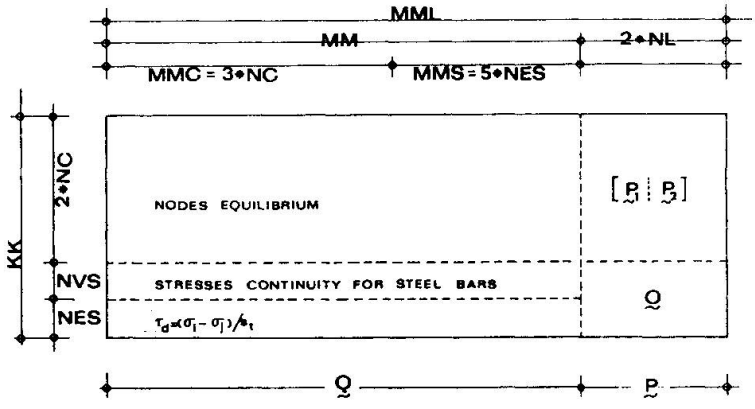

Fig. 1 - Matrix $\underset{\sim}{Q}$

Obviously, Eqs (1) are necessary, but not suffient conditions for equilibrium, because all the virtual kinematic filed have not been considered, but only a subset of them. Now let it be consider checking the yield condition (with analytical representation of concrete experimental data by Kupfer, Hlsdorf and Rüsch [3], von Mises criterium and comparison with maximum bond strength for steel)

$$f_i = \varphi_i(\rho\underset{\sim}{\sigma}) \leqslant 1, \ (i = 1, .., NF), \ (NF = NC + 3 \cdot NES) \tag{2}$$

the limit analysis problem is solved by the unconstrained minimization of the nonstrictly convex function

$$\Phi(\underset{\sim}{\sigma}^*_K) = \max_i \left[f_i(\underset{\sim}{\sigma}^*_K)\right] \quad (k = 1, .., LL) \tag{3}$$

where $\sigma^*$are the LL = MM - NN undependent parameters. The irregular function Φ is replaced by a sequence of every-where regular approximation of this function:

$$\varphi_\alpha = \left[\frac{1}{NF} \quad \Sigma_i \ \varphi_i^\alpha\right]^{1/\alpha} \tag{4}$$

In this paper, the numerical problems are examined more accurately then in previous papers [7], [8], [9].

3. EQUILIBRIUM MATRIX FOR A STEEL ELEMENT

It may be obtained by taking into account a rectangular element composite with two triangular elements. If the equilibrium matrices for triangular elements having linear distribution for stress and strain fields, and if a side of this rectangular element approaches to zero, then the equilibrium matrix for a linear element is obtained for the nodal stresses σ_i, σ_j, τ_i and τ_j.

4. FREE AND DEPENDENT PARAMETERS

The matrix $\underset{\sim}{Q}$ has zero rows, for the boundary kinematic condition, and since the problem:

$$\underset{\sim}{Q}\ \underset{\sim}{\sigma} = \rho\ \underset{\sim}{p}_1 + \underset{\sim}{p}_2 \tag{3}$$

has solutions, such general solution can be obtained in the form

$$\underset{\sim}{\sigma} = \underset{\sim}{\sigma}^*_o + \underset{\sim}{Q}^*\ \underset{\sim}{\sigma}^* \tag{4}$$

where

$$\underset{\sim}{\sigma}^*_o = \underset{\sim}{\rho}\ \sigma^*_{o2} + \underset{\sim}{\sigma}^*_{o2}$$

where $\underset{\sim}{\sigma}^*_o$ is a particular solution, $\underset{\sim}{\sigma}^*$ is linearly independent vector and $\underset{\sim}{Q}^*$ are arbitrary parameters.

The program is able to find the rank, designate the rows and the columns which provide a nonsingular square submatrix of that rank, and give the value of the determinant of that submatrix by using the Gaussian elimination process shown by Ralston [2].

When any of the divisors q_{ii} (diagonal element in Q^*_D) is small in magnitude compared with other elements q_{ij} of same matrix, then a serious round off error may be incurred.

To avoid these divisions, a technique called *positioning for size* is used. At the i-th stage of calculation (i = 1, ..., NN) it consists of the following:

- rows are interchanged to get nonzero rows in the first NN positions,
- columns are interchanged in order to locate that element q_{ii} of greatest absolute magnitude.
- then the elements in the i-th row are calculated by the so-called back substitution.
- the rows and columns interchangings are memorized in two vectors IROW and ICOL.

Finally, the matrix assembled as in Fig. 3 is obtained

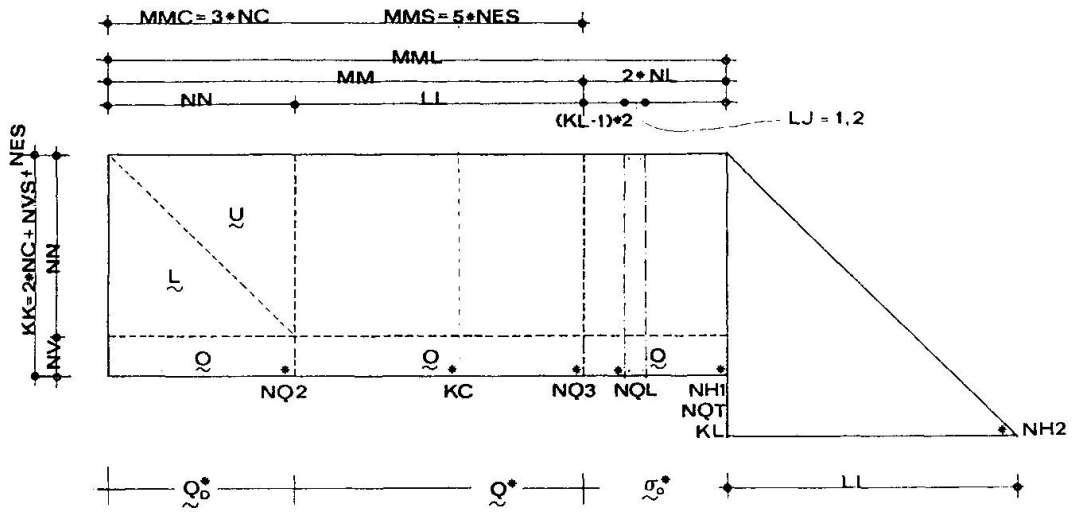

Fig. 2 - Resolutive matrix Q

where, NN is the rank of $\underset{\sim}{Q}^{*}_{D} = \underset{\sim}{L}\ \underset{\sim}{U}$ and of the dependent parameters, LL = MM - NN is the free parameters number. The triangular matrix at the right side of Fig. 3 represents the gradient coefficients for the free parameters and are computed by partial derivatives of plastic power $\Phi(\underset{\sim}{\sigma}^{*})$.

5. TESTS CHECKING

The tests (g), (i), (j) and (l) in the flow-chart of Fig. 2 are a very tiklish and important elements of the computer program.
The test (l) in the loop 1 permits to find the new cracks pattern for the stresses field which minimizes the plastic power Φ.
Let the following terms be considered:

$$\varepsilon_1 = | 1 - \varphi_{max} |, \quad \varphi_{max} = \max_i \varphi_i \ (i = 1, \ldots, NC) \tag{6}$$

$$\varepsilon_2 = | 1 - \varphi^{+} | \tag{7}$$

$$\varepsilon = \max (\varepsilon_1, \varepsilon_2) \tag{8}$$

where φ^{+} is the maximum value of function φ computed between the not cracked nodes with positive value of the first principal stress.
To take into account the value ε_2 is very important because only the cracking in the nodes subjected to tension may produce substantial variation of the stress

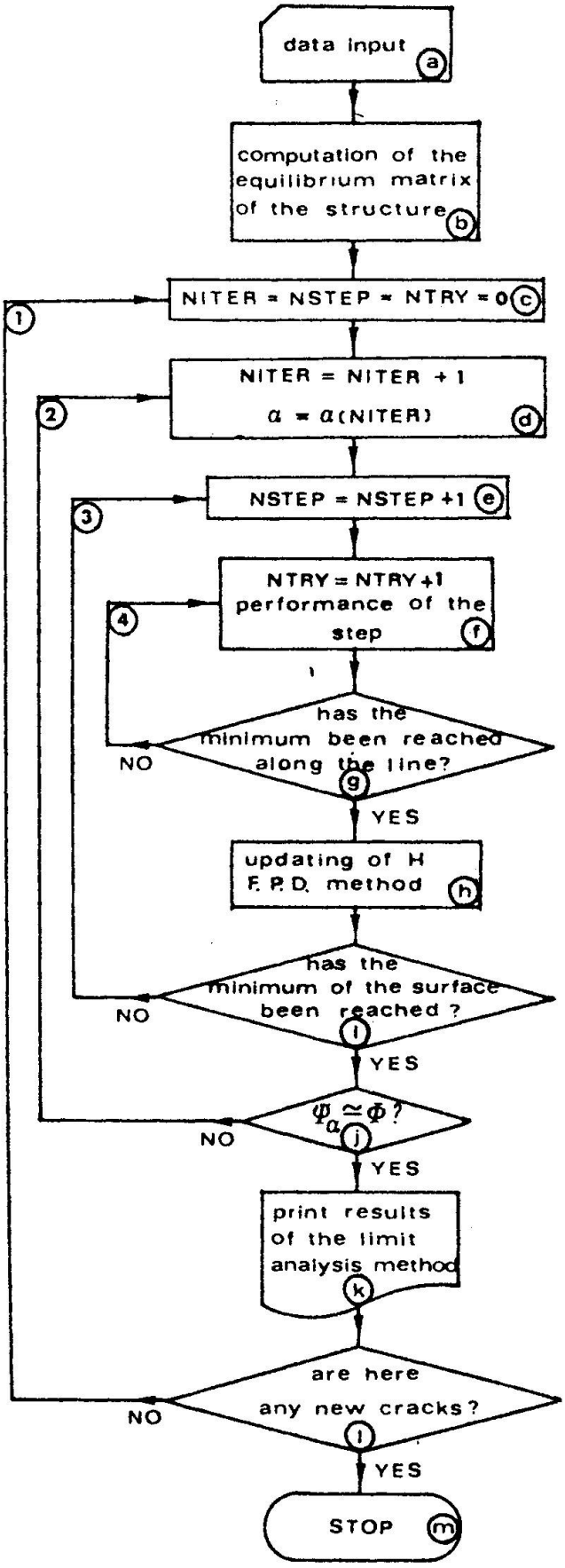

FIG. 3. - Flow-chart of the process; cycles ② , ③ and ④ constitute logical outline of limit analysis by nonlinear programming

field.
From a computational viewpoint, a new crack in a node produces a reduction of the failure domain only in the tension-tension or tension-compression zones. Then, if the point of the stress state was in this zone in the neigh-bouring of the yield line, after the cracking it will shift brusquely causing a substantial change in the whole stress field for the equilibrium of the same.
The value ε is used to calculate the following prescribed small positive value $\bar{\varepsilon}$ depending on the ratio between the two principal stresses

$$\bar{\varepsilon} = c_1 \varepsilon, \qquad \text{for } (\sigma_2 + 3\sigma_1) \leqslant 0 \tag{9}$$

$$\bar{\varepsilon} = c_2 + \frac{c_2 - c_1}{3} \frac{\sigma_2}{\sigma_1} \varepsilon, \qquad \text{for } \sigma_2 > 0,\ \sigma_2 \leqslant 0 \tag{10}$$

$$\bar{\varepsilon} = c_2 \varepsilon \qquad \text{for } \sigma_1,\ \sigma_2 \geqslant 0 \tag{11}$$

A node will became cracked if it is:

$$\varphi \geqslant 1 - \bar{\varepsilon} \tag{12}$$

It agrees to assume for c_1, c_2 the following values

$$c_1 = 1{,}5 \div 2{,}0\ ; \qquad c_2 = 3 \div 6 \tag{13}$$

In such a way, the biaxial tension stress states are penalized greatly than the biaxial compression stress states with linear interpolation for middle states. Smaller values will be selected for c_1 and c_2 parameters if it is deemed to follow the cracking phenomenon with greater accurancy; obviously, this behaves much more steps in the evolutive process.
The process is illustrated in the following Fig. 4

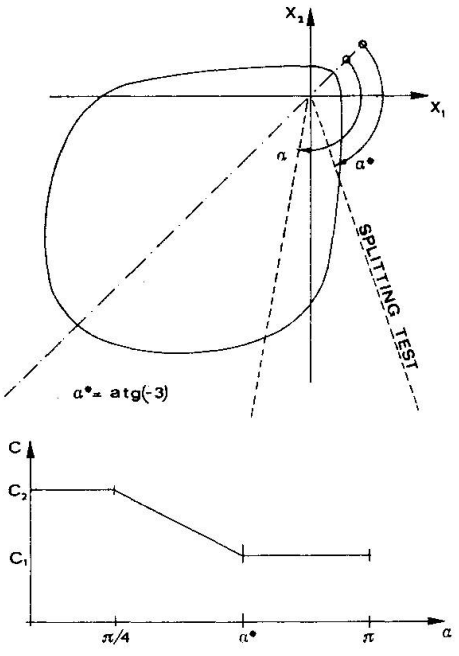

Fig. 4 - Computation of the parameter c (σ_1, σ_2)

The test (h) for the loop 2 checks that two surface ψ_α and Φ are enough close between themselves. When the minimum on the surface ψ_α has been ottained, the collapse multiplier for the node i-th having $\varphi_{max} = \max \varphi_k$ (K = 1, .., NC) is computed. The failure function is a fourth order polinominial and the condition:

$$\varphi_i \ (\rho_i \ \sigma) = 1 \qquad (14)$$

leads to four roots. Related to the Fig. 5 two kind of solution are possible:
- for the stress state represented by the point A, four real roots are obtained,
- for the stress state B, two real roots and two complex roots are obtained;
the true solution is the smaller real positive root (like points A_2 and B_1).

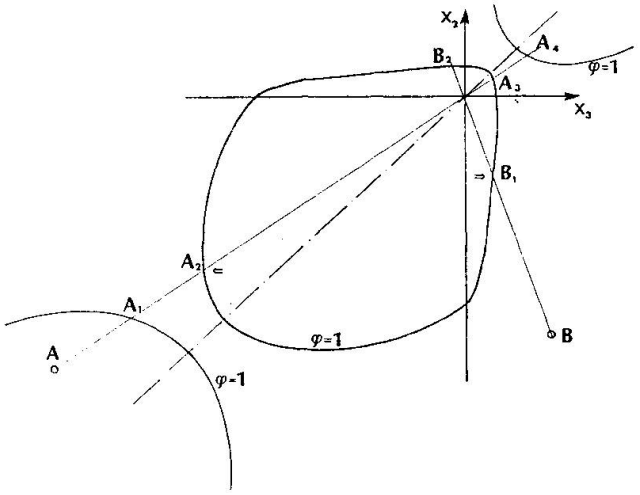

Fig. 5 - Solution of the fourth order polinomial

The error on this value of ρ_α is computed by the aim of the following Fig. 6.

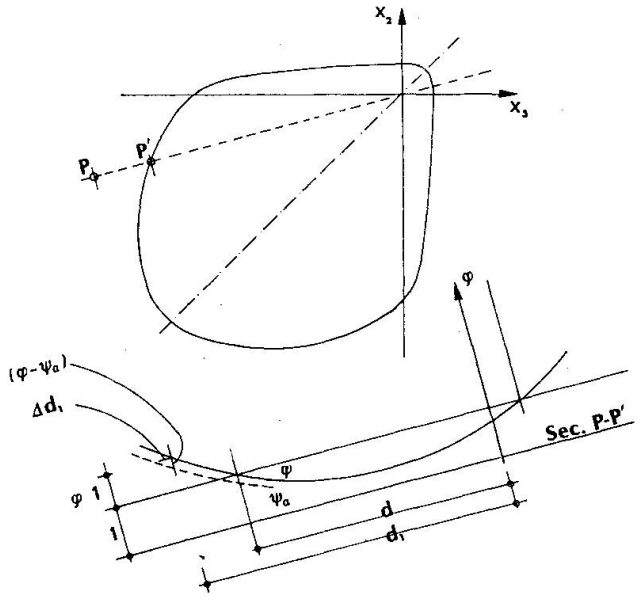

Fig. 6 - Error on the collapse multiplier computation

This error is deduced by the following relationships:

$$\rho_\alpha = \frac{d}{d_1} \quad f(d_i) \tag{15}$$

$$\Delta\rho_\alpha = \frac{df}{dd_1} \quad \Delta d_1 = \frac{d}{d_1^2} \quad \Delta d_1 \tag{16}$$

$$\Delta d_1 = (\varphi - \psi_\alpha) \ (d_1 - d)/(\varphi - 1) \tag{17}$$

$$\Delta\rho_\alpha = \rho_\alpha \ (\varphi - \psi_\alpha) \ (1 - \rho_\alpha)/(\varphi - 1) \tag{18}$$

The test (h) consists in the checking:

$$\Delta\rho_\alpha/\rho_\alpha \leqslant \varepsilon_{tol} \tag{19}$$

Where ε_{tol} is a prescribed small positive quantity. The test (i) in the loop 3 checks that the minimum position of the surface ψ_α has been ottained, this happen when between the initial and final values ψ_o, ψ_1 is

$$2 \ (\psi_o - \psi_1)/(\psi_o + \psi_1) \leqslant s_{lim} \tag{20}$$

This condition, in spite of its simplicity, displays itself to like better than other more complex, like gradient modulus.
The test (g) in the loop 4 checks that the minimum of the line has been attained; it is admitted that this test is satisfied when a value ψ_α less then all the preceding values on the line is obtained. The loops 2 , 3 and 4 are better shown by the paper of Fletcher and Powell [1]
The value S_{lim} is a prescribed small quantity; for $\varepsilon_{tol} = 10^{-2} \div 10^{-3}$, the better computational value was:

$$S_{lim} = 10^{-6} \div 10^{-7} \tag{21}$$

6. RUNNING TIME FOR THE EVOLUTIVE PROCESS

This computer time necessary to the program running may be subdivided into three parts:
- data memorization,
- computation of equilibrium and non singular matrices $\underset{\sim}{Q}$ and $[\, Q_D^* \quad Q^* \ \sigma_o^* \,]$ respectively
- minimization times for each step.

The first two computer times represent a derisive part of the total time, then the third part is the more important time.
In the following Fig. 7 the computer times for a single minimization in absence of cracked nodes is represented.
This time is placed near the relationship:

$$t = 10^{-2} \ (1 + 75 \ \alpha) \ LL \quad NC \tag{22}$$

where $\varepsilon_{tol} = 10^{-\alpha}$ is the prescribed small value for ρ_α in the minimization.
If cracked node exist, and if NCl is the number of the nodes having the tensile first principal stress before the cracking, the minimization time is greather

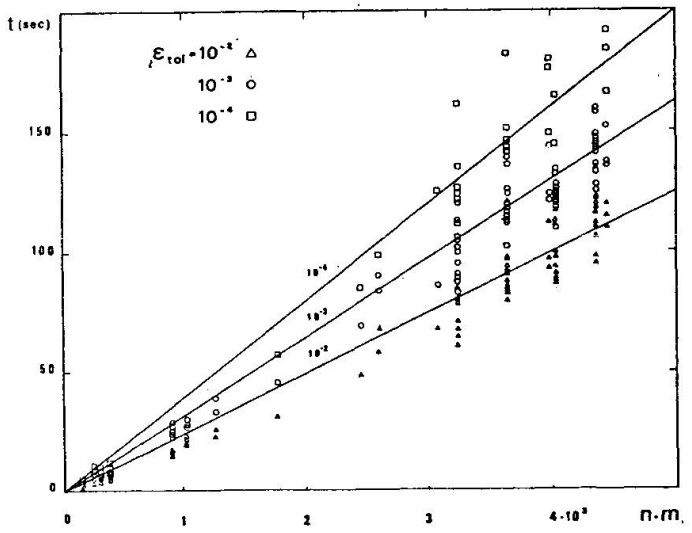

Fig. 7 - Minimization time in absence of cracked nodes.

then the aforementioned time according to the relationship:

$$t = 10^{-2}(1. + .75\ \alpha)\ LL\ \ NC(1. + 3.5\ NC1/NC) \qquad (23)$$

These relationships are obtained:

- by the numerous computer solutions of analogous problems for bodies with material according to Von Mises yield criterium,
- by the numerical solution of the famous beam tested by Bresler and Scordelis and of the concrete ring specimen numerical solved.

These computer times are related to UNIVAC 1100.

7. STORAGE USED

By the aforementioned notations this computer storage is defined by the following relationship:

$$55 \cdot NC + 4 \cdot NEC + 37 \cdot NES + 5 \cdot LL + 22 \cdot NL + 8 \cdot NC \cdot NL + (2 \cdot NC + 2 \cdot NS)\ (3 \cdot NC + 4 \cdot NES + 2 \cdot NL) + LL^2/2 + 2 \cdot NF + 20.000 \qquad (22)$$

8. NUMERICAL EXAMPLE

In the Malhota paper [5] regression analysis were carried out to establish correlation between inside diameter ring tensile strength and 4x8 in. (10x20 cm) cy-

linder compressive strength. All the reported data had been carried out using two kind of specimens like in following Table 1:

Table 1 - Ring specimens data

Specimen N.	Inside diameter	high	wide	P_{iu}	σ_t	ε
1	6 in (15cm)	1½ in. (3.8cm)	1½ in (3.8cm)	21.040	54.704	9.408
2	12 in (30cm)	3 in (7.5cm)	3 in (7.5cm)	20.960	54.496	8.992
				kg/cm^2	kg/cm^2	%

The Author found the following relationship:

$$Y = .063X + 17.5 \text{ kg/cm}^2$$

where Y and X are the inside diameter ring tensile strength and the cilinder compressive strength, respectively. Besides this the Author says that the tensile stresses in the ring section vary linearly from a maximum of 2.6 P_i at the internal periphery to 1.6 P_i at the outside periphery, where P_i is the applyed hydrostatic pressure.

In the subsequent discussion, Pandit [6] says that none of the existing methods for the determination of the tensile strength of concrete campare favorably as regard reproducibility or reliability with the compression test.

The aforementioned specimens have been represented by the finite element mesh in the following Fig. 8.

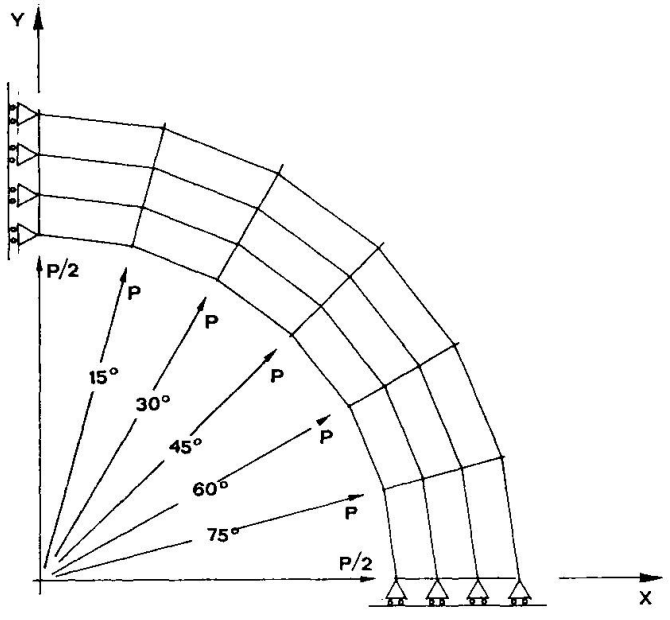

Fig. 8 - Finite element mesh

For these specimens the tensile and compressive strengths were 50. and 500. kg/cm^2 respectively and the ultimate hydrostatic pressures were those shown in Table 1. By admitting that the maximum tensile stress in the ring section is 2.6 P_{iu} at the inside periphery, there is the tensile stresses in the Table 1.

REFERENCES

1. FLETCHER, R. - POWELL, M.J.D.: "A rapidly convergent descent method for minimization", computer Jrn., Vol. 6, 1963.

2. RALSTON, A.: "A first course in numerical analysis", Mc Graw Hill, New York 1965, Chapter 9 § 3.

3. KUPFER, H. - HILSDORF, H. - RÜSCH, H: "Behavior of concrete under biaxial stresses,", Proceedings ACI, Vol. 66, August 1969.

4. CASCIARO, R. - DI CARLO, A. - VALENTE, G.: Discussion on "Plane stress limit analysis by finite elements" by T. Belytschko and P. Hodge jr., Dec. 1970, Proc. ASCE, EM5 1971.

5. MALHOTRA, V.M.: "Concrete rings for determining tensile strength of concrete", ACI jrn., april 1970.

6. PANDIT, G.S. - Discussion of paper [4], ACI jrn., october 1970.

7. VALENTE, G.: "Nonlinear analysis of reinforced concrete by finite elements", Istituto di Scienza delle Costruzioni, Facoltà di Ingegneria, ROMA, paer n. II-185, November 1976.

8. VALENTE, G.: "Nonlinear analysis of prestressed reactor pressure vessels", 4th SMiRT Conference, San Francisco, California, U.S.A., August 1977.

9. VALENTE, G.: "Ultimate criteria of concrete under bi-axial loading", 5th SMiRT Conference, Berlin, Germany, August 1979.

Biaxially Loaded Slender Reinforced Conrete Columns

Colonnes en béton armé élancées et chargées d'une façon biaxiale

Schlanke Stahlbetonstützen unter doppelter Biegung

DR. KULDEEP S. VIRDI
Lecturer in Civil Engineering
The City University
Londen, United Kingdom

SUMMARY

The paper describes an analytical method for the calculation of the "exact" ultimate load of a reinforced concrete column under conditions of biaxial bending. Nonlinear material properties, both for concrete and steel, are assumed. The analysis aims at monitoring the load versus deflection response of the column up to collapse. At each stage of loading the equilibrium deflected shape is calculated, using the second order Newton Raphson method. The moment thrust curvature relations required in the process are computed using Gauss quadrature, resulting in very rapid calculations. The question of accuracy of the method is discussed. The method is shown to give good agreement with test results from two previously reported papers.

RÉSUMÉ

Cette publication décrit une méthode analytique de calcul "exact" de la charge ultime d'une colonne en béton armé soumise à la flexion biaxiale. Propriétés non-linéaires du béton et de l'acier sont pris en considération. L'analyse vise à simuler le comportement de la colonne jusqu'à la rupture. Après chaque étage du chargement, la flexion de la colonne est calculée par la méthode Newton-Raphson du second ordre. Les relations entre flexion composée et courbure ont été programmées par la méthode des quadratures de Gauss, ce qui permet un calcul très rapide. La précision de la méthode est discutée. Les résultats numériques correspondent aux données expérimentales de deux recherches précédentes.

ZUSAMMENFASSUNG

Der Beitrag beschreibt eine analytische Methode zur Berechnung von Stahlbetonstützen unter doppelter Biegung, wobei nichtlineares Verhalten von Beton und Stahl berücksichtigt werden. Mithilfe der Newton-Raphson-Methode zweiter Ordnung wird die Gleichgewichtslage unter jedem Belastungsschnitt berechnet. Die Methode ziegt ausgezeichnete Übereinstimmung mit Versuchsergebnisse.

INTRODUCTION

The problem considered in this paper is that of a reinforced concrete beam-column with biaxial end restraints which may be dissimilar at the two ends of the column. It is assumed that the cross section is rectangular. Longitudinal reinforcement is represented as notionally concentrated point areas. Complete flexibility in the choice of material stress-strain characteristics is allowed. Warping and torsional effects are, however, not considered. Proportional or non-proportional loading paths can be specified.

A solution to the problem can be based on the notion that the ultimate load of a column corresponds to that level of loading for which the column stiffness in terms of its capacity to sustain additional loads is reduced to zero. The column stiffness is not calculated explicitly. Instead, the column deflected shape in equilibrium with the applied loading is calculated for increasing levels of applied loading, starting with a sufficiently low level. As expected, the rate of change of deflections with respect to the changes in loading increases with increasing levels of the applied loading. Eventually, for a load level higher than the ultimate load of the column, no equilibrium deflected shape is obtainable. Thus, the calculations are aimed at determining the ultimate load as the highest load for which an equilibrium deflected shape can be obtained.

When considering material and geometric nonlinearities, the determination of the deflected shape of the column in equilibrium with the external loading requires the solution of two separate subproblems.

First, an algorithm has to be selected to relate the curvatures in the column to the internal stress resultants. This forms the moment thrust curvature relationship for the cross section and its material properties. The inclusion of arbitrary nonlinear material stress strain characteristics renders the moment thrust curvature relationships unobtainable in the form of simple formulae. Inevitably, a numerical procedure has to be adopted. One commonly used algorithm, adopted by several investigators [1,5,14], with minor variations, is based on the subdivision of the cross section into a grid of sufficiently small areas, followed by the calculation of strains and stresses at the centroids of these areas, and finally the direct summation of forces and moments so obtained. It has been found that such an algorithm employs about two-thirds to three-quarters of the total time required for a complete analysis of a given column. It is clear that any technique aimed at reducing the computation time required for the moment thrust curvature relationship will lead to savings in the overall computational effort. Description of one such rapid algorithm forms a main part of this paper.

The second subproblem relates to the determination of the deflected shape satisfying the condition that the internal stress resultants at any point have to be in equilibrium with the external loading. Here, two types of approach can be adopted. The first is an integration type approach, and resembles the well known Newmark's method [8] for elastic beam columns. The second is based on finite differences, and is aimed at arriving at the values of the deflections at discrete points along the length of the column by some sort of iteration. Other options available for example, to use a first order iteration with Aitken's or some other type of accelerator for convergence, or to use a second order Newton Raphson type iteration. The author has found that, providing that at any stage of the computation process use is made of the results obtained thus far, the Newton Raphson iteration is very rapid and it is this method which is described later in the paper.

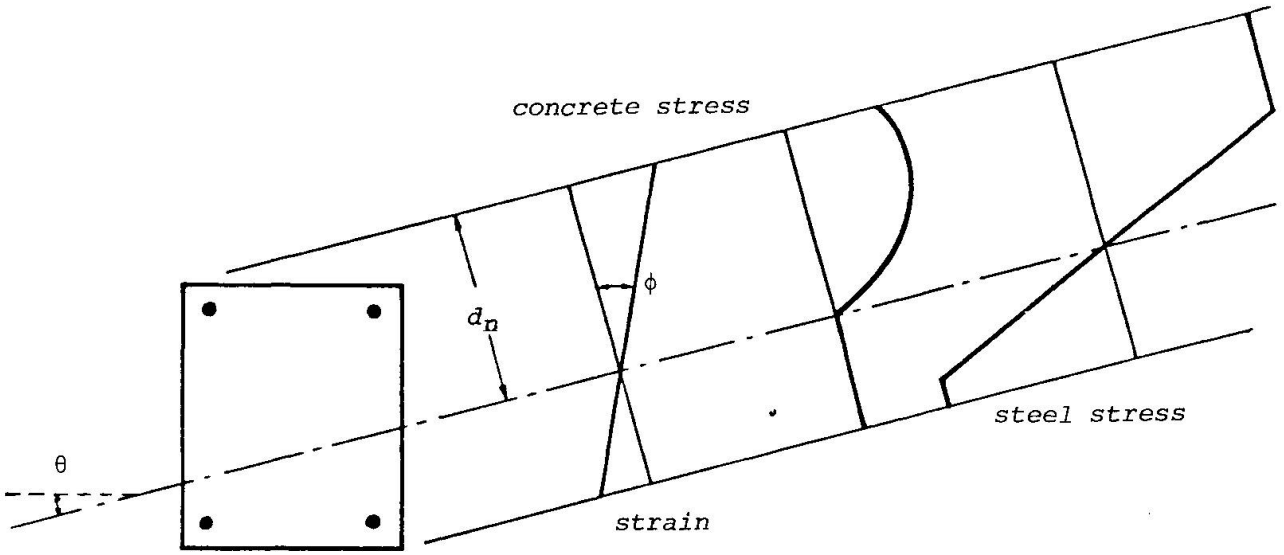

FIGURE 1 - Strain and Stress Distribution under Biaxial Curvatures

MOMENT THRUST CURVATURE RELATIONS

Where torsion and warping of the cross section are ignored, as in the present study, the biaxial moment thrust curvature relations involve six quantities: axial thrust P, biaxial moments M_x and M_y, biaxial curvatures ϕ_x and ϕ_y, and a sixth parameter required to establish the strain distribution, and hence the stress distribution, at a cross section uniquely. A convenient choice for the sixth variable becomes the distance d_n of the neutral axis from a predetermined point in the cross section, for example from the most highly stressed corner (Figure 1). Assuming that plane sections before bending remain plane after bending, the two biaxial curvatures can be compounded to yield the total curvature ϕ and the direction of the neutral axis θ:

$$\phi = (\phi_x^2 + \phi_y^2)^{\frac{1}{2}} \tag{1}$$

$$\theta = \tan^{-1}(\phi_y/\phi_x) \tag{2}$$

With the strain distribution in the cross section thus established, the strain at the centroid of a small area dA can be obtained and that, in turn, can be used to calculate the stress σ acting on the elemental area from the stress strain characteristic, which may be nonlinear, for the material concerned. The three stress resultants are then given by:

$$P = \int_A \sigma dA \tag{3}$$

$$M_x = \int_A \sigma x dA \tag{4}$$

$$M_y = \int_A \sigma y dA \tag{5}$$

These equations, together, represent the moment thrust curvature relations. In general, by assigning known values to any three of the six unknowns the other three can be evaluated uniquely. In the present analysis, at each stage in the determination of the deflected shape of the column by the method to be outlined later, the curvatures ϕ_x and ϕ_y, and the applied thrust P are regarded as the

independent variables. The problem is thus reduced to varying d_n in such a manner so as to yield the correct thrust P. The biaxial moments M_x and M_y are then available as by-products of the above process. The author has found that Newton's iteration technique is very efficient in this regard.

Whatever be the technique adopted for carrying out the iteration between d_n and P, the most important step involved remains the evaluation of the three integrals in Equations (3)-(5). Referring to the typical reinforced concrete column cross section shown in Figure 1, it is plain that a closed form solution is not easy, if not impossible, especially when arbitrary nonlinear material stress-strain characteristics are involved.

USE OF GAUSS QUADRATURE

According to the Gauss quadrature formulae, a definite integral between the limits -1 and +1 can be replaced by a weighted sum of the values of the integrand at certain specified points:

$$\int_{-1}^{1} f(\xi)d\xi = \sum_{i=1}^{m} H_i f(\xi_i) \qquad (6)$$

where H_i are the weighting coefficients and $\xi = \xi_i$ are the specified Gauss points. The integration is exact if $f(\xi)$ is a polynomial of degree up to $(2m-1)$. Values of ξ_i and H_i are available [6,16] in tabular form for values from 2 to 16.

A double integral can be replaced by a double summation as follows:

$$\int_{-1}^{1}\int_{-1}^{1} f(\xi,\eta)d\xi d\eta = \sum_{i=1}^{m}\sum_{j=i}^{m} H_i H_j f(\xi_i,\eta_j) \qquad (7)$$

The square area implied by the limits -1 and +1 in the two directions can be successfully mapped on to a quadrilateral area (Figure 2) by the following transformations using the so-called natural co-ordinates (ξ,η):

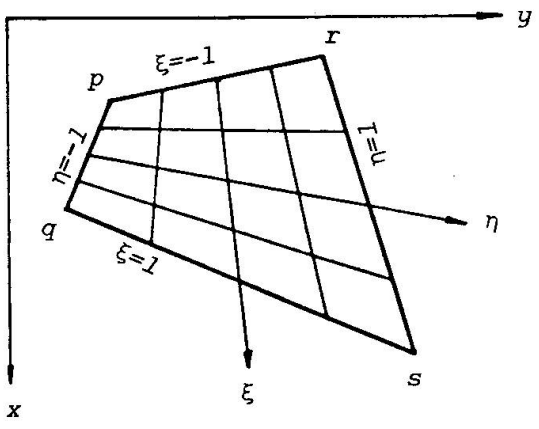

FIGURE 2 - Natural Co-ordinate System for a Quadrilateral

$$x = \frac{1}{4}\left[(1-\xi)(1-\eta)x_p + (1+\xi)(1-\eta)x_q + (1-\xi)(1+\eta)x_r + (1+\xi)(1+\eta)x_s\right] \quad (8)$$

$$y = \frac{1}{4}\left[(1-\xi)(1-\eta)y_p + (1+\xi)(1-\eta)y_q + (1-\xi)(1+\eta)y_r + (1+\xi)(1+\eta)y_s\right] \quad (9)$$

where (x_p, y_p), (x_q, y_q), (x_r, y_r), and (x_s, y_s) are the co-ordinates of the points p, q, r, and s, respectively.

The elemental area $dxdy$ in the cartesian co-ordinates is related to the area $d\xi d\eta$ in the natural co-ordinate system through the relation:

$$dxdy = |J|\, d\xi d\eta \quad (10)$$

where $|J|$ represents the determinant of the Jacobian matrix:

$$[J] = \frac{1}{4}\begin{bmatrix} -(1-\eta) & (1-\eta) & -(1+\eta) & (1+\eta) \\ -(1-\xi) & -(1+\xi) & (1-\xi) & (1+\xi) \end{bmatrix}\begin{bmatrix} x_p & y_p \\ x_q & y_q \\ x_r & y_r \\ x_s & y_s \end{bmatrix} \quad (11)$$

MOMENT THRUST CURVATURE RELATIONS USING GAUSS QUADRATURE

There are several alternative ways by which the Gauss quadrature formulae can be applied to obtain the integrals in Equations (3)-(5). Description of one such method was given in an earlier paper [11], in which a rectangular area was first subdivided into trapezoidal or triangular areas by lines parallel to the neutral axis and coinciding either with the corners of the rectangle or with any points marking a deviation in the material stress strain curve. The method had the merit of generality in its application to a variety of cross sections with material stress strain characteristics in the form of linear or curved segments. The following method, though perhaps slightly less accurate than the method given in Reference [11], is simpler to program and is considerably faster for an equal number of Gauss points chosen in the analysis. As indiated earlier, accuracy can always be improved by increasing the number of Gauss points used in a given problem, and in this connection some guidance is given later in the paper.

COMPUTATION PROCEDURE

In the context of reinforced concrete column sections, it is assumed that the integration is being carried over a rectangular area and the longitudinal reinforcing bars are considered as point area. The steel stress values obtained for these point areas are adjusted for the area of concrete replaced by the steel bars.

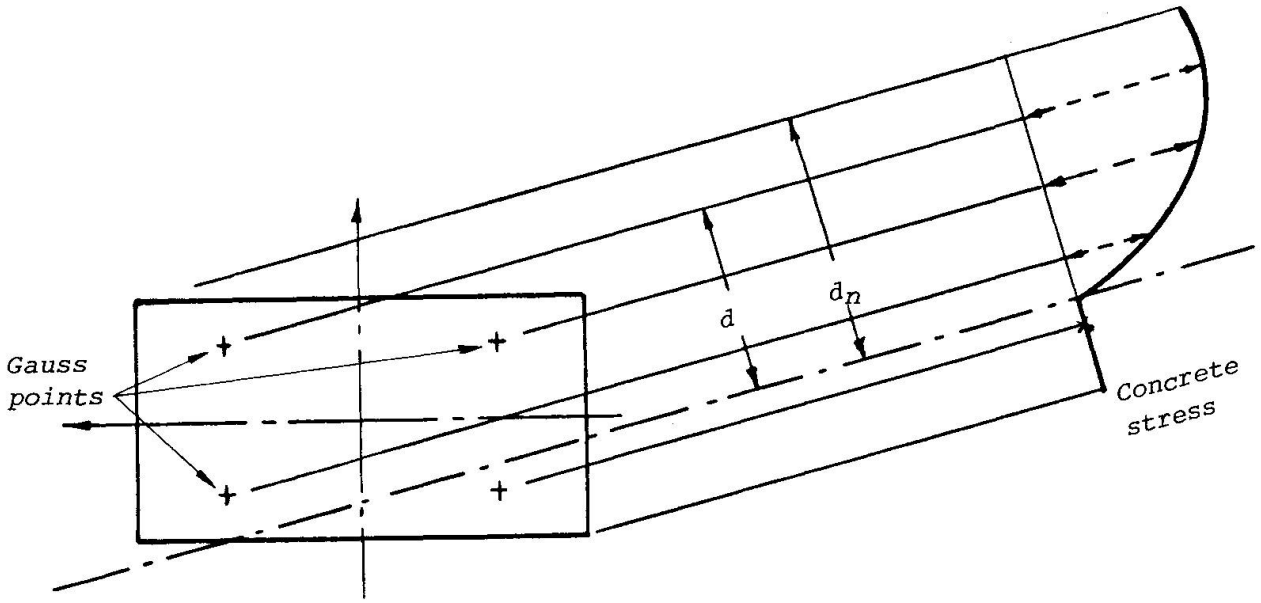

FIGURE 3 - Stress at Gauss Points

Assuming that ϕ and θ (or ϕ_x and ϕ_x) are known, the integration for a given value of d_n can be carried out as follows:

Step 1. For each Gauss point (Figure 3), repeat Steps 2-7.

Step 2. Determine the cartesian coordinates of the Gauss point from the predetermined natural coordinates using Equations (8) and (9).

Step 3. From the coordinates obtained, calculate the distance d from the neutral axis.

Step 4. Calculate the imposed strain ($\varepsilon = \phi d$) at the Gauss point.

Step 5. Using the material stress strain curve, calculate the stress at the Gauss point.

Step 6. Evaluate the Jacobian $|J|$ at the Gauss point using Equation (11).

Step 7. Obtain the summations implied by the Equations (7) and (3)-(5).

Step 8. As in Step 4, calculate the strain at the centroid of each of the reinforcing bars.

Step 9. From the material stress strain characteristics, calculate the steel stress and then the concrete stress, and hence the net stress for each reinforcing bar.

Step 10. Augment the summations obtained in Step 7 appropriately.

It is worth noting that at a given cross section, in Step 6, once the number of Gauss points is fixed, the value of the Jacobian $|J|$ and hence of the product $|J|H_iH_j$ needs to be evaluated only once for each Gauss point, thus offering additional savings in computational effort.

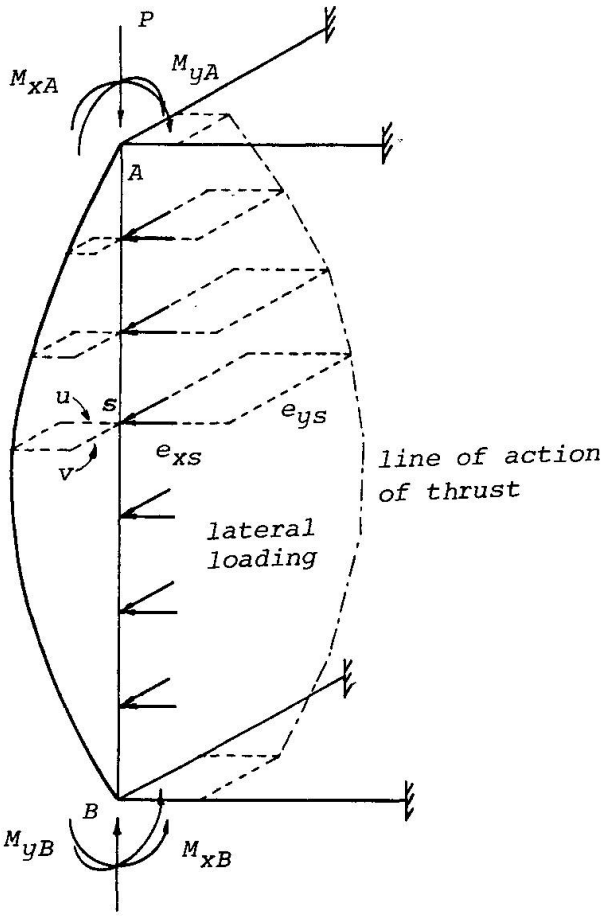

FIGURE 4 - Sign Convention for a Biaxially Loaded Restrained Column

DETERMINATION OF THE EQUILIBRIUM DEFLECTED SHAPE

Figure 4 shows the deflected shape of a beam column with generalised end conditions under generalised end loading together with some lateral loads. The deflections at the top and bottom of the column are assumed to be zero. Implicitly the following analysis is restricted to columns with ends which are not allowed to translate, but can rotate subject to the beam restraints. Thus columns suject to sway are not covered. under the initial conditions, the column initial deflected shape is assumed to be in equilibrium.

At any stage of loading, the column undergoes additional deflections, and hence end rotations. The end rotations induce moments in an opposite sense to the directions of the rotations. After allowing for the corrections to the applied end moments, the column deflected shape can be thought of as being in equilibrium with an eccentrically located thrust which has a variable line of action, as shown in Figure 4. This line of thrust would follow the notional bending moment diagrams in the two bending planes, due to the applied loading but corrected for the restraining end moments. In the absence of any lateral loads, the effective line of thrust would be a straight line passing through the effective end eccentricities at the two ends. The solution to the problem requires that the internal stress resultants induced by the biaxial curvatures in the column be balanced at each point along the length of the column by the applied thrust acting at a total biaxial eccentricity, obtained by summing the deflections and the deviations of the line of action of the thrust with respect to the column axis in both the bending planes.

BASIC RELATIONSHIPS

The biaxial curvatures at any point along the column length can be approximated by:

$$\phi_{tx} = -\partial^2 u/\partial x^2 \quad (12)$$

$$\phi_{ty} = -\partial^2 v/\partial y^2 \quad (13)$$

where, u and v are the total deflections in the two bending planes. If u_o and v_o are the initial deflections, the initial curvatures can be similarly expressed by:

$$\phi_{ox} = -\partial^2 u_o/\partial x^2 \quad (14)$$

$$\phi_{oy} = -\partial^2 v_o/\partial y^2 \quad (15)$$

The net curvatures are obtained by subtracting the initial curvatures from the total curvatures:

$$\phi_x = \phi_{tx} - \phi_{ox} \quad (16)$$

$$\phi_y = \phi_{ty} - \phi_{oy} \quad (17)$$

The internal stress resultants induced by the net curvatures can be obtained at all points in the column by knowing the values of these curvatures from the moment thrust curvature relations adopting the procedure outlined earlier. Let M_x and M_y be the bending moment stress resultants so obtained. For equilibrium:

$$u = (M_x/P) - e_x \quad (18)$$

$$v = (M_y/P) - e_y \quad (19)$$

where e_x and e_y are the biaxial eccentricities of the effective line of action of the thrust P for the particular column cross section measured with respect to the originally straight column axis.

Recognising that M_x and M_y are nonlinear functions of u and v, the solution to the problem now requires a simultaneous solution of Equations (18) and (19) at all points along the column length.

The column length is subdivided into n equal parts, each of length h. The resulting nodes are labelled $1,2,\ldots,(n+1)$. The equilibrium is then satisfied at the $(n-1)$ internal nodes only. Clearly, the larger the value of n, the more accurate the solution obtained will be.

At each station, the biaxial curvatures can be calculated by adopting the finite difference approximations:

$$\phi_{sx} = -(u_{s-1} + 2u_s - u_{s+1})/h^2 \quad (20)$$

$$\phi_{sy} = -(v_{s-1} + 2v_s - v_{s+1})/h^2 \quad (21)$$

Keeping in mind the implied moment thrust curvature relations, Equations (18) and (19) may now be stated thus:

$$u_s = U(u_{s-1}, v_{s-1}, u_s, v_s, u_{s+1}, v_{s+1}) \quad (22)$$

$$v_s = V(u_{s-1}, v_{s-1}, u_s, v_s, u_{s+1}, v_{s+1}) \quad (23)$$

or, even more generally as:

$$\{w\} = \{W(w_1, w_2, \ldots\ldots w_{2n-1}, w_{2n})\} \tag{24}$$

where, $w_{2s-1} = u_s$ and $w_{2s} = v_s$. The solution to nonlinear problems of the type expressed by Equation (24) can be obtained by the Newton Raphson method. The method states that if $\{w^k\}$ represents an approximate solution to Equation (24), a better approximation $\{w^{k+1}\}$ can be obtained by the following equation:

$$\{w^{k+1}\} = \{w^k\} - [I - K]^{-1} \{w^k - W(w^k)\} \tag{25}$$

In Equation (25), $[I]$ is an identity matrix and $[K]$ is a Jacobian matrix, the elements of which are:

$$K_{ij} = \frac{\partial W_i}{\partial w_j} = \frac{\Delta W_i}{\Delta w_j} \tag{26}$$

The elemental definition is of more relevance where the derivatives have to be calculated numerically, as in the present case. For the next iteration, $\{w^k\}$ is replaced by $\{w^{k+1}\}$, and the process is repeated until satisfactory convergence has been obtained.

An inspection of Equations (22) and (23) would reveal that, at each node s, the evaluation of the Jacobian matrix requires one basic and 6 incremental computations of the moment thrust curvature relations. However, by keeping Δu numerically the same at all stations, and noting that

$$\frac{\Delta\phi_{sx}}{\Delta u_{s-1}} = \frac{\Delta\phi_{sx}}{\Delta u_{s+1}} = -2\,\frac{\Delta\phi_{sx}}{\Delta u_s} \tag{27}$$

and similar other relationships, the entire procedure can be reduced to one basic and only two incremental computations of the moment thrust curvature relations at each node. Clearly, this simple device reduces the computation time required by more than half.

In the absence of any end restraints, the Jacobian matrix in Equation (25) will be a banded matrix. However, when end restraints are present, a change in displacements near the column ends would alter the end slope and hence the restraining moments at the ends, and this in turn would alter the computed displacements $\{W\}$ at all stations. In this case the Jacobian matrix would no longer be banded. If, for example, a difference formula of the type

$$\psi_{1x} = (4w_3 - w_5)/2h \tag{28}$$

is used to calculate the end slopes, it is clear that the derivatives with respect to the eight end deflection components involved would have to be evaluated. Once again, by noting that

$$\frac{\partial\psi_{1x}}{\partial w_5} = -\frac{1}{4}\,\frac{\partial\psi_{1x}}{\Delta w_3} = \frac{1}{2h} \tag{29}$$

and similar other equations related to the end deflections involved, it is possible to calculate elements of the Jacobian $[K]$ influenced by end restraint effects, without having to do any further moment thrust curvature calculations.

Because of the incremental nature of the computations involved, the end restraint characteristic does not have to be perfectly elastic. Nonlinear moment rotation curves for the end restraints can be handled with no penalty on the efficiency of the procedure. The procedure has been described in considerable detail in Reference [13].

STABILITY ANALYSIS

The procedure described above for the determination of the deflected shape of the column can be applied, in general, for the nonlinear analysis of any structure subjected to a given loading. Stability analysis further requires that the deflection response of the structure be monitored for increasing loads until, at some stage, equilibrium is no longer possible. Thus, if α is defined as a load fator on the initial loading $\{F_o\}$, the structure is analysed for varying loads $\{F_\alpha\}$, given by:

$$\{F_\alpha\} = ((\alpha-1)[G] + [I])\ \{F_o\} \qquad (30)$$

in which $[I]$ is an identity matrix and $[G]$ is a diagonal matrix, the elements of which are either 1 or 0, depending upon whether the corresponding load component varies with α or not. The highest value of α so obtained would be the load factor corresponding to the ultimate limit state of collapse. In the case of the biaxially loaded column the vector $\{F_\alpha\}$ consists of five components namely, the applied thrust and the biaxial moments at the two ends.

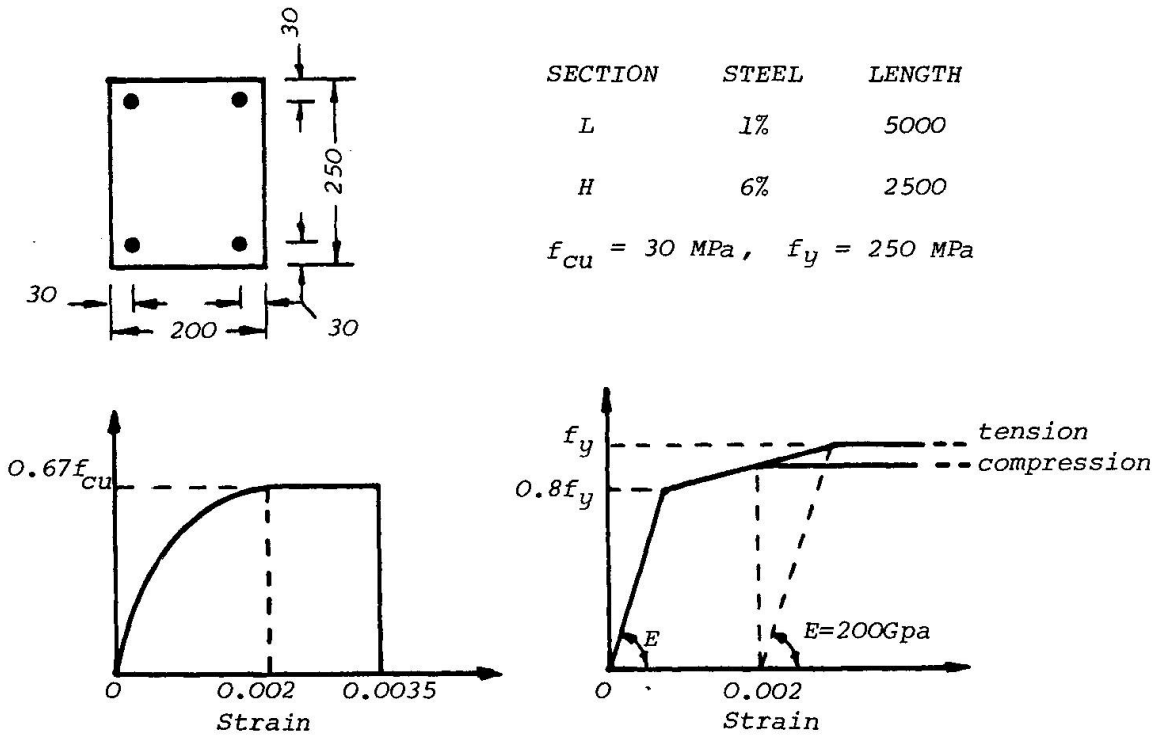

FIGURE 5 - Basic Data for Columns Referred in Table 1

ACCURACY OF THE PROPOSED METHOD

The method outlined above has been used to calculate the failure loads of columns of two cross sections shown in Figure 5. The percentage of steel in the two sections was 1% and 6% respectively. The material properties for both cases were the same. For steel a trilinear stress strain characteristic in line with the recommendations in CP110 [2] was chosen with a characteristic yield stress of 250 MPa and a Young's modulus of 200 GPa. For concrete, a parabolic rectangular characteristic in line with the CEB-FIP recommendations [3] was chosen with a characteristic strength of 30 MPa, a peak strain of 0.002, and a crushing strain of 0.0035. For the column with 1% steel, a column length of 5000 mm was chosen, whereas for the other section a stockier length of 2500 mm was adopted. The columns were assumed to be loaded with equal eccentricities of magnitudes 50 mm and 100 mm respectively, at both ends in the plane of the major axis. Both columns were assumed to have an out of plane initial deflection of magnitude 0.001 time the column length, resulting in biaxial mode of bending.

Table 1 gives the results for the two columns for different number of Gauss points, varying from 2 to 6, and for different number of column segments along the length, varying from 8 to 20. A close look at the failure loads obtained shows that for a given number of column segments, use of 4 Gauss points in each direction yields results within 0.5% of the convergence value. It appears that use of only 2 Gauss points tends to overestimate the failure load by about 2-3%. Use of 3 Gauss points, on the other hand, gives similar error on the safe side. On the question of the number of column segments along the length, it is noted that no significant improvement in accuracy is obtained by taking more than about 8 column segments. This, of course, would be true for columns in single curvature bending only. For columns in double curvature bending, a suitable number of column segments along the length would be about 16. It is worth noting that in the case of double curvature bending, having fewer segments may result in errors on the unsafe side [13].

TABLE 1 - Results with Varying Number of Gauss Points and Column Segments

Section	Number of Column Segments	Failure Load (kN) for Number of Gauss Points				
		2	3	4	5	6
[L]	8	428.6	408.2	418.3	417.7	418.3
	10	430.3	409.0	418.6	418.2	418.5
	12	429.7	409.3	419.1	418.6	418.9
	16	430.3	409.5	419.4	418.8	419.3
	20	430.6	409.5	419.5	419.0	419.4
[H]	8	688.1	696.6	683.8	686.7	686.5
	10	688.2	696.7	683.9	686.8	686.6
	12	688.2	696.8	683.9	686.8	686.6
	16	688.2	696.8	683.9	686.8	686.7
	20	688.2	696.9	684.0	686.8	686.7

COMPARISON WITH EXPERIMENTAL RESULTS

A very large number of test results are available for slender reinforced concrete columns. Very few of these, however, involved columns in biaxial bending. Two series of tests described in recent literature have been chosen to show typical agreement with experimental results [4,9].

In the first series by Pannell and Robinson, seven small scale columns with biaxial eccentricities were tested. In the second series, by Cranston and Sturrock, the columns had a narrow rectangular shape, and although the applied eccentricity was only in the major axis, small imperfections in the minor axis could easily have triggered biaxial mode of failure. For this reason, a minor axis initial lack of straightness of magnitude 0.001 times the column length has been adopted for the latter series. In both cases, for steel an elastic perfectly plastic stress strain characteristic has been used. For concrete, a stress strain curve of the type shown in Figure 5 has been adopted, except that the factor 0.67 on the cube strength has not been used. In all other respects, the data given in the original publications [4,9] has been used.

Table 2 shows the comparison between the experimental and analytical results. It will be noted that for the 12 columns analysed, the computed results are always on the conservative side. The mean value of the ratio of the theoretical and experimental failure loads is around 0.69, which indicates that the results based on the proposed method can be accepted with confidence.

TABLE 2 - Comparison with Test Results

Reference	Column Label	Failure load (kN) Test	Failure load (kN) Theory	Ratio Theory/Test
[9]	11	40	22.1	0.553
	12	40	26.1	0.653
	13	20	13.8	0.689
	14	20	12.2	0.610
	15	50	29.3	0.586
	16	30	24.0	0.800
	17	20	15.8	0.790
[4]	3	273	224.4	0.822
	4	463	301.0	0.650
	5	349	272.2	0.780
	6	321	195.2	0.608
	7	378	274.0	0.725
			Mean =	0.689
			Standard Deviation =	0.093

APPLICATIONS

Several studies in the past few years have shown that analytical techniques similar to the one described in the paper agree well with experimental results [4,7,12]. It is recognised, however, that such complex methods are unlikely to be used in the design office. The usefulness of these methods lies in their application to parametric studies of a wide range of practical columns, and then summarising the results by means of simple formulae which inevitably would be less accurate, and would also have limited range of applicability, but would be amenable for use in design office.

The method described in this paper has been used to verify the accuracy of a new design procedure [15]. Current areas of investigation include the problem of columns of varying profile along the length as used in bridge structures.

CONCLUSIONS

The exact method of analysis for biaxially restrained reinforced concrete columns with nonlinear material properties in the past has suffered from the drawback of requiring large amount of computer time so that parametric studies undertaken have had to be of limited scope. As shown in this paper, use of Gauss quadrature at the stage of computing the moment thrust curvature relations can reduce the computational effort significantly. It is shown that using only 4 Gauss points in any direction yields results within 0.5% of the convergence value for a given number of column segments. It is shown that for columns in single curvature bending, even for the biaxial case, use of 8 column segments along the length yields results within 0.1% of the convergence value. For columns in double curvature bending, it is suggested that use of 16 column segments would yield comparable level of accuracy. The method has been shown to give good agreement with two separate series of tests available in the literature, the computed results always being on the conservative side.

APPENDIX I - REFERENCES

1. Basu, A.K. and Hill, W.F. A more exact computation of failure loads of composite columns. Proc. Instn. Civ. Engrs., 1968, May, pp 37-60.

2. British Standards Institution. CP110:1972, The structural use of concrete. British Standards Institution, London, 1972.

3. CEB-FIP. International recommendations for the design and construction of concrete structures. Cement and Concrete Association, London, 1970, p 41.

4. Cranston, W.B. and Sturrock, R.D. Lateral instability of slender reinforced concrete columns. RILEM International symposium, Buenos Aires, 1971, Theme I, pp 117-141.

5. Gesund, H. Stress and moment distribution in three dimensional frames composed of nonprismatic members made of nonlinear material. Chapter 13 : Space Structures. Blackwell, Oxford and Edinburgh, 1967, pp 145-153.

6. Kopal, Z. Numerical Analysis. 2nd Edition, Chapman and Hall, London, 1961.

7. Milner, H.R. and Gent, A.R. Ultimate load calculations for restrained H-columns under biaxial bending. Civ. Engrg. Trans. Instn. Engrs. Aust., 1971, CE 13, April, pp 35-44.

8. Newmark, N.M. Numerical procedures for computing deflections, moments, and buckling loads. Trans. Am. Soc. Civ. Engrs., 1943, p 1161.

9. Pannell, F.N. and Robinson, J.L. Slender reinforced concrete columns with biaxial eccentricity of loading. Magazine of Concrete Research, 1968, December, pp 195-204.

10. Virdi, K.S. Inelastic Column Behaviour - Its application to composite columns in biaxial bending and stiffened plates in compression. PhD Thesis, University of London, 1973.

11. Virdi, K.S. A new technique for the moment thrust curvature relations for columns in biaxial bending. Sixth Australasian Conference on the Mechanics and Strength of Materials, Christchurch, New Zealand, 1977, August, p 307-313.

12. Virdi, K.S. and Dowling, P.J. The ultimate strength of composite columns in biaxial bending. Proc. Instn. Civ. Engrs., London, Part 2, 1973, March, pp 251-272.

13. Virdi, K.S. and Dowling, P.J. The ultimate strength of biaxially restrained columns. Proc. Instn. Civ. Engrs., London, Part 2, 1976, March, pp 41-58.

14. Warner, R.F. Biaxial moment thrust curvature relations. J. Struct. Div. Proc. Am. Soc. Civ. Engrs. 1969, May, pp 923-940.

15. Wood, R.H. and Shaw, M.R. Developments in the variable stiffness approach to reinforced concrete column design. Magazine of Concrete Research, 1979, September, pp 127-141.

16. Zienkiewicz, O.C. The Finite Element Method in Structural and Continuum Mechanics. McGraw-Hill, London, 1967, pp 263-265.

Software Engineering Aspects of Flexible Structural Analysis Systems

Des aspects "software" pour des systèmes flexibles d'analyse des structures

Software-Aspekte von flexiblen Konstruktionsrechensystemen

FRITS C. DE WITTE
Research engineer
IBBC-TNO, Software-engineering dpt.
Rijswijk, Holland

GER M.A. KUSTERS
Research engineer
IBBC-TNO, Software-engineering dpt.
Rijswijk, Holland

SUMMARY

This paper stresses the need for and presents a flexible computer system for structural analysis. Especially in the field of Research and Development modifications should be easily to deal with. Guidelines for the implementation of such a flexible system include: Use a highly modular program architecture, separate logical and physical data structures and separate the control structure from the rest of the system. Two examples, related to non-linear FEM-analysis, are given to demonstrate that this approach, indeed, leads to a flexible system.

RÉSUMÉ

Dans cette publication l'importance et la réalisation du développement des systèmes flexibles pour l'analyse structurelle sont accentuées. Surtout dans un domaine de Recherche et Développement il est avantageux que les modifications peuvent être traitées facilement. Comment assurer le "software" à jour et vivant dans un tel domaine? La réponse donnée dans ce rapport est triple: appliquez une architecture de programme d'une conception bien modulaire, séparez des structures de data logiques et physiques, séparez la structure controlée du reste du système. On donne deux exemples, concernant la méthode des éléments finis, qui démontrent que cette méthode résulte dans un système flexible.

ZUSAMMENFASSUNG

In dieser Abhandlung werden die Bedeutung und die Realisierung der Entwicklung flexibler Konstruktionsrechensysteme betont. Besonders auf dem Gebiet der Forschung und Entwicklung müssen Veränderungen berücksichtigt werden können. Die Frage ist wie man die "software" lebendig und neuzeitlich halten kann unter solchen Umständen. Die Antwort in diesem Berichte bezieht sich auf drie Hinsichten: verwende eine weit in Modulen entwickelte Programm-architektur, trenne logische und physische Datastrukturen und trenne das Steuerungssystem von den übrigen Systemen. Zwei Anwendungsbeispiele in Bezug auf die nicht-lineare Finite-Elemente-Analyse werden dargestellt um zu erlautern dass diese Methode zu einem flexiblen Systeme führt.

1.0 INTRODUCTION

1.1 Environment Of Use

The aspects of software engineering described in this paper are very much related to R&D-user environments in general and that of the authors in particular.

The latter is the Software Engineering Dept. of a R&D institute in the field of Structural Analysis and Material Behaviour. As computer simulation nowadays is an essential part of this research the support of an engineering analysis system based on the finite element method (FEM) is necessary..

1.2 Requirements

As research is, by nature, related to non-standard problems the system should be well suited for modification and extension in order to achieve easy adaptation to the non-standard problems on hand. This requirement is called Flexibility.

The need for flexibility not only stems from R&D in material- and structural behaviour but also from developments in numerical analysis (new methods), software engineering (languages, operating systems) and hardware (memory sizes, mini- and micro-computers).

Flexibility guards the integrity and consistency of the system. Without that, maintenance costs and unreliability will frustrate its use.

With respect to the D of R&D an important requirement for software systems is Portability [1], because of the fact that results of research should be available on different hardware configurations, both for customers and in-house use.

Some additional requirements for application software in general and R&D-software in particular are Efficiency - i.e. a minor load for the hardware - and User-friendlyness - i.e. a minor load for the user - .

Some ten years ago we had to decide, considering the above-mentioned requirements, either to use one (or more) of the existing and commercial available FEM-software systems or to develop our own system. Mainly because of the fact that the existing systems were not flexible enough we decided to develop our own FEM-software package (called DIANA for DIsplacement method ANAlyser). In this paper we describe some Software Engineering problems, mainly with respect to the flexibility requirement, and how these were solved during the development of DIANA.

2.0 IMPLEMENTATION LANGUAGE

The first problem is the choice of the programming language. For DIANA FORTRAN-IV was chosen as the system implementation language mainly because of the general availability of compilers and programmers for this language. Unfortunately this language is not very suitable for the development of flexible software systems. The main lack's are:

- Not well suited for realisation of a modular systems architecture
- Poor data-management facilities

So special care had to be taken about these short-commings. Some aspects related to it will now be described.

3.0 SYSTEMS ARCHITECTURE

A modular architecture is very important for large software systems. Modularity means that specific functions in the system, for instance the solution of the system of equations, are performed in specific parts of the program, called modules. Each module "M" has a clearly defined function and further-more a communication 'interface' "i" to other modules of the system for exchange of data. This architecture is shown in fig. 1.

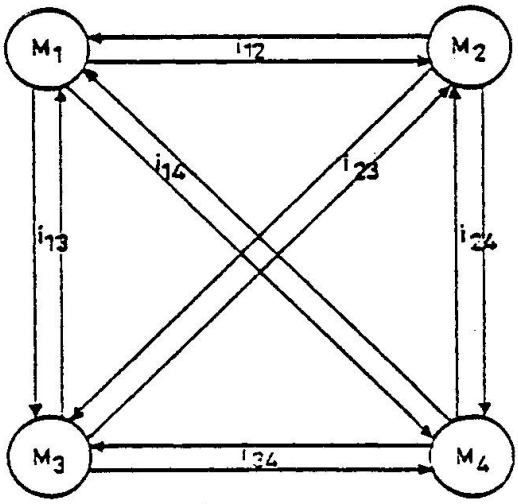

Figure 1

It is clear that the implementation of the performance of a module may be changed as long as the communication interfaces remain unaltered. It is possible, for instance, to change the solution method for the system of equations, without changing the other modules. This is the first step towards flexibility.

Problems with the architecture as shown in fig. 1 may arise when the number of modules increases. When each module of the system has its own interface to the other modules it is very difficult to connect new modules to the system. Many new interfaces have to be defined in that case.

A solution of this problem is to define one interface for the whole system and to connect all the modules to this interface. The interface separates the data from the modules of the system as shown in fig. 2.

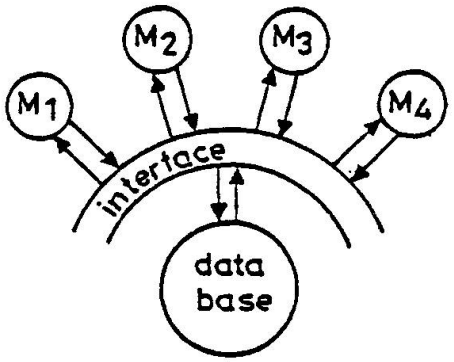

Figure 2

The data separated in this way may be called a database. The system modules communicate with the database via the interface, which may be considered as a database management system.

In DIANA we followed the approach as indicated in fig. 2. We will now describe the architecture of the DIANA system in more detail.

3.1 Modules

From the Users point of view the system is divided into Modules. Each Module performs a specific type of analysis. For instance:

- Module SOLVE for the solution of the system of equations.
- Module NONLIN for Physical and Geometrical non-linear analysis.
- Module SHOCK for dynamic analysis using direct time-integration.

The end-user activates a certain Module by a special command, followed by problem oriented Module-commands.

3.2 Segments

From the system's point of view Modules are built up from what are called Segments. Segments perform a specific function in a Module, for instance Segment DECOMP in Module SOLVE for decomposition of the system of equations. Each Module contains a special Segment for interpretation of the commands which are specific for that Module. For reasons of flexibility each Segment is linked independently from all other Segments and is in fact a stand-alone program for the computer.

In Fortran-terms a Segment consists of a Main-program and a number of Subroutines (and Functions). These routines are functionally collected in two groups:

1. Routines to perform a task specific for the Segment.

2. More general routines, to perform tasks which may be applicable in various Segments. These routines are assembled in Service Libraries, which are specified by the programmer during the Link-process of each Segment. For instance Service Libraries do exist for:
   - Data-management
   - Matrix end vector multiplication
   - Text manipulation.

The architecture described garantees a highly flexible software tool for R&D in the field of FEM-analysis. The standard versions of the Segments may be used as a tool-kit for FEM-programmers. However, they may adapt the system to their own needs by creating experimental versions of one or more Segments, without the need to Link the whole DIANA-system. A special command can be supplied, specifying the alternative version-name of the Segment. This feature is extremely usefull during development and implementation of new applications and theories in FEM-analysis.

Unfortunately some disadvantages are inherent to the concept of independently Linked Segments:

1. A large number of Segments have to be controled, i.e. to be loaded in the computer for execution in a specific sequence. This may need a large number of machine-dependent Job-Control statements, whereas special control structures as LOOPS and JUMPS may be even impossible on some machines.

2. Segments can only communicate via background storage. This may cause a large amount of data in the database which is very intensively accessed during the calculations. So special care has to be taken about the data management, both logical (for reasons of flexibility) and physical (for reasons of efficiency) .

In the next two sections we will describe how these two problems were

solved during the development of the DIANA-system.

4.0 CONTROL STRUCTURE

Two main aspects are related to the control of a DIANA-job:

1. The end-user likes to control the system by means of commands, related the problem he wants to solve (user--commands).

2. The DIANA-system can only control the loading and execution of the Segments (control-commands).

In some cases a conflict occurs between these two aspects. For instance, using the Module NONLIN to execute the next 5 loadsteps in a non-linear analysis the user would give a command like:

```
EXECUTE 5 LOAD STEPS
```

while the control of the Segments would be something like:

```
LOOP 5 TIMES
"LOAD SEGMENT INISTEP OF MODULE NONLIN"
"LOAD SEGMENT .......  OF MODULE SOLVE"
"LOAD SEGMENT ......."
 ........
END LOOP
```

In this case the user-command has to be interpreted and expanded into several control-commands. We now describe how this process works in the DIANA-system.

4.1 User Commands

The user activates the DIANA control-system by a single (machine dependent) Job-Control statement, like:

```
$RUN DIANA                    for VAX/VMS, or:

$$DIANA                       for HARRIS/Vulcan, etc.
```

Next he supplies a module command indicating the Module he is going to use:

```
*NONLIN                       for the Module NONLIN.
```

The DIANA control-system now activates the command interpretor Segment of the appropriate Module. This interpretor scans the module dependent user-commands including parameters etc. that follow the module command, for instance:

```
EXECUTE 5 LOAD STEPS
SIZE 1.2(5)                        "Five equal sized steps of 1.2"
PERFORM NEWTON-RAPHSON MI=10       "Max. 10 equilib. iterations"
```

Commands are interpreted and checked on correct syntax until the next module command or a special 'end' command:

```
*END
```

If no errors are detected the interpretor generates the necessary control-commands.

4.2 Control Commands

The generated control-commands are stored in the database. These commands exists of a list (the command-list), containing the names of the DIANA Segments to be loaded for execution. Special commands are generated if it is necessary to execute the Segments conditionally (JUMP) or more than once (LOOP, END LOOP). Some examples will be given later on.

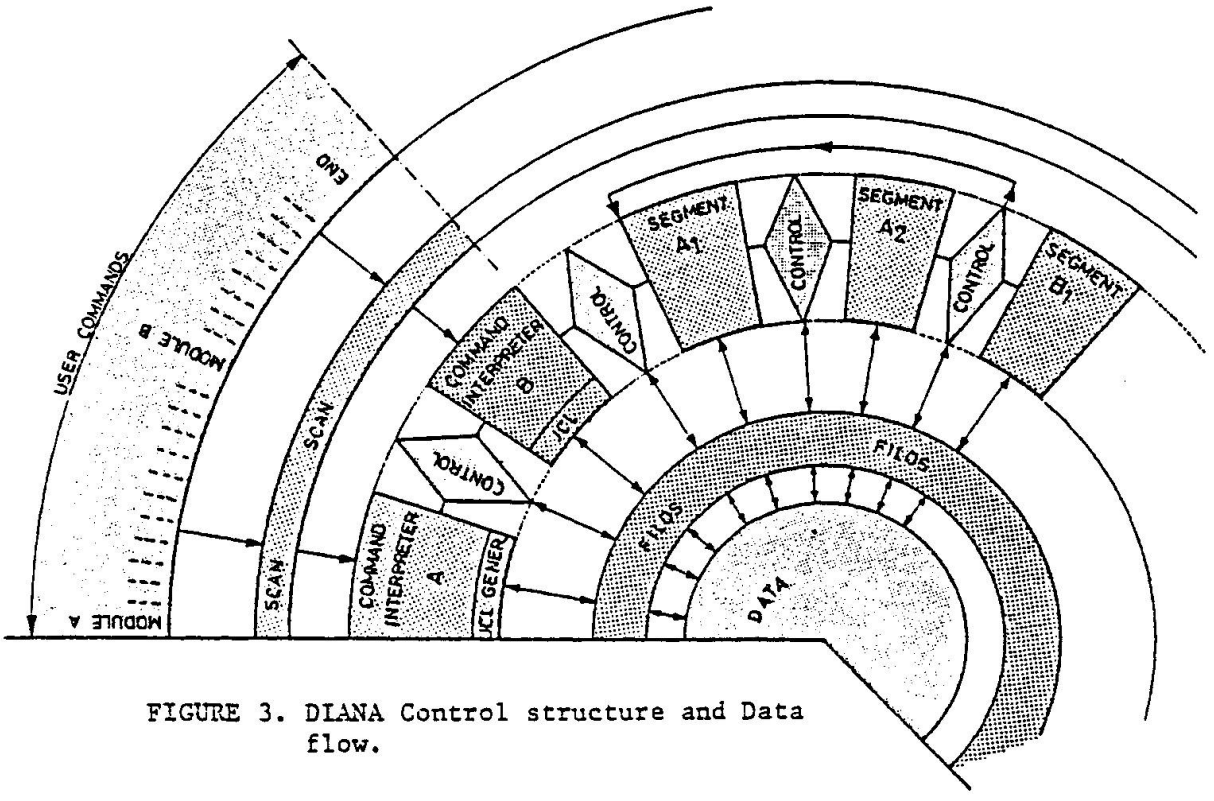

FIGURE 3. DIANA Control structure and Data flow.

When all user-commands are interpreted and all control-commands generated, the first Segment of the command-list is loaded for execution via a (machine dependent) Fortran-call.

After the execution of each Segment the DIANA control-system is activated to find out which is the next Segment to be executed. A special control-command (END) indicates the end of the command-list. The Control structure of the DIANA system is indicated in fig. 3.

The next section deals with data communication between Segments.

5.0 DATA MANAGEMENT

For a number of reasons much attention had to be paid to the organisation of the data management during the development of the DIANA--system:

- Complicated analysis of complex structures needs large amounts of data.
- Segments can only communicate via background storage (Disc--Files).
- The Fortran-IV language only gives a standard for sequential--access. Direct-access is often available, but is, especially in case of bufferd I/O, not portable.
- The Fortran-IV language does not provide for dynamic memory allocation.

Both portable and flexible data management can be realized using a "Database Management System". Unfortunately those systems generally are designed for administrative applications. Logical data-structures may be build for various kinds of access, but the physical organization of data in background memory is not tailored for minimal accestime.

For applications in an Engineering environment like DIANA the physical structure of the data in the database has to be designed for "High--volume I/O", i.e. minimal access-time is more important than minimal data-transport.

In DIANA therefore a severe distinction has been made between physical and logical data structures. The first are handeled by a dedicated service library, called FILOS for File Organisation System [6] . Although developed for DIANA, FILOS may also be used in other application software. It consists of a set of Fortran-callable routines to perform the following tasks:

- Data transport from foreground memory to background storage:
  - Data records may be accessed directly or sequentially, by name or by number.
  - All data may reside on one physical file, the database or FILOS-file.

- Organisation of data on the FILOS-file dedicated to minimal access-time. This is achieved by:
  - Buffering of Data-records, if appropriate.
  - Multiple buffering including a LRU-swapping algorithm.

- Dynamic memory allocation.
  Necessary Foreground memory is allocated at run-time, dependent on the size of the problem and the type of analysis.

FILOS acts as a machine independent, consistent interface to a physical data structure for Engineering applications. Logical data structures for dedicated applications may be given a physical representation using FILOS as a tool-kit.

In DIANA, for instance, logical data structures are designed for:

- Element data.
  Data records are accessed by name (STRESS, STRAIN etc.) for each element in the FEM-model. Data is organized in several levels (element, integration point etc.) and in several generations (Father-Son etc.).

- Material descriptions.
  Each material is described by a set of named data records.

- Node coordinates.

The logical data structures are very important for the flexibility of the DIANA-system. Each Segment may access, without major modifications, all the data stored by any other Segment of any other Module.

6.0 SOME APPLICATIONS

In this section we will demonstrate how the features of the DIANA-system described in the previous sections are used to implement different types of analysis methods.

6.1 Equilibrium Iteration Schemes

In this example we will show how the flexibility of the system is used to make different iteration procedures available in physical non-linear calculations. We will describe three different iteration schemes [2], [5]:

1. Constant stiffness matrix method, no updating of the stiffness matrix.

2. Modified Newton-Raphson, before each new loadstep the stiffness will be updated.

3. Normal Newton-Raphson, before each iteration the stiffness matrix is updated.

To perform a non-linear analysis with plasticity using the constant stiffness matrix method the user has to supply the following commands:

```
*NONLIN
   INITIALIZE
      ANALYSIS PHYSICAL GEOMETRICAL
      OPTIONS PLASTICITY CREEP
   END INITIALIZE
   EXECUTE nstep LOAD STEPS
      PERFORM CONSTANT MI=miter
      ANALYSIS PHYSICAL
      USE PLASTICITY
      SIZE r (nstep)
   END EXECUTE
*END
```

Where:

```
miter:  maximum number of iterations per loadstep.
nstep:  number of loadsteps to be performed.
r     :  size of loadstep increments.
```

The interpretor Segment generates the following command-list to perform a non-linear analysis with plasticity using the constant stiffness matrix method:

```
NONLIN INITIA              "Initialize data for non-lin. analysis"
LOOP nstep                 "Load-step loop"
   NONLIN LOAD             "Set up incremental load vector"
   SOLVE  SUBSTI           "Calculate incrementai displacements"
   NONLIN PHYSNL           "Determine internal load vector"
   LOOP miter              "Equilibrium iteration loop"
      SOLVE  SUBSTI
      NONLIN PHYSNL
   END LOOP
 END LOOP
```

To perform a non-linear analysis with plasticity using the Modified Newton-Raphson iteration method the user has to change the perform command in:

```
PERFORM MODIFIED NEWTON RAPHSON MI=miter
```

The interpretor Segment will generate the same command-list as previous but with some segments added at the beginning of the loadstep:

```
LOOP nstep
   NONLIN LOAD
   NONLIN TANGST          "Form new stiffness matrix"
   SOLVE  ASSEMB          "Assemble system of equations"
   SOLVE  DECOMP          "Decompose system of equations"
   SOLVE  SUBSTI
   NONLIN PHYSNL
   LOOP miter
      SOLVE  SUBSTI
      NONLIN PHYSNL
   END LOOP
END LOOP
```

The same segments added in the inner loop will result in the normal Newton-Raphson iteration procedure:

```
LOOP nstep
   NONLIN LOAD
   NONLIN TANGST
   SOLVE  ASSEMB
   SOLVE  DECOMP
   SOLVE  SUBSTI
   NONLIN PHYSNL
   LOOP miter
      NONLIN TANGST
      SOLVE  ASSEMB
      SOLVE  DECOMP
      SOLVE  SUBSTI
      NONLIN PHYSNL
   END LOOP
END LOOP
```

The example showed the flexibility of the system: by simply adding some Segments to the command-list different analysis methods became available, without the need to modify any of the used Segments.

6.2 Dynamic Analysis

In this example we will show how non-linear material behaviour can be included in a dynamic analysis using an implicit time integration method.

To perform a dynamic analysis, with implicit time integration the following equilibrium equations have to be solved [3], [4]:

$$M * {}^{t+\Delta t}\ddot{U} + C * {}^{t+\Delta t}\dot{U} + K * {}^{t+\Delta t}U = {}^{t+\Delta t}P - {}^{t}F \qquad \{1\}$$

Where:

M = mass matrix

C = damping matrix

^{t}K = tangent stiffness matrix at time t which includes the linear and non-linear material effects, and/or geometrical non-linear effects.

$^{t+\Delta t}P$ = externally applied forces at time $t+\Delta t$

^{t}F = nodal point forces vector equivalent to the stresses of the elements at time t.

$^{t+\Delta t}\ddot{U}$ = nodal point accelerations at time $t+\Delta t$

$^{t+\Delta t}\dot{U}$ = nodal point velocities at time $t+\Delta t$

$^{t}\ddot{U}$ = nodal point accelerations at time t

U = displacement increment from time t to time $t+\Delta t$

Solving equation (1) with the implicit Newmark Beta step by step integration procedure the following steps may be distinguished:

Initial calculations:

(I) Initialize:

^{0}U ; $^{0}\dot{U}$ and $^{0}\ddot{U}$

Calculate the constants a0 to a10 for Newmark Beta.

(II) Form effective coefficient matrix Ke:

$$Ke = K + a_0 * M + a_1 * C$$

In <u>linear analysis</u>:

(III) Triangularize effective coefficient matrix Ke (assemble and decompose).

For each <u>time step</u>:

(IV) Form effective load vector:

$$R^{t+\Delta t} = P^{t+\Delta t} + M * (a_0 * U^{t} + a_2 * U^{t.} + a_3 * U^{t..}) + C * (a_1 * U^{t} + a_4 * U^{t.} + a_5 * U^{t..})$$

(V) Solve for displacement increments:

$$Ke * U^{t+\Delta t} = R^{t+\Delta t} \; ; \quad U^{t+\Delta t} = U^{t+\Delta t} - U^{t}$$

(VI) Calculate new accelerations, velocities and displacements:

$$U^{t+\Delta t..} = a_6 * U^{t} + a_7 * U^{t.} + a_8 * U^{t..}$$

$$U^{t+\Delta t.} = U^{t.} + a_9 * U^{t..} + a_{10} * U^{t+\Delta t..}$$

$$U^{t+\Delta t} = U^{t} + U$$

To include non-linear material behaviour in the analysis the following steps are necessary per time step:

(III) Form new stiffness matrix K^{t}.

(IV) Form effective coefficient matrix Ke:

$$Ke = K^{t} + a_0 * M + a_1 * C$$

(V) Assemble and decompose effective coefficient matrix.

(VI) Form effective load vector:

$$R^{t+\Delta t} = P^{t*\Delta t} + M * (a_2 * U^{t.} + a_3 * U^{t..}) + C * (a_4 * U^{t.} + a_5 * U^{t..}) - F^{t}$$

(VII) Solve for displacement increments:

$$K_e * U = {}^{t+\Delta t}R$$

(VIII) If required, iterate for dynamic equilibrium:

(a) Initialize displacements U and inner iteration number i:

$$U = {}^{(0)}U ; \quad i=0$$

(b) i=i+1

(c) Calculate (i-1)st approximation to accelerations, velocities, and displacements:

$${}^{t+\Delta t..(i-1)}U = a_0 * {}^{(i-1)}U - a_2 * {}^{t.}U - a_3 * {}^{t..}U$$

$${}^{t+\Delta t.(i-1)}U = a_1 * {}^{(i-1)}U - a_4 * {}^{t.}U - a_5 * {}^{t..}U$$

$${}^{t+\Delta t\ (i-1)}U = {}^{(i-1)}U + {}^{t}U$$

(d) Calculate (i-1)st effective out-of-balance loads:

$${}^{t+\Delta t\ (i-1)}R = {}^{t+\Delta t}P - M * {}^{t+\Delta t..(i-1)}U + C * {}^{t+\Delta t.(i-1)}U - {}^{t+\Delta t\ (i-1)}F$$

(e) Solve for i-th correction to displacement increments:

$$K * {}^{(i)}\Delta U = {}^{t+\Delta t\ (i-1)}R$$

(f) Calculate new displacement increments:

$${}^{(i)}U = {}^{(i-1)}U + {}^{(i)}\Delta U$$

(g) Check for convergence, if not return to (b) for next iteration, otherwise continue:

$$U = {}^{(i)}U$$

(IX) Calculate new accelerations, velocities and displacements:

$$\overset{t+\Delta t}{U} = a_6 * \overset{t}{U} + a_7 * \overset{t}{U} + a_8 * \overset{t}{U}$$

$$\overset{t+\Delta t}{U} = \overset{t}{U} + a_9 * \overset{t}{U} + a_{10} * \overset{t+\Delta t}{U}$$

$$\overset{t+\Delta t}{U} = \overset{t}{U} + \overset{t}{U}$$

To perform a dynamic analysis with linear elastic material behaviour the user has to supply the following commands:

```
*SHOCK
   INITIALIZE dtime
      ANALYSIS NEWMARK alfa beta
   END INITIALIZE
   EXECUTE nstep TIME STEPS
      PERFORM LINEAR
   END EXECUTE
*END
```

Where:

dtime:	time increment.
alfa :	constant for Newmark Beta.
beta :	constant for Newmark Beta.
nstep:	number of time steps to perform.

The interpretor Segment generates the following command-list to perform a dynamic analysis with linear elastic material behaviour for nstep time steps (the number in brackets indicate the previously mentioned part of the integration procedure):

```
SHOCK INITIA          (I)
SHOCK EFCOEF          (II)
SOLVE ASSEMB          (III)
SOLVE DECOMP          (III)
LOOP nstep
   SHOCK EFFLOD       (IV)
   SOLVE SUBSTI       (V)
   SHOCK VELACC       (VI)
END LOOP
```

To perform a dynamic analysis with non-linear material behaviour and/or geometrical non-linear effects the execute command block has to be changed in:

```
EXECUTE nstep TIME STEPS
   PERFORM NEWTON RAPHSON MI=miter
   ANALYSIS PHYSICAL GEOMETRICAL
   USE PLASTICITY
END
```

The interpretor Segment generates the following command-list to perform a dynamic analysis with non-linear material behaviour and/or geometrical non-linear effects for nstep time steps:

```
SHOCK INITIA          (I)
LOOP nstep
   NONLIN TANGST      (III)
   SHOCK  EFCOEF      (IV)
   SOLVE  ASSEMB      (V)
   SOLVE  DECOMP      (V)
   SHOCK  EFFLOD      (VI)
   SOLVE  SUBSTI      (VII,VIIIa)
   NONLIN PHYSNL      (VI) F-term for i+1 .
   LOOP miter         (VIIIb)
     SHOCK  OOBFOR    (VIIIc,d)
     SOLVE  SUBSTI    (VIIIe,f,g)
     NONLIN PHYSNL    (VIIId) F-term for i+1 or next time step.
   END LOOP
   SHOCK VELACC       (IX)
END LOOP
```

In this example we see once more the flexibility of the system. The only new Segment to be programmed in order to make non-linear material behaviour available, is the Segment OOBFOR in Module SHOCK. Whereas the Segment PHYSNL of Module NONLIN may simply be added as it is.

7.0 CONCLUSIONS

For application software, especially when used in a R&D environment where all kinds of technological developments take place, change is the major factor to deal with. To keep the software alive and up-to-date Flexibility is the most important requirement. Therefore three considerations have to be kept in mind during the development of application software:

1. Use a highly modular program architecture. This facilitates the maintenance of a consistent set of software, avoiding the danger of rigidity.

2. Separate the logical and fysical data structures. This leads to both flexible data management and efficient inter-modular data communication.

3. Design a special control structure. This gives a flexible control over the execution sequences of segments from various modules. Different analysis methods may be implemented simply by an assembly of control-commands.

That these considerations indeed lead to flexibility, is demonstrated by two examples, taken from the DIANA FEM-software system:

- The implementation of different iteration schemes in non-linear analysis.
- The inclusion of non-linear material behaviour in a dynamic analysis.

8.0 REFERENCES

[1] van Beinum, Gerlach E.; Tolman, Frits P. and de Witte, Frits C.: "Portability Aspects of DIANA, A large Engineering Analysis System", Proc. 4th EASIT-Conference on 'Problems and experiences with quality assurance and portability of software', Luxembourg, 12-13 May 1980.

[2] Zienkiewicz, O.C.: "The Finite Element Method", Mc. Graw-Hill, London, 1977.

[3] Bathe, Klaus-Jurgen and Wilson, Edward L.: "Numerical Methods in Finite Element Analysis", Prentice-Hall, Englewood Cliffs, New Jersey, 1976.

[4] Bathe, Klaus-Jurgen: "Static and Dynamic Geometric and material Nonlinear Analysis using Adina", MIT Cambridge Massachusetts, May 1976.

[5] Kusters, Ger M.A.: "Non-linear material behaviour of reinforced concrete using the Finite Element Method", TNO-IBBC report nr. BI-77-36/07.1.22110, March 1977 (in Dutch).

[6] "File Organisation System - FILOS, Users Manual, version 1.2", TNO-IBBC, 1981.

Leere Seite
Blank page
Page vide

Session 2, part 1: Structural Modelling for Numerical Analysis

Introduction by Bergan, chairman (Norway); at the beginning of the session.

I am very pleased to have this opportunity of chairing this morning session on structural modelling for numerical analysis. This title indicates that we are now moving from the fundamental mechanisms and concepts in reinforced concrete on to computational techniques that may be used for solving real, practical problems. Coming from Norway I know that there is a great need for more sophisticated methods for non-linear analysis of reinforced concrete structures. I am of course particularly thinking of development of designs of gravity platforms for the North Sea. Already fourteen such gravity platforms have been built, and these structures are really enormous. I think that you have to see one in order to comprehend how enormous they really are. Some of these are nearly 200 m high and contain 500,000 tons of reinforced concrete. And the price for the concrete structure alone is close to one billion (10^9) Norwegian crowns, that is about 200 million U.S. Dollars. Concepts for structures that are supposed to stand in nearly 350 meters of water depth are now being worked out. And if you now consider the linear scale to be doubled you see also that the volume of these new structures will be much, much larger than those that we already have.
Economy and safety aspects are of course essential and it is therefore evident that we need some very powerful and accurate methods of analysis for analysing these structures.
Having said this, I must also add that ten years of research in non-linear finite element analysis of reinforced concrete structures have taught me to be a little bit sceptical as to what can be achieved by these methods. In fact I must admit that three, four years ago I was a little bit more optimistic than I am today. The reason for this is not at all that so little has been achieved during the last few years, but it has become apparent to me that there are still so many questions that are unanswered and it seems that new problems arise all the time. I particularly had this feeling yesterday: each talk seemed to raise more questions than it really answered. This may of course be a good thing for us, who are working in research; we just have to convince our sponsors about all these problems that still are not solved and we will be sure of keeping our jobs for the coming years. But seriously, it is also an indication that our insight is constantly growing and that the interphase to what we do not know is growing at the same time.
Undoubtedly, modelling of reinforced concrete structures is very difficult and a challenging field to be working in. It is somewhat frustrating that you do not have an exact solution to compare with. Of course there are experiments, but if you do the same experiment twice, you are likely to get two different answers. You may think that you have a perfect model that gives exact results, but then somebody comes along and shows that there are some other effects, that you have not considered, and that these effects are of vital importance for the behaviour of the structures. So there are many traps to fall into. And the biggest one among these is to believe that you have achieved a general solution technique when you only have been able to, should we say, post-predict one experimental test by means of adjusting some material parameters in your model. Considering all the important information that we got yesterday, how should we then go about developing our computation models? Is it really necessary to use a general three-dimensional finite element model, that accounts for every detail in the concrete, including pores, aggregate, paste, detailed reinforcement, that follows the development of each individual crack, that accounts for slip, interlocking, friction sliding, temperature, moisture, history effects, aging etc.?

Where will this bring us to? Well, I am sure that in this session we will hear some interesting papers that will point out the way to go, in order to achieve more efficient and better numerical models for analysing real structures.
This session begins with an introductory paper by Prof. Christian Meyer of the Columbia University, who will talk about dynamic finite element analysis of reinforced concrete structures. It is a great pleasure to give the word to Prof. Meyer.

For discussion on the Introductory Report by Prof. Meyer see 5 pages further.

DISCUSSION

Session 2, part 1: Structural Modelling for Numerical Analysis

Paper by Cope/Rao, United Kingdom

Crisfield (U.K.): It would be useful to have a break-down between the number of BFGS -iterations, in which updating was applied compared to the number of line searches. Could it be that in some cases the line search, rather than the BFGS, is the more dominant feature?

Cope: I do not have the numerical evidence here, but I can recall that the rate of convergence was in fact most influenced by the line search. Setting CONDMAX as low as 10^3, whereby there would only perhaps be one or two updates of the inverse of the stiffness matrix per increment, gave very similar results to setting CONDMAX equal to 10^5. So the answer is that we feel that the line search is the most important part of the acceleration procedure.

Bazant (U.S.A.): I think it is rather interesting that you found it to be a significant phenomenon that the directions of the principal moments rotate, and therefore that the use of orthotropic models gives better results if you rotate the directions of the axes of these models. However, although you get better results if you do that, it implies rotating the defects within the material. Therefore this formulation is to some extent physically objectionable. This comment also relates to all the so-called "equivalent uniaxial stress" models. These models have the orthotropic form and, by virtue of the fact that they have zero terms connecting normal stress and shear strain, and shear stress and normal strain, they are not invariant with regard to the choice of coordinates. Therefore, these models may lead to significant discrepancies.

Cope: With slabs the main behaviour is in fact influenced by the steel after cracking, and I do not think that the invariance is particularly important. Although it is obviously not a rigorous analytical model that we are using, we are trying to aim for economy, and to some extent we may have violated a rigorous approach in order to achieve that. I do not know how we would get over it, because with multiple load patterns there is no doubt, that cracking occurs between and inclined to established cracking. Also, where there is inclined cracking at a point, the direction of the applied principle moment determines which cracks dominate the response.
We found in extreme cases, where we have analysed panels subjected first to flexure and then to torsion, that if we fix the material property axes, we then cannot get the stiffness to rotate properly to treat the torsion case.
Yesterday someone mentioned having eight possible crack directions. We tried a similar approach in which material property axes were held in direction until the principal strains rotated by say 30 degrees, then we would allow them to rotate. But this is again, I think, an empirical rather than a rigorous approach.

Blaauwendraad (The Netherlands): Your conclusion that you can omit tensile stresses is correct, but only for this special structure and its typical loading (pure bending). I think that one should be more careful if you would have combinations of shear and bending, which may dominate the failure of the structure.

Cope: The point is accepted: the results were for Kirchhoff plate bending elements, in which transverse shear was not modelled. The Heterosis element, which includes the capability of taking tranverse shear into account, gives very similar results when we do not degrade the transverse shear modulus. We have not yet started doing studies that involve both flexure and shear cracking. For the sort of slab bridges that we have been looking at, it is not a usual failure criterion.

Paper by Rossi/Bazzi, Switzerland

Collins (Canada): I should like to congratulate you on a really first class paper: I very much enjoyed your presentation. In the comparisons between the predictions of your model and some other predictions for the beam in shear, I noticed that you seemed to be using situations where all of the steel yielded. I am wondering if you attempted to compare the more difficult situation where the steel does not yield, in either one direction or both directions prior to failure.

Rossi: As I mentioned in the presentation, this model till now works just for situations where the steel yields. The adopted yield condition of Drucker-Prager is not very useful for cases with high multiaxial compression, because we will get too high values for the strength. We intend to do some more research in this field.

Bazant (U.S.A.): Dr. P.D. Bhat carried out at Northwestern University a similar investigation of hysteresis, where he used the endochronic theory with layered beam elements, with non-normal cross-sections, and calculated the hysteresis loops. One aspect which he found significant in the response was expansion of the concrete during deformation cycling, which was putting into action the transverse reinforcement. It was a calculation according to the beam theory, where one unknown was also the mean transverse strain in addition to the angle between the cross section and a normal to the beam axis. Have you studied this effect and, if yes, what was your conclusion?

Rossi: So far we are not able to use this shear model for cyclic loading, since it is a plasticity model. We cannot expect good results for cylic loading because we have no possibility to simulate closing and reopening of the cracks; therefore, we have no experience in this case.

Blaauwendraad (The Netherlands): A remark and some questions. You referred to our paper in Copenhagen, which is describing a similar model. The difference is that we used a layered approach. Personally I feel that the difference is not that big, because it does not take much more time to do a correct integration over the cross-section.
Now my questions. We had some difficulties with the distribution of the vertical strains transverse to the bar axis; we started with the same approximation as you, a linear displacement field, resulting in a constant strain field. Specially when you have a compression zone, the vertical strains there will be considerably lower than in the cracked zone in the tensile area.

Did you deal with that? Furthermore, we feel that we should extend this model with a special element for the beam-column connection. Now that we can treat the beams and columns so well, we feel that the weakest part in the calculation of the frame structure is the connection. Do you have proposals for that?

Rossi: With regard to your first question, we had the same problems with the vertical strain distribution and we intend to adopt an approach using different models for each Gaussain point in the vertical direction, for instance three different ones. This means that we would have three more internal unknowns, which we should iterate first. We intend to follow this approach as a next step. To your second question: Until now we have not thought about modelling of the joints.

Paper by Muto/Sugano/Miyashita/Inoue, Japan

Blaauwendraad (The Netherlands): I understood that the intention of this presentation was the simulation of what will happen during earthquakes. If you regard a connection between a column and beam, is this loading case then a relevant one? Should not you consider moments of opposite sign on both ends of the connection? That may result in slip of the reinforcement, and influence the behaviour quite a lot.

Inoue: We had only the intention to obtain results in a short time; we studied the general characteristics, such as the load-deflection relation and the strain of the longitudinal reinforcement and I did not consider all details. In a further study we will extend the scope of the program.

Bergan (Norway): An eight-mode brick element is used, with a 2 by 2 Gaussian integration. It is well known that when you subject this element to bending modes, you get a lot of spurious shear deformations, and when you analyse concrete, that may be rather critical. Would not it be better to use a selective integration of shear strains, like taking the shear strains at the centroid, rather than in the Gaussian points? This choice is rather critical when non-linear material properties for concrete are considered.

Bazant (U.S.A.): I just should like to comment in defense of Mr. Inoue's analysis, that this pure shear effect would only be important for very slender members and that the members we are talking about here are very bulky. So I do not think that this effect could have been of significance in this particular example.

Bergan: I think that it is significant anyhow as long as you consider bending.

Bazant: There is a limit for very slender member.

Bergan: But he is not only considering axial loading on these columns.

Paper by Mang/Floegl, Austria

Gambarova (Italy): What do you think about the minor role of crack spacing, with reference to tension-stiffening effects? I would have expected it to be a major factor.

Mang: It is very difficult to answer this question, having only limited numerical evidence available. What I would say is that consideration of tension-stiffening within the given framework that I presented, acts, as we could say, as a stabilizator for the analysis. It may be not so important what the stabilizing parameters are. This might be an explanation, but I would not be astonished if counter-examples were found, showing a different state of affairs. We hoped, specially with respect to Prof. Bažant's remark about objectivity of some of the constitutive laws used, that analysing large cooling tower structures would give an answer to some of the problems, but this did not happen; even the whole tension-stiffening effect was not important. So also any refinements in the tension-stiffening formulation did not have an influence. Another aspect that was raised by one of the previous speakers refers to the behaviour of slabs; it was stated that the tension-stiffening effect was unimportant. We found, again within the scope of our limited numerical evidence, the same; there was hardly any influence of the tension-stiffening effect on these results. So for these problems of course a variation of the $b_{ij}^{(1)}$ term is unimportant. We hope to develop a rational method, from the standpoint of mechanics, to incorporate the initial crack spacing.

Mehlhorn (F.R.G.): I did not understand how you consider the influence of the angle between reinforcement and the crack. Did you check this influence by tests?

Mang: It is considered in a term containing the direction cosinus between the reinforcement and the crack, such that the special cases of perpendicular intersection would lead to the conventional result, and that the other case, when the reinforcement is parallel to the concrete strut, would result in the lower bound of the tension-stiffening factor, namely 1. There was not time enough to explain this in my lecture. The concept is brought into effect such that in a shell - where you can have the limiting cases of a pure bending state, or a pure membrane state - for the case of a pure membrane state you will arrive at the results for a plane situation. It would be too difficult to explain now all the terms; but it is accounted for.

Bergan (Norway): It is a little bit surprising that your tension-stiffening effect is so important for the ultimate loading; normally one thinks that it is important mainly for lower loading stages, with the initial cracking. Are you absolutely sure that this is correct?

Mang: I expected this question. I may say that we analysed the influence of variations of the meshes and variations of the input parameters, and we found the same thing in all the analysis. I can only be sure as far as correct coding is concerned, but I know that it is a well disputed fact.

Crisfield (U.K.): The stiffness of the material is important if instability effects, such as buckling, are involved in the analysis. Is this the explanation that in the shell example that you presented, tension-stiffening is affecting the ultimate load?

Mang: If the structures would have been built in steel, buckling would be a mechanism to be considered. However, in all typical reinforced concrete structures which we analysed (I mentioned that we analysed large hyperbolic cooling towers), there was no indication of buckling at all.

Collins (Canada): I just like to add to the comments about whether the tension-stiffening affects the ultimate strength. You would be perhaps interested to know that in our panel tests we have found that tension-stiffening does affect the ultimate strength, provided that failure occurs before all of the steel yields. If the steel in both directions fully yields prior to failure, then tension-stiffening has no effect.

Mang: I am glad you made this comment which corroborates our findings.

Bazant (U.S.A.): I would like to come back on the subject of crack spacing, further to what has been said earlier by Dr. Gambarova. Whether or not there is a tension-stiffening effect makes a significant difference, and the influence of the effect should clearly depend on the crack spacing, falling down to zero if the crack spacing becomes infinitely small. You did not find an influence of the crack spacing. This can only be true if the range of crack spacing which is considered is limited. Differences in crack spacing of about 100% are important; differences of 20-30% do not affect the behaviour very much, as can be shown by calculations.

Mang: What we hoped is to show this with a large shell structure, but we did not succeed as I said, because the structure we analysed showed a sudden collapse and the whole matter does not come into the play. What we are looking for now is to find examples in which it would really have some effect.

Discussion on not orally presented papers

Paper by Aguado/Murcia/Mari, Spain

Bergan (Norway): In your paper you gave results for moments. Are you also capable of calculating deformations with your solution procedure?

Mari: The deformations can be calculated only by integration of the curvatures. If the structure is an isostatic structure, the deformations are the addition of the linear deformations and the imposed deformations. But if the structure is hyperstatic, the deformations will be the sum of the linear deformations, the hyperstatic deformations and the imposed deformations.

Paper by Menegotto, Italy

Bergan (Norway): It was not clear from the paper what type of integration you used over the cross-section of the beams. You indicate that you divide the inter-subareas as a basis to find the Culmann-ellipses. Could you comment on how you find these stiffnesses?

Menegotto: The interntal forces are integrated over the section just by multiplying the stresses by the areas and summing up. The areas are small layers of concrete and spot steel areas. The point is that there can be an infinite number of definitions of the stiffness for a step of loading. Among these, that one is chosen which is deemed to be the most correct one, i.e. the one related to the local linearization of the stress-strain paths corresponding to the assumed loading step. In that sense I would like also to discuss Mr. Rossi's and Bazzi's paper, who find a non-symmetric stiffness matrix for the section. I think that among the infinite possibilities the symmetric matrix which one can find would be better.

Blaauwendraad (The Netherlands): I appreciated your paper very much. You are speaking in terms of a "very general approach". Is your procedure so general, that you can extend it to cases in which you have not only combined bending but also torsion?

Menegotto: Up to now it is only referred to combined normal forces and skew bending, but I think that the stiffness criterion can be generalized.

Introductory Report by Meyer, U.S.A.

Blaauwendraad (The Netherlands): I understood from you that you use a combination of integration in time, material non-linearity and maybe geometrical non-linearity. I am wondering how many hours computer time you need to process a real structure of the size you showed us, and what type of computer you have available to do such jobs.

Meyer: That was one of the reasons why I illustrated the various levels of sophistication. If you endeavour to analyse a multi-story building you cannot afford to break up every beam and column into hundreds of finite elements and integrate them all through the time domain. That is why I personally prefer the full member approach, at least for analizing buildings, although the layered or semi-finite element models may be also possible. About the last examples that I showed at the end, the 3-dimensional models for blast loading, which I got from Dr. J. Isenberg, I can add that these calculations were carried out for the Defense Department of the United States, and, as you know, money is of little concern to them.

Blaauwendraad (The Netherlands): What is the tendency in the U.S.: should we think of super-computers, such as Cray 1, or should we think in terms of "Super-Vax" in combination with an Array Processor? How will people handle the job in practice?

Meyer: It really depends on what kind of structure you are talking about. For example, for a simple slab cover over a missile tube, you can perform a full dynamic analysis on man common computers without requiring execessive funds. But on the other hand, in the case of some of the examples I have been involved with - some very complicated internal structures in a submarine, for example - you may speak of several hours of computer time on the Cray-machine. And if you know what an hour on the Cray costs, you can imagine what that means. But for common civil applications we really have to be concerned about simplifying our models. Otherwise calculations are simply not feasible, definitely not in engineering practice, for example on the civil engineering profession, where the final objective is to design and build structures, not to spend all the money analyzing them. You just have to draw lines somewhere. I consider all these approaches which have been discussed here only as a means of understanding concrete behaviour, that should help us ultimately to come up with simplified models.

General discussion

Crisfield (U.K.): I just want to show very briefly something relating to what Dr. Cope said this morning about various "rogue" solutions with the BFGS-method. He said one should look out for those rogue solutions. But they are still equilibrium states. He rejected them because he had the experiments, but you do not always have the experiments before the case.

I would like to talk about some of these alternative equilibrium states that can arise and relate this to the issue of tension-stiffening that has already been talked about, strain localization, discussed earlier by Bažant, and mesh dependency.
The mechanism of cracking and its effect can be represented in a way as shown in Fig. A. If a crack occurs at constant strain the stress falls down to a lower level. If the stress is then increased again a new ascending branch is followed until new cracking occurs.

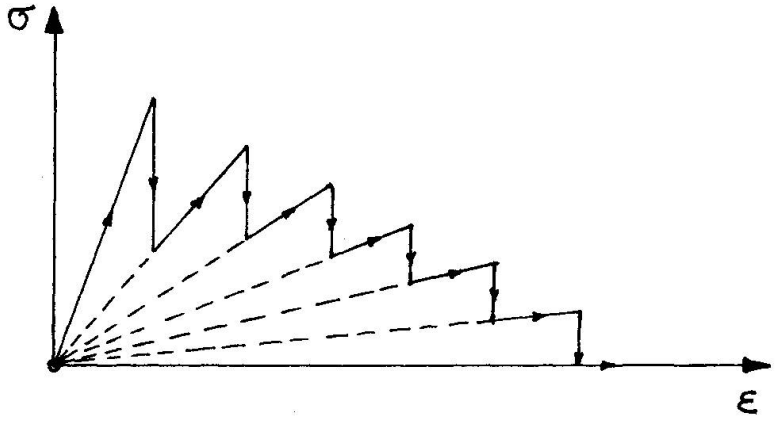

Fig. A

In fact these jumps are dynamic. Most of our analysis techniques involve pseudo-static methods of analysing these things. In general we nowadays replace such a discontinuous relation by a single line (Fig. B) at the element level.

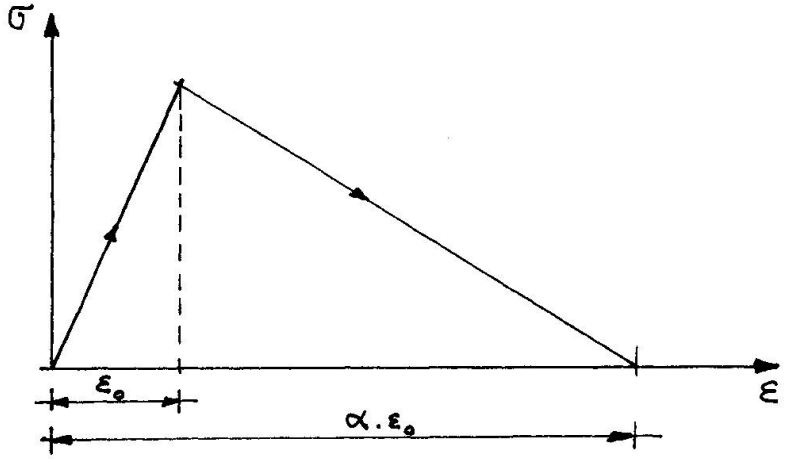

Fig. B

However, as the mesh gets finer, the stepped response of fig. A may be inevitable at the structural level, because of the strain localization effects. Even worse, pseudo-static analyses can result in nasty responses as shown in Fig. C.

If the inclination of the softening branch, represented in Fig. B, is small (so α is large), no problems will occur, but if this branch is steep, this may result in trouble. This is illustrated in Fig. D, displaying the load-deflection curve of a one-way slab, subjected to two concentrated loads.

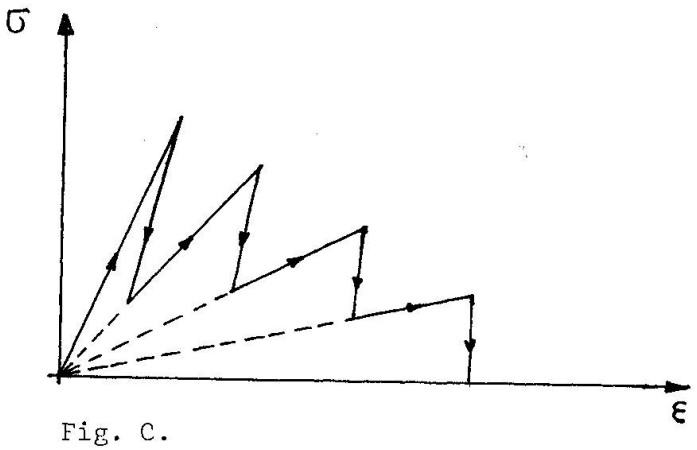

Fig. C.

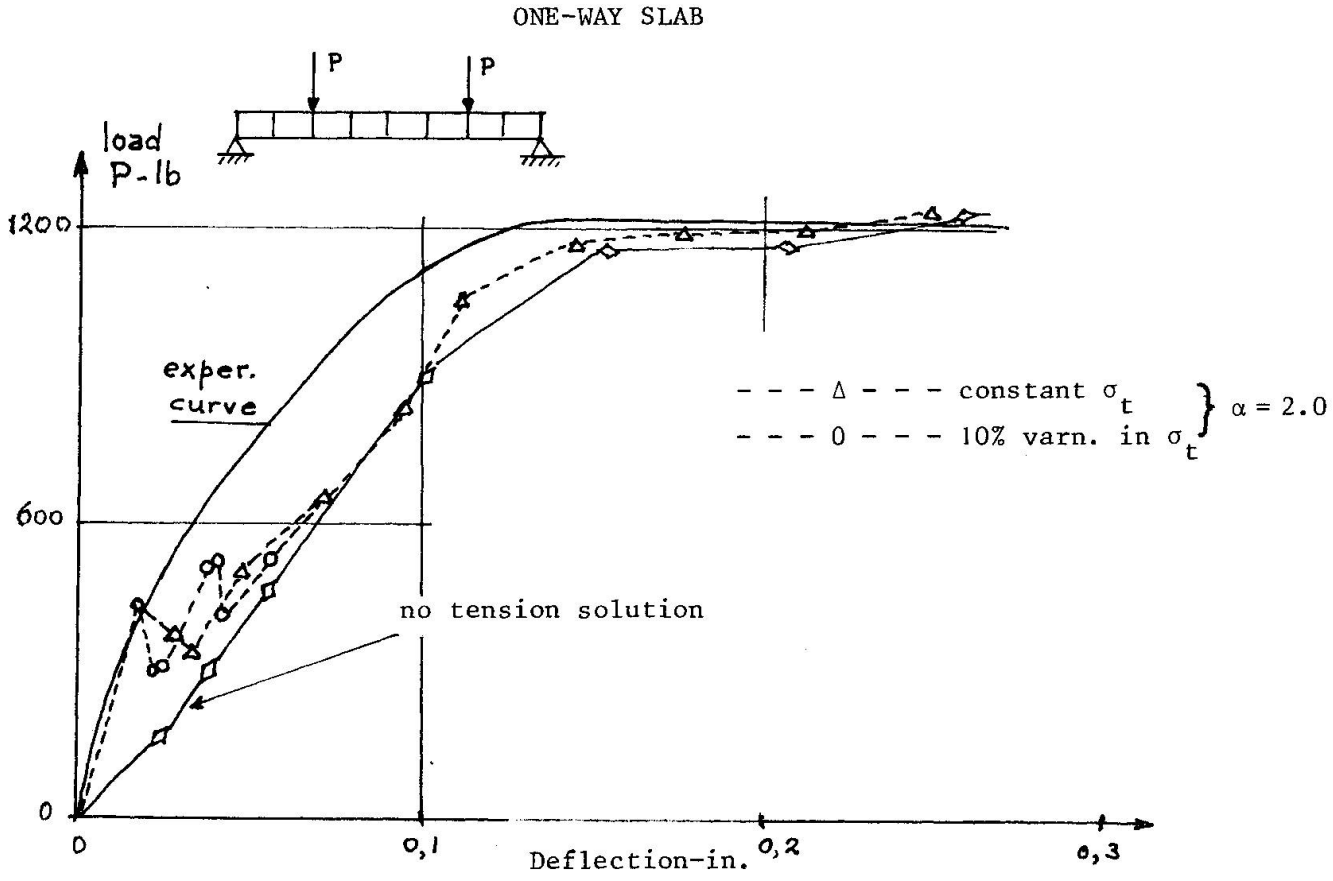

Fig. D

The upper, solid, line represents the experimental relation. The lower line shows the solution, obtained with a no-tension approach. In addition, two finite element solutions are given, both based on a steeply descending softening branch, with $\alpha = 2$. One of the lines is found, assuming that the tensile strength of the concrete σ_t in the area between the loads, is constant. After a local maximum in the curve, at first cracking, the load decreases and then three negative pivot points for the tangent stiffness matrix are obtained; however, convergence still occurs to an equilibrium state.

The reason that there are three negative pivots is because there are three excess Gauss-points, going down the strain softening path, where elastic unloading could occur as a result of the strain localization. So this situation is unstable. The second line which is represented, is obtained with the assumption that the tensile strength in one of the elements between the loads is 10% less than in the adjoining elements. Hence an alternative equilibrium path is obtained; after the first local maximum the load is reduced to a minimum, which is still an unstable situation because one extra Gauss-point is now "redundant". Subsequently again a local maximum, followed by a local minimum is obtained. This is definitely a very mesh-dependent situation.
If we took the variation in tensile strength (which in theory could be as small as 1%) between Gauss-points, we could even obtain a "snap-back" (as in fig. C) with many local load-maxima, depending on the mesh size in the constant moment zone. It may be not very practical but it is important to realize that these problems exist and that our solution codes are often trying to trace some very complicated things like this.

Bažant (U.S.A.): In several papers the use of orthotropic or equivalent uniaxial strain models was mentioned. I would like to call attention to the lack of invariance of these models with regard to rotation of the coordinates. I mean models the incremental stress-strain relation of which is characterized by zero terms connecting normal stress to shear strain and shear stress to normal strain:

$$\begin{Bmatrix} \Delta\sigma_x \\ \Delta\sigma_y \\ \Delta\tau_{xy} \end{Bmatrix} = \begin{bmatrix} x & x & 0 \\ x & x & 0 \\ 0 & 0 & x \end{bmatrix} \begin{Bmatrix} \Delta\varepsilon_x \\ \Delta\varepsilon_y \\ \Delta\gamma_{xy} \end{Bmatrix}$$

Such a model can principally be used in two ways. The first way is represented in Fig. 1. According to the standard rules the coordinate axes can be chosen arbitrarily with regard to the material in the initial state. However, when the element starts deforming, the coordinate axes have to be kept attached to the material. So if initially a uniaxial stress is applied, as in Fig. 1a, and subsequently an increment of a uniaxial stress that is oblique, is applied, (as in Fig. 1b), we get a combination of hydrostatic pressure and shear; however, in spite of this combination, in a vertical plane no shear deformation can occur.

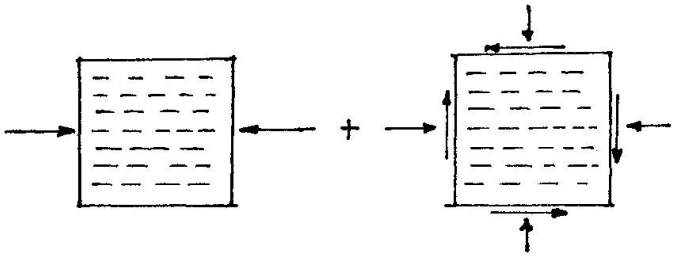

a. b.

Fig. 1 Coordinate axis fixed

The second way is represented in Fig.2a. An oblique orientation of the coordinate axes is adopted. Now the second increment in Fig. 2b, similar to that applied in Fig. 1b, is a uniaxial stress. However, now a shear deformation increment $\Delta\gamma$ is obtained as a result of a normal stress increment. If in both cases the first stress is 80% of the ultimate stress, the difference between the values of the maximum strain in both cases can be shown to be up to 50%, which can be rather significant. So there is no objectivity in this sense.

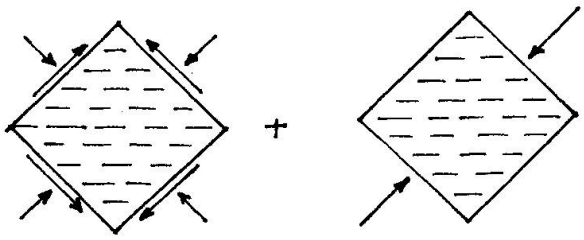

Fig. 2 Coordinate axes rotated against material

a. b.

Another possibility of the use of such models is that the coordinate axes are rotated in such a way that they always coincide with the direction of the principal stresses. In this case the model is invariant, but this is physically objectionable, because it implies that we get some oriented defects, e.g. microcracks, when we rotate them with the axes (Fig. 3).
A crack, however, cannot be rotated in the material.

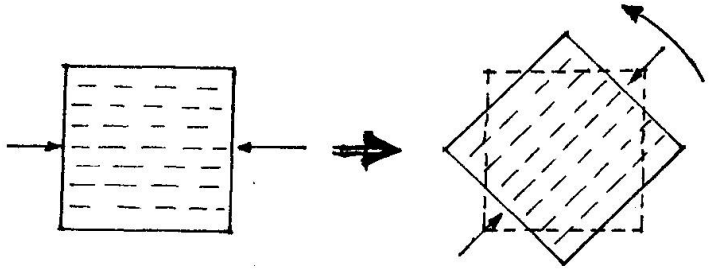

Fig.3. Rotation of cracks against the material is physically unacceptable

Of course it may be said that there is trouble with every model; we have no perfect model and a number of objections can be raised against plastic, endochromic or plastic-fracturing models. However, it should be pointed out that there are two kinds of troubles, those which are so complex that we do not know how to deal with them and those which can easily be avoided.
The trouble which has been discussed here can be easily avoided: therefore such errors should not be commited, because there are other models which are free of these errors.

Simplified Calculations of Concrete Problems

S. Turk,
D.Sc., Professor for concrete and timber-structures,
University of E. Kardelj
Ljubljana, Yugoslavia

The method given here is based on the fission(splitting)of deformations into an active part,which causes further rheological phenomena,and a passive part,which remains unchanged,as is the case for materials without creep.The fission is executed at the moment in time"i"(Fig.1/a)so that the active part D_{ai} of the deformation D_{fi},caused by a brought(planted)deformation D_{bo} at the moment "0" determines by itself the creep as though this active deformation had been brought(planted)in the structure at the moment "i" (Fig. 1/b),which has been chosen for the fission.The passive part D_{pi} of the deformation D_{fi} remains unchanged from this moment "i" onward,i.e.it maintains a constant value.These two parts,i.e.the active part D_{ai} and the passive part D_{pi},together,completely substitute the deformations D_{Ti} from the moment "i" onward,caused by the brought deformation D_{bo} at the moment "0"(Fig.1/a).In such a way the influence of the active part D_{ai} and that of the passive part D_{pi} together provide a complete substitute for the influence of the real brought deformation D_{bo} from the moment "i" onward,and by introducing them,we can cut off the whole rheological history from the moment "0" up until the moment "i".

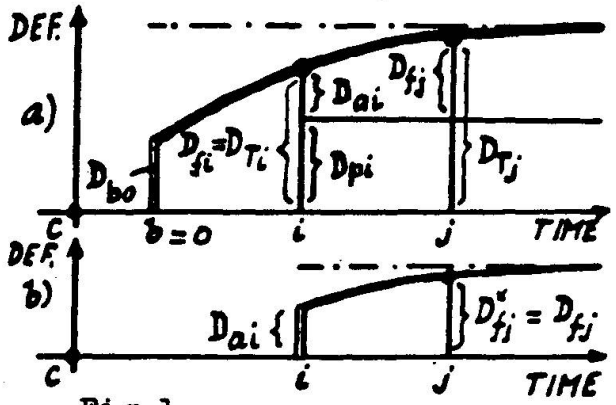

Fig.1

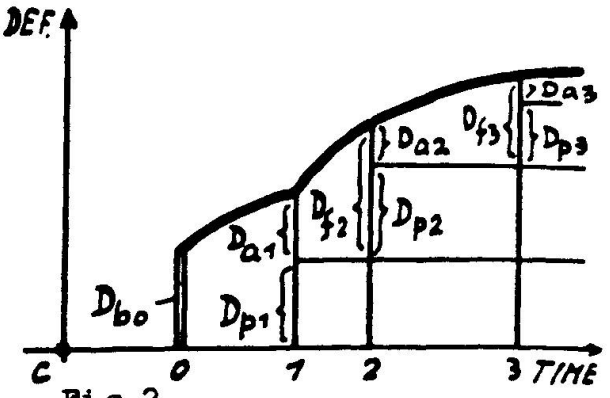

Fig.2

In the case of pure creep this procedure makes it possible to consider one climate in the first interval 0-1 (Fig.2),and then in the second interval 1-2 another climate which is decisive for the development(growing) of the deformation D_{a1}.At the moment "2" the climate can change again.In this case the fission of the"fissionable" deformation D_{f2},-caused by the active deformation D_{a1} at the moment"1"-is carried out,into active part D_{a2} and the passive part D_{p2},and for the development of the active part D_{a2} the climate in the interval 2-3 is considered. In this simple manner the creep resulting from an inconstant climate can be predicted.

The method further permits that the loading is changed at the moment of fission.For example at moment "1"(Fig.3)the deformation

D_{b1} is brought and this brought deformation is added to the active deformation D_{a1}, and from then on the common "working" deformation $D_{w1}=D_{b1}+D_{a1}$ for the further development of creep in the interval 1-2 is considered. The additional deformation can be an unloading, too, e.g. a deformation D_{b2} at the moment "2". At the moments "1", "2" etc., the climate can change, too. In this case the development of the working deformation D_{w1} in the interval 1-2 is subjected to another climate as the development of the working deformation $D_{w2}= D_{a2}-D_{b2}$ in the interval 2-3.

If, using this method, the total deformation D_{T1} ($=D_{f1}$), given by the first brought deformation D_{bo}, is diminished by means of a brought deformation D_{b1} so that at the moment "1" the initial deformation D_{bo} is reobtained (Fig.4), and if the same operation is carried out at moments "2", "3" etc., too, then at the moments "1", "2", "3" etc. a constant deformation D_{bo} is obtained. And if the intervals 0-1, 1-2, 2-3 etc. are very short, then by means of this procedure the phenomen of relaxation is obtained.

The fission of deformations must be always carried out at the moment when the structure changes, e.g. when a second span (part) is to be built into a first span, and a simply-supported beam turns into a continuous beam over two spans. Because of creep-phenomena, here a rheological redistribution of bending moments will occur here. This rheological redistribution can be easily predicted by the described method, and a simultaneously changing climate can be

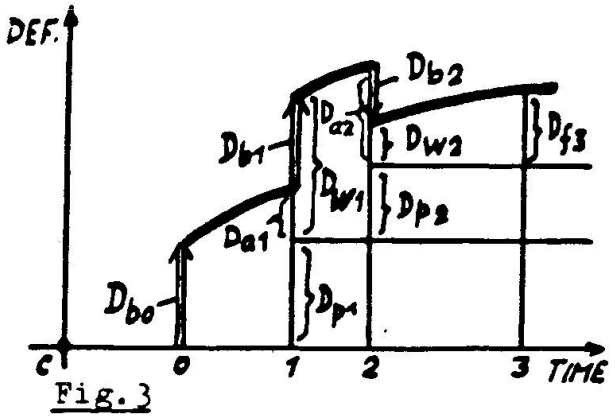

Fig.3

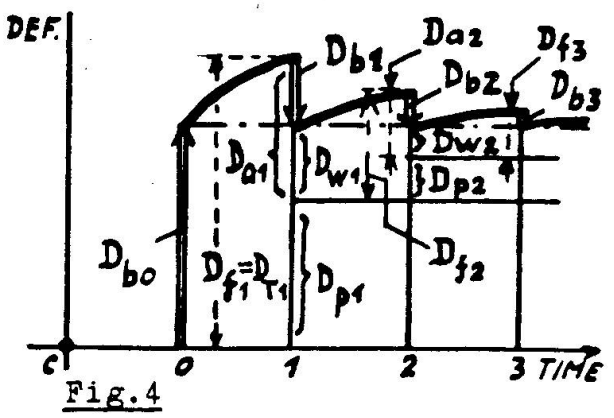

Fig.4

considered, too. Naturally, a fission of deformations must be arranged when a third span is built into in the second one, etc.

In the case of rheological redistribution, too, infinitely small intervals are used. That is in the case when the structure changes in a continuous manner. Such a case occurs if the second span is not a precast member (part), but is concreted directly onto the first span. In this case the stiffness $(E.I)_{II}$ grows from zero to the end-value [$\doteq (E.I)_{I}$]. (First span.. $(E.I)_{I}$, second span.. $(E.I)_{II}$)

The method is confirmed by experimental results obtained at the "Institute for Research of Materials and Structures" (=ZRMK) in Ljubljana. These results and numerical comparisons with results of other authors confirm a good accuracy for the technical practice.

DISCUSSION

Session 2, part 2: Structural Modelling for Numerical Analysis

Introductory Report by Willam/Argyris, F.R.G.

Schnobrich (U.S.A.): In the beam model that you showed you smeared cracks and consequently you have infinite bond between the steel and concrete and yet with that model you have been able to reproduce strain conditions, even in the cracked zone that looked extremely good to me. So I am wondering what your comment is on the smeared crack approach.

Willam: My comment is that you should use the simple tools first. Thus we assumed full bond between the steel and concrete in that first stage. We were also considering to introduce bond slip with spring elements. However, this was discussed after looking at material data from Dr. Eifel at the BAM, Berlin, who showed that if you account for plastification of the steel bar in the tensile flexural zone and if you introduce local cracking in heavily reinforced sections, i.e. for reinforcement ratios of higher than 0.6%, then there is virtually no difference between the perfect bond and the bond-slip formulations.

Ingraffea (U.S.A.): I would like to object to your objections about objectivity. Your comments are perfectly correct on the basis of the examples you showed. Prof. Bažant is also correct on the basis of his examples. But there are fundamental differences among the examples. Of the two cases you showed, in the one with the thick-walled cylinder, you will have a classically globally stable crack propagation problem, that is the load must continually rise to push the crack. In the case of the reinforced concrete beam you will have a stable crack propagation problem because of the reinforcement acting as a crack arrester. The load must constantly increase to push the crack. In the case of Prof. Bazant's example of a crack in an unreinforced plate there is a globally unstable system. Once the load reaches the necessary level to start the crack, the system is destroyed. Objectivity in the sense of Prof. Bažant is correct in his example because in the limit, as the element gets smaller, the load necessary to get the crack to propogate goes to zero. But in your case since you have load redistribution capability because of the stable propagation, objectivity in the sence that he uses is irrelevant. The accuracy in the sense that you use it is accurate. So one has to be careful about whether you talk about unstable crack propagation or stable crack propagation when talking about objectivity in either sense.

Willam: My point is that we should not be talking about objectivity if we consider stable or unstable crack propagation. Objectivity in mechanics is referring to the invariance of the material formulation with regard to rigid body motion and in particular coordinate transformations. We are discussing here the question of accuracy of your finite element lay-out. We have a discrete formulation and the approximate solution is certainly dependent on the mesh refinement. In that sense I did not like the term objectivity, because objectivity refers to the invariance with regard to the coordinate rotations. However, Prof. Bazant observed correctly, that you have to use energy criteria instead of local stress criteria, since the local stress concentration goes to infinity because of the singularity at the crack tip. In my thinking the different sensitivity of the finite element results with regard to the failure criteria has nothing to do with objectivity.

Prof. Bažant made a discussion on the evolution of parallel cracks in concrete which may be summarized as follows. Formation of secondary cracks halves the crack spacing, but that is not the only possibility. The crack spacing can also double. Under certain loading, for example for bending, or cooling, or shrinkage stresses, one observes the closing of every other crack (see figure), with the effect that the opening of the open cracks doubles as the loading increases (In more detail, see Bazant, ASCE-EMD Journal, 1979, p.873 and IASS 1980, p.97).

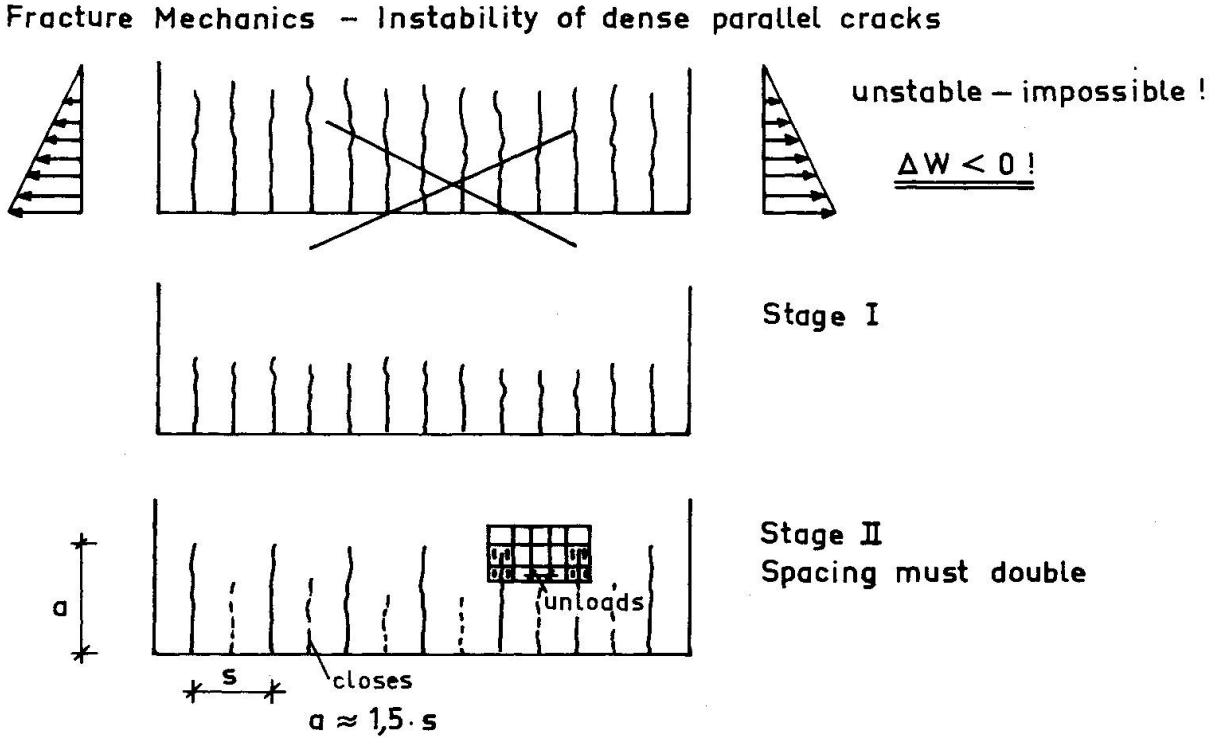

Kotsovos (U.K.): As the maximum load-carrying capacity of a beam under flexure is approached large tensile strain concentrations in the transverse direction occur in the compressive zone of the cross sections where flexural cracks appear. This causes a transverse deformation profile of the top surface along the length of the beam similar to that shown in fig. 1. It is apparent from this figure that such a shape of deformation profile will result in transverse internal forces (see fig. 1). Furthermore, the beam is subjected to internal forces acting in the loading direction due to its deflected shape (see fig. 2). The above forces combined with the longitudinal forces cause a complex triaxial, predominantly compressive state of stress in the compressive zone as indicated in fig. 3. In view of this triaxial state of stress which develops at load levels near the ultimate strength level, is it realistic to attempt to obtain, or indeed to expect, close predictions of ultimate load and corresponding deflexion of beams on the basis of a plane stress finite element analysis? (see page 496).

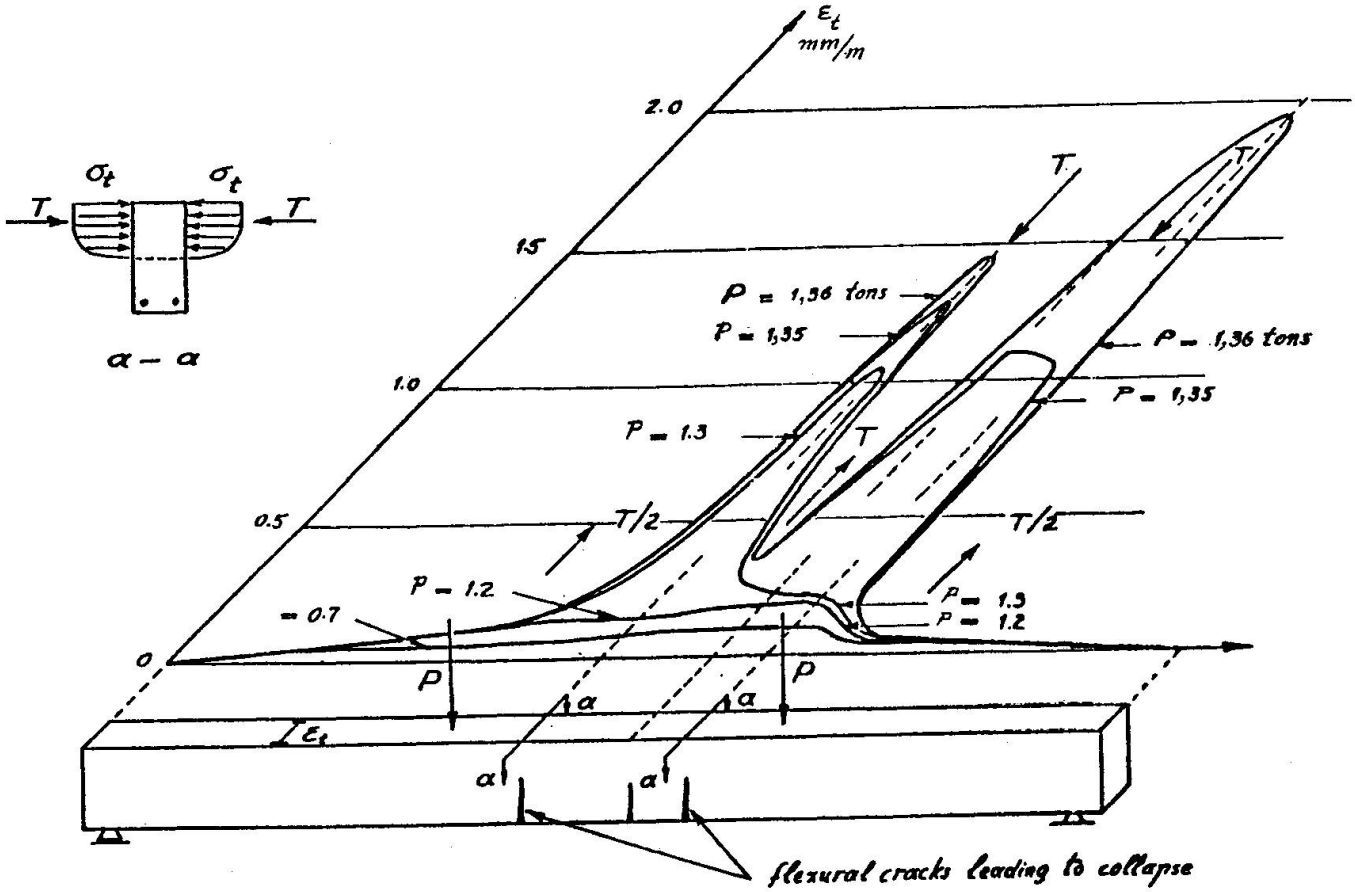

Fig. 1

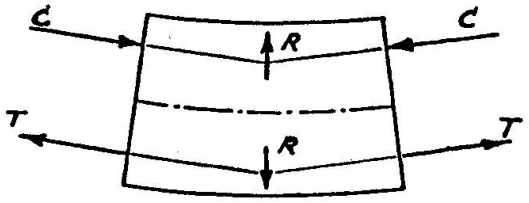

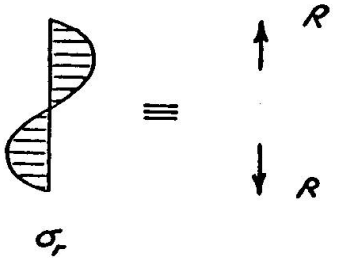

Fig. 2

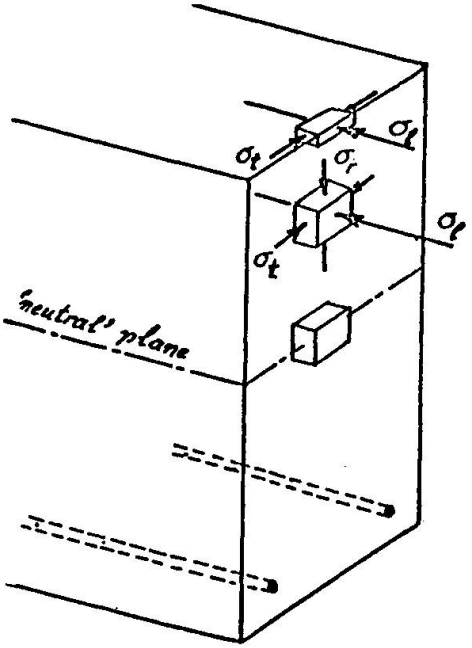

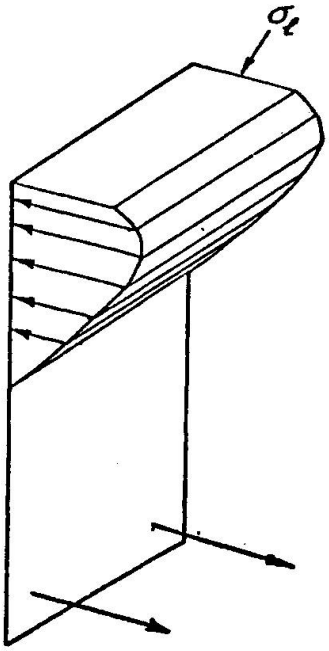

Fig. 3

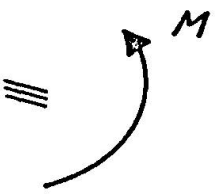

Willam: Let me repeat, we performed a plane stress analysis where the stresses perpendicular to the plane of bending are assumed to be zero. You could of course think of a three-dimensional analysis and our programs are perfectly capable of performing a fully three-dimensional analysis, but we had already 1624 degrees of freedom in the case of the fine mesh with computer times in the range of several hours. So you can imagine what is going to happen if you would adopt a three-dimensional idealisation of the beam problem which is "normally" solved as a one-dimensional flexural problem. Perhaps our Japanese colleagues have sufficient computing power to tackle this problem, but we are at ISD somewhat limited by the capacity of our University computer center.

Braestrup (Denmark):
1. Does the tensile strength affect the ultimate load and why did you use such a high tensile strength?
2. Concerning the compressive strength why didn't you use a kind of effective strength block instead of the cylinder strength in order to get a better agreement with test results?

Willam: To your first question: The tensile strength does not have any influence on the ultimate load behaviour. It has an influence on the cracking load; this occurs on a lower level. In order to get a good agreement with the test data, we had to use a high tensile strength value from the rupture test since we used no tension softening, i.e. brittle post-cracking behaviour.

To your second question: Within the framework of the Mohr-Coulomb formulation, the program predicts a compressive strength block automatically if sufficient stress redistribution takes place. However, the form of the compressive stress block is also a question of mesh refinement; how many elements are available in order to pick up the non-linear stress distribution in the compressive zone? Anyway, this was the main reason for the considerable differences in the ultimate load of all reinforced concrete beams when predicted by the coarse and fine mesh lay-out.

Paper by Saouma/Ingraffea, U.S.A.

Cervenka (Tsjechoslovakia): In your analysis the spacing of cracks was dependent on the size of the mesh. So the analysis is not suitable for determination of crack location, but only shows crack propagation.

Saouma: The initiation of the crack is based on the point with the highest tensile stress. This tensile stress is compared with the tensile strength; when this is exceeded the crack is initiated.

Bažant comments on this that in the case of a homogeneous stress distribution you do not know where the crack is initiated when you use a strength criterion. The right answer comes from fracture mechanics. You have a certain minimum spacing, you can calculate energy contained in the structure before cracking and then you take a finite jump to the cracked state. That jump requires a certain consumption of energy for the formation of the crack. From this one can calculate the minimum crack spacing. That is how you have to start in my opinion. That is the final conclusion of prof. Bažant.

Cervenka (Tsjechoslovakia): If the mesh size is sufficiently fine in order to describe the stress concentration, then the analysis can properly determine the crack location.

Paper by Blaauwendraad/Grotenboer, The Netherlands

Ingraffea (U.S.A.): First a comment because you referred to the previous paper which involves my work and dr. Saouma's work. In fact our cracks are not at all constrained by the mesh. The mesh does exactly what the cracks want it to do.
Now the question:
What criterium or what method do you use to predict the angle at which the crack is going to propagate at each increment and how do you predict how far the crack will go in each load increment?

Blaauwendraad: I understood that your mesh is not dominating the position and the propagation of your cracks. But you have to make a new mesh. I hesitate to believe that we have to go this way, because it has enormous consequences regarding renumbering of elements and nodes, rearrangements of matrices etc. We succeeded in avoiding that. Concerning your question:
The direction in which the crack propagates is determined by the main principal tensile stress and when the crack enters into an element it immediately splits up the total element. It means that in practice we have to use a sufficiently fine element mesh to allow for this.

Bažant (U.S.A.): What is your opinion on the assumption that the crack goes in the principal stress direction or do you believe that there are also other criteria for crack propagation?

Blaauwendraad: Until now I have no reason to take another criterium. But it is open for better proposals. We use an aggregate interlock model which in fact is of a rigid plastic nature. The stress level at which slip occurs is dependent on the crack opening. This model can be changed in a model in which shift occurs first when a certain amount of crack opening is reached. We have to study if this means that we have to change the criterium for cracking. I dare not say it at this moment.

Saouma (U.S.A.): What is the reason of taking a reduction factor of 20% to 30% in your tensile strength, and do you use the same factor if you are analyzing another type of structure?

Blaauwendraad: The amount of reduction is a result of tuning the model. First we did not use the reduction and found erraneous results of crack propagation. After lowering the tensile strength to approximately 20% to 30%, we found in a number of situations, that this leads to satisfying results in practice. We have no information at this moment, whether or not this value is dependent on the stress situation or type of structure we examine. We did not find a typical correlation.

Paper by Dotreppe, Belgium

Fawzi (The Netherlands): Have you taken the modulus of elasticity as a constant? (see also written comment Fawzi on p.p. 501-506).

Dotreppe: I have not spoken about the material properties; this would have been too long for the paper. Of course you have to take into account the decrease of all material properties, such as compressive strength, tensile strength, modulus of elasticity and so on.

Paper by Hinton/Abdel Rahman/Zienkiewics, U.K.

Willam (F.R.G.): The quasi Newton-Raphson method is an approximation of the actual Newton-Raphson method, so you would expect that the quasi Newton-method needs more iterations than the Newton-Raphson method. You found the contrary. Why?

Hinton: The Newton-Raphson method does indeed require fewer iterations than the Quasi-Newton method. However, in the example quoted in the paper, when the Newton-Raphson method was adopted, on the penultimate load increment premature failure occurred. This was probably due to ill-conditioned stiffness matrices.

Crisfield (U.K.) (answer to question of Willam): The Newton-Raphson used is a method without line searches; the quasi Newton method is a method with line searches. If in both methods the line search is used you will find that the Newton-Raphson method will use less iterations than the quasi Newton method. This is the explanation.

Bazant (U.S.A.): Mathies and Strang developed an efficient method for elastic-plastic analysis with a sudden change of incremental stiffness. This method has been tried with the ADINA program with a great improvement in efficiency. In your problem, you have a gradual change in stiffness, so I cannot see how you can expect an improvement there.

Hinton: Our experience to date shows that for the non-linear analysis of reinforced concrete plates the best overall method is the Quasi-Newton method with line searches. However, it should be mentioned that our program PLASAN includes a large number of alternative solution strategies and we are still experimenting.

Crisfield (U.K.): I would like to make a brief comment on the arc length method. It seemed the best method in your limited examples. I have tackled the same problem with the arc length method. Indeed, for a reasonably high value of tension-stiffening it is effective. I have found that if the strain softening is coming down fast, you are then in trouble with the standard version of the arc length method. I think that this relates to the whole issue of line searches. My conclusion has been that the really important thing with concrete cracking is the line search business. It is difficult to introduce the line search into the standard versions of the arc length methods. But one certainly can take even a standard modified Newton-method and include the line search. For concrete analysis this will give a great improvement in performance.

Hinton: From subsequent analyses it was found that for problems with no tension stiffening, a slight ripple occurred in the load-displacement curve at the onset of cracking. However, after this happened, the solution progressed to the correct failure load. Further investigations are being carried out to determine the reasons for this unusual behaviour.

Proposal Collins (Canada): Issues an invitation to a blind test.
There are several people here with models for the behaviour of reinforced concrete. All these models have many open parameters which have to be given values in order to get the model fit with the results of experiments. What we suggest now is that we ask for predictions before you know the answer of the tests. We are currently conducting a series of these panel tests that I explained yesterday. At the end of this summer we come to the more general stress situations, having a general plane stress situation in the reinforced concrete panel (see figure).

We ask for doing predictions for the behaviour of these panels. Write to us in Toronto what kind of input parameters you need to conduct your predictions.

In august 1981 we can provide you with all the material characteristics and the data on the reinforcement of the panels. We can tell how we plan to load the panel. Probably it will be a combination of shear stress and compression in one direction and tension the other way. What we are asking for is make a prediction for this experiment on what will be the maximum value of the load as expressed for instance by the shear; it will be monotonically increased to failure and the ratio's between the shears and the normal stresses will be maintained constant throughout the test. We want to receive your predictions in december 1981, so that we can publish the test results together with the various predictions in january 1982.

Bažant (U.S.A.): suggests a more complex loading path but Collins rejects this suggestion. His philosophy is "simple loading paths first".

INVITATION TO A BLIND TEST

M.Collins, University of Toronto

Given :

ρ_x , ρ_y , ... etc.

f_{yx} , f_{yy} , ... etc.

f'_c , ε_o , ... etc.

$\sigma_x = k_x . \tau$

$\sigma_y = k_y . \tau$

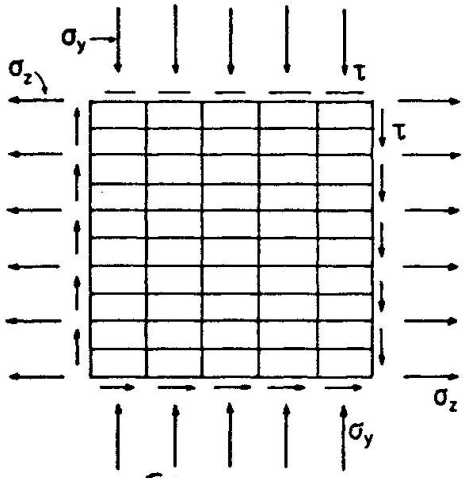

Predict :

τ_{max} and strains in panel at

$0,25\,\tau_{max}$, $0,50\,\tau_{max}$,

$0,75\,\tau_{max}$, $1,00\,\tau_{max}$.

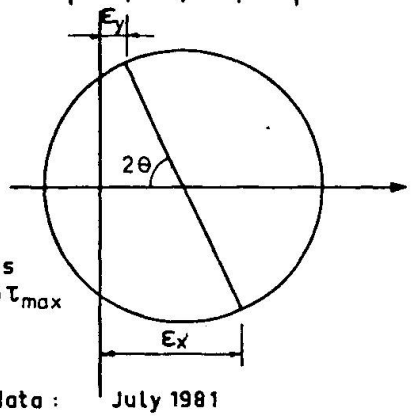

e.g. strains at say $0,5\,\tau_{max}$

Timing :

Submit names + list of desired data : July 1981

Give out data : Aug. 1981

Receive predictions : Dec. 1981

Publish results : Jan. 1982

COMMENTS ON DR. DOTREPPE PAPER

ADVANCED MECHANICS OF REINFORCED CONCRETE

IN STRUCTURAL FIRE ANALYSIS

Prepared by
Dipl.-Ing. A.E.R. Fawzi
Consulting Engineer
Rotterdam, The Netherlands

In the Paper of Dr. J. Dotreppe "Advanced mechanics of reinforced concrete-in Structural Fire Analysis" a numerical model for the evaluation of the fire resistance of reinforced concrete structures at elevated temperature is presented.

Under point 2 of the paper "Material properties" which is subdivided into: 1) Thermo-physical- and 2) Mechanical properties of materials. These material properties will be significantly affected due to the high temperatures, therefore, they have to be considered in the numerical model.

In a step by step numerical analysis, in addition to the classical mechanical properties, such as ultimate strength in tension and compression, yield stress and modulus of elasticity, the instantaneous stress-strain relationship as well as the thermal creep of concrete and steel have to be considered.

The stress-strain relationship for concrete at high temperature is indeed the basic topic for numerical analysis.

The heat function relation for the elevated heat propagation through the structural element

$$f(\sigma, \bar{\sigma}, \varepsilon, E, \theta, t) = 0 \quad \text{---------- (1)}$$

is characterizing the material behaviour under varying loading and temperature conditions.

The modulus of elasticity E, is not included in equation (1) of Dr. Dotreppe's paper, i.e. he assumed it as constant.

As a matter of fact the modulus of elasticity has to be determined for the test, and must be considered for the numerical analysis as varying with the time t in respect of the elevated temperature. The stress-strain curve in our problem is distinctly non-linear and may be represented by the following equation of P.H. Thomas

$$\frac{\sigma}{\sigma\ max} = \frac{\varepsilon}{\varepsilon\ max} \exp\left(1 - \frac{\varepsilon}{\varepsilon\ max}\right)$$

Over the whole range of $\varepsilon/\varepsilon\ max > 0$

for the small values of $\varepsilon/\varepsilon\ max$ the curve is approximately linear so that:

$$\frac{\sigma}{\sigma\ max} = C\ \frac{\varepsilon}{\varepsilon\ max}$$

where C is constant, i.e. $\sigma = \left(C\ \frac{\sigma\ max}{\varepsilon\ max}\right) \varepsilon$

but $\sigma = E\varepsilon$ (elastic range)

then $E = C.\ \frac{\sigma\ max}{\varepsilon\ max}$

The constant C can be determined from the values of E and $\frac{\sigma}{\sigma\ max}$ at ambient temperature.

It is well known that E is the tangent of the stress-strain curve in elastic range which gives

$C = 2.18$ and $E = 2.18\ \frac{\sigma\ max}{\varepsilon\ max}$ ----------(2)

The variation of the modulus of elasticity E with temperature can be determined by using equation (2) by which σ max and ε max can be derived from stress-strain curves.

Actually the modulus of elasticity of concrete is influenced directly by the vaporization of the capillary water and the associated shrinkage phenomena.

At 200°C the reduction of the modulus of elasticity is about 25% of its original value at room temperature

i.e. $\frac{E\theta\ 200°C}{E\theta\ 20°C} \cong 75\%$

By increasing the temperature up to 500°C a significant reduction occurs in the range of 70%

i.e. $\frac{E\theta\ 500°C}{E\theta\ 20°C} = 30\%$

Since the range of our investigation is up to 800°C, there is a tremendous reduction factor in modulus of elasticity. The additional thermal stress equ. (9) in the paper.

$\Delta\sigma = E\Delta\varepsilon$ must be $\Delta\sigma = E_t\Delta\varepsilon$

$= E_t\ (-\alpha\Delta\theta + \Delta\varepsilon o + \Sigma\ \Delta\chi)$

This is valid for Equ. (10) through (13).

The restrain stresses $E\alpha\Delta\theta$ on page 299, must be $E_t\alpha\Delta\theta$

The stifness matrix ($E_t I$) is directly related to the modulus of elasticity, E, as time, temperature dependent. This means that the stiffness of a concrete structural member diminishes at high temperatures and plastic hinges are capable of large rotational capacities, the ductility of concrete will be higher at elevated temperatures.

My last contribution point is about the thermal creep of concrete and steel. Dr. Dotreppe left this important topic open because of the complexity of the creep models for both materials. In the course of the last years, there are many different tests, studies and investigations about thermal creep under steady state, non steady state, isothermal creep and transitional thermal creep.

The transitional thermal creep "according to Illston and Sanders" which can fit in our model of analysis is defined as "the creep strains appearing during very short heating periods, which are far beyond those values according to creep measurements at constant temperatures. In my opinion, it is possible nowadays to predict with good accuracy the thermal creep laws.

One of the phenomenal studies on this subject, is the work of Dr. U. Schneider, "Ein Beitrag zur Klärung des Kriechens und der Relaxation von Beton unter instationärer Temperatureinwirkung".

Creep and transitional creep laws:

$$\left(\frac{\partial \varepsilon}{\partial t}\right)_{\sigma} = \sigma \cdot \left(\frac{\partial J\ (\bar{\sigma}, t)}{\partial t}\right)_{\sigma} \text{---------- (3)}$$

$$\varepsilon - \varepsilon o = \int_{\vartheta o}^{\vartheta} \left[\frac{\bar{\sigma}\left(\frac{\vartheta - \vartheta o}{W}\right)}{E\left(\frac{\vartheta - \vartheta o}{W}\right)} + \sigma \left(\frac{\vartheta - \vartheta o}{W}\right) \cdot \left(\frac{\partial J}{\partial \vartheta}\right)_{\sigma} \right] d\vartheta \text{ -------- (4)}$$

$$\varepsilon = \frac{\bar{\sigma}}{E(\vartheta)} + \bar{\sigma} . J\ (\sigma, \vartheta) \text{ -------- (5)}$$

$$J = \frac{1}{E(\vartheta)} \cdot \Phi\ (\bar{\sigma},\ \vartheta) \text{ ---------- (6)}$$

$$\varepsilon = \frac{\bar{\sigma}}{E(\vartheta)}\ [1 + \Phi\ (\bar{\sigma},\ \vartheta)] \text{ -------- (7)}$$

Where $\Phi\ (\bar{\sigma},\ \vartheta)$ as creep function of concrete

$\Phi = C_1 \tanh \gamma_1\ (\vartheta - \vartheta o) + C_2 \tanh \gamma_2\ (\vartheta - \vartheta_1) + C_3$

The parameters can be seen in Table 1.

See also fig. 1.

The general creep law for Reinforcement (Steel)

$\dot{\varepsilon}_{cr}\ (\sigma) = C_1\ \sigma^{c2} + tB\sigma^{n}$

Where B = creep rate intercept at log stress 1.0, a material constant for a given temperature.

C_1 and C_2 = Const. (material depend.)

The rupture time is:

$\log T_r(\sigma) = C_3 + C_4\sigma$ (at a temperature)

The time interval ΔT_i with a stress σ_i the damage fraction equals

$$F_i = \frac{\Delta Ti}{Tri(\sigma)}$$

See elevated temperature properties of carbon steel ASTM special tech. Publication No. 180.

Table 1
Parameter for Φ function

Parameter	Dimension	Wert
c_1	1	2,51
γ_1	$°C^{-1}$	$2,72.10^{-3}$
ϑ_0	°C	$2,0.10^{1}$
c_2	1	3,0
γ_2	$°C^{-1}$	$7,5.10^{-3}$
ϑ_1	°C	$6,0.10^{2}$
c_3	1	2,9

Conclusion:

The influence of the Modulus of Elasticity and Thermal Creep on the numerical model for the analysis can not be smaller than the possible accuracy of measurements in such kind of tests.

I wonder how we could achieve such good agreement between theoretical analysis and experimental results.

Finally, I look forward to seeing further results along the lines of Dr. Dotreppe's work especially when the topics of my comments are included. A particularly valuable feature of this work is the development of the numerical analysis methods in parallel with the test programme on the structures he is analysing.

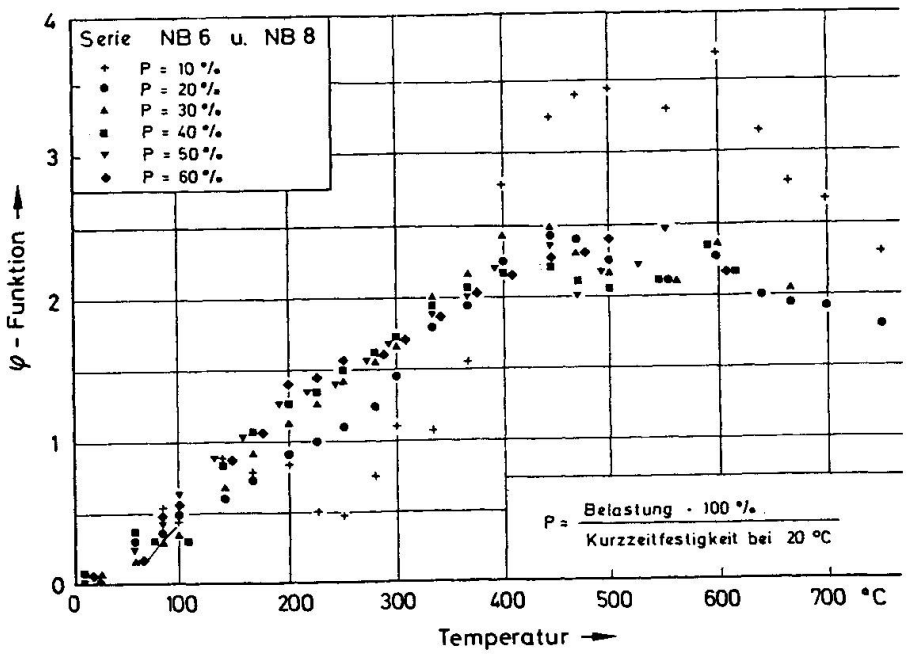

Fig. 1 $P = \frac{\text{load} \cdot 100\%}{\text{short time strength at } 20°C}$